OBSERVATION OF THE DEVELOPMENT OF FRACTURE PROCESS ZONES IN CONCRETE UNDER TENSION

by

Mark Edward Raiss, MA, MSc, DIC, CEng, MICE

October, 1986

A Thesis submitted for the degree of Doctor of Philosophy
of the University of London.

Department of Civil Engineering
Imperial College
London, S.W.7

Abstract

A review of current theoretical models for the fracturing of concrete has highlighted a lack of experimental data regarding the initiation, propagation and characteristics of fracture process zones. The aim of the work described in this thesis has been to provide such data.

A test has been developed in which controlled fracture occurs and can be observed. Specimens of concrete are loaded in direct tension by a closed loop servo-controlled testing machine, using the axial extension of the specimen as the control parameter. The combination of extension control and stiff testing frame has allowed stable failure to be achieved and the full post-peak portion of the load/extension relationship to be obtained.

The full field surface strain of the specimen is measured using moire interferometry, which yields local strains throughout the area of observation. Both initiation and propagation of the fracture process zone have been observed, together with their effects on the surrounding material. The extent of the fracture process zone and crack opening characteristics under increasing extension have also been measured. Localisation in the strain field occurs prior to the attainment of maximum load, with subsequent propagation during the post-peak portion of the load/extension relationship. In the majority of tests it was noted that more than one fracture process zone was initiated but that only one of these zones propagated across the specimen leading to final failure.

An improved model for the stress transferred across a fracture process zone has been suggested based on a local stress/fracture zone opening relationship. The model is suitable for use in the finite element analysis of concrete structures undergoing cracking.

To Kathryn and Beth

Acknowledgements

This work was undertaken in the Concrete Section, Department of Civil Engineering, Imperial College.

I am greatly indebted to Professor John Dougill and Dr. John Newman for their continued encouragement and supervision.

I also wish to acknowledge the help received from the following:
The staff of the Concrete Laboratories, in particular Roy Loveday, Peter Jellis, John Hall, Bill Bobinski and John Turner, for technical support during the experimental work.
Richard Packer, for assistance with the photography.
Dr. Colin Walker and Dr. Jim McKelvie of the University of Strathclyde and Professor Luigi Cedolin of the Politecnico di Milano, for advice concerning the techniques for moire interferometry.
Nigel Metcalf and Bill Greenaway of R.D.P.-Howden Ltd., for assistance with the servo-controlled testing machine.

I am grateful to the Science and Engineering Research Council for financial support through grant number GR/C/36711.

Most of all I am indebted to my wife, Kathryn, not only for typing the manuscript but also for her support and encouragement throughout the period in which this research was undertaken.

CONTENTS

Nomenclature

A	area
A_{eff}	effective cross-sectional area
a	semi-crack length
b_0	intermolecular spacing at equilibrium
COD	crack tip opening displacement
COD_c	critical tip crack opening displacement
D	damage modulus
d_y	length of yield zone
E	Young's modulus
E_t	tangent strain-softening modulus (Section 2.4.3)
f'_c	cylinder strength
f_{cu}	cube strength
f_t	tensile strength
G	strain energy release rate
G_c	critical strain energy release rate
G_f	fracture energy
J	J-Integral
J_c	critical J-integral
K	stress intensity factor
K_c	critical stress intensity factor
K'_c	effective fracture toughness
k_1	testing machine stiffness
k_2	parallel bar stiffness
k_g	specimen grip stiffness
k_s	specimen stiffness
l	length
l_{ch}	characteristic length (Section 2.4.2.1)
l_p	length of fracture process zone
N	fringe order
P	load
p	moire reference grating pitch
p'	moire specimen grating pitch
q_t	intrinsic tensile strength (Section 2.3.1)
r	distance ahead of crack tip
S	moire fringe spacing

S'	surface energy
s	net stress (Section 2.3.2.1)
$\underline{T}$	traction vector
U	stored strain energy
$\underline{u}$	displacement vector
u_{11}	crack opening displacement
W	strain energy density function
w	fracture zone opening
w_c	width of fracture process zone
x_i	Cartesian coordinates
Γ	path for J-Integral
γ	surface energy per unit area
γ_{xy}	shear strain
δ	extension
δa	crack extension
ε	strain
$\tilde{\varepsilon}$	equivalent strain (Section 2.3.2.2)
$\varepsilon_{x,y,z}$	principal strains
λ	wavelength
μ	cracking parameter (Section 2.4.3)
ν	Poisson's ratio
ξ	stress at microscopic level (Section 2.3.1)
ρ	crack tip radius
σ	stress
σ_0	remote applied stress
σ_{11}	local stress
σ_c	critical applied stress
σ_{max}	maximum applied stress
σ_y	yield stress
ω	scalar damage parameter

Chapter 1 Introduction

The dual phenomena of localisation and strain-softening in the fracture of concrete are of considerable theoretical and practical interest. The phenomena cause difficulties both in the interpretation of experimental results to obtain valid material parameters and in the analysis of concrete structures undergoing fracture. These difficulties are commonly associated with the term 'size effects' by which is meant the apparent change in the fracture characteristics of a material with a change in size of the specimen or structure. A more detailed understanding of the fracture processes which occur in concrete is essential if the results of laboratory tests on strength and cracking are to be properly applied in the design of plain, reinforced and pre-stressed concrete structures.

Localisation and strain-softening have been observed both in uniaxial compression (Van Mier, 1984) and uniaxial tension (Petersson, 1981b) and it is suggested that these phenomena are fundamental to the fracture of concrete. Failure in multi-axial stress states occurs generally by opening of cracks in a direction perpendicular to the direction of maximum principal tensile stress. The aim of the current research is to study the localisation and strain-softening behaviour of concrete fracturing under tension. It is believed that an understanding of tensile fracture is of primary importance in the investigation of failure in concrete, not only under uniaxial tensile stress, but also under more complex stress states. Even the failure of concrete in uniaxial compression occurs by lateral tensile splitting although the link between compressive and tensile behaviour is not yet fully understood.

Until the early 1960's little research had been conducted into the tensile fracture of concrete which was assumed to be both brittle and weak. As a result the tensile properties of concrete were taken to be of little importance in the design of structures. During the last two decades advanced methods for the analysis of concrete structures have

been developed. Numerical techniques and computer hardware have been greatly improved allowing the analysis of complicated structures under complex loading conditions. With these developments, the demand for improved material models has grown. Hughes & Chapman (1966a) demonstrated the existance of a post-peak portion to the stress/strain curve for concrete in tension. Since that time there has been an increasing awareness of the importance of the role of the tensile behaviour of concrete in the performance of structures. For example, the strengths both of the anchorage of a steel reinforcing bar in concrete and of beams in shear depend on the post-peak behaviour of concrete in tension, as do the ductility and deformation of concrete structures.

Kaplan's (1961) application of linear elastic fracture mechanics to concrete signalled the beginning of a extensive research effort into the tensile failure of concrete, which has, as yet, not reached a satisfactory conclusion. The main difficulty faced by the researchers was the dependence of the parameters measured on specimen size. It has been suggested (Gustaffson, 1985) that direct tensile tests are less susceptible to these size effects. Non-linear constitutive models have been developed based on the data from stable direct tensile tests despite the severe experimental difficulties encountered in conducting such tests. Evidence of the recent interest in direct tensile testing of concrete may be gained from the fact that in the three years since the start of the research reported in this thesis, six different research establishments working in four countries have published details of such tests. This compares with only five different establishments in the previous seventeen years. Part of the increased interest in this particular type of test stems from the need for improved constitutive relationships and part from the advent of servo-controlled testing machines.

The fracture of concrete is characterised by the formation and propagation of fracture process zones. It has been suggested that these zones are initially formed by microcracks which subsequently coalesce into a macroscopic defect. It is essential that the localised nature of the fracture process zones is understood when interpreting experimental results and when postulating models for the strain-softening behaviour of concrete. It is towards achieving a

better understanding of the role of fracture process zones and of the correct interpretation of the results of direct tensile tests that the research reported in this thesis has been directed.

During the last 20 years, research undertaken within the Concrete Section at Imperial College has reflected the increasing demand for improved material models for concrete. The experimental work has ranged from direct tensile tests (Ward, 1964) to tests under multi-axial stresses (Vile, 1965; Newman, 1973). The data from the tests has formed the basis of analytical models for the deformational behaviour of concrete under multi-axial stress states (Kotsovos, 1978) which have been applied to real problems using the finite element method (Bedard, 1983). In the models, concrete has been taken to be a brittle fracturing material. The increased interest in tensile deformation behaviour led as a natural extension of the earlier work, to the initiation of the current research project.

The primary aim of the current research has been to develop a stable direct tensile test in which the failure processes could be studied. For the test results to be useful several stringent limitations have had to be applied to the condition of the specimen, the method of loading and the technique used for strain measurement. In the test developed, necked specimens were loaded by a stiffened servo-controlled testing machine. The response of the specimen was monitored using a full field surface strain measurement technique. A series of tests was conducted to validate the techniques and to obtain initial results.

A review of the tensile failure of concrete is described in Chapter 2 in which the application of linear and non-linear fracture mechanics as well as continuum mechanics is discussed.

Chapters 3 and 4 are concerned with the direct tensile testing of concrete. In Chapter 3 the testing techniques and test results published in the literature are reviewed and the requirements for further work are discussed. In Chapter 4 the development of that part of the direct tensile testing technique concerned with controlled loading of the specimen is discussed.

Full field surface deformation measurement techniques are reviewed in Chapter 5 and the technique adopted is described in detail in Chapter 6.

The experimental programme is discussed in Chapter 7 and the results are given in Chapter 8. Chapter 9 discusses the results and compares them with those obtained by other researchers. As part of the discussion a model for the stress transferred across a fracture process zone is described to allow a clearer understanding of the test results.

The conclusions which may be drawn from the research presented in this thesis are given in Chapter 10 and recommendations for further research are given in Chapter 11.

Chapter 2 Review of the tensile failure of concrete: Theories and Models

2.1 Introduction

In Chapter 1 the need for a detailed understanding of the fracture processes of concrete in tension was established. In this chapter, theoretical descriptions of these processes are reviewed together with their experimental evaluation. The fracture of concrete is characterised by the development of fracture process zones within which, initially, microcracking is thought to occur with subsequent concentration at one or more discrete cracks. This is a continuous process and subdivision into separate, well defined stages is not possible. Even after a discrete crack can be observed significant load carrying capacity remains (Petersson, 1981b). The simple strength criterion, with elastic behaviour up to maximum stress followed by complete loss of load carry capacity, cannot be a valid description of the fracture of concrete.

Two basic approaches to the description of the complex fracturing phenomena have been used. The first, Fracture Mechanics, considers the stresses and strains around a crack and defines the conditions which are required for the crack to propagate. The second, Continuum Mechanics, relates the stresses and strains throughout the material by continuous constitutive relationships. Both approaches are idealisations of the true properties of the material in which, initially, the continuum description is more appropriate but as the fracture processes develop significant strain localisation occurs and a discrete crack is formed. These two approaches are described in Section 2.2 and 2.3 respectively.

In Section 2.4 non-linear, finite element modelling of the fracture process zone is discussed. The models described embrace both of the approaches mentioned above.

It should be noted that unless stated otherwise only Mode I cracking,

that is opening perpendicular to the crack, has been considered. It is believed that this mode is of primary importance in the fracture of concrete and that all cracks induced by proportional loading (with the possible exception of crushing under large hydrostatic stresses) occur by separation perpendicular to the principal tensile stress. Only when Mode I cracking is more fully investigated can other situations, for example shearing across an already formed crack, be understood.

2.2 Fracture Mechanics

2.2.1 The development of fracture mechanics

2.2.1.1 Linear elastic fracture mechanics

2.2.1.1.1 Introduction

Fracture mechanics has been developed following work by Griffith (1921) who attempted to explain why the strength of materials was very much less than their theoretical strength based on the inter-molecular attraction. He supposed that a macroscopically homogeneous test sample might contain small defects, or flaws, which caused stress concentration. The stress in the material adjacent to the flaw could then approach the theoretical fracture stress.

The stress concentration around an elliptical hole, in an infinite, linear elastic plate, under uniform tensile stress, had previously been calculated by Inglis (1913). He showed that for an ellipse (Fig. 2.1) whose major axis was normal to the direction of the applied stress, σ_0, the stress at the tip of the major axis is given by:

$$\sigma_{11} = \sigma_0 (1 + 2\sqrt{(a/\rho)}) \qquad (2.1)$$

where a = semi-major axis of ellipse
ρ = radius at the tip of the ellipse.

It can be seen that when the ellipse degenerates into a circle $\sigma_{11} = 3\sigma_0$, and when the minor axis is very much smaller than the major axis (or $\rho << a$) then $\sigma_{11} = 2\sqrt{(a/\rho)}\sigma_0$. Inglis showed that the exact shape of the hole was unimportant provided that it was similar to an ellipse at it's tip. Thus for fracture to occur:

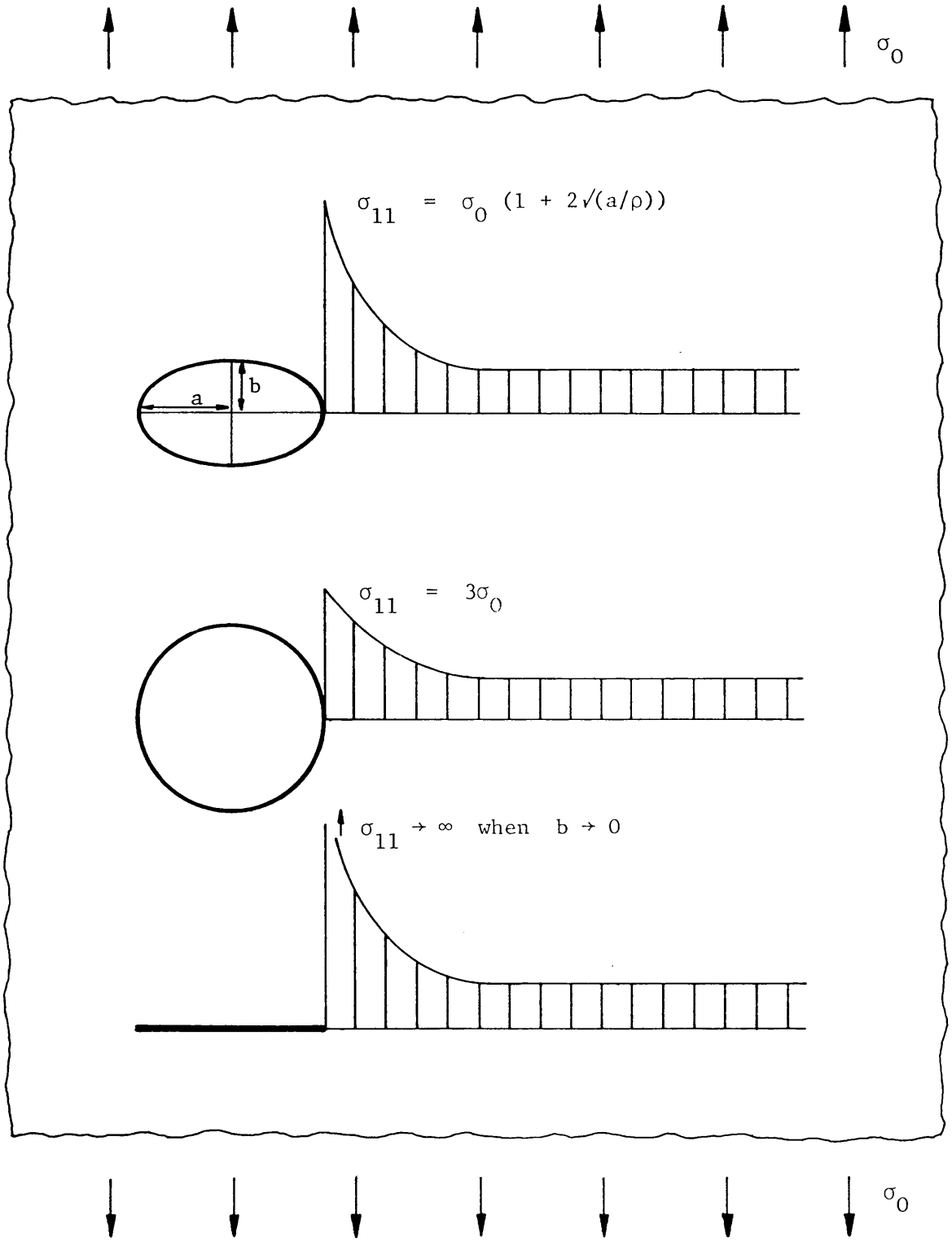

Fig. 2.1 Stress distributions close to an elliptical hole, a circular hole and a crack in an infinitely large elastic plate subjected to uniform stress. (Inglis, 1913)

$$\sigma_c = \sqrt{\frac{\rho}{4a}}\ \sigma_{11} \tag{2.2}$$

where σ_c = critical applied stress

σ_{11} = maximum stress sustainable adjacent to the hole.

The theoretical maximum stress based on averaging the intermolecular attraction is given by:

$$\sigma_{max} = \sqrt{\frac{E\,\gamma}{b_0}} \tag{2.3}$$

where E = Young's modulus

γ = surface energy per unit area

b_0 = intermolecular spacing at equilibrium.

Equating σ_{max} with σ_{11} provided the condition for fracture to occur:

$$\sigma_c = \sqrt{\frac{E\,\gamma\,\rho}{4\,a\,b_0}} \tag{2.4}$$

The minimum possible value for ρ is b_0. Therefore for the worst possible defect:

$$\sigma_c = \sqrt{\frac{E\,\gamma}{4\,a}} \tag{2.5}$$

This result was obtained using the Inglis stress concentration equation, based on linear elastic theory, and the theoretical maximum intermolecular force based on non-linear intermolecular force/displacement laws. This is not very satisfactory but it does indicate the dependence of the strength on the size of the flaws as well as the material's Young's modulus and surface energy.

In linear elastic fracture mechanics two different parameters are used to assess the strength of materials containing flaws. These parameters, both being measures of the toughness or resistance to crack growth of the material, are described in the following two sections.

2.2.1.1.2 Energy criterion.

Griffith was able to circumvent the problem of combining linear elasticity with non-linear intermolecular force laws by proposing a thermodynamic criterion for fracture. He suggested that just as in a liquid, a solid possesses a surface tension which is a form of potential energy. In order for a crack to propagate the increase in potential energy required by the formation of new surfaces must be provided by the reduction in the potential of the strain energy and the applied forces (Griffith, 1924).

There was an error in Griffith's mathematical formulation pointed out by Orowan (1948-9) and what follows is a summary of the development of the energy criterion up to 1950.

Integration of the product of stress and strain over the whole of a linear elastic, infinite plate containing a crack, gives the stored strain energy, U. For the case of uniaxial tension the rate of change of stored strain energy with respect to increase in crack length may be shown to be:

$$\frac{\partial U}{\partial a} = -\frac{2\pi a \sigma_0^2}{E} \qquad \text{(plane stress)} \quad (2.6)$$

$$\frac{\partial U}{\partial a} = -\frac{2\pi a \sigma_0^2}{E}(1 - \nu^2) \qquad \text{(plane strain)} \quad (2.7)$$

where a = semi-crack length

σ_0 = tensile stress applied remotely and perpendicular to the crack

E = Young's modulus

ν = Poisson's ratio.

$(\partial U/\partial a)$ is normally termed the strain energy release release rate and is denoted by the symbol, G.

The rate of change of surface energy, S', with increase in crack length is given by:

$$\frac{\partial S'}{\partial a} = 4\gamma \tag{2.8}$$

Griffith's thermodynamic criterion stated that the total stored energy is unchanged with increase of crack length, i.e.

$$\frac{\partial U}{\partial a} + \frac{\partial S'}{\partial a} = 0 \tag{2.9}$$

Therefore, for fracture to occur, the critical applied stress is given by:

$$\sigma_c = \sqrt{\frac{2E\gamma}{\pi a}} \times \alpha \tag{2.10}$$

where α = 1 for plane stress

= $1/\sqrt{(1-\nu^2)}$ for plane strain.

This is shown graphically in Figure 2.2. The critical strain energy release rate, G_c, can then be defined as:

$$G_c = 2\gamma = \frac{\sigma_c^2 \pi a}{E} g \qquad (2.11)$$

Where g is a factor dependent on specimen geometry and loading type. For a central crack of length 2a, in an infinite plate, g = 1 for plane stress, g = $(1-\nu^2)$ for plane strain. It should be noted that this criterion is defined only for the onset of unstable crack growth in brittle materials.

Griffith (1924) extended the basic theory to biaxial stress states and Sack (1946) took it further to the three dimensional case of an infinite solid with an internal penny-shaped crack. When a tensile stress was applied perpendicular to the crack the critical stress was simply $\pi/2$ times that for the uniaxial plane strain case. It is interesting to note the strong similarity between Orowan's (1948-9) plot of Griffith's biaxial failure criterion, Figure 2.3, and the biaxial failure envelope for concrete, Figure 2.4, (Vile, 1968).

The Griffith formulation describes both a necessary and sufficient condition for fracture to occur in brittle materials where the only mechanism for energy absorption is the formation of the new surfaces. It is often used as a reasonable approximation for some materials in which the inelastic region near the crack tip is small compared to the crack and specimen dimensions. For other materials the energy absorbed in plastic deformation, heat generation, sound emission and kinetic effects must also be considered in the energy balance. For such cases an additional term is required in the equation for G_c:

$$G_c = 2(\gamma + \gamma_p) \qquad (2.12)$$

where γ = surface energy per unit area

γ_p = other dissipated energy per unit area.

This result is again limited to situations where the inelastic region

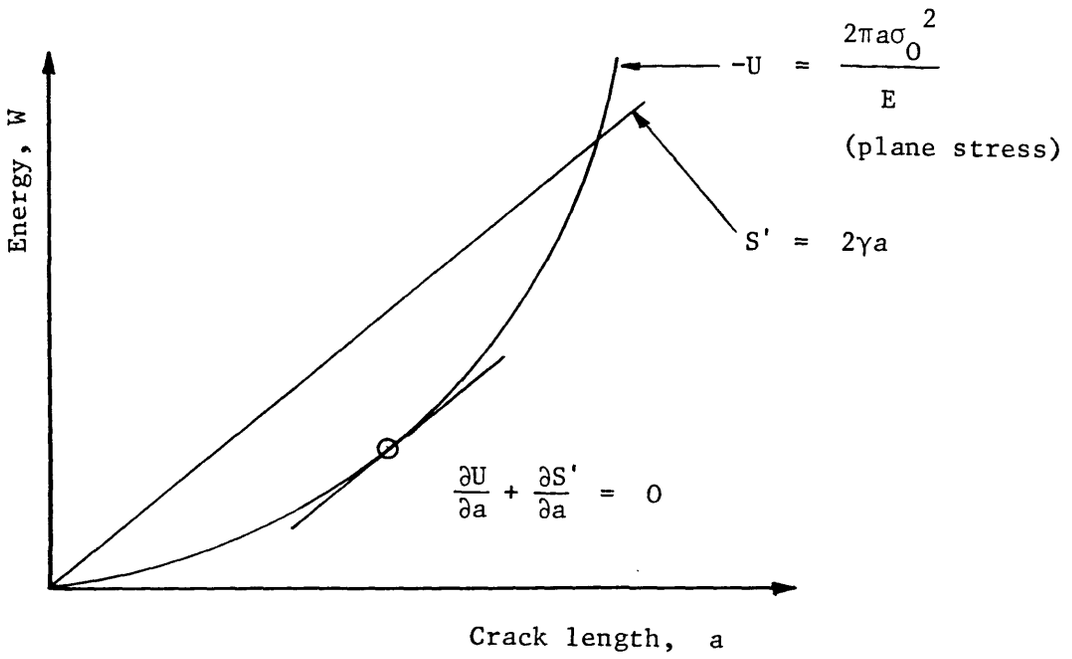

Fig. 2.2 Griffith's thermodynamic fracture criterion

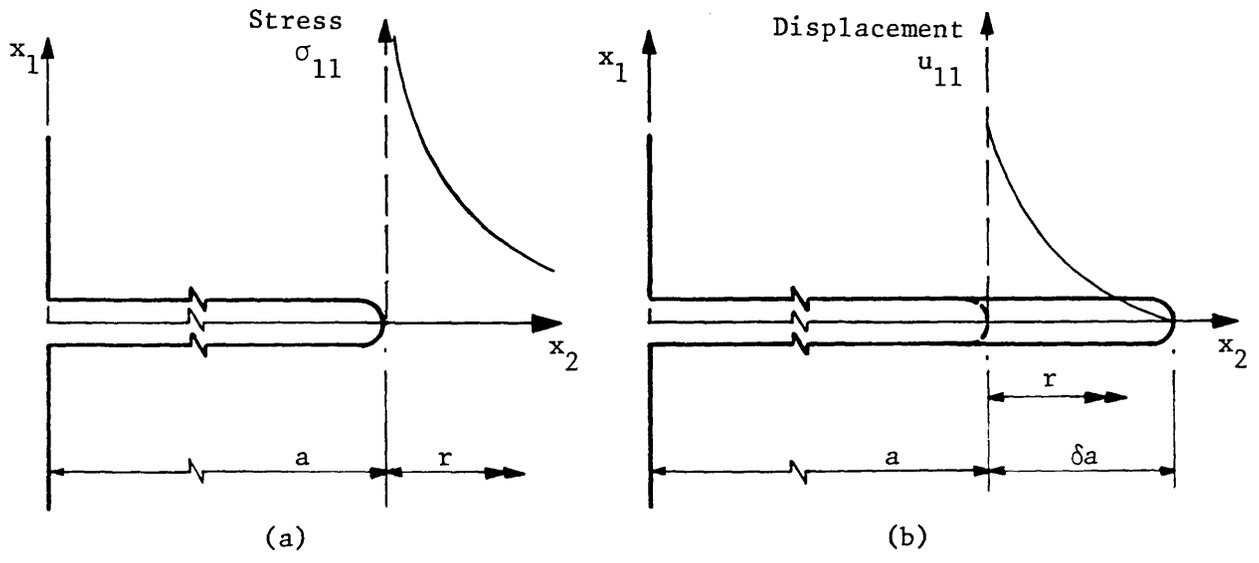

Fig. 2.5 (a) Stress distribution in front of a crack
(b) Displacement distribution during crack extension
(Westgaard, 1939)

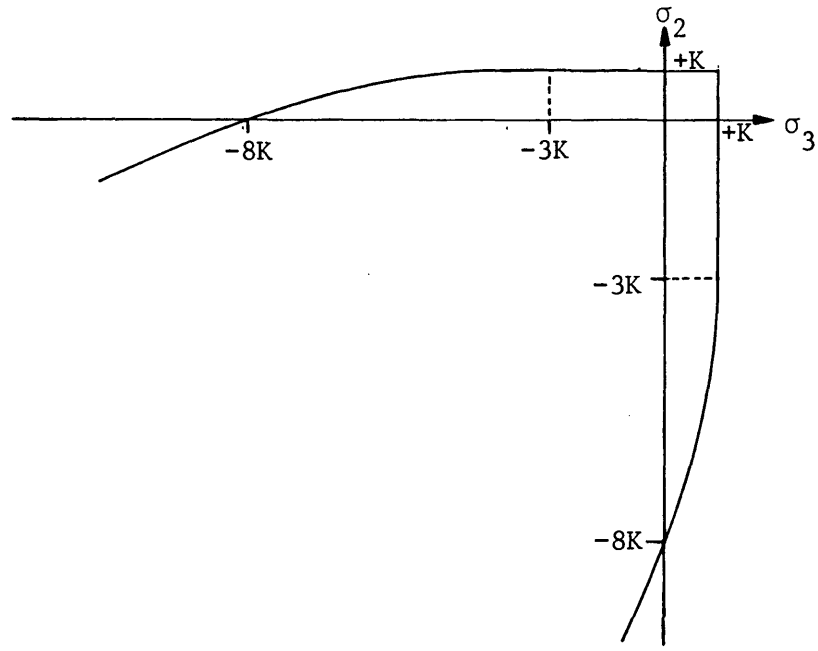

Fig. 2.3 Biaxial fracture criterion of Griffith (Orowan, 1948-9)

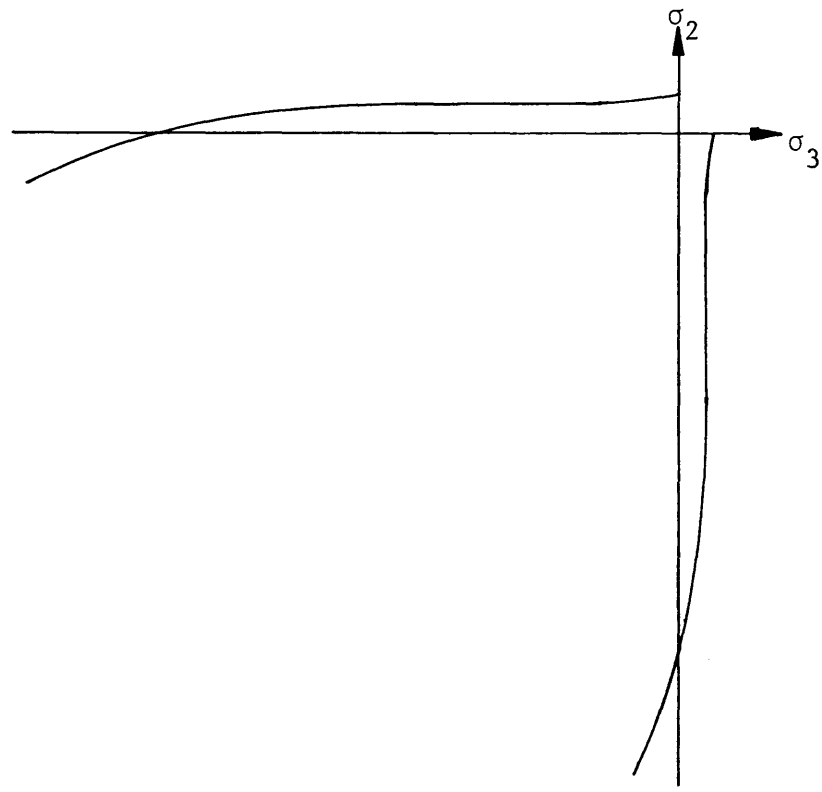

Fig. 2.4 Biaxial failure envelope for concrete (Vile, 1968)

is small.

2.2.1.1.3 Stress intensity criterion

The critical strain energy criterion considers the total change in stored energy in the body during crack propagation. As an alternative the stress intensity criterion concentrates on a crack tip region, which is small compared with the body as a whole, but sufficiently large with respect to molecular dimensions to enable linear elasticity to be assumed.

Westergaard (1939) determined the bearing stresses between imperfectly mating elastic bodies using a function of a complex variable as a stress function. He used the same technique to determine the stress distribution ahead of a crack of length 2a, and the displacement distribution within a crack of length 2x(a + δa) under uniform applied tensile stress (Fig. 2.5). The stress for $x_1 = 0$, with a crack length 2a, is given, for $x_2 > a$, by:

$$\sigma_{11} = \sigma_0 \frac{x_2}{\sqrt{(x_2^2 - a^2)}} \tag{2.13}$$

The crack opening displacement distribution for a crack length 2x(a + δa) under plane strain is given, for $x_2 < (a + \delta a)$, by:

$$u_{11} = 2(1-\nu^2) \frac{\sigma_0}{E} \sqrt{((a + \delta a)^2 - x_2^2)} \tag{2.14}$$

Substituting $r = (x_2 - a)$ and assuming $r <= \delta a$ and $\delta a << a$ we get:

$$\sigma_{11} = \sigma_0 \sqrt{(a/2r)} \tag{2.15}$$

$$u_{11} = 2(1 - \nu^2) \frac{\sigma_0}{E} \sqrt{(2a(\delta a - r))} \tag{2.16}$$

The stress intensity factor, K, for a sharp crack within an infinite plate is defined as:

$$K = \sigma_0 \sqrt{(\pi a)} \tag{2.17}$$

$$\therefore \quad \sigma_{11} = \frac{K}{\sqrt{(2\pi r)}} \tag{2.18}$$

The loss in strain energy of the body as a whole, as the crack propagates a distance δa, is equal to the work done by the surface forces across the length δa when the crack is closed from half-length $(a + \delta a)$ to half-length a, (Irwin, 1957).

The energy change per unit thickness may be expressed as:

$$\begin{aligned} G\,\delta a &= \int_0^{\delta a} \sigma_{11}\, u_{11}\, dr \\ &= \int_0^{\delta a} \left(\frac{K}{\sqrt{(2\pi r)}}\right) \left(2(1 - \nu^2) \frac{\sigma_0}{E} \sqrt{(2a(\delta a - r))}\right) dr \\ &= 2 \frac{K}{E} (1 - \nu^2)\, \sigma_0 \sqrt{(a/\pi)} \int_0^{\delta a} \left(\frac{\delta a - r}{r}\right)^{\frac{1}{2}} dr \end{aligned} \tag{2.19}$$

Substituting $r = \delta a \sin^2\omega$ it follows that, for plane strain:

$$G\,\delta a = 2\frac{K}{E}(1-\nu^2)\,\sigma_0\,\sqrt{(a/\pi)}\,\left(\frac{\pi\delta a}{2}\right)$$

$$= \frac{K^2}{E}(1-\nu^2)\,\delta a$$

$$\therefore \quad G = \frac{K^2}{E}(1-\nu^2) \tag{2.20}$$

Similarly for plane stress it can be shown that:

$$G = \frac{K^2}{E} \tag{2.21}$$

Equations 2.20 and 2.21 can be shown to hold for all specimen and loading geometries. Hence we have an alternative fracture criterion, based on the limiting value of the stress intensity factor and given in general by:

$$K_c = \sigma_c\,\sqrt{(a)}\;x\;f \tag{2.22}$$

Where f is a factor dependent on specimen geometry and loading type. For a central crack of length 2a in an infinite plate, $f = \sqrt{(\pi)}$ for both plane stress and plane strain.

There are some advantages to be gained by using the stress intensity criterion rather than the energy criterion (Swamy, 1979). The main one is that K varies linearly with applied stress and K values are therefore simply algebraically additive. Swamy also suggests that it is more rational to consider stress/strain distributions at crack tips rather than energy balances to determine conditions of fracture.

2.2.1.2 Non-linear fracture mechanics

2.2.1.2.1 Introduction

Except for the introduction of the additional energy term in Equ. 2.12, the effects of plasticity around the crack tip have been ignored in Section 2.2.1.1. Irwin (1957) showed that, provided the radius of the plastic region was small compared with the length of the crack, this assumption was valid. However, with yielding materials this condition may not be satisfied and many modifications have been made to elastic fracture mechanics to cater for the plastic region. Although these were originally devised for yielding materials, subsequent attempts have been made to use some of these techniques to describe the fracture of concrete. The techniques may be broadly subdivided into two groups, those which model the non-linear stress distribution around the crack tip (Section 2.2.1.2.2) and those which modify linear elastic fracture parameters to cater for non-linear effects (Sections 2.2.1.2.3-5).

2.2.1.2.2 The Dugdale model

Dugdale (1960) addressed the problem of stress distribution near the crack tip in an ideal elastic-plastic material. He assumed a constant tensile stress equal to the yield stress acting in a direction perpendicular to the crack, for a distance d_y ahead of a crack of length a (Fig. 2.6). By imposing the condition that the stress at $x_2 = (a + d_y)$ is finite and using Muskhelishvili's solution for stress around a straight crack, he was able to show that:

$$\frac{d_y}{a + d_y} = 2 \sin^2\left(\frac{\pi \sigma_0}{4 \sigma_y}\right)$$

$$\therefore \quad \frac{a}{a + d_y} = \cos\left(\frac{\pi \sigma_0}{2 \sigma_y}\right) \tag{2.23}$$

On using the binomial expansion for the left hand side and the cosine expansion for the right hand side of Equ. 2.23 and limiting the result to low stress levels ($\sigma_0 << \sigma_y$, $d_y << a$):

$$d_y = \frac{\pi^2 \sigma_0^2}{8 \sigma_y^2} \tag{2.24}$$

For high stress levels d_y becomes large and a situation of general yield would be produced for which the Dugdale model is less appropriate.

Barenblatt (1962) also investigated the stresses and strains near the crack tip by considering a crack in equilibrium with the loads applied to the body. He considered the intermolecular cohesive forces across the crack near the tip. When the loads were increased to such an extent that the cohesive forces were fully developed, he produced a formulation similar to that of Griffith (1921,4) but in which the stress at the crack tip was finite. Barenblatt's ideas are often linked with those of Dugdale since both models involve crack closing stresses.

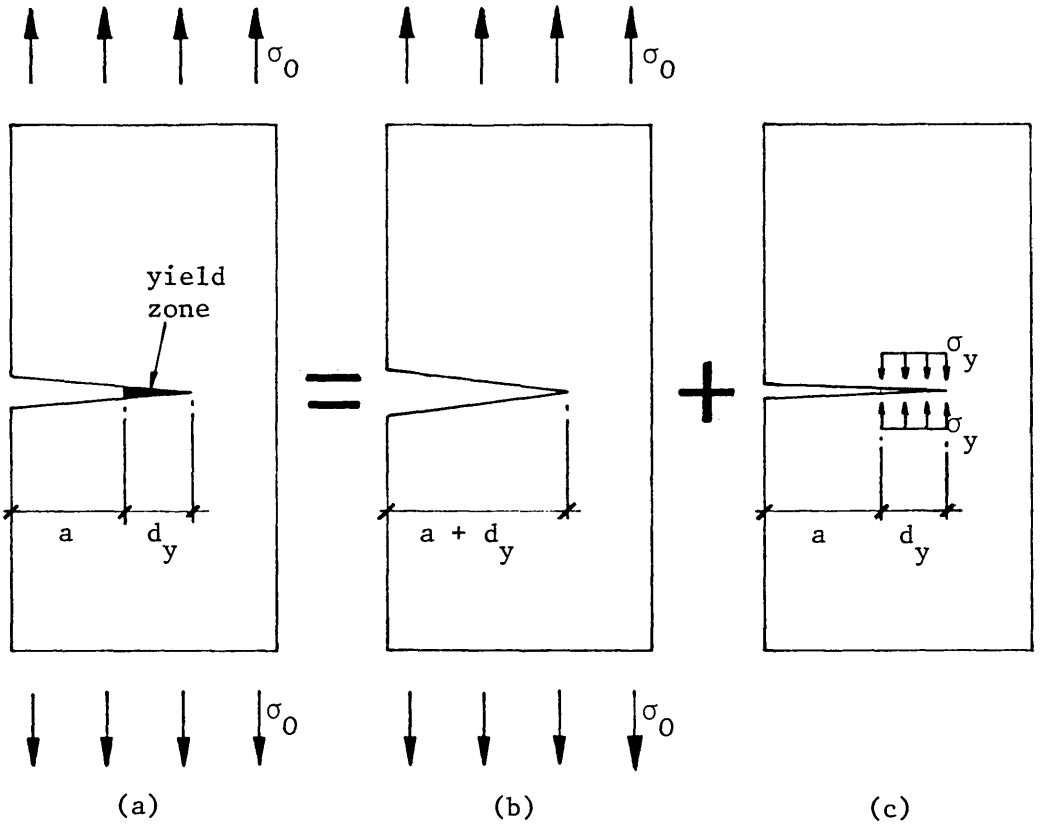

Fig. 2.6 The Dugdale model, loadcase (a) is identical to the sum of loadcases (b) and (c)

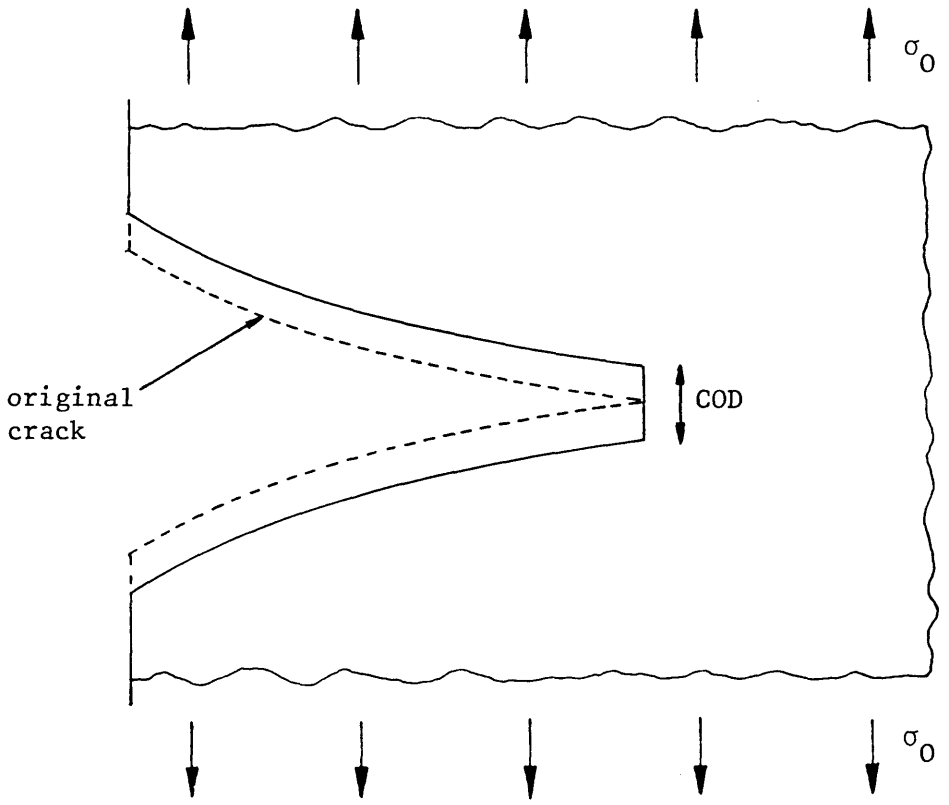

Fig. 2.7 Crack opening displacement, COD represents widening of crack tip

2.2.1.2.3 Crack opening displacement (COD)

Burdekin & Stone (1966), (following Wells, A.A., Crack propagation symposium, College of Aeronautics and the Royal Aeronautical Society, Cranfield, Sept. 1961) also obtained Equ. 2.24 but using as their starting point Westergaard type stress functions (Westergaard, 1939). They then went on to examine the opening of the crack tip at crack initiation (Fig. 2.7). They obtained an expression for the crack opening displacement, COD, given by:

$$COD = \frac{8\,\sigma_y}{\pi\,E}\,a\,\ln\left(\sec\left(\frac{\pi\,\sigma_0}{2\,\sigma_y}\right)\right) \qquad (2.25)$$

For low stresses this becomes:

$$COD = \frac{\sigma_0^{\,2}\,\pi\,a}{\sigma_y\,E} \qquad (2.26)$$

Assuming that the size of the plastic zone is not influential, COD may be related to the strain energy release rate, G, and the stress intensity factor, K, by:

$$COD = \frac{G}{\sigma_y} \qquad (2.27)$$

$$COD = \frac{K^2}{\sigma_y\,E} \qquad (2.28)$$

It should be noted that this calculation assumes plane stress but a similar calculation could be made for plane strain.

Burdekin & Stone assumed that at some critical value of the crack opening, COD_c, the crack was initiated. It has been shown that for some materials the value of COD_c is independent of specimen size provided that the notch width and depth remain constant. It is a

difficult experimental problem to measure COD_c, and it should be remembered that COD_c corresponds to crack initiation and not failure.

2.2.1.2.4 The J-Integral approach

An alternative method for assessing the toughness, or resistance to crack extension, of a cracked body which cannot be regarded as linear elastic, was proposed by Rice (1968). It relies on the determination of an energy term, which expresses the change in potential energy, when an existing crack is extended by an amount da. It is analogous to the strain energy release rate, G, in linear elastic fracture mechanics.

The line integral, J, on a curve, Γ, surrounding the notch tip (Fig. 2.8) is defined by:

$$J = \int_{\Gamma} \left(W \, dx_1 - T_i \frac{\partial u_i}{\partial x_2} \right) ds \qquad (2.29)$$

Where s = the arc length along the curve traversed in the anticlockwise direction

$\underline{T}$ = the traction vector on Γ according to an outward normal unit vector $\underline{n}$ (direction cosines, n_j), $T_i = \sigma_{ij} . n_j$

W = the strain energy density function,

$$= \int_0^{\varepsilon_{mn}} \sigma_{ij} \, d\varepsilon_{mn}$$

$\underline{u}$ = the displacement vector.

Rice showed that the value of J is independent of path, Γ, by considering 2 paths Γ_1 and Γ_2 (Fig. 2.9). The integral was carried out along Γ_1 anticlockwise and along Γ_2 clockwise, thus integrating around a closed loop. Since the crack faces are parallel to x_2, the value of J along the crack faces is zero. The total integration around a closed loop must be zero, therefore the integrals along Γ_1 and Γ_2 are equal

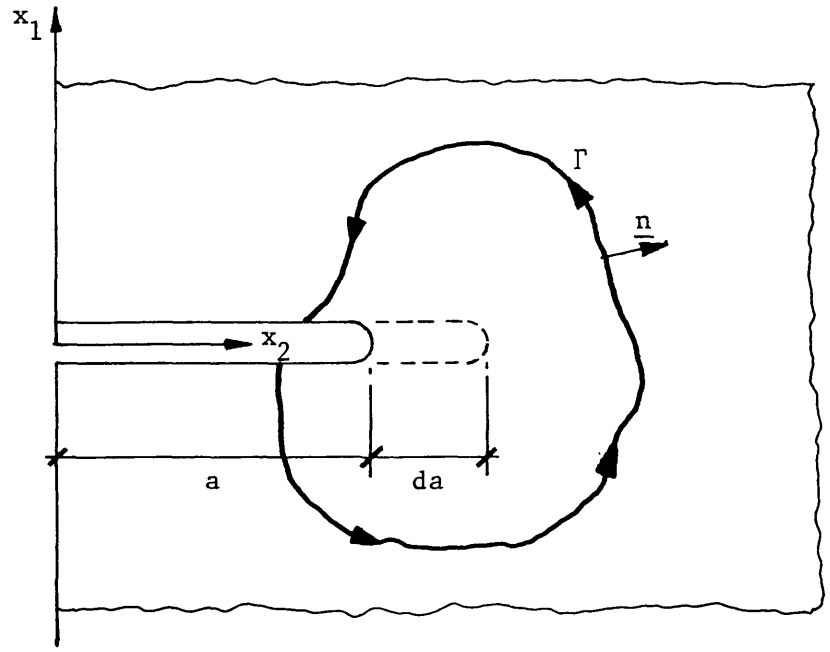

Fig. 2.8 The Γ-contour along which the J-Integral is evaluated

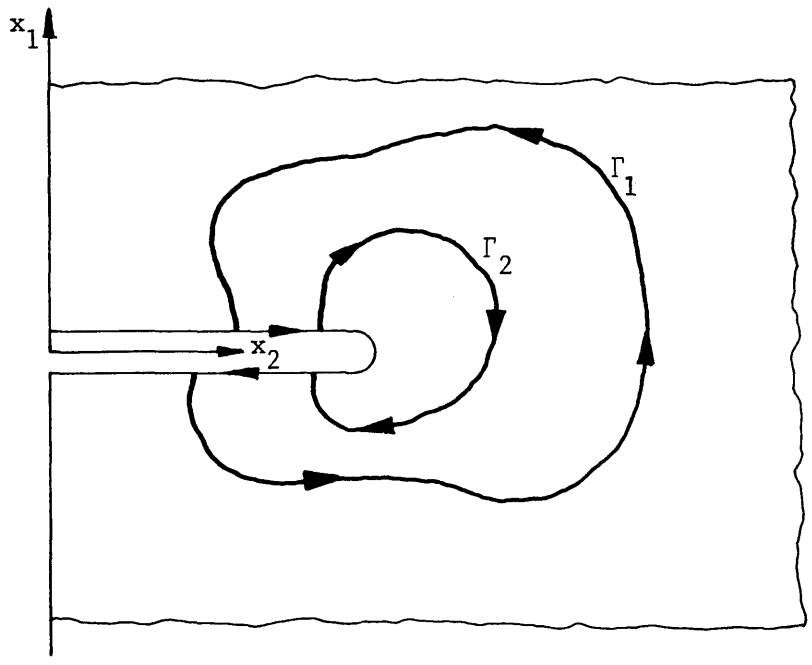

Fig. 2.9 Layout for the proof of path independence of J-Integral

and opposite. Hence J is path independent.

For small scale yielding (plastic zone small compared with specimen geometry), it can be shown that, for plane strain:

$$J = G = \frac{K^2}{E}(1 - \nu^2) \qquad (2.30)$$

It would seem reasonable, therefore, that there exists a critical value of J, J_c, which can represent a characteristic failure criterion. The results of some tests on an alloy steel, reported by Knott (1973), support the proposition that J might be a suitable failure criterion in situations where fracture is preceeded by significant amounts of yeilding. Although the J-Integral approach is now widely used, more needs to be done before this proposition can be fully accepted. One problem is that the theory requires the existance of the strain energy density function, W, and is strictly applicable to a non-linear elastic material rather than a real yielding material. The theory still applies for real materials provided that no unloading occurs. It is not yet clear how severe this limitation will prove to be.

2.2.1.2.5 Resistance curves

The thickness of sheet metal has a significant effect on it's fracture toughness. This is explained by the fact that there are two modes of failure in sheet metals corresponding to plane stress and plane strain (Knott, 1973). In thin plates the through the plate stress is negligible leaving the plate in a state of plane stress. Failure occurs by the antiplane strain (K_{III}) mechanism resulting in a 45 degree slant fracture surface (Fig. 2.10). In contrast to this, the central section of thick plates can be considered to be under plane strain and failure occurs by a cleavage (K_I) mechanism. This gives a square fracture surface with a small amount of slant fracture ('shear lips') at the edges (Fig. 2.11).

There is, however, a range between the two limiting cases above, in which the plane strain and plane stress regions make similar contributions. As the load is increased on a specimen in this intermediate range, square fracture begins to develop in the centre of the specimen but the side ligaments continue to carry load. The square fracture tunnels ahead into the specimen and may exibit a sudden 'pop-in'. Under increased load, the side ligaments begin to fracture and the crack extends with the square fracture tunneling ahead dragging the shear lips with it. As the crack extends, the size of the plastic zone in front of it increases which allows a relaxation of the through the plate stress. This results in more of the plate being under plane stress and the proportion of slant fracture to square fracture increases. This may continue until the square fracture disappears completely (Fig. 2.12). The fracture toughness increases with the increased proportion of slant fracture.

Knott following Krafft, J.M., Sullivan, A.M. and Boyle, R.W. (Proc. Symp. Crack Propagation, Cranfield (1961)), obtained "Resistance curves" by plotting crack growth resistance or strain energy release rate against absolute crack extension. These curves are, however, of limited use as they depend on the thickness of the specimen.

The concept of "Resistance curves" has been applied to the fracture of concrete although the failure mechanisms are different. This is discussed further in Section 2.2.2.3.5.

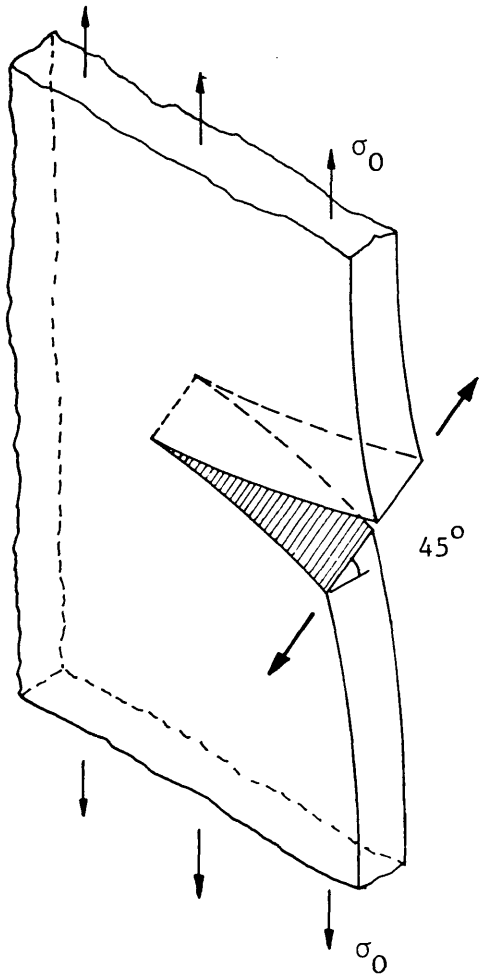

Fig. 2.10 45° slant fracture

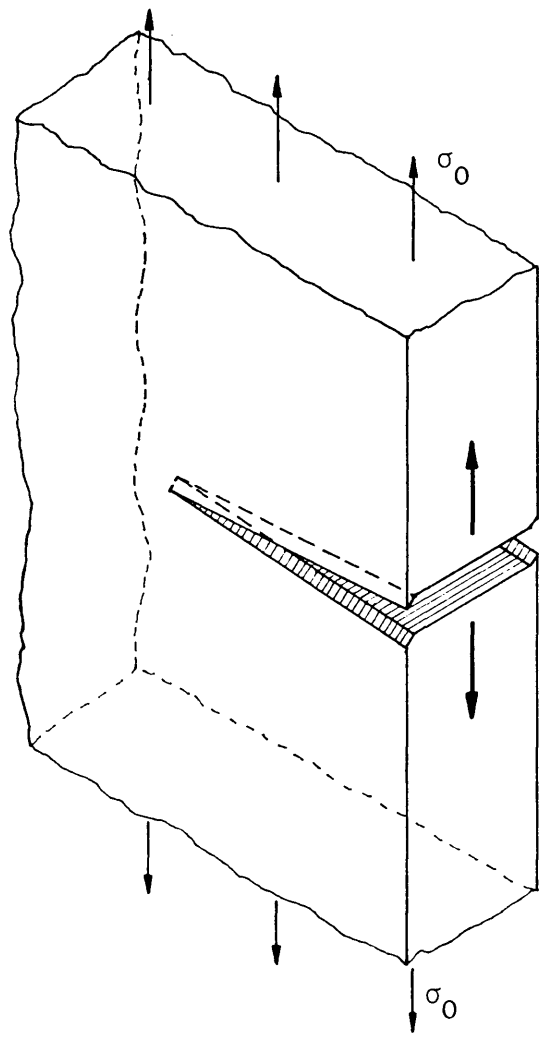

Fig. 2.11 Square fracture with shear lips

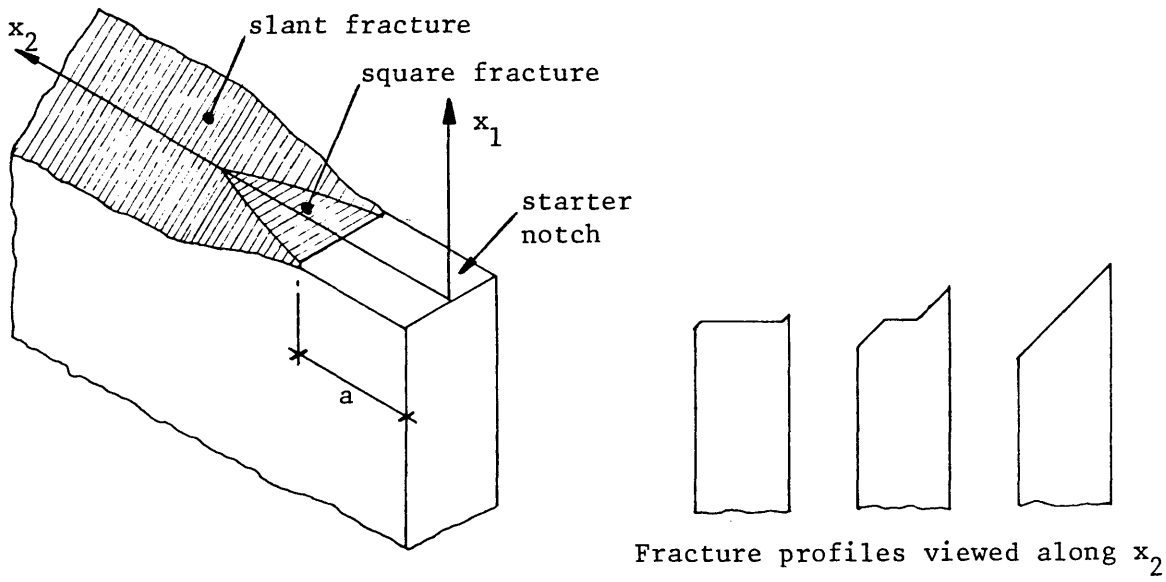

Fig. 2.12 Fracture in intermediate range

2.2.2 Fracture mechanics applied to concrete

2.2.2.1 Introduction

The fracture of concrete is characterised by the propagation of cracks. It was a logical development, therefore, when Kaplan (1961) started to study the fracture process of concrete by means of fracture mechanics. Linear elastic fracture mechanics, which Kaplan employed, is only applicable when the non-linear zone around the crack tip is small compared with the specimen dimensions. In concrete, the size of the fracture process zone is thought to be relatively large and related to the maximum aggregate size (Bazant & Cedolin, 1980), although there is, as yet, no direct experimental evidence to support these suggestions. It is, therefore, questionable whether or not linear elastic fracture mechanics is a useful tool for the analysis of fracture in concrete. Some of the linear and non-linear fracture mechanics methods originally developed for metals, which have also been applied to concrete, are discussed below.

2.2.2.2 Linear elastic fracture mechanics applied to concrete

2.2.2.2.1 Introduction

Table 2.1 gives details of some of the research over the last 25 years which has investigated the application of fracture mechanics to cement paste, mortar and concrete. It can be seen from the Table that many different types of tests have been conducted on specimens of differing geometry and size.

Kaplan (1961) obtained values for the critical strain energy release rate, G_c, in two ways. The first technique employed the analytical relationship between the stress at the notch tip and G_c, the second

Author	Year	Material	Test	Parameter	Dimensions (mm)	a (mm)	Comments
Kaplan	1961	M,C	3PB 4PB	G_c	76.2x101.6x406.4 152.4x152.4x508	0-38.1 0-76.2	
Hughes & Chapman	1966a&b	C	T	S/S	101.6x101.6x508	None	Neck: 63.5x63.5, Stable
Evans & Marathe	1968	C	T	S/S	Not given	None	Necked specimen
Heilmann, Hilsdorf & Finsterwalder	1969	C	T,ET	f_t,S/S	150x150x600	None	Neck: 90x150mm
Moavenzadeh & Kuguel	1969	P,M,C	3PB	G_c,K_c,G_f	25.4x25.4x304.8	10.2	
Naus & Lott	1969	P,M C	4PB 4PB	K_c K_c	50.8x50.8x355.6 101.6x101.6x304.8	6.35-25.4 12.7-38.1	
Welch & Haisman	1969	P,M,C	*	G_c,K_c	*	*	Bend test
Shah & McGarry	1971	P,M,C P,M,C	3PB T	NS NS	50.8x50.8x558.8 25.4x76.2x304.8	0-25.4 2.54-2.54	Notches, Central cracks
Brown; Brown & Pomeroy	1972,3; 1973	P,M,FRP P,M	4PB TWDCB	K_c K_c	38x38x250 50x100x350	5-20 75	
Cooper & Figg	1972	P	3PB	G_f	10x10x30 25x50x80	-	Special bend specimen, triangular ligament
Kesler, Naus & Lott	1972	C	T	K_c	50.8x304.8xb	2a/b= 0.1-0.5	Central cracked plate b=457.2-914.4

Table 2.1 Concrete fracture testing

Author	Year	Material	Test	Parameter	Dimensions (mm)	a (mm)	Comments
Walsh	1972,6	C	3PB	MR,K_c	bx1.5dx4d bxdx2d	d/2 d/2	d=50.8-254mm Re-entrant corners b=40-100, d=50-800
Carmicheal & Jerram	1973	M	CT	K_c	25 thick	*	
Higgins & Bailey	1976	P,M	3PB T	K_c K_c	25xdx5d bx50x150 bx25x75 bx50x75	0-10 10 5 2	d=5-110mm Double notched Double notched Neck: bx10, & notched
Mindess & Nadeau	1976	M,C	3PB	K_c	bx50.8x203.2	25.4	b=45-254mm
Gjorv, Sorensen & Arnesen	1977	P,M,C	3PB	K_c	50x50x550	0-25	
Hillemeier & Hilsdorf	1977	P,Bond	CT	K_c	40x100x105	15-60	
Mindess, Lawrence & Kesler	1977	P,M,FRC	4PB	G_c,K_c,J	76.2x76.2x381	0-50.8	
Cook & Crookham	1978	C	3PB	K_c	100x100x500	13.5	
Swartz, Hu & Jones	1978	C	3PB	K_c	76.2x101.6x406.4	10.2-81.3	
Strange & Bryant	1979	P,M,C	3PB	K_c	6x12x60- 100x200x1000	*	
		P,M,C	T	f_t,K_c	*	*	
Terrien	1980	M,C	T	S/S	36(diam)x140	None	Acoustic emission

Table 2.1 Concrete fracture testing (cont.)

Author	Year	Material	Test	Parameter	Dimensions (mm)	a (mm)	Comments
Kim, Ko & Gerstle	1980	M	3PB	K_c	76.2x76.2x292.1 76.2x38.1x292.1	30.5-46.5 1.5-26.2	
Mindess & Diamond	1980	M	CT	CL	12.7x23.9x31.8	12.7	Scanning Electron Microscope
Petersson	1980a&b	C	TPB	G_c,G_f	50x50x650	25	
	1981a&b	M,C	3PB	G_c,G_f	50x50x320- 50x200x2000	d/2	
			T	f_t	50x50x320	None	
			T	G_f,S/S	30x50x50		Neck or notched, 20x50
Velazco, Visalvanich & Shah	1980	FRM	4PB	K_c,J K_r,COD	38x76x457	0-57	
Visalvanich & Naamen	1980	M,FRM, AC	TDCB	G_c,K_c	50.8x304.8x584.2	101.6	
Wecharatana & Shah	1980a&b	M,C,FRM	TDCB	G_r	50.8x304.8x609.6	101.6	
	1982,3		DT	K_c,G_r	38.1x152.4x812.8	None	
Ziegeldorf, Muller & Hilsdorf	1980	P,M,C	4PB	NS	40x40x160 100x150x700	d/10	
Cedolin, Dei Poli & Iori	1981,3	C	T	-	40x70x200 approx	0-23	Some specimens necked Full field strain

Table 2.1 Concrete fracture testing (cont.)

Author	Year	Material	Test	Parameter	Dimensions (mm)	a (mm)	Comments
Cho, Kobayashi, Hawkins, Barker & Jeang; Barker et al	1984;5	C	DCB	CL,COD	50.8x381x457.2 76.2x571.5x685.8	113.4 200.2	
Go & Swartz	1984	C	3PB	COD	*		a/d=0.2-0.8 1/d=3.75-4.0
Gopalaratram & Shah	1984,5	P,M,C	T	G_c,G_f, S/S,COD	19.1x76.2x304.8 38.1x76.2x304.8	0-12.5	
Gylltoft	1984	C	4PB	G_f	120x200x1000	40	Cylic loading
Legendre & Mazars	1984	C	3PB CT	G_c	*x100x300 100x600x750	*	
Mindess	1984	C	3PB	K_c,G_f	100x100x840- 400x400x3360	d/2	
Reinhardt; Cornelissen, Hordijk & Reinhardt	1984,5; 1985a&b	C	T	G_f,S/S	50x50x250 50x180x250	5	Stable, cyclic loading Double notched
Barr & Sabir	1985	C	CC	K_c	100x150 cubes 100x100x125 100x100x150	20-45	Double notched specimen
Eligehausen & Sawade	1985	C	3PB T	K_c,G_c,G_f G_f,S/S	150x300x1200 120x180x600	40-65 10	Neck: 120x120mm.

Table 2.1 Concrete fracture testing (cont.)

Author	Year	Material	Test	Parameter	Dimensions (mm)	a (mm)	Comments
Nallathambi, Karihaloo & Heaton	1985	M,C	3PB	G_c,G_f	40x51x200- 80x152x600	2-20	
Rossi, Acker & Francois	1985	C	DCB	K_c	300x1100x3500	715	
Wittmann & Metzener-Gheorghita	1985	C	DT TWDCB TDCB NR	K_c K_c K_c K_c	150x500x1000 400x700x1440 150x1040x1150 600o.d., 300i.d. 200 thick	None * * 50	

Table 2.1 Concrete fracture testing (cont.)

Nomenclature:

P = Cement paste
M = Mortar
C = Concrete
FRP = Fibre reinforced cement paste
FRM = Fibre reinforced mortar
FRC = Fibre reinforced concrete
AC = Asbestos cement
Bond = Mortar/aggregate bond
a = Notch/crack depth
b = Width
d = Depth
l = Length
* = Not given

3PB = 3 point bending
4PB = 4 point bending
T = Direct tension
DCB = Double cantilever beam
TWDCB = Tapered web DCB
TDCB = Tapered DCB
CT = Compact tension
CC = Compact compression
DT = Double torsion beam
NR = Notched ring
ET = Eccentric tension
NS = Notch sensitivity
MR = Modulus of rupture

G_c = Critical strain energy release rate
K_c = Critical stress intensity factor
f_t = Tensile strength
G_f = Fracture energy
G_r = Resistance curve for G_c
K_r = Resistance curve for K_c
J = J-Integral
COD = Crack opening displacement
CL = Crack length
S/S = Complete stress/strain or load/extension curve

Table 2.1 Concrete fracture testing (cont.)

was a compliance technique which made use of the relationship between G_c and the rate of change of beam flexibility with respect to notch depth. The values he obtained for G_c did not vary significantly with notch depth but the smaller beams gave consistantly lower results. The value of G_c also depended on the type of loading and the analysis technique used. It should be noted that in this analysis the length of the crack is assumed to be the depth of the notch and growth of the crack prior to maximum load was not taken into account. Kaplan concluded that slow crack growth was significant but that linear elastic fracture mechanics should still be applicable to fracture in concrete.

2.2.2.2.2 Slow crack growth

Glucklich (1963; Glucklich & Cohen, 1967) discussed the mechanisms which allowed slow crack growth to occur. He examined the energy dissipation at the crack tip in concrete and postulated the existance of a "highly stressed zone in the form of a multitude of microcracks". The energy required for fracture was, unlike metals, still largely surface energy but the surface area created by crack propagation might be ten times larger than the effective fracture area. He suggested that the size of the highly stressed zone would increase with the propagation of the fracture and that as a result the energy requirement for frature would no longer be the straight line predicted by Griffith theory (as shown in Figure 2.2) but rather, a curve with increasing gradient (Fig. 2.13). He also suggested that the energy demand would increase when the crack encounted a "crack arrester". He suggested that crack arrest might occur after a crack had developed around an aggregate particle. The energy demand for continued propagation of the crack through the matrix was greater than that required to break down the aggregate/matrix bond. The crack would be arrested at this point until the energy available had risen sufficiently to allow propagation through the matrix. An initial crack of length, a_0, would begin to grow under a stress, σ_0, but would be checked at a_1, because of the increase in energy demand. If the stress was increased to σ_1 the crack would grow again to a_2. This would

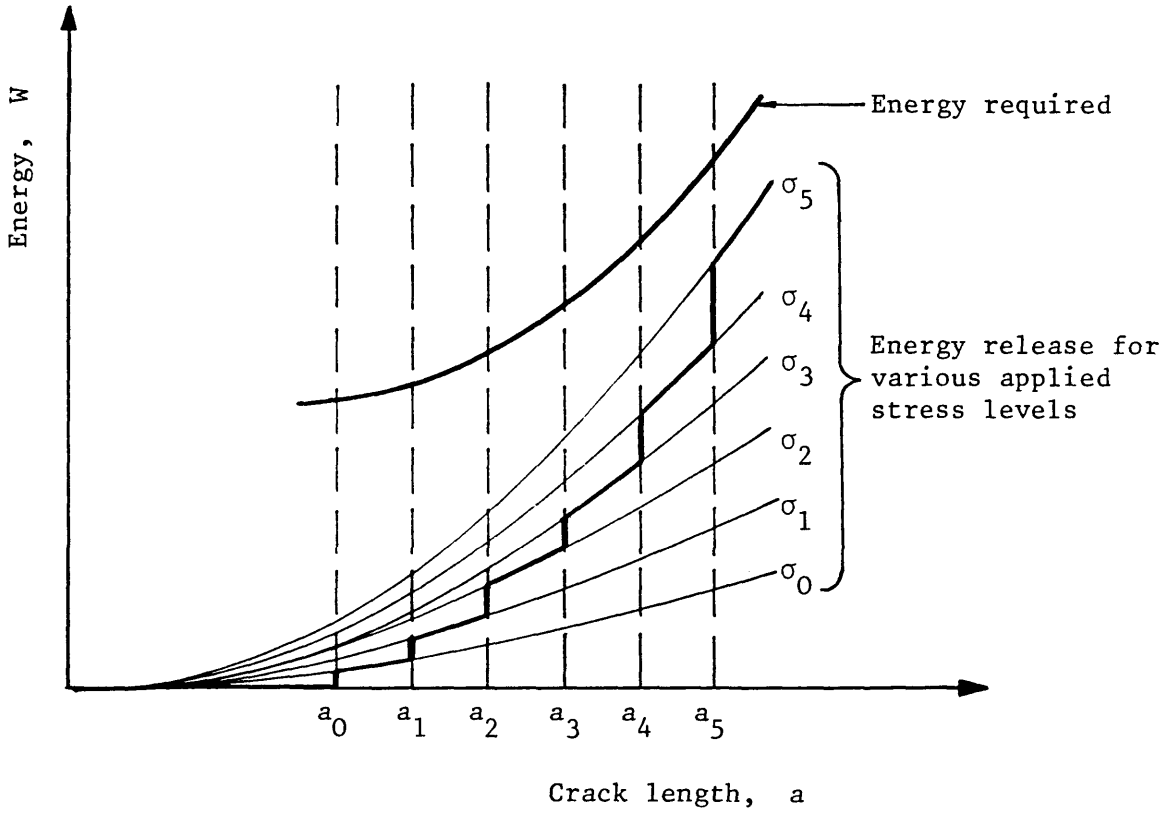

Fig. 2.13 Glucklich's postulated mechanism for slow crack growth

continue to crack length a_5 when the crack would grow spontaneously. Glucklick assumed that the value of G at the onset of instability was a material property and should be designated G_c. Figure 2.13 suggests a step-wise increase in the energy requirement, however, if it is remembered that the highly stressed zone has a finite volume, then the 'steps' will be averaged throughout the volume leading to a smooth increase.

The first detailed observation of the microcracking of concrete which precedes the formation of a macrocrack was made by Isenberg (1966) using X - radiography. He showed that the interface between mortar and aggregate was the major source for microcracks. These developed further by bridging between the aggregate particles. Contrary to Glucklich he said that the energy demand increased when the crack encountered an aggregate particle due to crack blunting rather than when it had propagated around the aggregate. Mindess & Diamond (1980) used a scanning electron microscope to photograph the cracking process in mortar specimens. The observed cracking process was complicated with energy dissipation by multiple and branch cracking. The cracks developed preferentially along interfaces between sand and paste but not only there.

Naus & Lott (1969) acknowledged the existance of slow crack growth but were unable to measure it. They used Brown & Srawley's (1966) equation for the stress intensity factor, (which assumed a homogeneous material with no slow crack growth) and called the results the "effective fracture toughness", K'_c. They showed that K'_c did not vary with notch depth (in agreement with Kaplan) but did depend on mix proportions and the age of the concrete. Welsh & Haisman (1969) noted a similar dependence of fracture parameters on mix proportions, however, they also stated that the values obtained for G_c and K_c are very dependent on the assumed crack length. They describe a compliance technique for the measurement of true crack length at failure in which the specimen compliance at failure was compared with a graph of the compliances of beams with varying notch depth. They concluded that linear elastic fracture mechanics should be applicable to concrete provided the true crack length was used.

In an interesting discussion of Gjorv, Sorensen & Arnesen (1977), Cook

& Crookham (1978) show the importance of a correct measurement of slow crack growth. They compared the failure of notched and un-notched concrete beams. If slow crack growth is ignored linear elastic fracture mechanics cannot be applied to un-notched beams, however, they used a compliance technique to obtain the crack length at maximum load. The ultimate stress carried by the notched beam was 72% of that carried by the un-notched beam and the crack lengths were 25.1mm and 15.2mm respectively. From the theory of linear elastic fracture mechanics the ultimate stress is inversely proportional to the square root of the crack length. In this case the ultimate stress ratio predicted would be 78%. They used this reasonable correlation to concluded that linear elastic fracture mechanics is applicable to concrete. Whilst this might be over optimistic it should be noted that a variation in K (calculated from notch depth rather than true crack length) with notch depth does not invalidate the applicability of linear elastic fracture mechanics to concrete.

2.2.2.2.3 Notch sensitivity

One necessary condition for the application of linear elastic fracture mechanics is the requirement that the material is notch sensitive (Ziegeldorf, Muller & Hilsdorf, 1980), ie. the presence of a notch reduces the tensile or flexural strength beyond that caused by a mere reduction of the cross-sectional area. Shah & McGarry (1971) found that paste was very notch sensitive whereas mortar and concrete were notch insensitive, at least for notches of up to a few inches in length. It followed that, in linear elastic fracture mechanics theory, the critical crack length in concrete would have been at least a few inches. They also demonstrated a dependence of the measured fracture energy on the notch length. They attributed the significant difference between paste and mortar or concrete to the crack arrest mechanics resulting from the presence of aggregate. Gjorv, Sorensen & Arnesen (1977) commented on Shah & McGarry's paper and showed that horizontal restraint at the supports of their beams had masked some of the results. In their tests mortar and concrete were also shown to be notch sensitive but not as sensitive as paste. The test results of

Strange & Bryant (1979) led to the same conclusion regarding notch sensitivity.

2.2.2.2.4 Analytical techniques

Until 1978 the majority of results for K_c were based on Brown & Srawley's (1966) analytical equation for the stress intensity factor for a notched beam. However, this is only an approximation and Swartz, Hu & Jones (1978) performed a finite element analysis of their beams leading to a reduction in the variability of the results. There followed a modified elastic analysis by Go, Swartz & Hu (1984) which gave similar results to those of the finite element method. They demonstrated that the Brown & Srawley formula was reasonable for low span/depth ratios but was significantly in error for a span/depth ratio of 8. Two new analytical formulae for K were obtained by Somayarji (1980) by differentiating the elastic expression for the strain energy with respect to notch length and using the relationship between G, the strain energy release rate and K. The first formula was based on the compliance of a prismatic beam of depth equal to the ligament of the notched beam, whilst the elastic compliance of a beam with a triangular notch was used for the second formula. The two formulae yielded upper and lower bounds of the value of K. The upper bound formula was shown to reduce the scatter of some of the tests reported in the literature. Somayarji's work emphasises the importance of a correct analysis of the specimen geometry when calculating values of K.

2.2.2.2.5 Specimen size

Walsh (1972,6) proposed a double failure criterion for concrete; Linear stress distribution from the notch tip with failure at the modulus of rupture for small specimens (notch insensitive) and linear elastic fracture mechanics for larger specimens. He suggested that the previous fracture mechanics testing of concrete had been conducted on specimens which were too small and that the results were consequently misleading. He suggested a minimum depth for a notched beam test of 230mm. for linear fracture mechanics to apply. It should be noted that Walsh did not take into account slow crack growth.

Kesler, Naus & Lott (1972) conducted tests on centrally flawed plates loaded at the flaw in tension. They showed a dependence of K_c on specimen geometry even if some slow crack growth was allowed for. They concluded that although concrete displayed some notch sensitivity, linear elastic fracture mechanics was not applicable to the specimen geometry used and therefore it's usefulness is questionable. As an alternative they suggested a "rigid plastic cracked strip model" which allowed for a non-linear zone at the crack tip. The model is discussed more fully in Section 2.4.1. Higgins & Bailey (1976) also reached the conclusion that K_c varied with specimen size for cement paste and that linear elastic fracture mechanics could not therefore be applied to laboratory sized specimens. They stated that cement paste was relatively notch insensitive; however, the comparision was with glass and cannot on it's own be considered to be very useful.

Saouma, Ingraffea & Catalano (1982) re-examined the results obtained by Kesler et al. using a finite element technique rather than the analytical approximation of the original authors for the calculation of K. When slow crack growth is allowed for the values obtained for K_c are sensibly constant and they concluded that linear elastic fracture mechanics is applicable. In further analysis of Kesler et al.'s results, Bazant & Oh (1983) and Gustafsson (1985) showed that linear elastic and non-linear fracture mechanics were both capable of reproducing the maximum experimental loads with reasonable accuracy. The differences related to the strains obtained ahead of the crack, which the non-linear analyses were able to predict much more

accuratly. Bazant & Oh suggested that the reason why the maximum loads agreed so well, was that the crack extension at maximum load for the type of specimen used, was small. They concluded that, in general, for concrete and mortar, non-linear fracture mechanics techniques should be used unless the specimen was very large.

An analysis of all the reported test series since 1979, in which size effects have been studied, shows that with the exception of the tests of Gopalaratnam & Shah (1985) the value of G_c or K_c increases with specimen size. The level of this increase varies between 50% for a change in beam size from 25x38x188mm. to 100x200x1000mm. (Strange & Bryant, 1979) and 100% for a change in beam size from 80x76x600mm. to 80x152x600mm. (Nallathambi, Karihaloo & Heaton, 1985). Gopalaratnam & Shah's tests showed no change in G_c for a doubling of their tensile specimen width but the specimen minimum dimension was only 1.9 times the maximum aggregate size which calls into question the validity of the results. However, the increases reported are not altogether consistant. For example, Mindess (1984) found the same value of K_c for 100mm. and 200mm. deep beams but an increase of 50% with a change to 400mm. beam depth.

Higgins & Bailey (1976) and Petersson (1980a&b) suggested that as specimen size increased, K_c would tend to a contant value. This could then be considered as the true fracture toughness and would be a material property. This supports Walsh's (1972) suggestion that the minimum depth of a notched concrete beam for linear elastic fracture mechanics testing to apply was 230mm. Several researchers have used specimens which allow for a large crack growth in order to obtain this constant value for K_c. Visalvanich & Naamen (1980) used tapered double cantilever mortar beams which allowed valid crack lengths of up to 16ins. and concluded that K_c could be predicted analytically provided that the specimen was large enough to accommodate crack growths greater than about 8ins.. Wittmann & Metzener-Gheorghita (1985) tested fairly large specimens of various types (see Table 2.1) and obtained similar results for K_c from each type of test. Very large, axially prestressed double cantilever beams were used by Rossi, Acker & Francois (1985) and K_c was approximately constant for crack lengths greater than 0.67m. Since these double cantilever beams were not tapered it was necessary to know the crack length to calculate K_c.

This was obtained by a compliance technique. It should be noted that the observed crack was always longer than the calculated effective crack, sometimes by as much as 0.20m. The extra length of the visible crack was attributed both to three dimensional surface stress concentration and to surface shrinkage cracking. The other possibility, not mentioned by the authors, is that the crack might still be able to transmit significant stresses even when it was visible.

2.2.2.2.6 Variation in fracture parameters with crack propagation

Brown (1972,3; Brown & Pomeroy 1973) used a similar compliance technique to that used by Welch & Haisman (1969) on notched beams to determine the variation in the value of K_c as the crack progressed. He also conducted double cantilever beams tests with varying web width to the same end. The advantage of this test is that the analytical value of K is independent of crack length and therefore the crack length need not be measured. He showed for the notched beams that there was little change in K_c with crack growth in paste but that in mortar K_c increases with crack growth of up to 7mm.. Beyond this the results are not clear. Similar results were obtained from the double cantilever beams except that the crack growth could be monitored up to 100mm.. Finer aggregate appeared to give a greater increase in K_c as the crack proceded. He also noted that the value of K_c for initation of the fracture was less than that required for propagation. Similar results were obtained for notched, glass-fibre reinforced cement beams as for the mortar beams.

In contrast Hillemeier & Hilsdorf (1977), using wedge-loaded compact tension paste specimens, found that K_c reduced with an increase in crack length and stabilised at a value which was repeatable in several tests. They attributed this reduction to a reduction in the size of the fracture zone at peak load (at which crack initiation was assumed to occur) towards a single crack. This contradicts Glucklich's (1963) suggestion that the fracture zone would increase in size with fracture propagation leading to an increasing K_c. Carpinteri (1985a&b)

suggested that the relationship between K_c and relative crack length should be bell-shaped, ie. that it should initially rise, reaching a plateau before falling off at sufficiently large cracks. He related this shape, not to the size of the fracture zone but to a transition in the mode of failure from 'collapse at ultimate strength' to 'crack propagation collapse' and then back again for large cracks. This is similar to Walsh's (1972,6) double failure criterion.

2.2.2.2.7 Comments

It can be seen from the above review, that the existance of valid linear elastic fracture mechanics parameters for paste, mortar and concrete is by no means certain. The results are generally dependent on specimen size and require careful analysis and measurement of slow crack growth. Walsh's (1972) double failure criterion of strength and linear elastic fracture mechanics dependent on specimen size has been extended by Bazant (1984a) to include a third non linear fracture mechanics criterion. Bazant performed a dimensional analysis of the three criteria which showed their different size dependent characteristics as shown in Figure 2.14. He reanalysed Walsh's data which gave support to the general shape of the non-linear fracture mechanics curve in the figure and claimed that the majority of other tests had been performed on specimens which were not suitable for the evaluation of the usefulness of linear elastic fracture mechanics. He suggested that the size of the fracture process zone could not be considered to be small compared with the sizes of the specimens. This contravenes one of the basic assumptions of linear elastic fracture mechanics. There are, as yet, no expermental data concerning the geometry of the zone during crack propagation, and further work is required in this area. In the past 10 years several researchers have claimed that non-linear fracture mechanics is more appropiate than linear elastic fracture mechanics to the failure of concrete. Non-linear fracture mechanics is discussed in the next section.

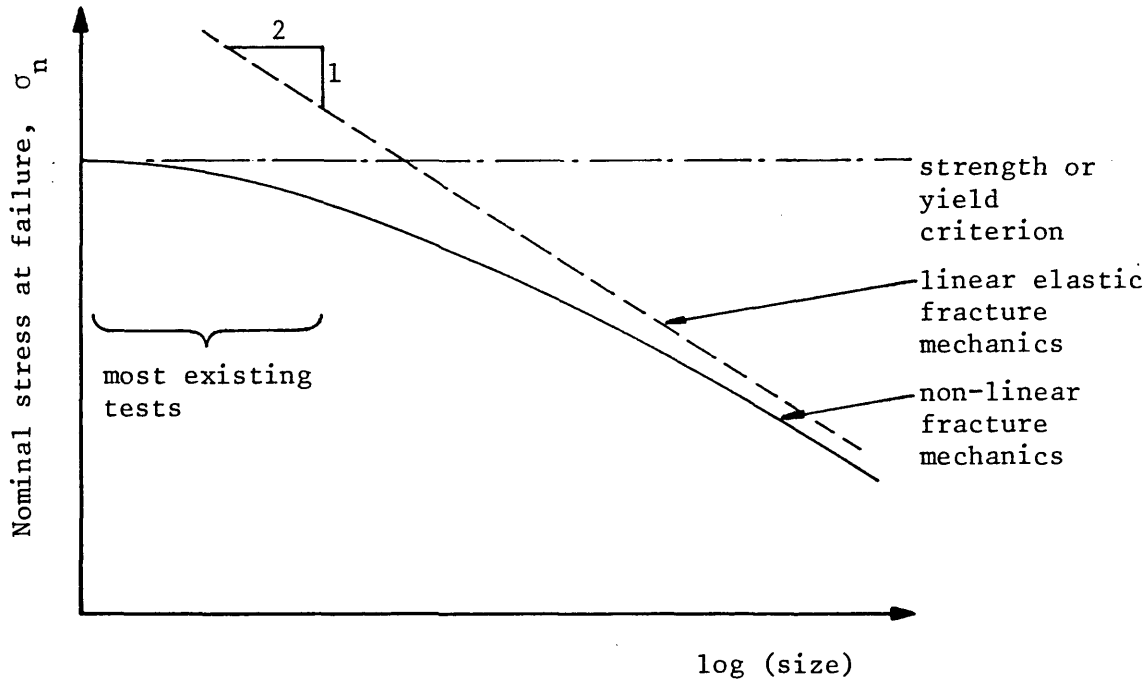

Fig. 2.14 Dimensional analysis of fracture criteria (Bazant, 1984a)

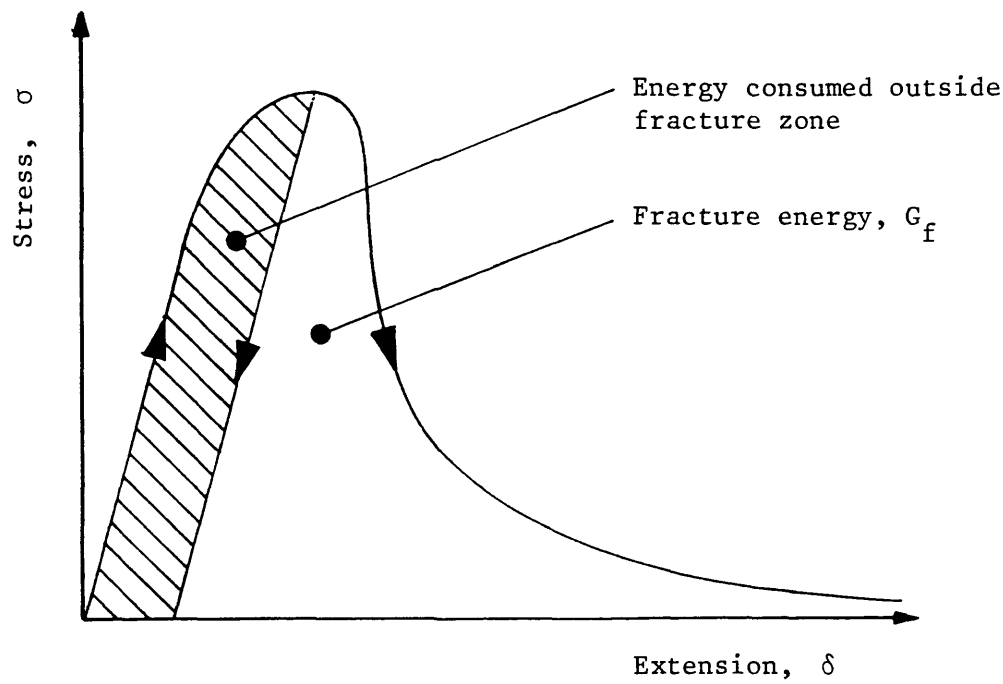

Fig. 2.15 Evaluation of fracture energy from direct tensile test according to Petersson (1981b)

2.2.2.3 Non-linear fracture mechanics applied to concrete

2.2.2.3.1 Introduction

In the previous section it was shown that the applicability of linear elastic fracture mechanics to concrete structures is limited and dependent on the structural size. During the fracture of concrete, non-linear effects arise from micro-cracking in the fracture process zone and subsequent aggregate interlock. The required size of a structure in which these non-linear effects can be ignored is subject to debate, however, many researchers believe that structures of common dimensions require the use of non-linear techniques for accurate analysis. The fracture energy, discussed in the following section, was first measured by Moavenzadeh & Kuguel (1969), and is strictly a non-linear fracture parameter since it averages the strain energy release rate during the whole fracture process. The other non-linear fracture parameters described in Section 2.2.1.2 have been applied to concrete and will be dealt with in Sections 2.2.2.3.3-5.

Various models for the fracture process zone have been suggested and, although these could be considered as a form of non-linear fracture mechanics, they will be dealt with separately in Section 2.4.

2.2.2.3.2 Fracture Energy

The fracture energy of concrete (G_f) is defined as the energy required to cause complete separation within the material. In a linearly elastic brittle material this would be the same as the critical strain energy release rate (G_c). In heterogeneous materials like concrete there are various mechanisms involved in the fracture process so that G_c may not be constant as the fracture propagates. G_f is an average measure of G_c for the complete fracture process. Most researchers have found that G_f is considerably greater than G_c measured either at crack initiation or peak load (Petersson, 1981b). This can be attributed to

the effects of slow crack growth and energy dissipation throughout the fracture process zone during propagation (Gopalaratnam & Shah, 1985).

G_f may be obtained by measuring the area under the full load/deformation graph of a suitable stable test. One must also be aware of the contribution to the fracture of the specimen self weight. Both Moavenzadeh & Kuguel (1969), and Shah & McGarry (1971) performed three point bend tests to measure G_f but made no allowance for beam self weight. Dispite this oversight, Moavenzadeh & Kuguel were able to show that G_f was more consistant than their measurements of G_c and K_c, provided that the failure was stable, ie. no kinetic energy loss. Petersson (1980a&b, 1981b) modified the calculation of G_f to include approximately, the energy supplied by the weight of the beam. He also stated that it is important to ensure that the energy consumed outside the fracture zone (eg. in crushing at the supports) must be negligible. The work of Hillerborg (1985a) and Petersson led to a draft RILEM recommendation for the determination of G_f by means of three point bend tests (RILEM, 1985), however, the confirmation of G_f as a basic material property is by no means certain. Indeed after reviewing several series of tests performed at different laboratories in accordance with a 1984 draft of RILEM (1985), Hillerborg (1984b) concluded that G_f increased by 20% for a doubling of the beam depth and by 30% for trebling of beam depth. Mindess (1984) found a 50% increase for a quadrupling of the beam depth, however, it should be noted that in his tests (based on a 1982 draft of RILEM (1985)) the span was increased in proportion to the depth, rather than in proportion to the square root of the depth (as in the later recommendations). This resulted in a much larger beam self weight effect for which Petersson's original approximations may not be adequate (Petersson, 1982). The effects of beam self weight could be overcome by the use of simply supported beams with either cantilevers or counterbalance weights outside the supports. Nallathambi, Karihaloo & Heaton (1985) found an even greater dependence of G_f on beam size, up to 100% increase for a doubling of beam depth. They do not state how they have allowed for beam self weight. G_f was also dependent on the relative notch depth and span to depth ratio, but in general G_f was less dependent than G_c on beam dimensions.

As an alternative to flexural tests, G_f may also be measured using a

stable direct tensile test. Although this test is significantly more difficult to set up than three point bend tests, one of the advantages is that the effects of specimen self weight are reduced by an order of magnitude. This approach has been used by Petersson (1981b), Gopalaratnam & Shah (1984,5), Reinhart (1984,5) and Eligehausen & Sawade (1985). Petersson differentiated between the energy absorbed outside the fracture process zone and that absorbed by the zone itself. He assumed that the zone was initiated at peak load and, therefore, that any energy absorption prior to peak load was not part of the energy required for the formation of the zone. He subtracted from the area under the load/extension graph, that area which he attributed to non-linear effects outside the zone. This he took to be bounded by the graph and an unloading line from the peak load, parallel to the initial tangent stiffness (Fig. 2.15). Although this was convenient, particularly when combined, as Petersson did, with the fictitious crack model (Section 2.4.2.1), there is, as yet, no justification for this approach. It assumed that all pre-peak non-linearities were associated with bulk energy absorption effects and not with the fracture process zone.

Gopalaratnam & Shah tested specimens whose dimensions were 76x19x305mm. and 76x38x305mm. and showed only a slight increase in G_f for the larger specimens, however, the concrete used had a maximum aggregate size of 10mm. and therefore there is some doubt regarding the validity of the smaller specimens. None of the other researchers have investigated the effect of specimen size on G_f as measured by direct tension tests.

The measurement of G_f is certainly a useful comparative tool for different concretes but it remains to be proven that G_f can be obtained in such a manner as to be considered as a material property.

2.2.2.3.3 Crack opening displacement

The concept of a critical crack opening displacement (COD_c) (Section 2.2.1.2.3) for fracture initiation has been applied to concrete by Go & Swartz (1984). They measured the crack mouth opening displacement for concrete beams in three point bending and assumed a centre of rotation at the strain reversal point. From this they were able to calculate the crack opening at the notch tip which they found to be relatively constant with respect to the notch depth to beam depth ratio. Velazco, Visalvanich & Shah (1980) measured the crack opening displacement directly using a microscope and found that COD_c was fairly constant for crack initiation but did not vary consistantly with fibre content. Visalvanich & Naamen (1980) suggested that a critical crack opening angle might exist for mortar based on their tapered double cantilever beam tests. This parameter does not appear to have been investigated by any other researchers and would require further work on specimens of differing geometries before any conclusion regarding it's usefulness could be reached.

2.2.2.3.4 The J-Integral approach

The J-Integral fracture criterion (Section 2.2.1.2.4) is a one-parameter average measure of the change in potential energy in the elastic-plastic field near a crack tip during initial crack extension. For linear elastic materials the critical value of the integral for crack initiation, J_c, is identical to the critical strain energy release rate. The J-Integral is strictly only applicable to non-linear inelastic materials providing no significant unloading occurs. Another limitation is that the integral is defined for crack initiation only and is not appropriate during slow crack growth. (Swamy, 1979).

Rice, Paris & Merkle (1973) investigated the application of the J-Integral to various specimen geometries. They showed that in order to obtain the value of J_c for a notched beam all that was required was to measure the area under the load/displacement curve for the beam, up

to the critical load. J_c was given by this area minus the equivalent area for a prismatic beam loaded up to the same level. Mindess, Lawrence & Kesler (1977) investigated the applicability of the J-Integral to cement paste, concrete and fibre reinforced concrete beams using this technique. J_c was evaluated at the maximum load (being much easier to identify than the load for crack initiation) even though this is not strictly correct. They found a greater scatter in J_c than G_c or K_c (based on Brown & Srawley's (1966) equation). For cement paste J_c was approximately equal to G_c, however, for concrete and fibre reinforced concrete J_c was greater than G_c. This could be attributed to the additional energy absorbed, due to non-linear effects, included in J_c that is not measured in G_c. One advantage of J_c over G_c was that it was more sensitive to change in fibre content. This result was not born out by the work of Velazco, Visalvanich & Shah (1980) who found that J_c did not vary consistantly with fibre contents. These latter workers evaluated J_c at initiation of slow cracking and termination of slow cracking (observed as kinks on a crack mouth displacement vs. load line displacement graph) as well as at maximum load. They suggested that resistance curves appeared to be more useful for fibre reinforced concrete.

2.2.2.3.5 Resistance curves

Several investigators have noticed a change in either the strain energy release rate or the stress intensity factor during crack growth (Section 2.2.2.2.6). This led Wecharatana & Shah (1980a&b) to attempt to use resistance curves (Section 2.2.1.2.5) to characterise the varying strain energy release rate, G_r, during crack propagation in tapered double cantilever beams and double torsion beams. They observed the crack tip position at each cycle in the loading and plotted G_r against crack extension. Using a modified evaluation of G_r to take into account the permanent deformation at the end of each cycle, they obtained similar graphs for mortar specimens of the two types studied. However, it was realised that plotting G_r against the extension of the visible crack might not produce the best results and, in further work (Wecharatana & Shah, 1983), they plotted G_r against

the extension of the visible crack plus the fracture process zone. They obtained the length of the fracture process zone, l_p, by means of an empirical model described in Section 2.4.2.2. The agreement between the resistance curves for the two different specimens was much greater than in the previous papers. However there is some concern regarding the validity of the model (Section 2.4.2.2).

Velazco, Visalvanich & Shah (1980) drew resistance curves for four point bend, fibre reinforced concrete beams. These curves plotted the stress intensity factor for propagation against the extension of the crack from a pre-existant notch. The curves were the same shape for a variety of notch depths and showed a significant variation with fibre content. They concluded that the resistance curves may be a useful material parameter for fibre reinforced concrete.

2.2.2.3.6 Comments

From the above review of non-linear fracture parameters applied to concrete it can be seen that there is still significant uncertainty regarding the adoption of any one of them as a material property. For this reason, research in the last 10 years has been extended to include strain-softening continuum theories and non-linear fracture process zone models. These two areas are reviewed in Sections 2.3 and 2.4 respectively.

2.3 Continuum Mechanics

2.3.1 Introduction

One of the drawbacks of the fracture mechanics techniques reviewed in Section 2.2 is the requirement for a starter crack. In concrete structures defects certainly exist prior to loading, however, their nature, size and orientation would not normally be known. This difficulty can be circumvented using continuum theories which do not look in detail at the stresses and strains around a crack tip, but consider constitutive relationships which are continuous functions throughout the material. Many continuum theories have been advanced to model the response of concrete under load. A detailed review of these theories is not within the scope of the present project, however, discussion of those theories which are intended to model tensile failure of concrete is appropriate.

The vast majority of continuum theories model concrete as brittle in tension (see, for example, Chen & Ting (1980) and Kotsovos & Newman (1981)). It has been shown by several researchers that the apparent brittleness of concrete in tension is not a material property but depends on the specimen size and loading regime (Chapter 3). It is, therefore, necessary to consider concrete as a strain-softening material in tension with a localisation of strain within a certain volume. These effects are related to the heterogeneity of the material and it's progressive degration through microcracking.

Dougill (1967,71) proposed a mathematical model for the progressive fracture of heterogeneous materials under uniaxial macroscopic stress, σ. The stress, ξ, at microscopic level is assumed to be normally distributed with mean $m\sigma$ and standard deviation $\alpha\sigma$. The normal distribution is truncated at $\xi = q_t$, the intrinsic tensile strength, and has a discontinuity at $\xi = 0$. The distribution is shown in Figure 2.16a. The discontinuity represents that proportion of the material which would have been in the shaded area had it not fractured at q_t. The parameter m increase from unity with progressive fracturing and is

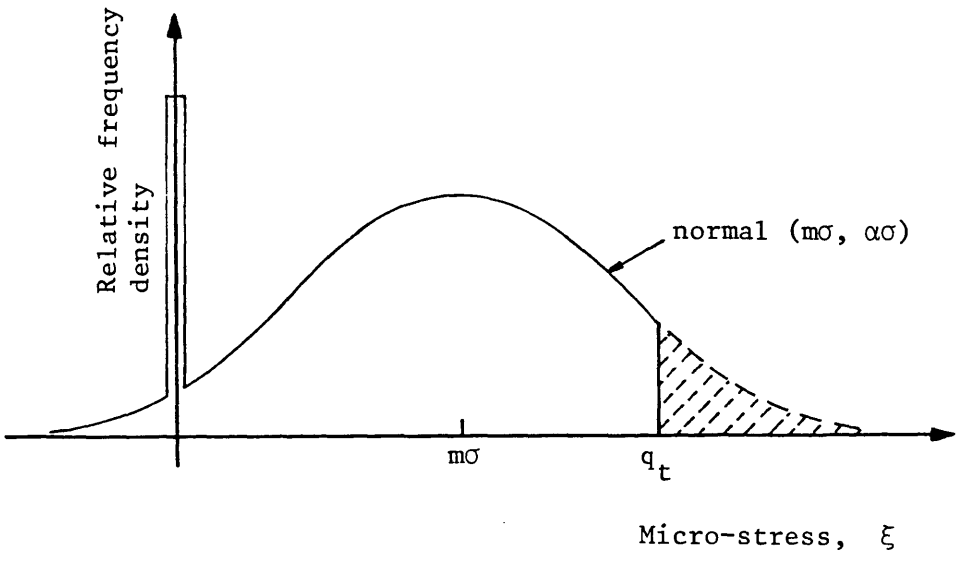

(a) Distribution of micro-stress

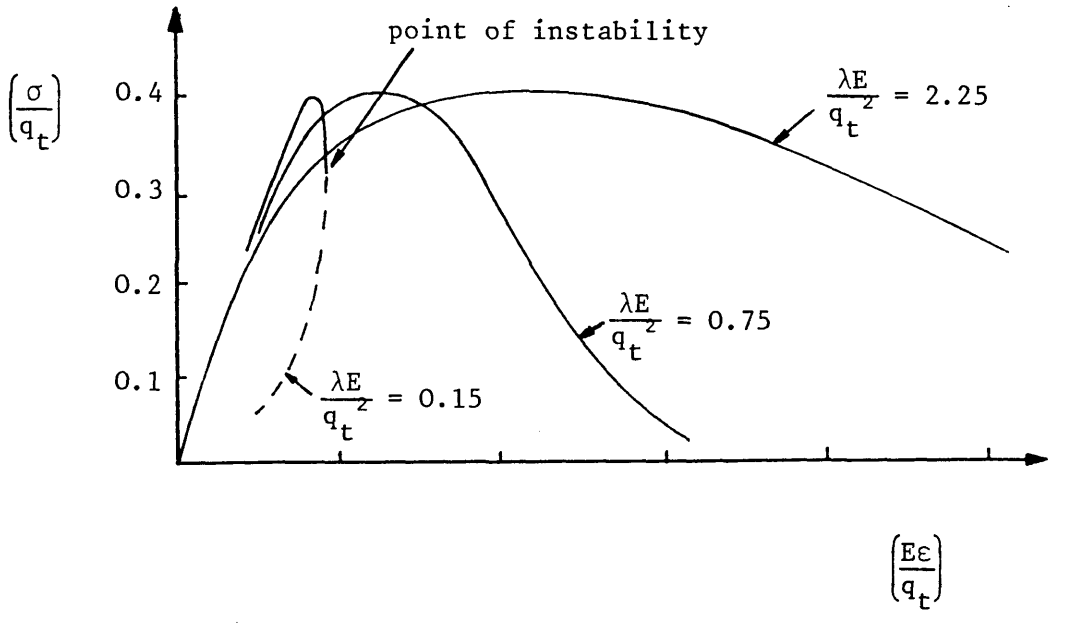

(b) Normalised stress/strain curves, $\alpha = 1$

Fig. 2.16 Dougill model for progressive fracture

thus a measure of the extent of microcracking. The parameter α is a measure of heterogeneity.

Dispite the simplification of the assumption that q_t is constant throughout the material, the model displays many of the characteristics of real fracturing materials. The tensile strength reduces with increasing heterogeneity reflecting the experimental results of Hughes & Chapman (1966b). If the micro-elements are assumed to linearly elastic up to fracture then stress/strain curves can be drawn, the shapes of which depend on the degree of heterogeneity, α, and a non-dimensional parameter $\lambda E/q_t^2$. Three curves for $\alpha = 1$ are shown in Figure 2.16b and it is interesting to note that for low values of $\lambda E/q_t^2$ instability occurs even in strain-controlled tests. This limit is analogous to that obtained for the width of the crack band (Equ. 2.43) in Section 2.4.3. The material property, λ, may be seen to be related to the value of G_f/w_c and is a measure of the fracture energy per unit volume rather than per unit area. The shapes of the curves in Figure 2.16b may be seen to be similar to those obtained for concrete under direct tension. However, it must be remembered that that the curves are drawn for three different material properties whereas to obtain similar curves for concrete three different gauge lengths would be used. The model is capable of displaying strain-softening but not the localisation effects of fracture in concrete.

It is interesting to note the similarity between Dougill's model, damage mechanics (Section 2.3.2) and the Crack band model (Section 2.4.3). In Dougill's model the degredation is characterised by the parameter m, in damage mechanics the damage parameter, ω, is used and the crack band model uses a parameter, μ, by which one term in the compliance matrix is multiplied. All three parameters serve the same purpose, to model strain-softening, only the detailed response is affected by the three different formulations.

Dougill (1983) also proposed a continuum theory, known as the 'progressively fracturing solid', for materials in which the non-linear behaviour was due solely to degradation of stiffness during loading. The theory was developed partly by analogy with the theory of hardening plasticity. It makes use of a fracture surface in

deformation space to distinguish between deformation accompanied by linear and non-linear behaviour. The theory was capable of modelling the strain-softening associated with the fracture of concrete.

Any classical or local continuum such as the ones proposed by Dougill, in which stress and strain are continuous functions that may be defined at any given point, suffers problems of instability when describing a material in which localised strain softening occurs. In such a material, prior to localisation the stress and strain may be related by a local continuum, however, after localisation has occurred a local continuum would yield non unique results (Dougill, 1985). For example consider a rod tension (Fig. 2.17a) which, up to peak load is linear elastic (Fig. 2.17b). after peak load strain softening occurs according to Figure 2.17c in a zone of length 1, whilst the rest of the rod unloads elastically. The response of the rod in terms of average strain (or of extension), Figure 2.17d, depends on the size of the softening zone. If no restraint is put on this size in a local continuum, then it reduces to the smallest possible dimensions with the result that the amount of energy absorbed in fracturing is reduced to zero. This cannot be representative of real materials (Bazant, Belytschko & Chang, 1984). The only local continuum models which can be used for strain softening materials impose a restraint on the size of the softening zone or on the fracture energy. An example of such a model, is the blunt crack band model described in Section 2.4.3. In this case the fracture energy is kept constant; the size of the fracture zone and the strain softening modulus are related to the fracture energy by Equ. 2.42. It is assumed that the strain is constant across the width of the fracture zone. A similar artifice of a controlled fracturing volume might be suitable for the Dougill model.

In Section 2.3.2 damage mechanics is discussed. Although damage mechanics is just one form of local continuum mechanics and as such suffers the problems of localisation, it is included in a separate section due to the interest shown in it's application to concrete within the published literature. In Section 2.3.3 a non-local continuum, the imbricate continuum, is examined which, in it's simplest form, degenerates to the crack band model but is capable of a greater resolution of the stresses and strains within the fracture

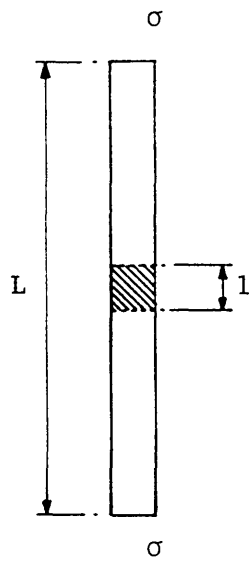

(a) Strain-softening rod

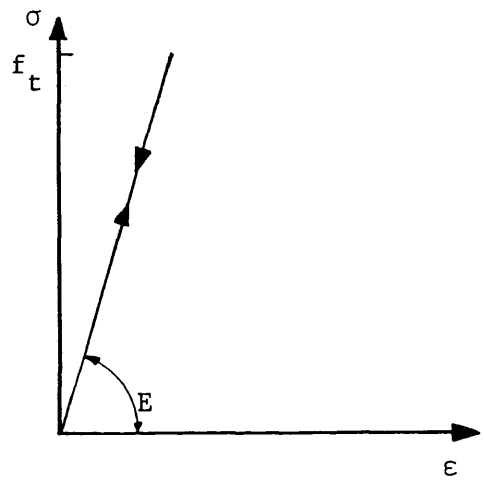

(b) Linear elastic up to f_t

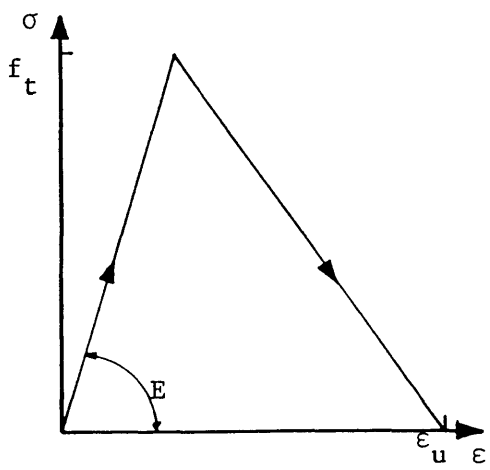

(c) Constitutive relationship strain-softening zone

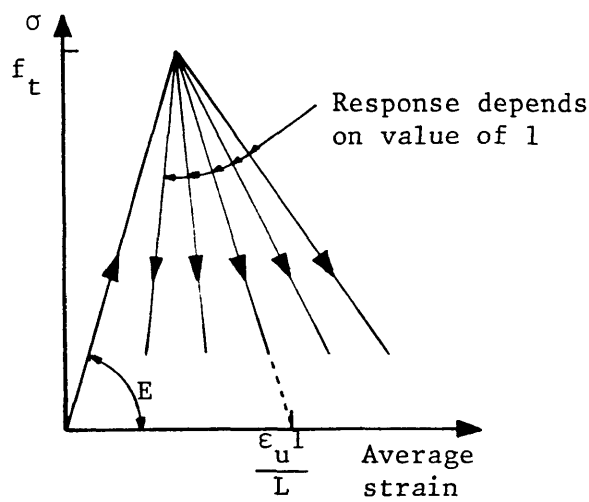

(d) Overall response

Fig. 17 Strain-softening rod in tension

zone than the simpler model.

2.3.2 Damage Mechanics

2.3.2.1 Introduction

Damage mechanics was first suggested by Kachanov (1958, 1971) in an attempt to describe the degradation of materials under creep conditions. Where fracture mechanics considers the initiation and propagation of a discrete crack, damage mechanics considers cracking over a distributed volume. The damage within the volume was characterised by a scalar quantity, ω, which was zero before any damage occurred and rose to 1 when the damage became complete and the material was fractured. This was later known as isotropic damage. When considering creep the damage was a function of time but under static conditions it may be related to strain or net stress (as described below).

The formulation given by Janson & Hult (1977) has been used by subsequent researchers into the application of damage mechanics to concrete and is outlined below.

Damage mechanics considers a reduction in load carrying area due to cracking. The damage parameter may be related to the effective area in either of two ways:

either linear damage:-

$$\omega = \frac{A - A_{eff}}{A} \qquad (2.31)$$

$$s = \frac{\sigma}{1 - \omega}$$

or logarithmic damage:-

$$\omega = \ln\left(\frac{A}{A_{eff}}\right)$$

$$s = \frac{\sigma}{1 - \omega} \qquad (2.32)$$

where σ = applied stress = P/A.

s = net stress = P/A_{eff}.

P = applied load

A = cross-sectional area

A_{eff} = effective cross-sectional area.

The strain and damage are related to the net stress by the general functions:

$$\varepsilon = G(s) \ , \quad \omega = g(s) \qquad (2.33)$$

These were simplified by Janson & Hult to be:

$$\varepsilon = s/E \ , \quad \omega = s/D \qquad (2.34)$$

where E = Young's modulus

D = damage modulus.

Hence:

$$\sigma = E\,\varepsilon\left(1 - \frac{E\,\varepsilon}{D}\right) \qquad (2.35)$$

The maximum applied stress occurs when:

$$\frac{d\sigma}{d\varepsilon} = 0$$

therefore for linear damage:

$$\sigma_{max} = D/4 \qquad (2.36)$$

and for logarithmic damage:

$$\sigma_{max} = D/2.72 \qquad (2.37)$$

It can be seen from the above discussion that the exact formulation is dependent on the description of the damage parameter and the relationships between strain, damage and net stress. Janson (1978) subsequently used an elastic/perfectly plastic, net stress/strain relationship, a power curve for the relationship between damage and net stress with an additional term in the yielding zone dependent on crack opening. This formulation resulted in a similar model to that presented by Dugdale except that the crack closing pressures varied along the yield zone. Unfortunately, in order to solve the equations, Janson approximated the variation of crack closing pressures to a constant pressure, less than the yield stress. However, this simplification could be easily avoided using numerical techniques. Janson also extended the model to include time-dependent damage by substituting strain rate for strain in the net stress/strain relationship.

As pointed out by Janson & Hult (1977), both damage mechanics (distributed damage) and linear elastic fracture mechanics (discrete damage) are highly idealised models for the fracture of materials. They described a combined approach for elastic-perfectly plastic materials.

2.3.2.2 Damage mechanics applied to concrete

Krajcinovic (1979) applied Janson & Hult's (1977) damage mechanics formulation to an unreinforced beam in bending. In looking for the ultimate load carrying capacity, he first calculated the load at which the extreme fibre applied stress dropped to zero. He assumed no damage in the compression zone. At this stage the neutral axis had already begun to move towards the compression fibre. He then calculated the load required for a section which was fully cracked over the bottom portion and partially damaged over the rest of the tensile zone. This he found to be less than that required for the former condition and concluded that the maximum load occurred when the extreme fibre stress just dropped to zero.

Loland (1980) used damage mechanics to model the uniaxial tension curves given by Evans & Marathe (1968). He used an elastic/perfectly plastic 'net stress'/strain relationship (Fig. 2.18a). He assumed an initial damage, ω_i, to account for existance of voids and other pre-existant defects. Subsequent damage was assumed to follow a power curve up to maximum applied stress after which damage increased linearly with strain (Fig. 2.18b). The resultant stress/strain relationship is shown in Figure 2.18c and can be seen to be similar to the experimental curves, despite the simple relationships shown in Figures 2.18a&b. One of the disadvantages of the approach noted by Loland was the lack of consideration of stress concentration effects. Legendre & Mazars (1984) and Mazars & Lemaitre (1984) have used a combination of damage mechanics and fracture mechanics. Damage mechanics was used up to peak load after which linear elastic fracture mechanics was assumed to be applicable. Unlike Loland they did not assume an initial damage which increased immediately on the application of a strain; instead they assumed elastic behaviour up to a damage threshold level. The level of damage which occurred beyond the threshold was dependent on a parameter which they called equivalent strain, $\tilde{\varepsilon}$, given by:

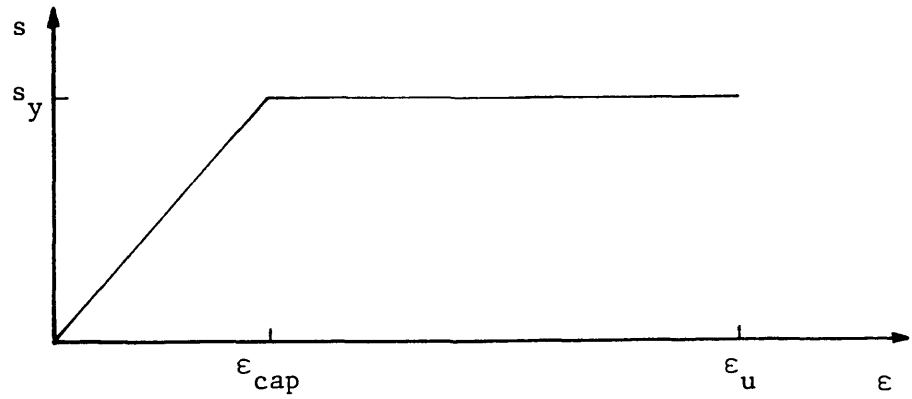

(a) Net stress/strain relationship

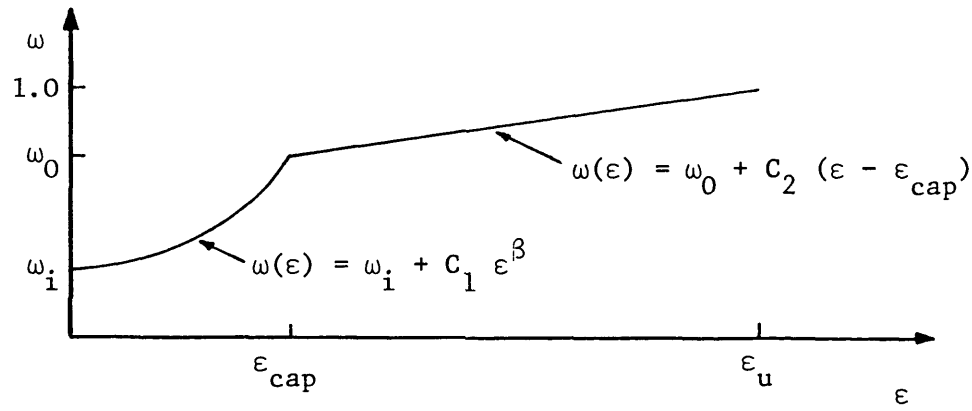

(b) Damage/strain relationship

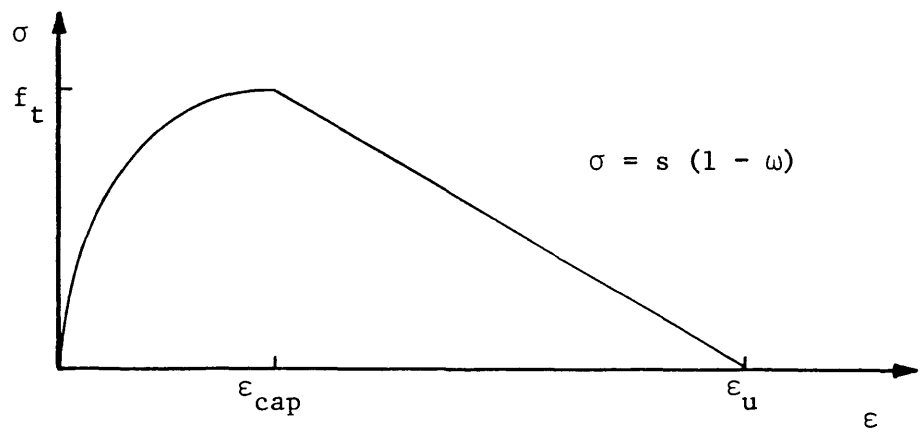

(c) Applied stress/strain relationship

Fig. 2.18 Loland's damage mechanics formulation

$$\tilde{\varepsilon} = \sqrt{(\sum_i \langle \varepsilon_i \rangle_+^2)} \qquad (2.38)$$

$$\langle \varepsilon_i \rangle_+ = 0 \quad \text{for } \varepsilon_i < 0$$

$$= \varepsilon_i \quad \text{for } \varepsilon_i > 0$$

ε_i = principal strains

The damage threshold was then defined by:

$$f(\tilde{\varepsilon},\omega) = \tilde{\varepsilon} - K(\omega) = 0 \qquad (2.39)$$

where ω = scalar damage parameter.

At peak load the analysis was switched from damage mechanics to fracture mechanics applied to a specimen including an "equivalent crack". The crack length was calculated by equating the energy required for it's creation with the energy dissipated in the formation of the damaged zone.

One advantage claimed for this technique is a reduction in computer time; also there is no need for any starter notch as in conventional linear elastic fracture mechanics. There are, however, disadvantages. Firstly it appears not to allow significant fracture propagation prior to peak load; secondly, the assumptions regarding the equivalent crack length have not yet been verified; thirdly, the critical strain energy release rate is taken to be constant throughout fracture propagation. The last point is not entirely consistant with the results given by Legendre & Mazars for the analysis of a compact tension specimen: nor with much of the published literature regarding tests on concrete. Despite the drawbacks the load/crack opening curve for a compact tension test could be modelled fairly closely.

2.3.3 The Imbricate continuum

Non-local continuum theories relate the stress at a point to the strain distribution over a certain representative volume rather than the strain at that point. This, in itself, does not obviate the problems of localisation, however, a new non-local continuum, the 'imbricate continuum', was proposed by Bazant and co-workers (Bazant & Chang, 1984a&b; Bazant 1984b, 1985; Bazant, Belytschko & Chang, 1984) which was suitable for the modelling of strain softening. This model was an extension of the crack band model (Section 2.4.3), but in this case could be applied to arbitrarily fine meshes without adjustment of the material properties of the finite elements. As the mesh was refined the behaviour was convergent and greater resolution of the stresses and strains within the fracture process zone was achieved.

The model was inspired by the work of Burt & Dougill (1977). They simulated, by computer, a random two dimensional network of pin-jointed elastic brittle bars (Fig. 2.19a). When loaded this network exhibited properties very similar to those obtained for concrete specimens. Of particular interest were the localisation of failure, strain softening and size effects (Figs. 2.19b&c). This was obviously a form of non-local overlapping continuum in which the stress in a bar was determined by the relative displacement of it's ends.

The imbricate continuum model makes use of two different types of finite elements. The first is an element similar to traditional local continuum models, known as the local element, which spans between adjacent nodes a distance h apart. The second type of element spans between nodes a distance l apart where l is a multiple of h. Since these elements overlap they are known as imbricate elements. A schematic representation of the finite elements is given in Figure 2.20b. As a mesh is refined in a local continuum the length of the

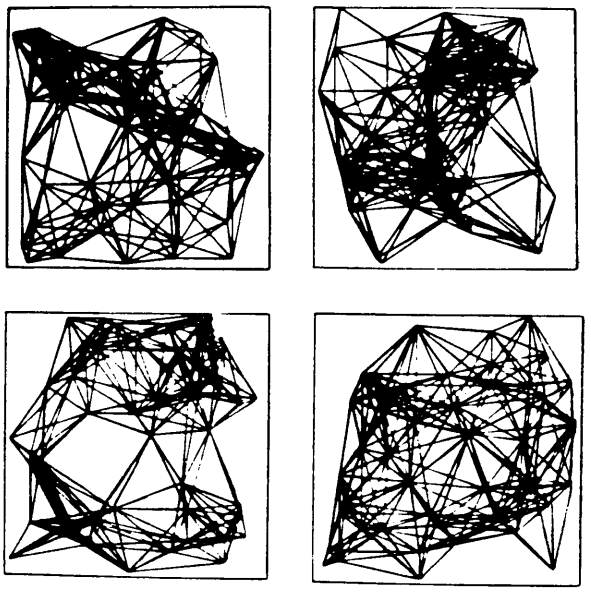

(a) Four typical random networks

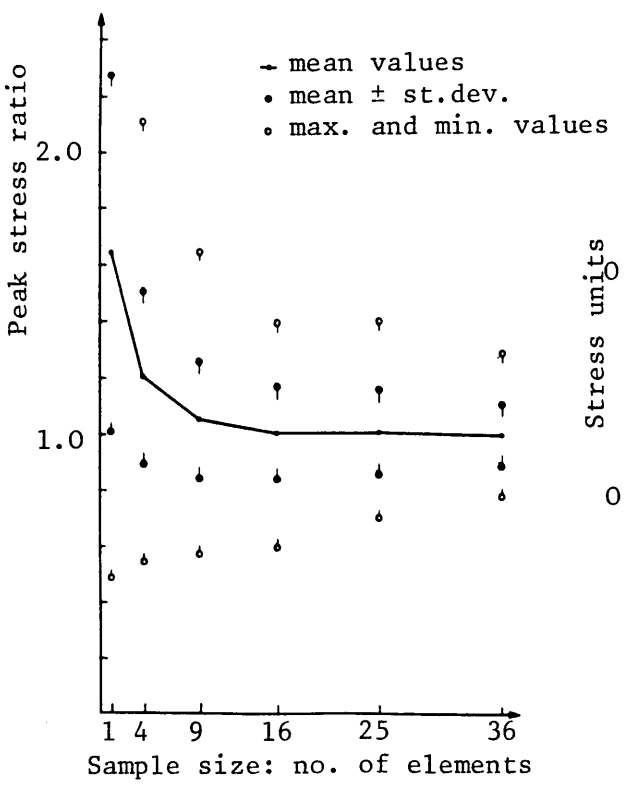

(b) Size effects on peak stress, samples from regular network

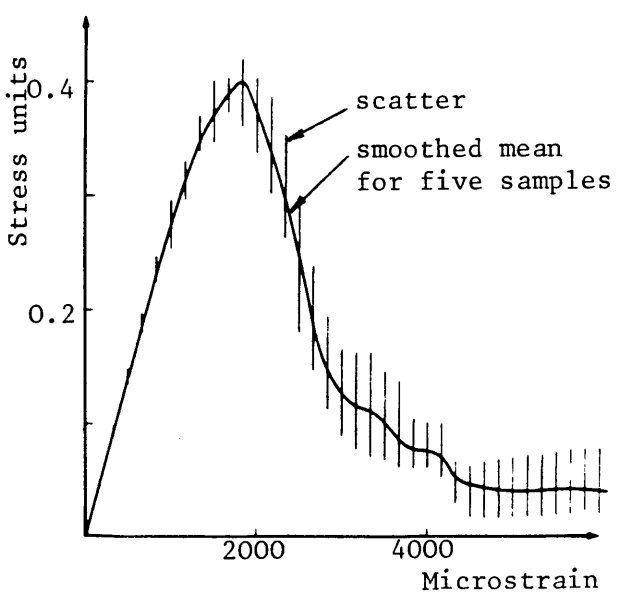

(c) Stress/strain curve showing strain-softening

Fig. 2.19 Burt & Dougill (1977) model

elements reduces, however, in the imbricate continuum only the local elements reduce in length. The imbricate elements stay the same length but extra layers are added with additional nodes (Fig. 2.20c). The reason why two element types are required is that the imbricate elements, which model the strain softening, (Fig. 2.20d) would not on their own be stable and would suffer the normal localisation problems of local continua. The addition of the local elements which are assumed to be elastic/plastic (Fig. 2.20e) overcomes this problem and stable behaviour ensures. The convergence of the model was demonstrated by Bazant, Belytschko & Chang (1984) by modelling a bar whose ends were subjected to two tensile step waves. When these waves met at the centre of a bar a fracture process zone was produced. The length of this process zone and the energy dissipated were approximately conserved as the mesh was refined. This one test of convergence presented cannot be considered as conclusive but it does suggest that the model is promising.

The finite element imbricate continuum model has been generalised into a continuum theory by increasing the number of elements to infinity, however there are still some problems with the boundary conditions for the continuum. At the other extreme if the number of elements is reduced until the imbricate elements no longer overlap, the model degenerates into the crack band model.

As yet there has been no experimental evaluation of the strains within the fracture process zone predicted by the imbricate continuum. The published information on the imbricate continuum fracture process zone does not include details of it's size, however, it is expected that it is of a similar size to that used in the crack band model, ie. three times the maximum aggregate size. Should this not turn out to be representative of real materials, it is expected that more realistic results may be obtained by either a change in the length of the imbricate elements, or a modification in the relative proportions of the local and imbricate elements, or changes in the constitutive relations of the elements.

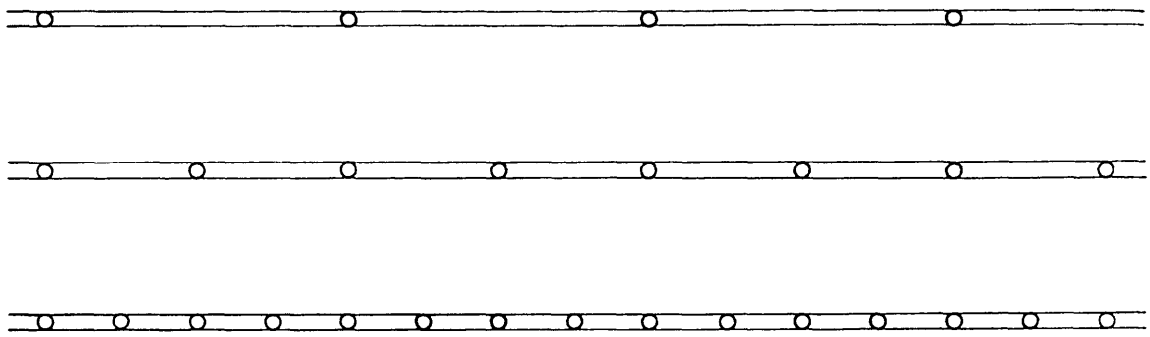

(a) Classical local continua, showing mesh refinement

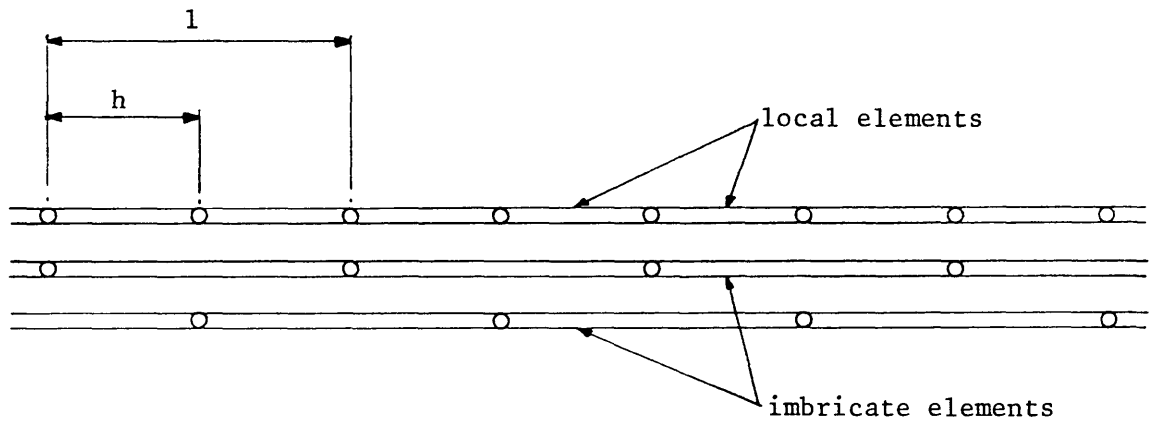

(b) Imbricate continuum, h = 1/2

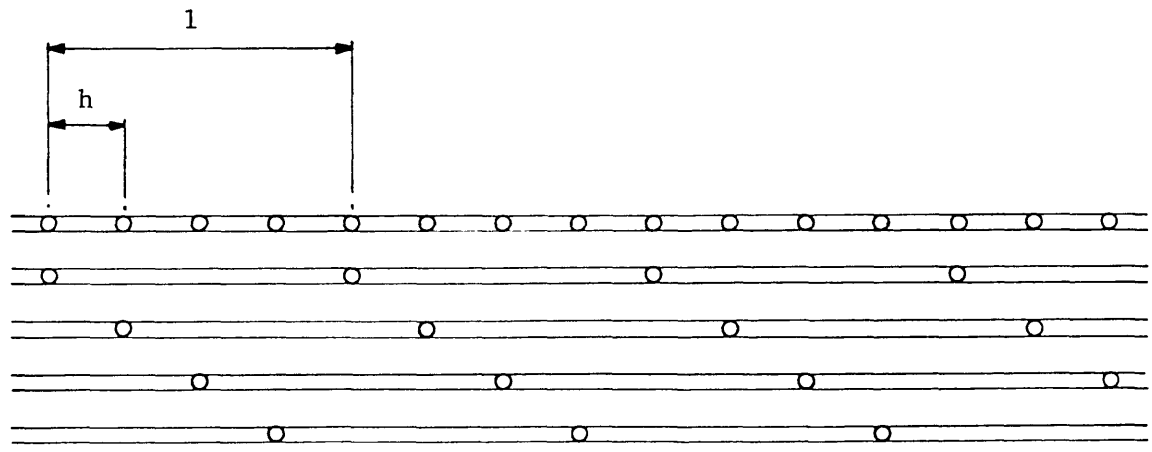

(c) Refined imbricate continuum, h = 1/4

Fig. 2.20 The Imbricate Continuum (sheet 1 of 2)
(Bazant, Belytschko & Chang, 1984a)

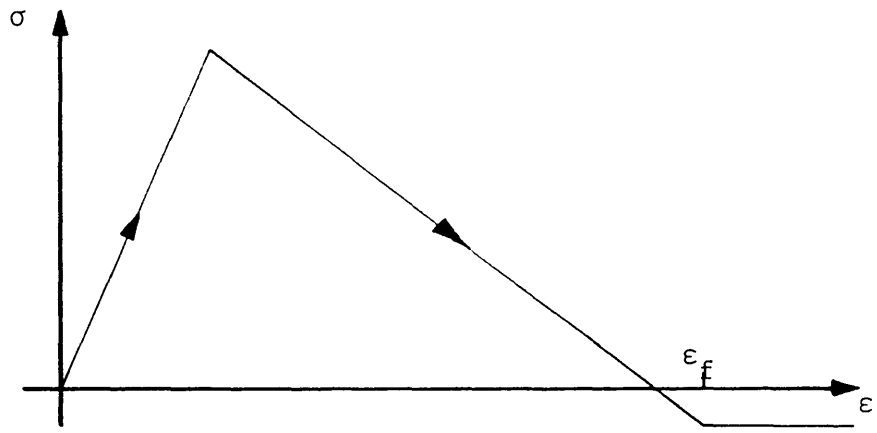

(d) Constitutive relationship, imbricate elements

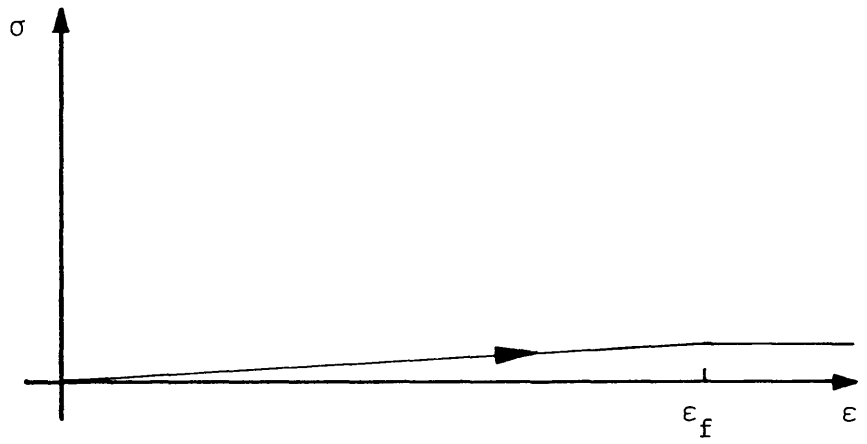

(e) Constitutive relationship, local elements

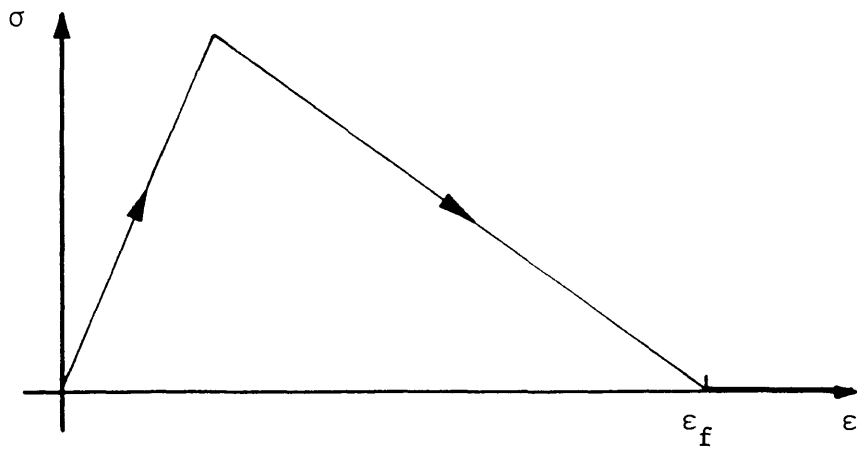

(f) Net constitutive relationship

Fig. 2.20 The Imbricate Continuum (sheet 2 of 2)
(Bazant, Belytschko & Chang, 1984a)

2.4 Fracture process zone models

2.4.1 Introduction

As has been shown in the previous sections of this chapter, there has been considerable difficulty in obtaining any usable single parameter to characterise the fracturing of concrete. In this section the modelling of the fracture process zone during the initiation and propagation of cracks will be considered. The use of these models has been greatly encouraged in the last decade, by the increased sophistication and reduced cost of finite element computer programs. Many of the models employ tensile stresses across the crack in a similar fashion to the Dugdale model (Section 2.2.1.2.2) for elastic-plastic materials. Kesler, Naus & Lott (1972) appear to have been the first to suggest the use of such a model for concrete. Their model consisted of a specimen divided into two elastic regions joined together along a strip of rigid plastic material. The joining strip contained a void, which simulated a crack, and an adjacent zone which corresponded to the region of inelastic deformation (Fig. 2.21). The model agreed qualitatively with their experimental findings but they did not do any detailed calculations based on the model. Models which consider the fracturing of concrete to be characterised by a discrete crack are discussed in Section 2.4.2 and those which assume distributed cracking, in Section 2.4.3.

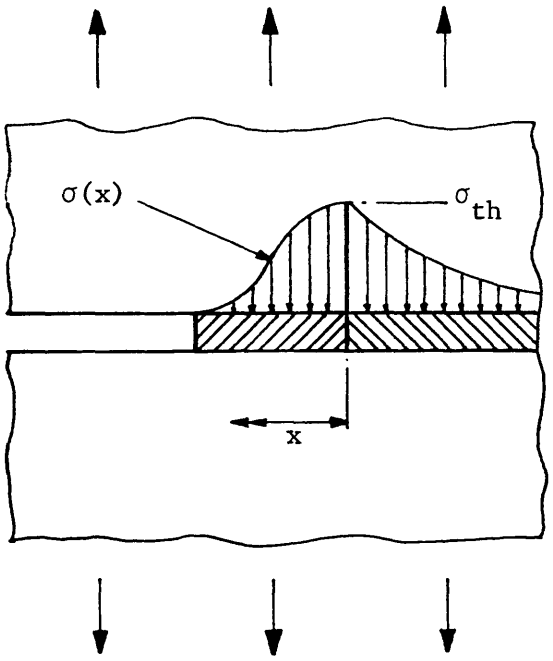

$$\sigma(x) = \frac{\sigma_{th}}{2}\left(1 + \cos\frac{\pi x}{\omega}\right)$$

Fig. 2.21 Crack model (Kesler, Naus & Lott, 1972)

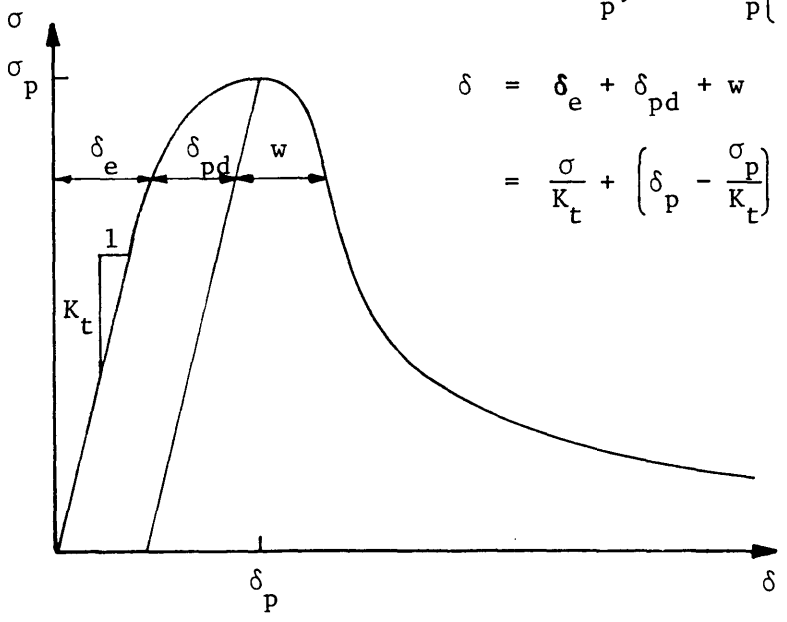

For $\delta < \delta_p$, $\sigma = \sigma_p\left(1 - \left(1 - \frac{\varepsilon}{\varepsilon_p}\right)^A\right)$, $A > 1$

For $\delta > \delta_p$, $\sigma = \sigma_p\left(e^{-kw^\lambda}\right)$, $\lambda > 1$

$$\delta = \delta_e + \delta_{pd} + w$$

$$= \frac{\sigma}{K_t} + \left(\delta_p - \frac{\sigma_p}{K_t}\right) + \left(-\frac{1}{K}\ln\left(\frac{\sigma}{\sigma_p}\right)\right)^{(1/\lambda)}$$

Fig. 2.23 Model suggested by Gopalaratnam & Shah (1984,5)

2.4.2 Discrete crack models

2.4.2.1 Fictitious crack model

The first fracture process zone model to be used in the analysis of concrete structures was proposed by Hillerborg, Modeer & Petersson (1976). This model, subsequently called the fictitious crack model, assumed that stresses would act across a crack as long as it was only opened a small ammount and that the stresses were dependent on crack opening. The model is shown in Figure 2.22a and can be seen to be similar to the Dugdale model except that the closing stresses are variable. It is interesting to note that approximately concurrently with the development of the fictitious crack model, Palmer & Rice (1973) proposed a similar model for the localisation into 'shear bands' of over-consolidated clay. The model related the shear stress to the relative shear displacement in much the same way as the fictitious crack model related the tensile stress and crack opening. Both models were capable of displaying the localisation and size effects present in the real materials.

The magnitude of the tensile stresses was determined from the direct tension test (Fig. 2.22b) from which two different constitutive relationships were obtained (Hillerborg, 1978). The first (Fig. 2.22c) was the stress/strain relationship for the material outside the fracture process zone. The second (Fig. 2.22d) was the stress-crack opening relationship for the fracture process zone which was originally assumed to have zero width and only to start widening when the peak stress was reached. These assumptions presume that the fracture energy is a material property.

Hillerborg et al. conducted a finite element analysis of a beam. For the purposes of this calculation the relationships of Figures 2.22c&d were simplified to those of Figures 2.22e&f. The material behaved elastically until the stress at the outermost node reached f_t. At this point the crack was allowed to open between the elements and the force at this node obtained in accordance with Figures 2.22f. The moment was

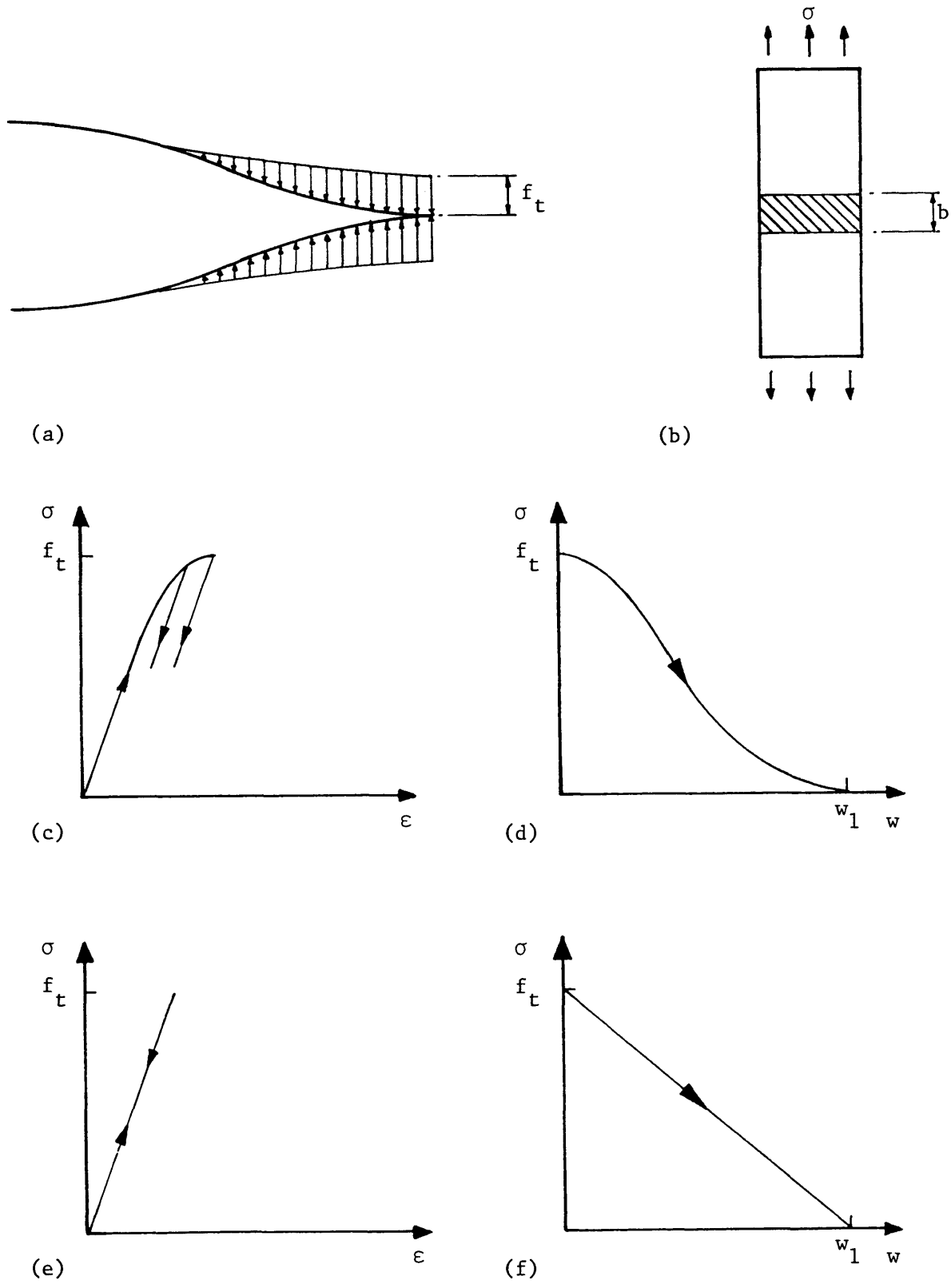

Fig. 2.22 Fictitious crack model (Hillerborg, Modeer & Petersson, 1976)
(a) Crack closing stresses
(b) Idealised direct tensile test
(c) Stress/strain relationship outside fracture zone
(d) Stress/opening relationship for fracture zone
(e) & (f) Simplified relationships used in calculations

increased until f_t was obtained in the second node. This process was repeated modelling the development of the fracture process zone and it's propagation through the beam. The maximum moment was not achieved until the tip of the fracture process zone was approximately one third of the depth of the beam above the soffit. From the calculations they obtained relationships between the ratio of bending to tensile strength and the beam depth which agreed reasonably well with results in the literature.

The fictitious crack model has been further investigated and more generally applied by Petersson (1981b) and Gustafsson (1985). Petersson described in detailed the application of the model using finite element analysis and also determined the material parameters required for the model using direct tensile and three point bend tests. Gustafsson compared the model with various other fracture theories, gave a more general basis for the model and then applied it to specimens of various geometries.

Some of Petersson's and Gustafsson's comments on the model may be summarised as follows:

1. There exists a characteristic length, l_{ch}, which is a measure of the brittleness of a material given by:

$$l_{ch} = \frac{G_f E}{f_t^2} \tag{2.40}$$

Where G_f = fracture energy
E = Young's modulus
f_t = tensile strength.

For a given shape of the stress/crack opening relationship the material becomes more brittle when the value of l_{ch} decreases.

2. The model can demonstrate size effects in concrete fracture. As the specimen size increases with respect to the material characteristic length the results become closer to those obtained by linear elastic fracture mechanics.

3. It is assumed that each infinitesimal volume of material behaves and fractures as in uniaxial tension. Two and three dimensional stress states are considered not to affect the fracture process significantly, provided the maximum principal compressive stress is not too large.
4. The shape of the stress/crack opening curve is important for the prediction both of specimen ductility and the maximum load capacity.

They also commented on the application of the model to concrete structures by means of finite element analysis:

1. The fictitious crack is required to follow the edges of the finite elements.
2. The stress singularly at the crack tip for linear elastic analysis requires a fine finite element mesh around the tip. This stress singularity does not occur in the fictitious crack model so that the finite element mesh may be relatively coarse. For concrete, the maximum node spacing along the crack should be of the order of 40-80mm.
3. The analysis is simplified if the crack path is predetermined, but unknown crack paths can be followed.
4. Any node through which the crack passes is required to be a double node to allow for crack opening.
5. The model is capable of analysing the development and propagation of fracture process zones in concrete specimens of many different geometries and predicting their response under load.

A model, very similar to the fictitious crack model, was used by Gopalaratnam & Shah (1984,5) to reproduce the stress/extension curves from their own direct tensile tests. The model, shown in Figure 2.23 includes the effects of pre-peak non-linearities and assumes a non-linear stress vs. crack width relationship.

2.4.2.2 Other discrete crack models

Wecharatana & Shah (1983) proposed a model (Fig. 2.24) which they used to calculate the length of the fracture process zone, l_p. They used this length, added to the length of the stress free crack, to improve the agreement between resistance curves for two different specimen geometries (Section 2.2.2.3.5). l_p was obtained by means of a trial and error method in which the basic steps are as follows:

1. Assume a critical crack opening displacement at the tip of the visible crack, η_{max}.
2. Assume a crack opening profile and a value for l_p.
3. Calculate crack closing stresses from the crack opening profile and the stress/crack opening results of direct tension tests.
4. Apply the external load and crack closing stresses using elastic beam theory, to a specimen with a crack length equal to the visible crack plus l_p.
5. Check for critical crack opening at tip of visible crack, if incorrect try new value of l_p.
6. Check the opening at the mouth of the crack with experimental results, if incorrect modify crack profile and repeat from step 2.

They found that the shape of the stress distribution in the fracture process zone had little effect on the results provided that the fracture energy was maintained constant. Consequently they used a uniform stress throughout the zone in all the calculations. In a discussion of Wecharatana & Shah's work, Hillerborg (1985b) made various comments which call into question the suitability of their approach. Firstly, the use of elastic beam theory is an approximation which may be sufficiently accurate for deformation at the loading point (underestimated by a factor of 1.5), but is no good for deformations near the crack tip (underestimated by a factor of up to 4.0). The second main objection is the assumption that the visible crack is a "traction free crack". It is likely that, unless special precautions are taken to avoid surface shrinkage, the lengths of the surface and internal cracks would be different (Legendre & Mazars, 1984). It is also true that even visible cracks can have significant traction capacity (Petersson, 1981b).

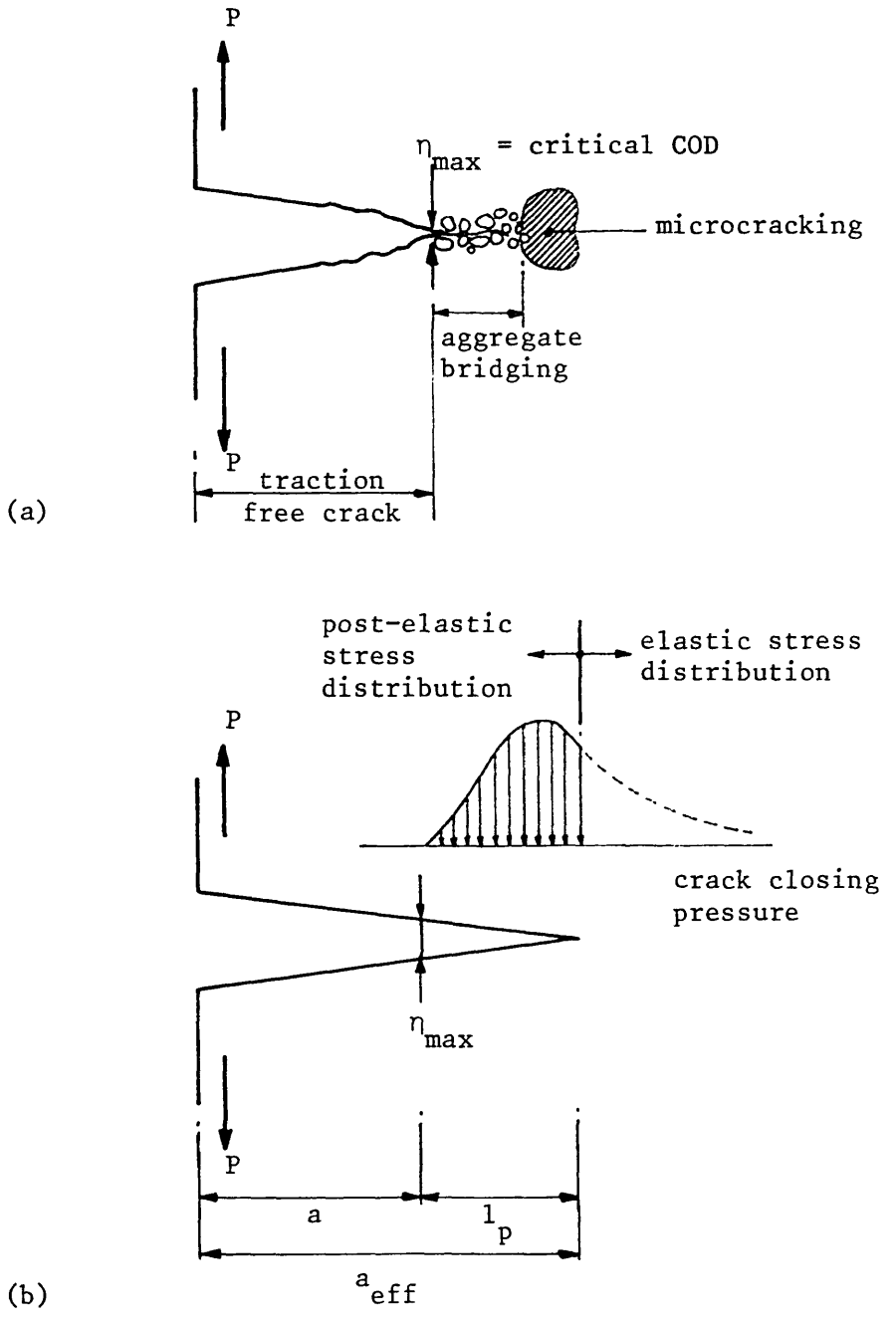

Fig. 2.24 Crack model proposed by Wecharatana & Shah (1983)
(a) Assumed physical actions
(b) Model

One of the problems in establishing realistic models for the fracture of concrete is the difficulty in measuring the various stages of degradation that the material passes through. The stages have been defined in many ways by different authors but may be broadly subdivided into microcracking, formation of a macro crack with aggregate interlock, and complete separation of the surfaces with no load transfer. The fictitious crack model is based on the stages as displayed by direct tensile tests. The model is then directly applied to specimens of any other geometry. Wecharatana & Shah's model assumes that the visible crack is the same as the stress free crack and that the other stages are lumped together in the fracture process zone. The fracture process zone length for a particular specimen, is obtained by the technique described above in conjuction with the experimental results for that specimen.

Cho, Kobayashi, Hawkins, Barker & Jeang (1984) (also Barker, Hawkins, Jeang, Cho & Kobayashi, 1985; Jeang & Hawkins, 1985) have attempted to measure directly the length of the total crack using a surface replica technique. They used the crack opening displacements (COD) at two positions on their double cantilever beam specimens to infer the effective and stress free crack lengths. The effective crack was calculated from a load/displacement graph using the secant stiffness. This length included the stress free crack length and some additional length to represent the effects of the fracture process zone. The stress free crack was obtained from the reloading portion of a plot of the two crack opening displacements against each other. It was assumed that the fracture process zone was included within the total crack as measured by the replication technique. Microcracking prior to the formation of a discrete crack was ignored. From the above results the length of the fracture process zone was inferred, it was then necessary to obtain the crack closing stresses in this zone. These were obtained by a trial and error method which was evaluated by comparing the predicted load/COD with that obtained experimently. The starting point was to assume a uniform stress equal to the tensile strength throughout the measured fracture process zone (Fig. 2.25a). This gave good agreement with the load/COD curves but had the disadvantage that no criterion was provided for crack propagation. As an alternative, the stress distribution shown in Figure 2.25b was

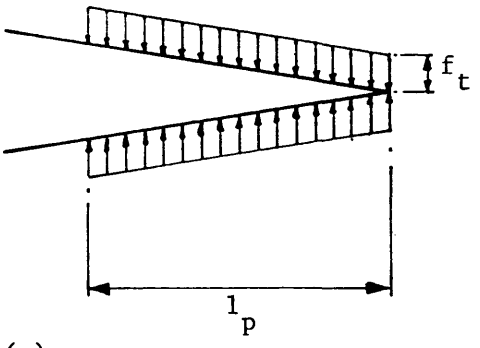

(a)

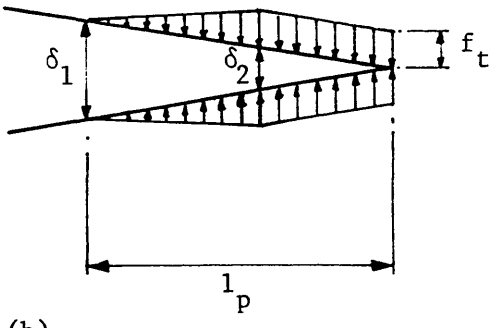

(b)

$\delta_1 = 1.5 \times 10^{-3}$ ins.

$\delta_2 = 0.5 \times 10^{-3}$ ins.

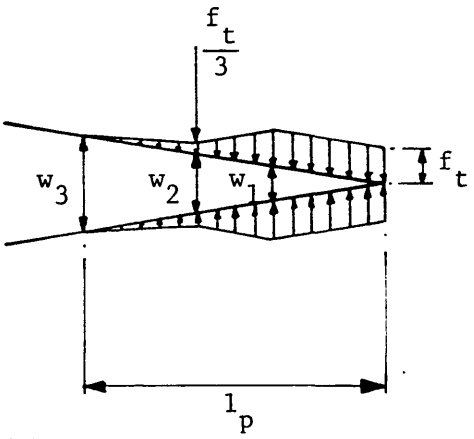

(c)

For $3470 \leqslant f'_c < 5010$:

$$w_1 = \left(\frac{0.10\ f'_c}{1000}\right) - 0.10$$

$$w_2 = 5\ w_1$$

For $5010 \leqslant f'_c < 9070$:

$$w_1 = 0.75 - \left(\frac{0.07\ f'_c}{1000}\right)$$

$$w_2 = \left(\frac{1.25\ f'_c}{1000} - 1.25\right).w_1$$

$$w_3 = w_2 + 9.0$$

w values in 10^{-3} ins.
f'_c in psi.

Fig. 2.25 Crack models (Cho, Kobayashi, Hawkins, Barker & Jeang, 1984; Barker et al., 1985; Jeang & Hawkins, 1985)
(a) Initial simple model
(b) Improved model
(c) Model dependent on f'_c

used. The crack tip opening displacement was now set to 1.5x10-3 in. which formed the propagation criterion. With this stress distribution, no longer restricted to the measured fracture process zone length, the load/COD curves could be equally well reproduced and as a check the calculated crack tip position was found to be close to the average position observed in the tests.

Jeang & Hawkins (1985) proposed a tri-linear stress distribution (Fig. 2.25c) which took into account the concrete strength in calculating the critical crack openings. In contrast to Wecharatana & Shah's (1983) findings, the load/COD response was found to be very dependent on the shape of the stress distribution. The maximum load sustained by a double cantilever beam specimen, assuming their tri-linear stress distribution, was only 80% of the value obtained assuming the stress distribution of Figure 2.25b, even though the total fracture energy was the same. Also the post-peak behaviour was significantly affected.

In order to assess the effect of the shape of the stress distribution, Reinhardt (1985) considered a centrally cracked infinite plate as shown in Figure 2.26a. He applied the fictitious crack model analytically whilst assuming a power function for the stress distribution within the fracture zone (Fig. 2.26b). The length of the zone was calculated by ensuring that no stress singularity occurred at the crack tip. This involved equating the linear elastic stress concentrations due to the remote applied stress and the crack closing stresses, a technique first used by Dugdale (Section 2.2.1.2.2). The existance of cracks or flaws in a material reduces it's tensile strength. Reinhardt showed the dependence of this reduction on the shape of the stress distribution (Fig. 2.26c). It can be seen that for large n, representing yielding materials, the existance of cracks has little effect on the strength, whereas for low n, representing brittle materials the strength is reduced significantly and approaches zero. Reinhardt conducted two series of tests, the first on narrow specimens to obtain stress/extension curves for concrete in direct tension, the second on wider plates to measure the strain distribution in front of a crack. By a combination of the results of these two tests he was able to obtain an indication of the stress distribution in the wider plates. Unfortunately, as Reinhardt pointed out, the test arrangement and choice of size for the wider plates were not ideal since they did

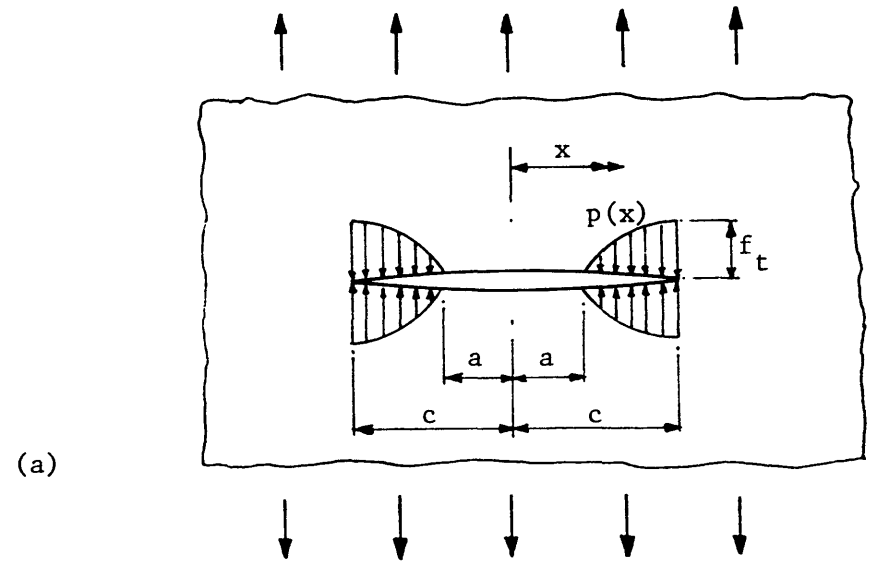

(a)

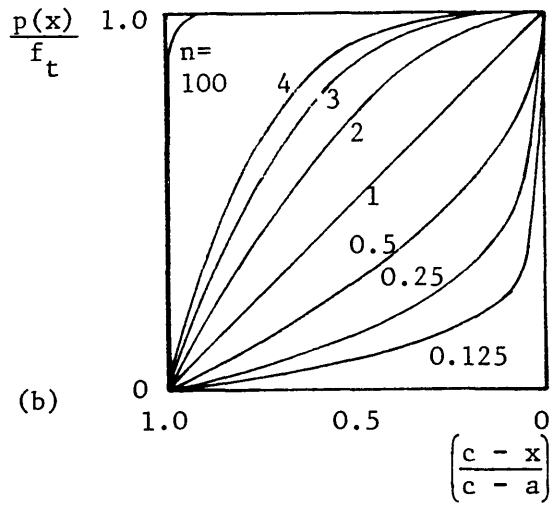

(b)

$$\frac{p(x)}{f_t} = 1 - \left(\frac{c - x}{c - a}\right)^n$$

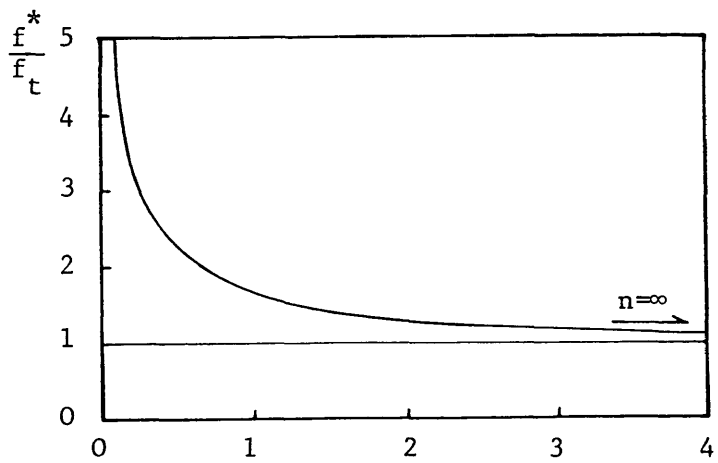

(c)

f^* = 'true' tensile strength of uncracked material

f_t = measured apparent tensile strength of specimens including defects

Fig. 2.26 Reinhardt's (1984) model
(a) Crack closing stresses for crack in infinite plate
(b) Stresses in softening zone, dependence on n
(c) 'True' to 'apparent' strength ratio as a function of n

not allow for a full fracture zone to develop in front of a stress free crack. However, this work does show the dependence of structural response on the stress distribution within the fracture process zone and the need for detailed measurements of the strains within the zone.

The models described so far have all been for monotonic loading. Gylltoft (1983,4) has used a model based on the fictitious crack model for fatigue loading of concrete. In this case, rather than using the double nodes of the former model with a stress/crack opening relationship, Gylltoft used very short linkage elements between nodes on either side of the predetermined crack path. These elements had the stress/strain relationship shown in Figure 2.27a for monotonic loading. There is no fundamental difference between these two models. The fatigue model is shown in Figure 2.27b. The energy supplied to the fracture zone in an unloading/reloading cycle, corresponding to the hysteresis loop, (Area A_1) is assumed to be equal to the reduction in subsequent energy required for complete separation (Area A_2). This equivalence ensures that the total energy consumed during fatigue fracture is identical to the fracture energy for monotonic loading. The validity of this energy approach is not entirely born out by Gylltoft's experimental results and contradicts the conclusion drawn by Gopalaratnam & Shah (1985) who found that cyclic loading, in direct tension, did not affect the envelope stress/strain curve. However, Gylltoft applied the model to a notched beam in four point bending and was able to reproduce the experimental results fairly accurately.

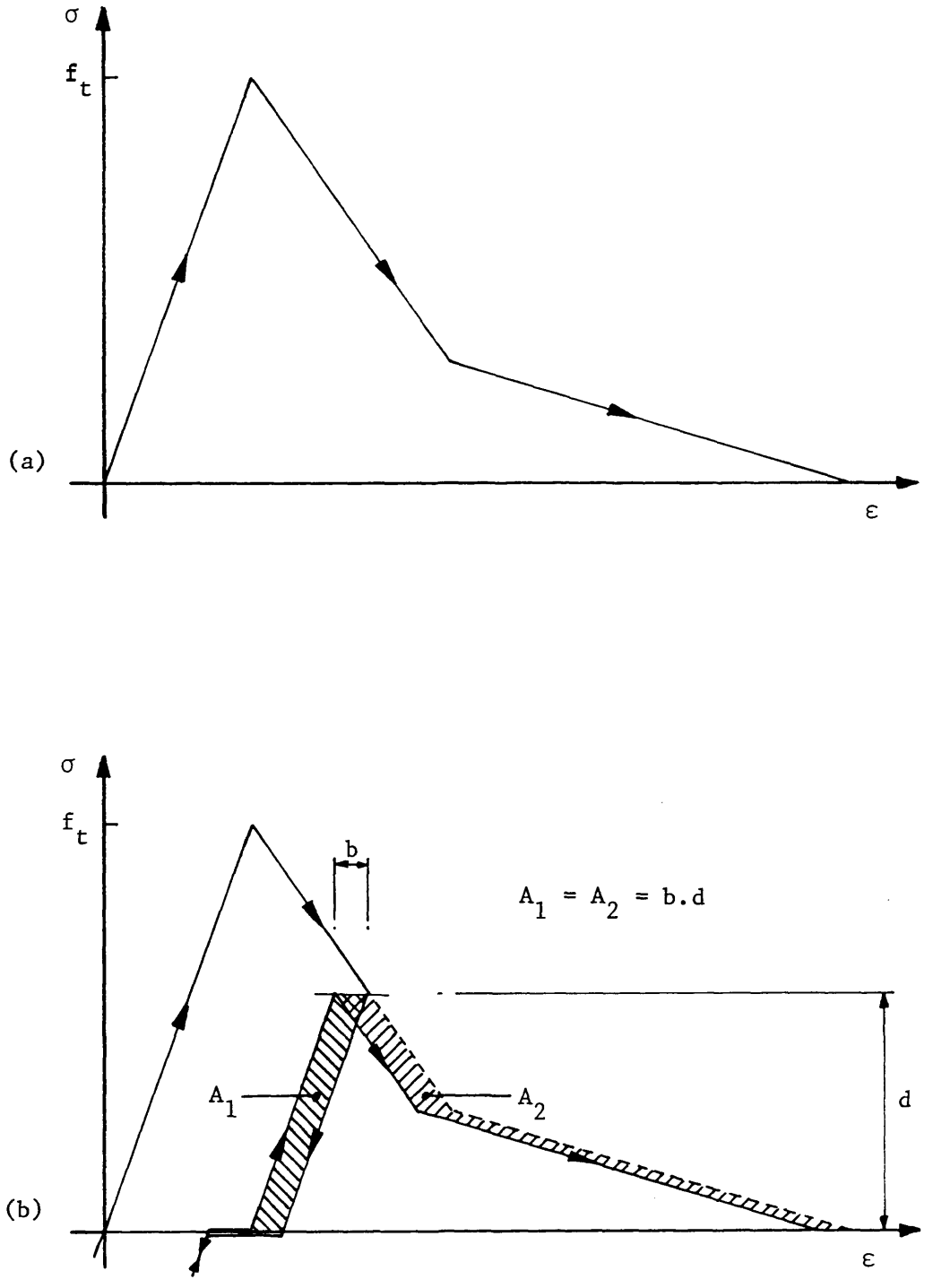

Fig. 2.27 Cyclic loading fracture model (Gylltoft, 1983,4)

2.4.3 Blunt crack band models

In the previous section, sharp interelement cracks were used in the finite element analysis of structures. In this section, the use of blunt, element wide crack bands is described.

The fracture process zone in concrete is that volume in which large strains take place. These large strains are normally attributed to progressive cracking at a microscopic level. Not until later in the degradation of the material does the fracture coalesce into a single crack. It seems, therefore, that a model which allows degradation within a volume might, in some ways, be more realistic than a sharp crack model. Blunt crack band finite element models make such an allowance in that the microcracking is assumed to be uniformly dispersed throughout the finite element. In practice there appears to be little difference in the results obtained when using the two crack models provided that appropriate finite elements are used. It has been suggested that blunt crack band models are easier to use (Cedolin & Bazant, 1981) and there are certainly three dimensional effects which can be included in blunt cracks which do not appear to be usable for discrete crack models (Bazant & Oh, 1983).

Bazant & Cedolin (1979; Cedolin & Bazant, 1981) investigated blunt crack band propagation for linearly elastic brittle materials (Fig. 2.28a&c). They found that, if a limiting stress such as the tensile strength was used as the criterion for element fracture then the model was not objective with respect to element size. This was because the stress intensity factor at the crack tip depended on the width of the crack band which was equal to the element size. As an alternative crack propagation criterion, they proposed that the energy required for crack extension should be equal to the fracture energy (assumed to be a material constant). This proved to be objective with respect to element size. The energy criterion was shown to be the same as an equivalent tensile strength criterion, where the strength was dependent on the element size.

Bazant & Oh (1981,3) used a strain-softening material, idealised by the bi-linear relationship of Figure 2.28d, to model the fracture of

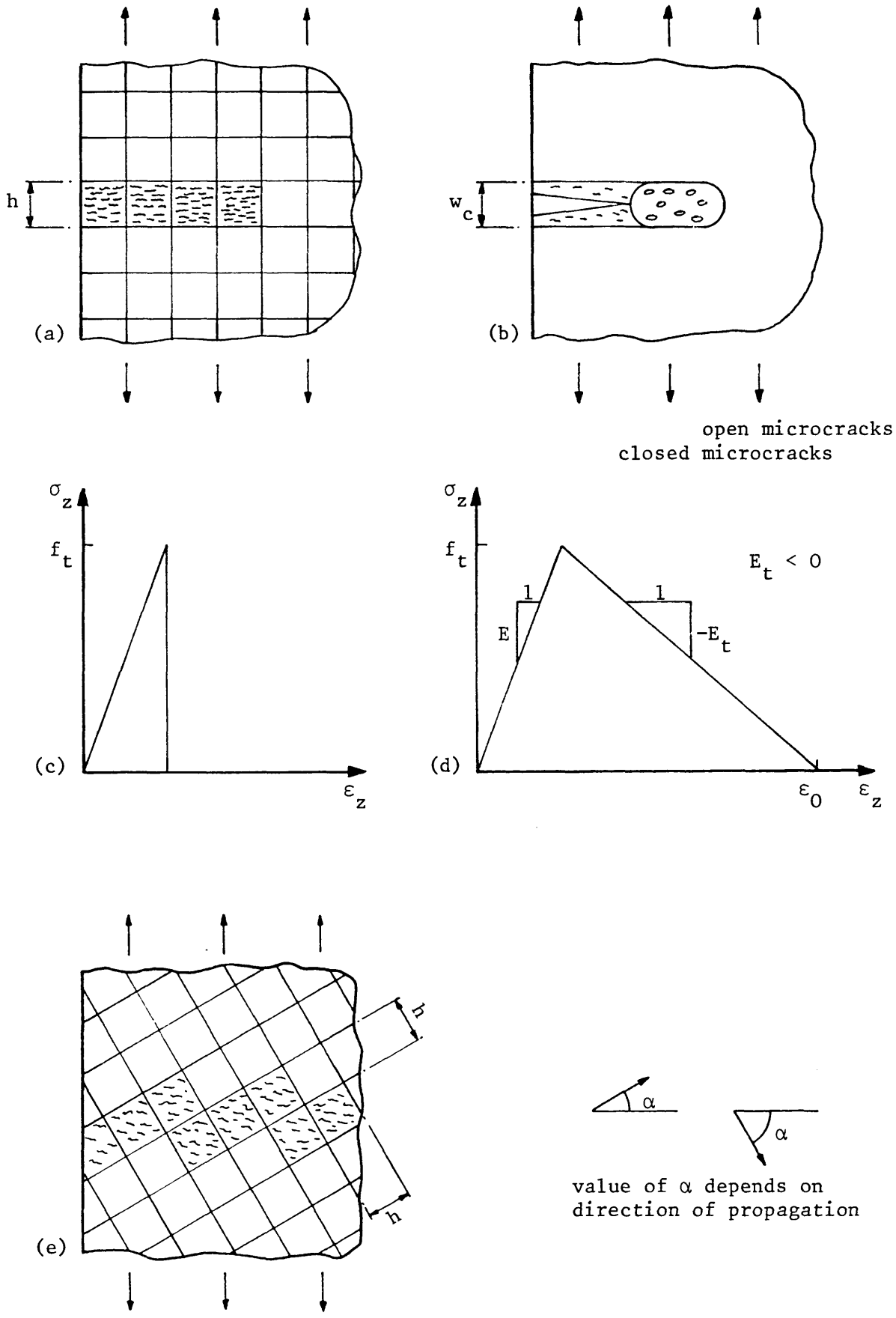

Fig. 2.28 Crack band fracture models
(a) Finite element mesh
(b) Assumed physical actions
(c) Elastic/brittle relationship
(d) Strain-softening relationship
(e) Zig-zag crack band

concrete. In this case it was not necessary to adjust the tensile strength to ensure objectivity with respect to element size, instead the slope of the strain-softening part of the stress/strain relationship, E_t, is related to the crack band width to ensure constant fracture energy. From Figure 2.28d it can be seen that the fracture energy (the area under the load/displacement curve) may be given by:

$$G_f = w_c \frac{f_t^2}{2} \left(\frac{1}{E} - \frac{1}{E_t} \right) \tag{2.41}$$

Or alternatively the width of the fracture process zone is given by:

$$w_c = \frac{2G_f}{f_t^2} \left(\frac{1}{E} - \frac{1}{E_t} \right)^{-1} \tag{2.42}$$

Since E_t must be negative, Equ. 2.42 puts on upper limit on the magnitude of w_c.

$$w_c \leqslant \frac{2\ G_f\ E}{f_t^{\ 2}} \tag{2.43}$$

Interestingly, this is double the characteristic length proposed by Petersson (1981) and, as such, if a single straight line softening were to be assumed, is the length of a prismatic concrete specimen in direct tension in which the stored strain energy is equal to the fracture energy. An element of this size will exhibit the brittle fracture characteristics of Bazant & Cedolin's model.

G_f, E and f_t were assumed to be material properties in which case E_t could be calculated from the value chosen for w_c. If the crack was parallel to the finite element mesh then the element size, h, and w_c were chosen to be equal. In the more general case of a crack direction that was not parallel to the mesh lines, the crack had a zig-zag shape (Fig. 2.28e). It was then necessary to chose a value, w_c, of the width of a smooth band which corresponded to the zig-zag band. This value

would have to be recalculated at each crack band advance and was given, for square meshes, by:

$$w_c = \frac{h}{\cos \alpha} \tag{2.44}$$

where α = direction of the mesh line along which the crack band advances.

Bazant & Oh considered concrete to be an isotropic linearly elastic material in which beyond peak stress, a system of uniformly distributed microcracks developed normal to the principal tensile stress, σ_z. The microcracks increased the strain, ε_z, but did not affect the strains, ε_x and ε_y. This could be expressed in a triaxial compliance relationship in which the progressive microcracking was modelled by a simple multiplicative parameter, μ, in one element only. The relationship is:

$$\begin{pmatrix} \varepsilon_x \\ \varepsilon_y \\ \varepsilon_z \end{pmatrix} = \begin{pmatrix} C_{11} & C_{12} & C_{13} \\ & C_{22} & C_{23} \\ \text{Sym.} & & C_{33}\mu^{-1} \end{pmatrix} \begin{pmatrix} \sigma_x \\ \sigma_y \\ \sigma_z \end{pmatrix} \tag{2.45}$$

where $\frac{1}{\mu} = -\frac{E}{E_t} \cdot \frac{\varepsilon_z}{\varepsilon_0 - \varepsilon_z}$, $0 < \mu \leqslant 1$

For $\mu = 1$ the material was uncracked and for $\mu \to 0$ the fully cracked state is approached.

As previously mentioned, one advantage of the blunt crack band over discrete crack models is a more realistic modelling of the distributed microcracking in the fracture process zone. Although this is true, it does not appear to have any significant effect on the results obtained. Other advantages claimed for the crack band model are that it is easier to handle in finite element programs, particularly when the propagation direction is unknown or when the crack path is curved. It also allows one to take into account the effect of the triaxial

stress state in the crack front region.

The use of simple parameter, μ, in Equ. 2.45 to describe the degradation of the material suggests a similarity between this model and damage mechanics (Section 2.3.2). The basic difference between the two approaches is that μ is related to a zone of a certain characteristic width, w_c, whereas the damage parameter within a continuum is not contained within any predetermined volume. It is for this reason that there are difficulties in the use of damage mechanics to model the localisation of fracture in concrete.

2.4.4 Comments on fracture process zone models

In the previous two sections, fracture process zone models have been described which provide powerful tools for the analysis of concrete structures. Several models have been applied to reinforced concrete as well as plain concrete (Cedolin & Bazant, 1981; Gylltoft, 1983; Gustaffson 1985). The models have been used to describe the behaviour of structures with reasonable accuracy. Some of the models, and in particular the fictitious crack and crack band models, provide both initiation and propagation criterion for fracture and would appear to have wide ranging applications.

There are, however, drawbacks to the models described. The discussion has concentrated on Model I cracking and it has been assumed that the principal stresses do not rotate after the fracture has initiated. In the discrete crack models the stress exerted across the crack after initiation is assumed to be perpendicular to the crack. In the crack band model the direction of principal tensile stress which causes initiation is maintained throughout the cracking process. There are cicumstances where these simplifications are not justified, for example curved crack paths (Jeang & Hawkins, 1985) or non-proportional loading. In such cases shear transfer must be allowed for as well as traction transfer. Models for these conditions have been suggested by Wium, Buyukozturk & Li (1984a&b), Jeang & Hawkins (1985) and Bazant & Oh (1985). None of these models has been properly verified and their discussion is beyond the scope of the present work.

One further drawback, implicit in the fictitious crack model and adopted by several other models, is the interpretation of the results of direct tensile tests to give basic material parameters. It is assumed that each infinitesimal volume of the material behaves in exactly the same way as the overall response of a specimen in the direct tensile test (Gustafsson, 1985). This is unlikely to be correct since the degredation of the material would probably not be uniform throughout the cross-section of the test piece. The tensile strength of all parts of the material is not reached at exactly the same stage, consequently the results provide some form of statistical average of the material properties. The same approximation is made when assuming

that the fracture energy is a material property. Ideally, very small specimens should be used, however, a specimen whose maximum dimension is less than approximately 3 times the maximum aggregate size cannot be considered to be suitable for testing the macroscopic behaviour of concrete. Reinhardt (1985) demonstrated that the responses of specimens of differing cross-sections were not the same. In the same way that strain softening can be considered as a localisation within the length of a specimen, the present problem may be considered as an initial localisation within the cross-section.

The models vary considerably regarding the size of the fracture process zone. The fictitious crack model assumes the opening of a zone whose initial width was zero. Gylltoft (1984) assumed a very narrow initial zone, whereas the crack band model assumes uniform degradation of the material within a finite width which can be taken to be three times the maximum aggregate size. None of these assumptions has yet been shown to be a realistic model of the fracture process zone.

2.5 Summary

The application of linear elastic and non-linear fracture parameters, continuum theories and fracture process zone models to the fracture of concrete has been discussed. The majority of the theories examined have some application to concrete structures, however, the breadth of that application depends on the ability of the theory to model the non-linear fracture processes which occur. A common theme throught the discussion has been the effect of structural size on the results obtained. Linear elastic fracture mechanics can only be applied to structures which are large compared with the fracture process zone. The minimum size of such a structure is a matter for debate but it is likely that the majority of structures and certainly most laboratory specimens are too small for linear elastic fracture mechanics to be applicable.

Non-linear fracture mechanics parameters and models are more widely applicable since they are able to reflect more closely the non-linear fracture processes. Similarly, continuum theories and models, which are formulated in such a way as to be able to model strain softening reasonablly well, can also be applied to structures of most common sizes. The current difficulty is in obtaining realistic material parameters for use in these theories.

The material parameters for both non-linear fracture mechanics and continuum mechanics have been obtained from the load/displacement graphs for stable direct tensile tests. It is assumed that the fracture process zone opens equally across the whole cross-sectional area of the specimen. It is by no means certain that this does, in fact, happen and it is suggested that lateral localisation of the strain field may occur as well as longitudinal localisation. Given the heterogeneity of the material it would not surprising if some areas begin to fail before others. It is known that, due to the longitudinal strain softening, the length of a specimen effects the shape of it's load/displacement relationship. Similarly, it is expected that the cross-section and lateral localisation within the specimen will also effect the load/displacement relationship. If this effect is

significant, it will not be possible to use this relationship as a material property since a change in size would require a change in material properties. It is necessary, therefore, to look in greater detail at the propagation of the zone of localisation across the specimen. It would be possible, in theory, to evaluate the effects of the lateral localisation by comparing the load/displacement relationships for specimens of differing cross-sections, however, as the specimen cross-sectional area increases the testing machine stiffness requirements become more stringent (Section 3.2). Gopalaratnam & Shah (1984&5) attempted such tests, but there is some doubt regarding the validity of their specimen dimensions (Section 2.2.2.3.2).

It would be of interest to investigate some of the areas of uncertainty highlighted in this review of theoretical models for the fracture of concrete. These might include:

1. The stage at which crack initiation occurs.
2. The size of and strain distribution within the fracture process zone.
3. The unloading of material outside the zone.
4. The possibility of crack branching or the formation of secondary zones of high strain.

It is suggested that these questions may be most successfully resolved using direct tensile tests and, for this reason, the application of such tests to concrete is reviewed in Chapter 3.

Chapter 3 Review of direct tensile testing of concrete

3.1 Introduction

Until the 1960's concrete was assumed to be brittle in tension. Up to this time, testing was concerned primarily with the determination of elastic properties and tensile strength. The full tensile properties were not considered to be of major importance to the design and performance of concrete structures and this, combined with the significant difficulties in conducting direct tensile tests, led to the concentration of research effort in areas other than tensile testing. Since that time interest in the tensile fracture properties of concrete has significantly increased due to the following factors:

1. The application of linear elastic fracture mechanics to concrete by Kaplan (1961) opened a new area of research which has led to a greater understanding of the role of the tensile properties of concrete undergoing fracturing.
2. The use of linear elastic fracture mechanics principles in the analysis of large concrete structures such as dams and prestressed concrete pressure vessels (Carmicheal & Jerram, 1973) has demonstrated the potential usefulness of this approach.
3. The demonstration a significant post-peak portion of the load/deformation curve obtained from stable direct tensile tests (Hughes & Chapman, 1966a&b; Evans & Marathe, 1968; Heilmann, Hilsdorf & Finsterwalder, 1969).
4. The availability of servo-controlled testing machines allowing a wider range of tests to be conducted.
5. The use of increased sophistication in the non-linear analysis of concrete structures using finite element computer programs, demanding a greater knowledge of the tensile properties of concrete.
6. The application of non-linear analyses to both reinforced and mass

concrete structures to study the deflection, energy absorption, ductility, crack growth, shear strength, size effects and behaviour under cyclic loading of such structures.

During this period of development, various different test techniques have been used to study the tensile properties of concrete. These were discussed in Chapter 2. Recently greater interest has been shown in stable direct tensile tests. Hannant (1972) attributed this to the fact that all other test techniques required assumptions to be made regarding the elasticity or plasticity of the material in order to obtain the fracture stress, whereas the direct tensile test does not require the use of such assumptions. Reinhardt (1984) suggested that if a small specimen was used in a stable direct tensile test then the fracture processes would develop uniformly over the whole cross-section so that the average stress/deformation curve for this fracture zone could be considered to be characteristic of the material. This material property could then be applied to the zone ahead of a crack to determine it's characteristics. This may be a simplification, however, the majority of non-linear fracture models are based on the results of direct tensile tests using this simplification. The other tensile test techniques require even greater assumptions to be made in order to obtain usable data for non-linear fracture models.

Despite the fact that the stable direct tensile test is possibly the most difficult of the tensile tests to perform, it has been selected for the current project. The test can yield information on the initiation and propagation of cracks in concrete and also the stress transfer across an opening crack without the need for assumptions regarding the behaviour of the material outside the fracture zone. The other tests, which involve more complex stress fields do not yield such direct data concerning the fracture processes and are, therefore, not likely to be so useful. The secondary reason for the choice of this test technique is to enable an assessment to be made of Reinhardt's suggestion of uniform fracture processes across the specimen. Since this is the basis of the majority of non-linear fracture models it is important that the extent to which it is valid be identified.

The published literature on the complete load/deformation response of concrete subjected to direct tension is scarce and sometimes conflicting. However, the existance and general form of the post-peak softening response is generally accepted (Fig. 3.1b). The following factors, which will effect the measured response, have varied from one test series to another and must be taken into account when evaluating the test results and their applicability to the material within the body of a structure.

1. The type of testing machine used to ensure stable failure.
2. The means by which the specimen is held in the machine.
3. The shape of the specimen.
4. The strain measurement technique.
5. The crack detection and crack width measurement techniques.
6. The moisture state of the specimen during curing and testing.

Examples of the more recent test data are shown in Figure 3.1. Stress/strain curves are drawn in Figure 3.1a, which can be seen to be fairly consistant before the maximum load is reached but to vary considerably in the post-peak portion. If the stress is plotted against extension rather than strain (Fig. 3.1b), then the agreement between the curves up to the maximum is no longer so good, however, the variation post-peak is significantly reduced despite the different concrete qualities used. One of the main factors which may be expected to affect the post-peak shape of the curve is the size of the aggregate used. This varied from 16mm. (Eligehausen & Sawade) to 5mm. diameter glass spheres (Terrien). The agreement between the curves may be improved by plotting the stress against the opening of the fracture process zone (Fig. 3.1c). This latter figure is based on the assumption that the total extension is made up of two parts, that due to the elastic deformation outside the fracture process zone and the opening of the zone (see, for comparison Figures 2.22 and 2.23). The differences between Figures 3.1a, b and c, demonstrate the importance of understanding the effects of localisation when taking measurements across fracture process zones. Strain or extension, without a knowledge of gauge length, is meaningless. It seems that the ascending portion of the curves is best described in terms of stress and strain, whereas the descending portion is characterised by an elastic unloading of the material outside the fracture zone together with a

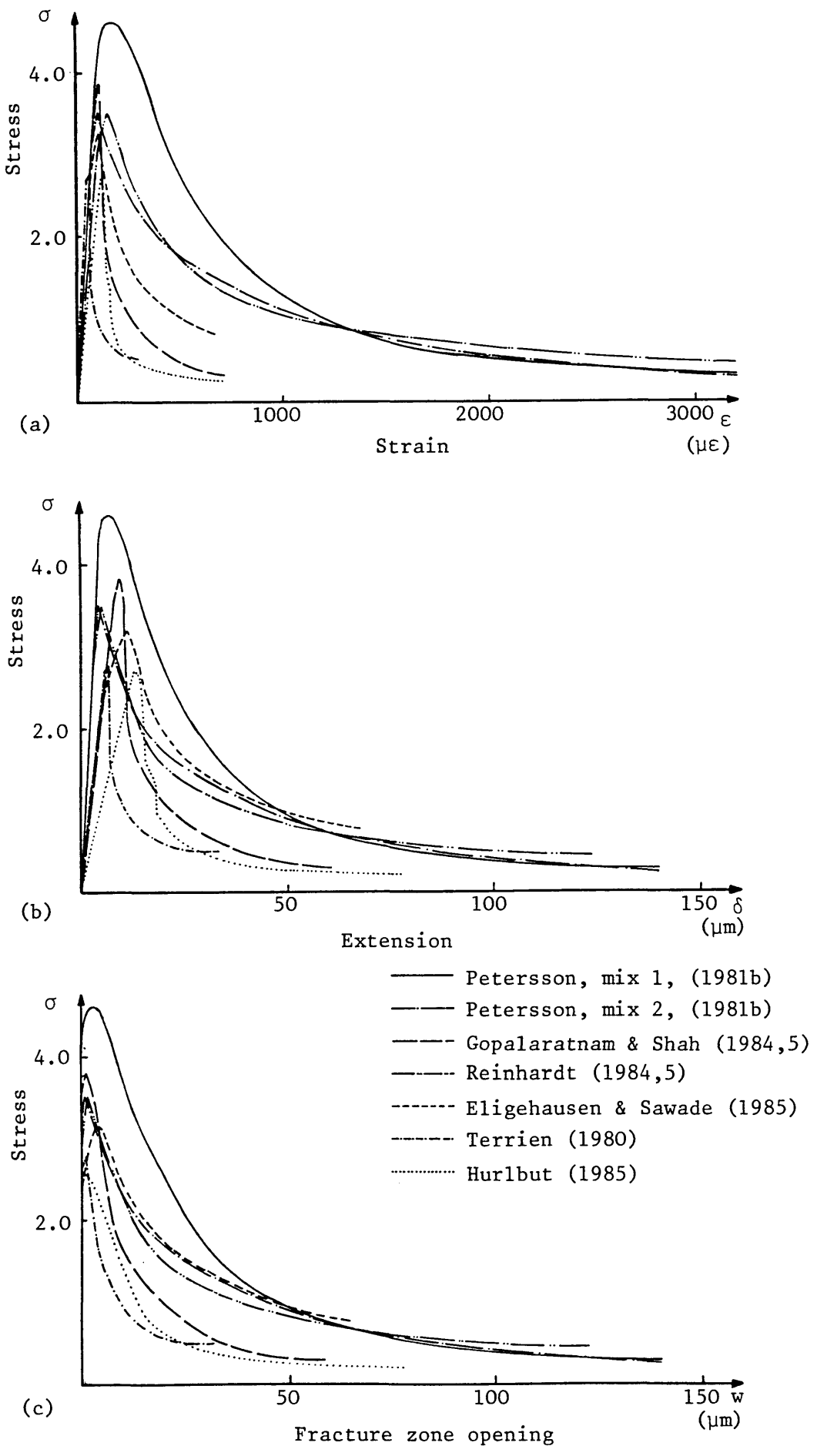

Fig. 3.1 Direct tensile test results
(a) Stress/strain relationship
(b) Stress/extension relationship
(c) Stress/fracture zone opening relationship

stress/fracture zone opening relationship. Fracture initiation and localisation may possibly be regarded as providing the transition between these two behavioural regimes, although the stage at which fracture initiates is not yet clear.

In the next section the requirements for stable direct tensile tests will be discussed. Section 3.3 will review the testing techniques which have been used by other researchers, Section 3.4 will discuss the results obtained and Section 3.5 will comment on these tests. In general, stable tensile tests will be discussed with reference to unstable tests only where necessary.

3.2 Requirements for stability in direct tensile tests

Stable failure at the structural dimensional level, is defined as gradual opening of the fracture process zone without any sudden releases of energy resulting in kinetic effects. The opening of the zone results from cracking at a micro-structural level as can be detected by acoustic emission. This micro-cracking may be brittle and have some kinetic effects, however, this is contained within the bulk of the surrounding material so that the behaviour is stable at the structural level. For stable failure to occur using a quasi-static testing machine, two conditions must be satisfied. Firstly, the loading applied to the specimen must, in effect, be controlled by extension rather than applied load. Secondly, the sum of the stored elastic strain energy release rates for the testing machine, specimen grips and specimen must be less than the energy rate required for the fracture zone opening. The first condition may be met in any of the following three ways:

1. A load controlled testing machine with stiffeners in parallel with the specimen in such a way that the sum of the stiffnesses of the specimen and stiffeners is always positive.
2. An indirect, extension controlled testing machine in which the extension of the specimen is controlled by some parameter other than applied load. An example of this would be the machine designed by Petersson (1981b) in which the extension of the specimen was controlled by the temperature of aluminium columns in parallel with the specimen.
3. A servo-controlled testing machine using any control signal which increases with opening of the fracture zone.

The second condition is met when the combined stiffness of the testing machine, specimen grips, the unloading portions of the specimen outside the fracture zone and any parallel stiffeners is greater than the maximum descending stiffness of the load/fracture zone opening relationship. This latter stiffness is equal to the product of the area of the specimen and the steepest slope of the curves shown in Figure 3.1c. Assuming that the portions of the specimen outside the

fracture zone are elastic, Petersson (1981b) showed that, for a prismatic specimen, this condition becomes:

$$1 < -\frac{E}{\left(\frac{\partial\sigma}{\partial w}\right)_{min}} - \frac{A\,E}{(k_1 + k_2)} \qquad (3.1)$$

Where 1 = length of specimen

E = Young's modulus

A = cross-sectional area of specimen

k_1 = testing machine stiffness

k_2 = paralled bar stiffness

$\left(\frac{\partial\sigma}{\partial w}\right)_{min}$ = greatest descending stiffness (negative) of the curves shown in Figure 3.1c.

If a necked specimen is used, this upper limit should be multiplied by the ratio of the overall specimen stiffness to the stiffness of a prismatic specimen of the same length and with a cross-sectional area equal to A. A is now the cross-sectional area at the neck.

Should there be any flexibility in the specimen grips Equ. 3.1 would become:

$$\frac{1}{k_s} < -\left(\frac{1}{A\left(\frac{\partial\sigma}{\partial w}\right)_{min}} + \frac{1}{k_1 + k_2} + \frac{1}{k_g}\right) \qquad (3.2)$$

where k_s = Specimen elastic stiffness

k_g = Specimen grip stiffness

For an infinitely stiff machine with no flexibility in the specimen grips, Equ. 3.2 may be re-written:

$$k_s + A\left(\frac{\partial\sigma}{\partial w}\right)_{min} > 0 \qquad (3.3)$$

Alternatively, the upper limit occurs when the descending portion of the graphs in Figure 3.1b become vertical.

The conditions for stable failure described above are for a quasi-static testing machine. It has been suggested (Gylltoft, 1983; Gustaffson, 1985) that with the dynamic reaction of a suitable servo-controlled machine the limits on the specimen and machine stiffness could be relaxed. However, this suggestion is based on the assumption that the machine could react and reduce the applied load more quickly than the fracture zone would shed it's load. The speed of propagation of a fracture zone across an unstable direct tensile specimen is unknown but might be at least 100m/s. If this is correct, for the specimens of the present project, the machine would have to respond in less than 0.6 milliseconds. This reaction time would have to allow for an electrical response signal, opening of the servo-value, flow of oil into and out of the actuator chambers and elastic unloading of the machine, grips and specimen outside the fracture zone, together with associated inertial effects. It seems unlikely that any available mechanical system could respond at this rate and that, therefore, the limits on specimen and machine stiffness described above continue to be applicable.

A similar suggestion (Gopalaratram & Shah, 1984,5) is that it may be advantageous to use the opening of a notch or a small portion of the specimen rather than the extension of the whole specimen as a feedback signal for the servo-control. Again, this will not assist the stability of the failure but may have advantages with regard to reducing the creep occurring within the fracture zone with unloading of the adjacent material.

3.3 Review of testing techniques

3.3.1 Specimens

Three basic specimen geometries are used for direct tensile tests; prismatic, necked and notched. Some of the specimens described in the literature are shown in Figure 3.2. Prismatic specimens can fail anywhere within their length, however, the stress perturbations caused by whatever technique is used to fix the specimen to the machine (Section 3.3.3) frequently cause premature failure at one end of the specimen. Failure can be forced to occur at any given cross-section by the introduction of notches. This has the advantage that the position of the failure cross-section is known in advance so that strain gauges etc. may be most effectively positioned. The disadvantages of notched specimens are that in forcing the failure at one cross-section, the statistical scatter of strength within the specimen is ignored and also that stress concentration effects around the notch tip are introduced which are not fully understood. Gopalaratnam & Shah (1984,5) obtained similar load/extension curves for both notched and prismatic specimens suggesting that concrete is not notch sensitive for notches of the depth used (13mm). Petersson (1981b) came to the same conclusion when comparing notched and necked specimens but both references do show a slight reduction in tensile strength for notched specimens. Necked specimens can be used to avoid the uncertainty regarding notch sensitivity and also can allow the concrete to fail at any section within the central portion of the specimen, wherever the material is at it's weakest. Naturally with necked specimens, the position of failure is less well defined in advance and, as suggested by Cedolin, Dei Poli, & Iori (1983), it is possible that more than fracture process zone may develop in parallel.

The maximum size of the specimen is determined by the stability criteria stated in Section 3.2. The minimum size of the specimen should be designed to ensure that it represents normal concrete. This is usually done by using a minimum dimension of at least 3.5 times the maximum aggregate size. Most tests have complied with this minimum,

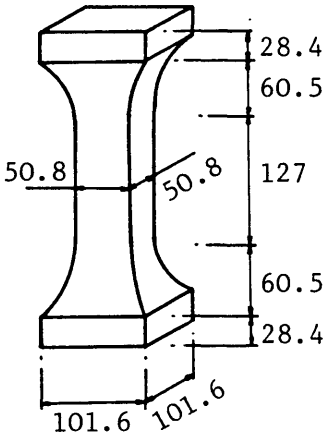

(a) Hughes & Chapman (1965)

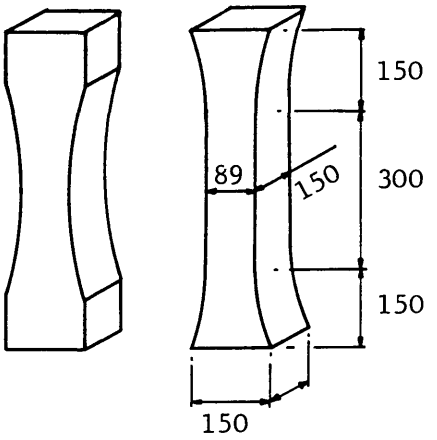

(b) Heilmann, Hilsdorf & Finsterwalder (1969)

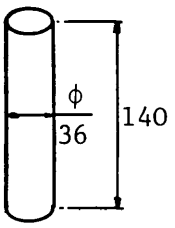

(c) Terrien (1980)

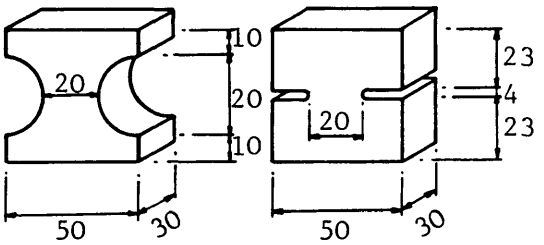

(d) Petersson (1981b)

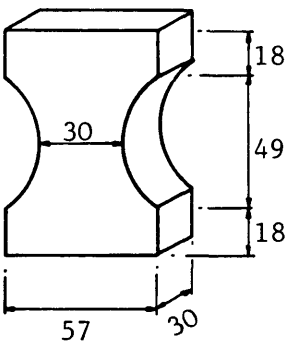

(e) Gylltoft (1983)

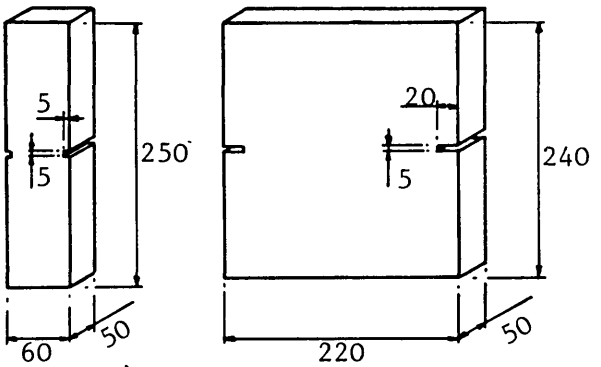

(f) Reinhardt (1984)

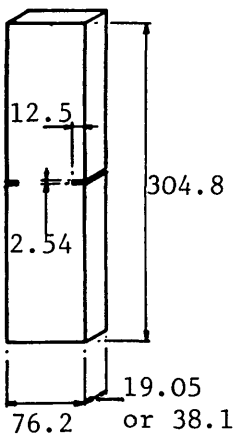

(g) Gopalaratnam & Shah (1985)

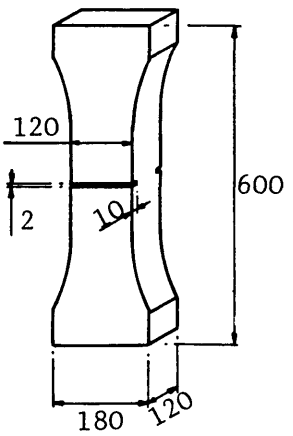

(h) Elighausen & Sawade (1985)

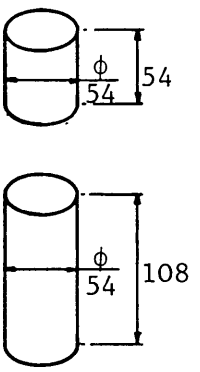

(i) Hurlbut (1985)

Fig. 3.2 Direct tension specimens (dimensions in mm.)

however, Petersson (1981b) used a ratio of 2.5 and Gopalaratnam & Shah (1984,5) used 2.0. Caution must be excersised when interpreting these results and it is interesting to note the significant difference between the results of the latter paper and the other graphs in Fig. 3.1b. The majority of tests assume that the deformation distribution is constant over the whole cross-section, which means that the fracture process zone should spread uniformly. However, this may not in fact occur and Reinhardt (1984,5) suggested keeping the cross-section as small as possible (given the above minimum dimension requirement) in order to keep the deformation as uniform as possible.

The moisture condition of concrete is important when considering the tensile properties. Cady, Clear & Marshall (1972) have demonstrated significant variation in strength with moisture gradients induced by drying at elevated temperatures. These effects would be reduced if drying occurred more slowly at room temperature and the moisture state was allowed to reach equilibrium. However, drying shrinkage would still occur leading to a reduction in strength (Elvery & Haroun, 1968; Petersson, 1981b; Carreira & Chu, 1986). If there is a requirement to produce specimens which are similar to concrete within the body of a structure then they should be sealed as soon as possible after casting, to prevent either moisture loss or gain. Specimens stored under water will absorb water and swell and this cannot be representative of concrete in most structures. Of the recently conducted tests in which the curing conditions were specified, Eligehausen & Sawade (1985) and Reinhardt (1984,5) allowed their specimens to dry at 20 degrees C and 60% Relative Humidity prior to testing, whereas Petersson (1981b) and Gopalaratnam and Shah (1984,5) stored the specimens in lime saturated water until the time of the test. Terrien (1980) tested both moist and dry specimens and found significant differences both in Young's modulus (greater for moist specimens) and tensile strength (greater for dry specimens).

One further variable regarding the specimens is the orientation during casting. Unless special precautions are taken, there will be a variation of material properties in the direction of casting due to bleeding, segregation and rising entrapped air. This is unimportant if the specimen is tested with the tension applied in the direction that was vertical during casting. On the other hand, with the tension

applied perpendicular to this direction, the fracture will initiate preferentially on the side which was uppermost when cast. In the literature the only specimens stated as being cast in the reclining position were those of Eligehausen & Sawade. This may account for the greater pre-peak non-linearity observed in these tests (Fig. 3.1c).

3.3.2 Loading Machine

Various types of machines have been used for direct tensile testing of concrete. The requirements demanded of these machines with regard to the stability of the test have been presented in Section 3.2. The standard testing machines commonly used for materials testing were found to be too flexible to be able to follow the descending portion of the load/extension curve of concrete in tension. In the early stable tests, this was overcome by loading stiffeners in parallel with the specimen. Equation 3.1 shows that the stiffeners add to the overall machine stiffness. Hughes & Chapman (1966a&b) used a standard 100 ton universal testing machine. To obtain the required overall stiffness, they placed a steel block in the compression testing space whilst the concrete specimen was being strained in the tension space. In this case the sum of the stiffnesses of the specimen and stiffener would always have been positive so that the extension of the specimen could be controlled by the applied load. Evans & Marathe (1968) also modified a 100 ton testing machine but this time with bars in parallel with the specimen. Heilmann, Hilsdorf and Finsterwalder (1969) obtained a few stable, direct tensile tests with a purpose built machine, although most of their specimens failed in an unstable manner. The specimen was glued between two end blocks. The blocks were separated, extending the specimen, using three hydraulic jacks, which also worked against tension bars giving the required stiffness. The loads in the jacks could be independently controlled so that either uniaxial or eccentric loading could be applied to the concrete.

A new type of stiff testing machine was devised by Petersson (1981b). Three aluminium columns were fixed between two concrete blocks and heating elements attached to the columns. The specimen was held

between the two blocks. The aluminium expanded when heated leading to extension of the specimen. The load applied to the specimen was measured by strain gauges attatched to one of the specimen end pieces. The columns could also be cooled allowing unloading of the specimen.

More recently, stiff closed loop servo-controlled testing machines have been used. The control signal can be any signal that increases with the opening of the fracture zone. This may be either the displacement of the actuator, the extension of the specimen or the extension of a portion of the specimen within which the fracture occurs. Gopalaratnam and Shah (1985) have commented on the importance of using an appropriate signal. They used the average signal from two extensometers placed on either side of the specimen. With the use of only one extensometer unstable failure could result if the fracture initiated at the notch on the other side of the specimen. It should be noted, however, that this implies a significantly greater opening on one side of the specimen compared with the other and relative rotation of the two halves of the specimen. This was allowed to happen since there were universal joints at the connections of the specimen to the machine. This condition cannot be considered to be representative of the material within the body of a structure as described in the following section. The use of servo-controlled testing machines is discussed in greater detail in Chapter 4.

3.3.3 Connection of specimen to machine

The means by which the specimen is connected to the testing machine for direct tensile tests is extremely important and will affect the results obtained. In an inquiry to various testing laboratories RILEM (1963) discovered four commonly used techniques:

1. Steel pieces cast into the ends of the specimen.
2. Clamping by means of wings or truncated cones.
3. Scissor grips or lateral clamping.
4. Sticking by means of adhesive.

All four techniques cause some disturbance of the stress field near to the ends of the specimen. The reasons for this disturbance are obvious for the first three techniques. In the adhesive technique the disturbance is caused by the differences in elastic properties of the concrete, adhesive and steel (Section 4.2). Hurlbut (1985) observed that fracture occurred within 1.0 inch of the ends of his prismatic specimens and, in order to produce failure remote from the ends, it is normal either to neck or notch the specimen. The other main difference between the various tests in the literature is in the articulation of the specimen connections. Hughes & Chapman (1966a) allowed rotation about one axis at the connections, whereas Gopalaratnam & Shah (1984,5) used full universal joints at both connections. Rotation at the connections allows self alignment of the specimen such that the centre of stiffness of the specimen is always on the line of action of the load. This might initially seem to be an advantage, however, it is not realistic for material within the body of a structure which cannot align itself in the same way. It is more realistic to prevent rotation of the ends of the specimen such that when, due to material heterogeneity or localised fracture initiation, the centre of stiffness shifts, restraining moments are applied to the ends of the specimen. In this case the boundary conditions for the specimen are controlled separation of the ends which are maintained parallel to one another. Petersson (1981b) applied this restraint using the bending stiffness of the connection pieces. Strange & Bryant (1979) used four "controlling arms" loaded in parallel with the specimen to reduce end rotation and Reinhardt (1984,5) provided a guiding device to the same end. Gylltoft (1983) suggested that the tensile strength measured when allowing end rotation would be reduced due to the stress gradients created.

3.3.4 Deformation and crack width measurement

Most tests have depended on either strain gauges or linear variable differential transformers (LVDTs) for the measurement of strain and crack opening. Unfortunately these techniques only yield average strain or relative displacement across the gauge length and, unless a very large number of gauges is used, only limited information regarding the localisation of strains is obtained. In order to ensure that the failure occurs within the gauge length, either long gauges or a large number of short gauges must be used or, alternatively, the specimen must be notched. Gauges placed on either side of the failure zone give information regarding the elastic unloading accompanying post-peak behaviour. A combination of the readings of gauges across the failure zone and those on either side can provide measurements of the overall opening of the fracture zone but do not give any information regarding the width of the zone or the distribution of strain within the zone. Gopalaratnam & Shah (1984,5) used an optical microscope to measure the crack width and showed that practically all the non-linear displacement during the post-peak response was due to the opening of a single crack. This suggests that there is little non-linearity either side of the crack once it has formed but no information is obtained regarding the strains prior to discrete crack formation. Eligehausen & Sawade (1985) used a flourescent dye to detect cracks of widths greater than about 0.001mm.. Cracks were detected at, or just before, maximum load and became visible to the naked eye when the load reduced to about 30% of the maximum. Branching cracks were occasionally observed. In contrast, Evans & Marathe (1968) detected cracks during the ascending portion of the curve when the load was only 68% of the maximum.

Cedolin, Dei Poli & Iori (1981,3) used a full field strain measurement technique known as moire interferometry to observe the development of fracture process zones in concrete in tension. This technique is discussed more fully in Chapter 5. Unfortunately, stable failure was not achieved but significant localisation prior to failure was observed. Single notched, double notched and necked specimens were used. The propagation of the fracture zone could be monitored in the notched specimens, particularly those with only one notch which, in

effect, had an eccentrically applied load. In the notched specimens, fracture zones only occurred at the cross-section which included the notches. However zones of high localised strain occurred in several parts of the necked specimen. The line of final separation passed through one of these zones.

3.4 Results of stable direct tensile tests on concrete

Due to the scarcity of reported test results and the diverse nature of the test techniques used, it is difficult to draw any firm conclusions regarding the deformation of concrete in direct tension. The existance of the descending portion of the load/extension curve is now without doubt, however, the following conclusions can only be regarded as tentative at this stage:

1. The initial tangent modulus is the same in tension and compression.
2. Cracks can be detected at, or before, maximum load and are visible to the naked eye at a load of approximately 30% of the maximum, on the descending portion of the load/extension curve.
3. The strain at maximum load is of the order of 90 - 140 microstrain for normal weight concrete and approximately 180 microstrain for lightweight aggregate concrete.
4. After the maximum load is reached the stress is carried by a combination of aggregate interlock and unbroken ligaments of the matrix.
5. No unique stress/strain relationship exists for concrete undergoing strain-softening, rather, an average stress/average crack opening relationship seems more appropriate.
6. The softening response is related to the opening of a single crack with occasional branching.
7. The crack passes round aggregate particles which are stronger than the matrix but passes through weaker aggregate.
8. The envelope within which load/extension curves lie is not significantly affected by load cycling.
9. The tensile strength and fracture energy increase with increasing age and with a decrease in water/cement ratio. These parameters are also dependent on the composition of the concrete, particularly the type of aggregate, but the nature of the dependence is not yet clear.
10. It is necessary to make a realistic assumption regarding the shape of the long tail of the softening branch of the load/deformation curve, when calculating the fracture energy (G_f). None of the

tests continued to the point where the tensile stress reduced to zero. Reinhardt (1984) fitted a curve to the unloading branch and calculated that G_f = 132 N/mm^2. Using a modified curve for the same data, Cornelissen, Hordijk & Reinhardt (1985a) calculated that G_f = 100 N/mm^2.

11. For a true measurement of the fracture energy, the test must be stable.

3.5 Comments and requirements for further work

In the previous section some tentative conclusions were drawn regarding the fracturing of concrete in tension. These were based on a limited number of test series with considerably different test techniques. Some of the assumptions made, and test techniques used, are doubtful and the purpose of the present project is to develop an improved test based on the information available from the previous work. This is necessary to ensure a suitable basis for non-linear fracture models to be used in the analysis of concrete structures. Wider application of such analytical techniques is only possible if the models are based on a correct understanding of the test results.

There are several requirements for the new test as follows:

1. The testing machine shall be capable of loading the specimens in such a way that the extension can be controlled and that stable failure occurs. This can be achieved by ensuring that the requirements of Section 3.2 are fulfilled.
2. The specimens shall have a minimum dimension of 3.5 times the maximum aggregate size and shall be cast such that the tension can be applied in the direction of casting.
3. Moisture migration into, or out of, the specimen shall be prevented from the time of casting until after the test.
4. The stress purtabations at the ends of the specimen shall be minimised and the specimen designed such that failure occurs within the body of the specimen but is not forced to occur at any predetermined section.
5. The specimen shall be loaded in uniaxial extension such that it's ends are restrained against rotation.
6. A full field strain measurement technique shall be used to provide information regarding the initiation and propagation of fracture process zones in the specimen. The opening of the fracture process zone shall also be measured.

In the analyses of the test series reported in the literature, it was assumed that, for narrow specimens, the opening of the fracture zone

was uniform across the width of the specimen and that, consequently, the average stress/average crack opening relationship was a material property. It can be seen from the results given by Reinhardt (1984,5) that, for the portion of the curve just past the peak stress, this was not true. The fracture zone initiated on one side of the specimen before propagating across the full width. At peak stress there was a slightly greater opening on one side, but at the point where the stress had dropped to 75% of the maximum, the opening on one side of the specimen, was approximately 2.2 times the opening on the other side. The fracture zone opening did not become uniform again until the stress had dropped to 30% of the maximum, when the opening was 35 microns. Hence the load/extension curve for the test cannot be considered to be representative of the material but some account must be taken of the propagation of the fracture across the specimen. Full field measurement of strain would allow a greater understanding of the fracture process zone propagation and would provide a more suitable basis for the analysis of the test results.

Chapter 4 Development of the direct tensile test technique

4.1 Introduction

In Chapter 3, the direct tensile tests in the published literature were reviewed. It was shown that there were drawbacks with all these tests and that consequently only tentative conclusions could be drawn regarding the fracturing of concrete in tension. Section 3.5 described the ideal requirements for a new tensile test. In practice, the design of the test must take into account the layout of the laboratory, any equipment available, financial restrictions and the time needed for development, as well as the more theoretical requirements listed in that section. A direct tensile test has been developed and those parts of the technique concerned with achieving controlled stable failure are discussed in this chapter. The full field strain measurement technique is discussed in Chapters 5 and 6. Section 4.2 outlines the choice of specimen size, shape and moisture state as well as it's connection to the testing machine. Section 4.3 discusses various possible testing machine arrangements, initial trials and the system finally adopted. A significant proportion of the development time was devoted to control systems for the servo-controlled testing machine used and this is discussed in Section 4.4.

4.2 Specimens

The design of appropriate specimens and their connection to the testing machine is crucial when developing stable, direct tensile tests for concrete. The requirements for the current project are as follows:

1. The concrete shall, as far as possible, reflect that used on construction sites. This puts limits on material types and sizes and on workability.
2. The minimum specimen dimension shall be least 3.5 times the maximum aggregate size to ensure that the specimen is representative.
3. The shape of the specimen shall be designed to allow the selected full field strain measurement to be used.
4. The overall specimen stiffness shall be such that, when combined with that of the particular testing machine, the requirements of Section 3.2 are fulfilled so that failure occurs in a stable manner.
5. The specimen shall be cast in a manner that allows the tension to be applied in the direction which was vertical during casting.
6. Moisture migration either into, or out of, the specimen shall be prevented from the time of casting until after the end of the test.
7. The stress perturbations at the ends of the specimen shall be minimised, and the shape of the specimen designed such that failure occurs remote from the ends but not at any predetermined position.
8. The ends of the specimen shall be restrained against rotation.

Of the various possible specimen connection details described in Section 3.3.3, the only one already available in the laboratory was the scissor grip designed by Ward (1964). He commented that the adhesive technique would be better but that there were no suitable adhesives available at that time. For the present project, where machine stiffness is very important, and also for which rotational restraint of the ends of the specimen is required (Section 3.3.3), the scissor grips are not suitable. The use of the adhesive would also seem to minimise the perturbations in the stress field and consequently this technique was chosen in combination with a necked

specimen to ensure failure within the body of the specimen.

A large number of adhesives were tested for adhesion to damp concrete. By definition sufficient adhesion was achieved if, when loaded, the concrete failed rather than the adhesive. Since the early work of Hughes & Chapman (1965) which required the development of a suitable adhesive, adhesive technology has significantly improved and several adhesives for use with damp concrete are now available. The adhesive finally chosen was Sikadur 31, Rapid grade, supplied by Sika Ltd.. This is a filled, two part epoxy resin specially formulated for use in the construction industry. Most epoxy resins cannot be used in the presence of moisture since the hardener combines preferentially with the water rather than with the resin. In the material used this is not so. The filler is added to the material in order to reduce it's shrinkage. One drawback of this material is that it requires approximately 18 hours to gain sufficient strength for the test. Since it is not possible to actuate the testing machine after sticking the specimen to the plattens (Section 4.4.2.2.2), and it was considered impractical to leave the machine running during the adhesive cure (as was done by Hurlbut (1985)), it was necessary to stick small steel end plates onto the specimen. These plates could then be stuck to the machine platens using Loctite Multibond 330, a cyanoacrylate adhesive which gained sufficient strength in 45 minutes. This latter adhesive layer also catered for any lack of parallelness in the end plates and platens.

The maximum length of the specimen is dependent on the testing machine stiffness, the maximum unloading slope of the stress/crack opening curve for the specimen, the cross-sectional area of the neck and the severity of the necking (Section 3.2). The first two parameters were unknown and the specimen length and overall cross-section had to be estimated from the information provided by Petersson (1981b). The 250mm. long, 100mm.x100mm. specimen was originally designed for use with 20mm. aggregate and was necked to 100mm.x75mm.. The was subsequently reduced to 75mm.x75mm. and then to 60mm.x60mm.. The reason for this reduction in neck cross-section was that with the original neck a significant proportion of premature failures occurred adjacent to the adhesive. These premature failures were caused partly by incompatability of the elastic properties of the concrete, adhesive

and steel end plates. This effect was first described by Hughes & Chapman (1965). The unrestrained lateral strain of each of the three materials depends on the ratio of Poisson's ratio to Young's modulus. The ratios of these strains are approximately 1 : 80 : 5 for steel : adhesive : concrete. If the adhesive layer is thin then the effect of the steel on the concrete is significant, the concrete is restrained from lateral contraction and is subjected to an outward shear stress. The shear stress combined with the axial tensile stress increases the principal tensile stress leading to failure in the concrete adjacent to the adhesive. As the adhesive layer becomes thicker the shear stress reduces eventually changing sign. Hughes & Chapman assumed that there was some critical thickness at which the shear stress became zero. This is an oversimplification of a complex three dimensional problem and in an attempt to understand the stress distribution more clearly, a simplified two dimensional elastic model of the adhesive layer has been studied. The details of the analysis are given in Appendix A. The results can only be taken as a guide but they suggest a significant reduction in principal tensile stress, with increase in adhesive layer thickness of up to 5mm.. Beyond this the reduction is much less pronounced. The adhesive layer thickness, originally 1mm. was increased to 3mm. and then to 4.7mm. in order to reduce the outward shear stresses.

As an alternative solution, aluminium end plates could have been used, the lateral strain of aluminium being similar to that of concrete. However, this might have led to elastic incompatability problems between the end plates and the steel platens with the possibility of failure at this adhesive interface. The other disadvantage with aluminium is that, being softer, the end plates would have been prone to damage during cleaning between uses.

As a result of the reduced neck dimensions the maximum aggregate size that could be used with the final specimen dimensions was 17mm.. The specimens for the present project were made with 10mm. aggregate. The rectangular or square shape of the cross-section was dictated by the full field strain measurement technique. The specimens were cast vertically in a pair of specially designed moulds (Section 7.2.1) and after stripping were sealed in polythene bags to prevent moisture migration.

There may also be effects, other than elastic incompatability, which promote premature failure at the ends of the specimen. For example, grinding may cause some damage to the ends of the specimen. It was also noticeable that the majority of premature failures occurred at the upper end of the specimen as cast. This is due to the reduced quality of the concrete near the top of the specimen. Whatever the causes of these failures, it was found that, with a cross-section of 60mm.x60mm. and an adhesive layer thickness of 4.7mm. they did not occur. With either a larger neck or a thinner adhesive layer premature failure sometimes occurred. The final shapes of the specimen and associated end plates are shown in Figure 4.1.

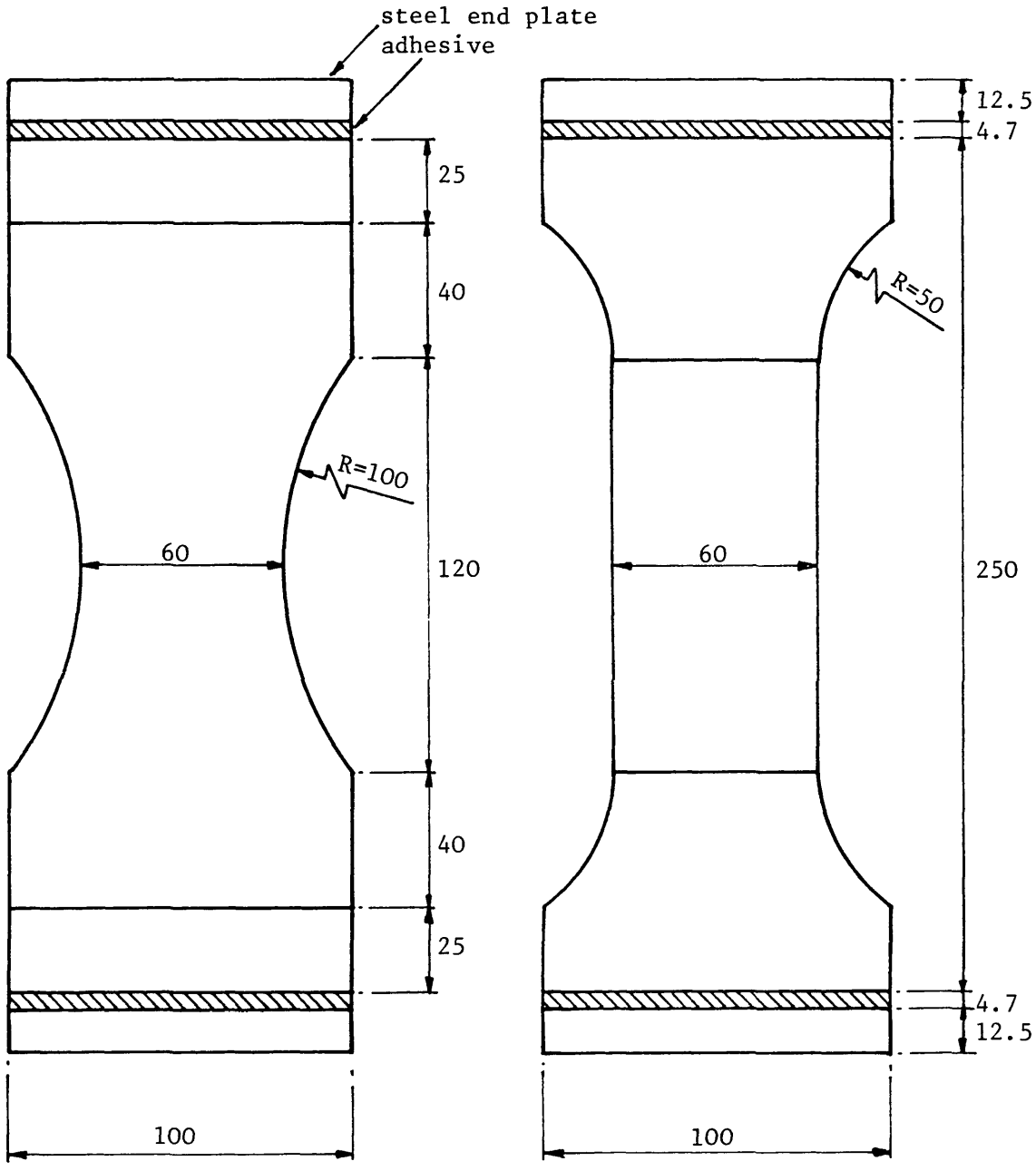

Fig. 4.1 Direct tensile specimen with end plates attatched (dimensions in mm.)

4.3 Testing machine

Section 3.2 described the testing machine requirements for stability in direct tensile tests, one of which was that the loading of the specimen must, in effect, be controlled by extension. This is most easily obtained using a servo-controlled machine. Such a machine was available in the laboratory at the start of the project and it was decided to attempt to use it, with some modification, for the tests. There remained three options for the use of this testing machine to obtain stable failure:

1. The use of the applied load as a control feedback signal with a stiff device loaded in parallel with the specimen. In this case the sum of the stiffness of the device together with the maximum negative stiffness of the specimen would have to be positive.
2. The use of the extension of the specimen, or part of the specimen, as a control feedback signal in combination with a stiff testing machine. The stiffness requirements when using extension control (Section 3.2) are less severe than those for load control and do not necessary demand that any device be loaded in parallel with the specimen.
3. The use of the dynamic response capability of the machine to 'freeze' the crack by unloading more rapidly than the specimen can unload itself due to fracture propagation.

The first option puts unnecessary stiffness requirements on the machine and was therefore rejected. The actuator available at the beginning of the project was double acting, with capacities of 100T in compression and 50T in tension. These capacities were much larger than required by the test, however, the construction of the actuator was extremely robust and as a result very stiff. Even though the hydraulic power pack could supply oil at 19 litres/minute, this would have been insufficient to allow such a large actuator to respond sufficiently quickly to 'freeze' the crack. Consequently, the first tests were conducted using this actuator in combination with a stiff testing frame. The frame was constructed using precast reinforced concrete

blocks prestressed to the laboratory floor in the form of an arch. The actuator was bolted to the floor under the arch and the specimens glued between the actuator and a plate bolted to the upper concrete block. It soon became apparent, however, that the friction in the actuator (approx. +/-1.0KN.) was too great to allow controlled loading of the specimen and also that a load cell rather than a differential pressure transducer would have to be used to measure the applied load. This might introduce excessive a flexibility and cause the failure to be unstable. It was therefore, decided that a different actuator was required.

In the design of the new actuator, several factors had to be taken into account. Firstly, in order to attempt to 'freeze' the crack the actuator had to respond extremely rapidly. This meant using the large flow capacities of the existing Hydraulic Power Pack and Servo-valve, together with an actuator with a small volume. Also, to reduce the response time the ram friction and inertial effects would have to be reduced. Unfortunately, the reduction in inertial effects would have led to a more flexible actuator which might have allowed to unstable failure to occur and so some form of compromise was required. The other main constraint on the actuator design was that of the project's finances, an 'off the shelf' actuator would have been significantly cheaper than one specially designed for the tests. As a result an 'off the shelf', 5T. equal area actuator was purchased. The large load capacity was chosen to allow for the use of additional stiffeners should they be required. The actuator was fitted within a similar stiff frame to that used for the larger actuator but, in the event, it was found that the dynamic response was insufficient to prevent unstable failure. Given the inadaquacy of this combination of a small actuator with a large flow capacity servo-valve and hydraulic power pack, it seems unlikely that any servo-controlled machine would be able to respond quickly enough to 'freeze' the crack. Section 3.2 also discusses the possibility of using dynamic response to 'freeze' cracks.

As described above, in order to obtain high speed dynamic response, the new actuator was of a much lighter construction than the original one. Unfortunately, this meant that new actuator was significantly more flexible and was unable on it's own either to produce stable

failure or restrain the rotation of the end of the specimen. These two drawbacks were overcome by fixing four steel bars in parallel with the specimen both to stiffen the test set up axially and to restrain rotation of the lower platten. The specimen assembly, together with the transducer measuring the extension of the specimen which also provided the feedback signal, is shown in Figure 4.2. The four parallel bars are strain gauged and the load on the concrete is calculated by subtracting the bar loads from the load applied by the actuator. The actuator load was measured using a differential pressure transducer such that the actuator friction was included in the measured load. Part of this friction occurred in the seals around the ram at the top and bottom of the actuator body. In order to improve the load measurement, the backing rings from the seals were removed resulting in a reduced contact between the seals and the ram, less efficient sealing and some loss of oil but also a reduction in the friction from approximately +/-0.3KN. to +/-0.15KN.. With this set up, shown in Figure 4.3, it was eventually possible to obtain repeatable stable failure. It should be noted that by the time this final test frame was built, it had become clear that moire interferometry would be chosen for the strain measurement and that, as far as possible, vibrations of the specimen should be reduced. The new frame was built on a different part of the laboratory floor which was independently supported on springs so as to be isolated from vibrations in the main floor. The hydraulic power pack, which itself caused significant vibration was left on the main laboratory floor.

The load and extension data were recorded using a Hewlett Packard data logger (Section 7.4.1). The data logger was programmed so that readings were taken either on demand or at given extension or time intervals. Measurement of the load applied by the actuator and the extension were available through outputs on the back of the Monitor Unit in the machine control console. The load taken by the bars was measured using the strain gauges on the bars and was subtracted from the total applied load to calculate the load applied to the specimen. The data logger reading cycle took approximately 3 seconds. In order to have continuous information on the load and extension, which was necessary during setting up of the test, the Monitor Unit outputs were also connected to a digital voltmeter to measure total applied load and a plotter to plot extension against time.

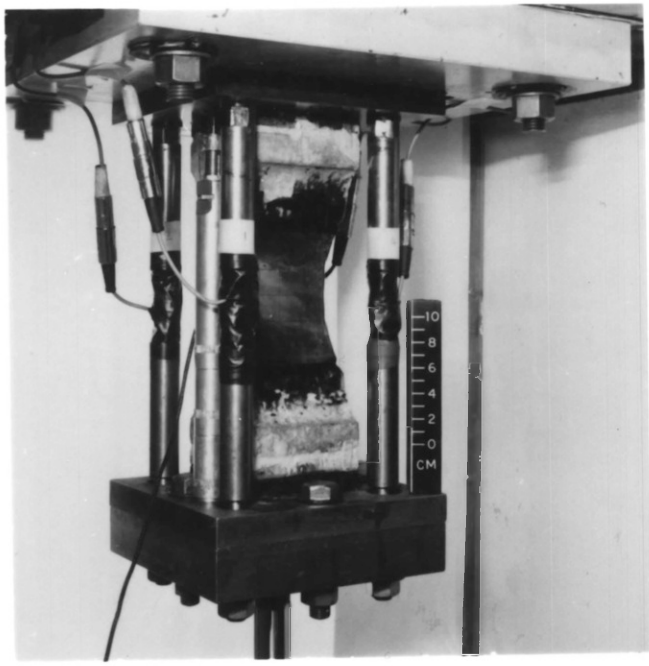

Fig. 4.2 Specimen mounted in testing machine

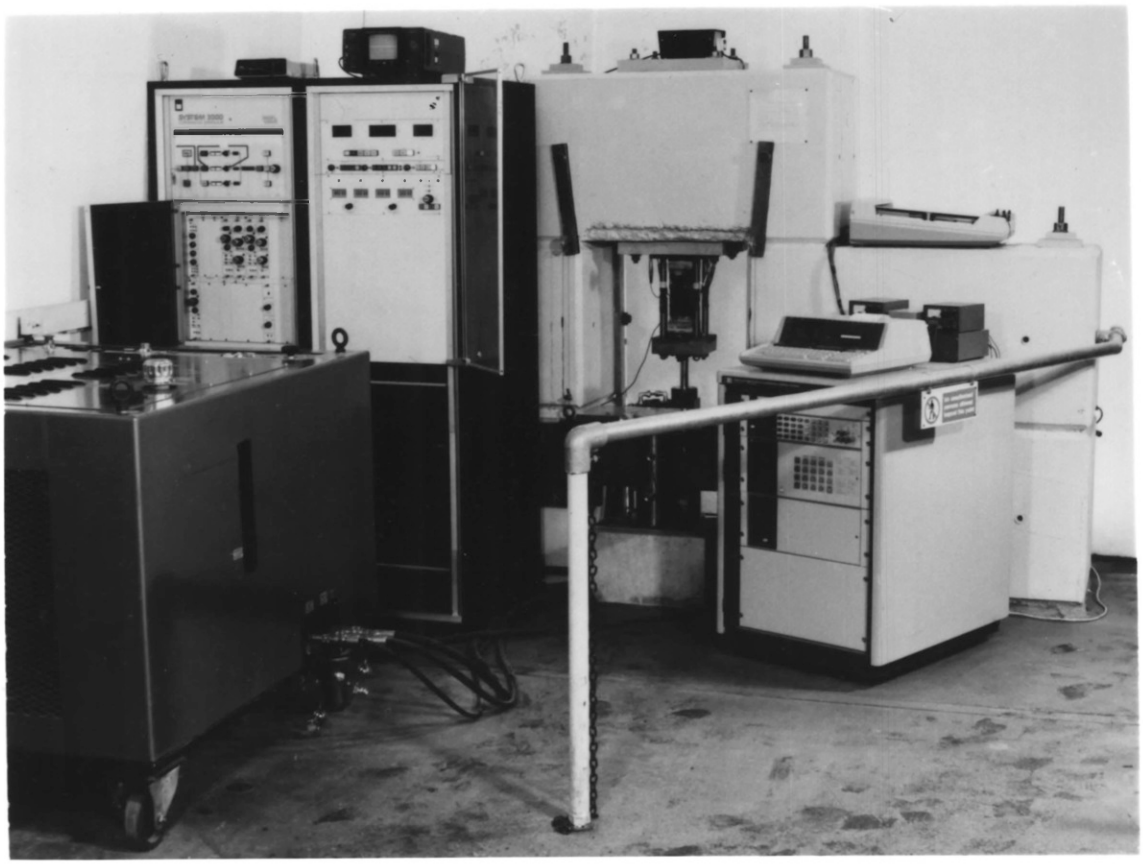

Fig. 4.3 General arrangement of testing machine

4.4 Closed loop servo-controlled hydraulic testing machine

A closed loop servo-controlled hydraulic testing machine is a complex piece of equipment which must be properly understood for safe and effective use. This is particularly true of the machine used for the present project which is capable of high speed response but was required to move extremely slowly and in a very carefully controlled manner. The general principles of this type of machine are discussed in Section 4.4.1, with the details of the particular machine used described in Section 4.4.2.

4.4.1 General principles

The general arrangement of a closed-loop servo-controlled testing machine is shown in Figure 4.4. Hydraulic oil is supplied at a constant pressure by the power pack, via the servo-valve, to the actuator causing movement of the ram. The flow of oil into and out of the upper and lower chambers of the actuator is controlled by the valve, the opening of which is, in turn, controlled by the drive current supplied by the servo-valve drive amplifier (SVDA). The drive current is an amplification of the error signal, which is the difference between the required demand signal and the feedback signal. The level of amplification is given by the gain of the SVDA. The feedback signal is an electrical signal resulting from either the ram displacement, the applied load, the specimen strain or any other parameter which is related to the movement of the ram. The servo-valve directs the oil flow in such a way that the pressures in the actuator chambers are adjusted to ensure that the feedback signal continually follows the demand signal. The demand signal may simply be a static voltage or may be the output of a function generator. It is essential that the movement of the ram should cause a change in the feedback signal. If this is not true the ram may move out of control of the system.

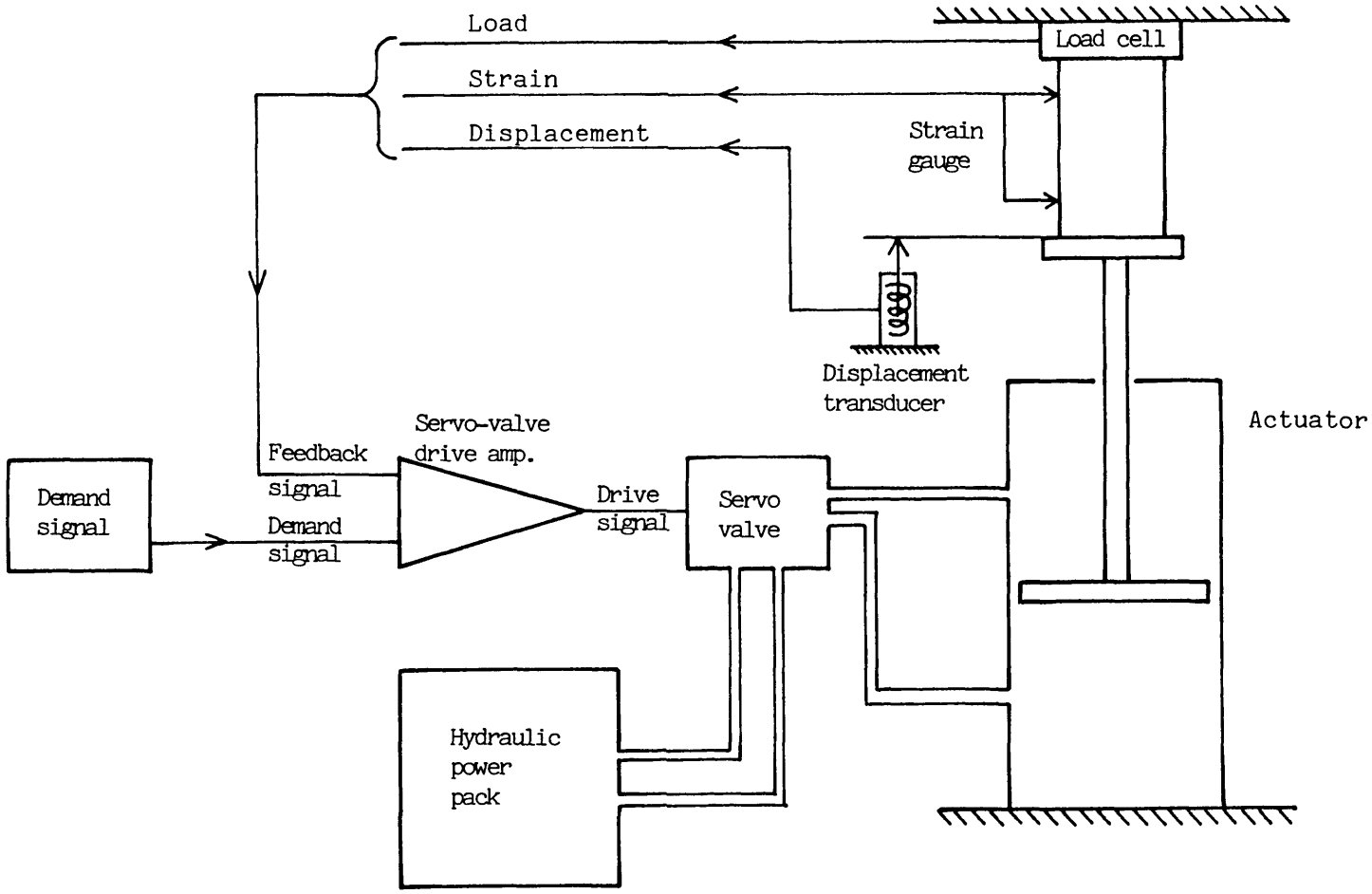

Fig. 4.4 General arrangement of a closed loop, servo-controlled testing machine

The allowable error between the demand and feedback signals can be set by adjusting the gain of the SVDA such that as the gain is increased, a smaller error results in the same drive signal. There is an upper limit on the gain which can be used. If this limit is exceeded then a small error signal will cause too large a response of the ram leading to an increased, rather than decreased, error signal. The machine quickly goes out of control and starts to oscillate at it's natural frequency. The upper limit on SVDA gain depends on the gains of the other parts of the closed loop. The gain of the servo-valve may be considered to be the oil flow per unit of drive signal current, and the gain of the actuator is the ram movement per unit of oil flow. The gain of the specimen and feedback transducer combined may be considered to be the change in the feedback signal voltage per unit ram movement. It is the cumulative effect of all these gains, the overall system gain, which must be limited to ensure that instability does not occur. If the gain of any one of the elements of the closed loop is altered then, for optimum performance, the change must be counteracted by adjustment of the gain of one of the other elements, normally the SVDA.

4.4.2 R.D.P.-Howden System 2000

R.D.P.-Howden System 2000 is a range of sophisticated closed loop servo-controlled testing machines. Each machine is assembled from a variety of elements to suit the particular application. A free standing, twin bay cabinet houses the electronic control elements of the machine. A block diagram showing the different elements of the machine is given in Figure 4.5. The basic principle of operation is the same as for any other servo-controlled machine, however, there are a number of additional features which will be described in more detail.

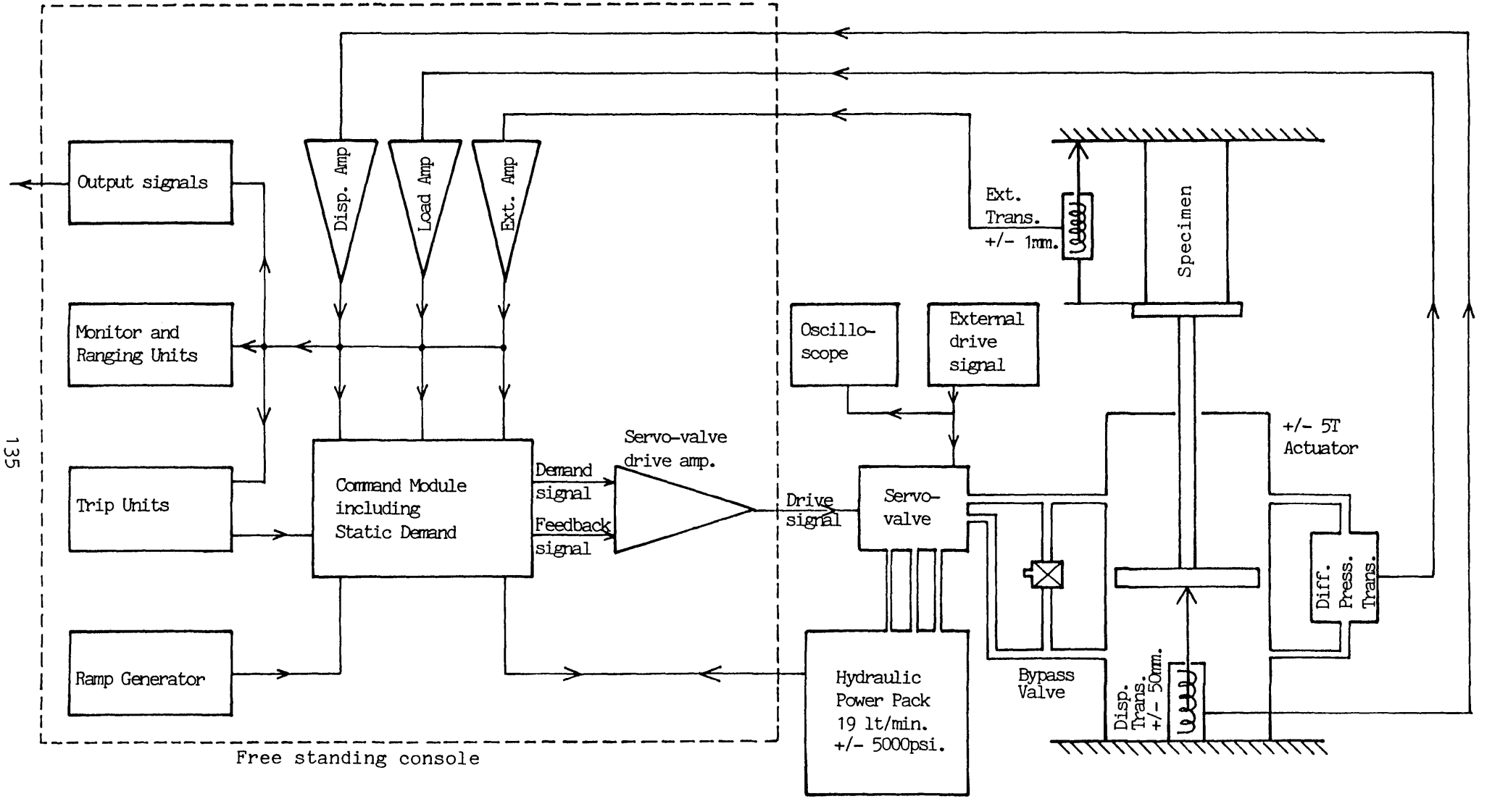

Fig. 4.5 Block diagram of the R.D.P.-Howden System 2000 Testing Machine

4.4.2.1 Description of testing machine used

System 2000 allows up to three different control parameters to be used. The first parameter, which is selected when the machine is turned on, is the displacement of the ram. This is measured by a linear variable differential transformer (LVDT) situated within the body of the actuator. The other two channels, called 'Load' and 'Strain' on the machine, may be connected to any transducer, the output of which is related to the movement of the ram. A differential pressure transducer, fitted across the two chambers of the actuator was connected to the 'Load' channel and a +/-1mm. travel LVDT, which measured the extension of the specimen, was connected to the 'Strain' channel. In the following this latter channel will be referred to as the 'Extension' channel. The control of the machine may be switched to any of the three channels simply by operation of the push buttons on the System 2000 Command Module. The Command Module ensures no large jump of the ram during change over. When switching to displacement control the static demand level of that parameter must be adjusted until it is equal to the actual displacement of the ram. When switching to either of the two control modes it is not necessary to 'balance' the static demand. When the machine is turned on, 'Standby' conditions are selected which means that only low oil pressure is applied and that the oil supply rate is restricted. On changing to 'Test', the oil pressure increases to that set on the hydraulic power pack with maximum flow capacity. The Command Module also allows the selection of two other input demand signals which are additive to the static demand signal. The Ramp Generator is connected to the first of these input signals. All systems operations which would result in uncontrolled specimen loading are inhibited by the Command Module logic and 'hidden legend' displays are illuminated to indicate the required action. 'Hidden legend' displays are also provided to give warning of overload of parts of the system and to display error conditions.

The three feedback transducers are energised by a 5V. 5KHz. signal. Each feedback signal is passed through an amplifier by which the signal is rectified and amplified to give +/-10V D.C. for the maximum / minimum values of that parameter. The zero and gain of the

amplifiers may be adjusted on the front panel. The output of the three amplifiers may be displayed on the Monitor Unit and may also be sent to other equipment, such as a data logger, via connectors on the back of this unit. The 'Static' display gives the mean value of the parameter whilst the 'Peak' and 'Trough' displays show the maximum and minimum values of the parameter since they were last reset. The parameter to be displayed is selected by a push button on the Monitor Unit and is automatically ranged by the Ranging Unit. The Ranging Unit may be adjusted to display either the voltage output from the parameter amplifier, the percentage of the maximum value of that parameter or the actual value of the parameter. As set up during the present project, when the machine is turned on the displacement and extension channels are displayed in millimetres, whereas the load channel is displayed as amplifier output voltage (1V = 5KN).

The Ramp Generator may be programmed to provide trapezoidal wave forms. Some typical wave forms are shown in Figure 4.6 together with the required settings. The four time constants, T_1 - T_4, can be varied between 0.01 and 100,000 seconds. The output level is set as a proportion of the maximum of 10V. The demand signal is the sum of the Static demand set on the Command Module together with the output signal of the Ramp Generator.

The Servo-Valve Drive Amplifier (SVDA) compares the feedback signal with the demand signal to obtain an error signal. This error is multiplied by the amplifier gain to produce the servo-valve drive current. There are three types of gain in this amplifier. The first, Proportional gain, multiplies the error signal by the same value irrespective of the frequency of the error signal. The other two, Integral and Differential gain, increase the gain for low frequency and high frequency signals respectively. Additional trimpots are provided to adjust the relative proportional gains for the three control channels such that it is not necessary to adjust the proportional gain when changing control parameter. A Dither signal (200Hz) is superimposed on the drive current to reduce the effects of the stiction in the servo-value. The amplitude of the Dither signal may be adjusted by means of a trimpot on the SVDA. The maximum drive current is set internally (20mA for one valve) but can be reduced if required using the Current Limit control.

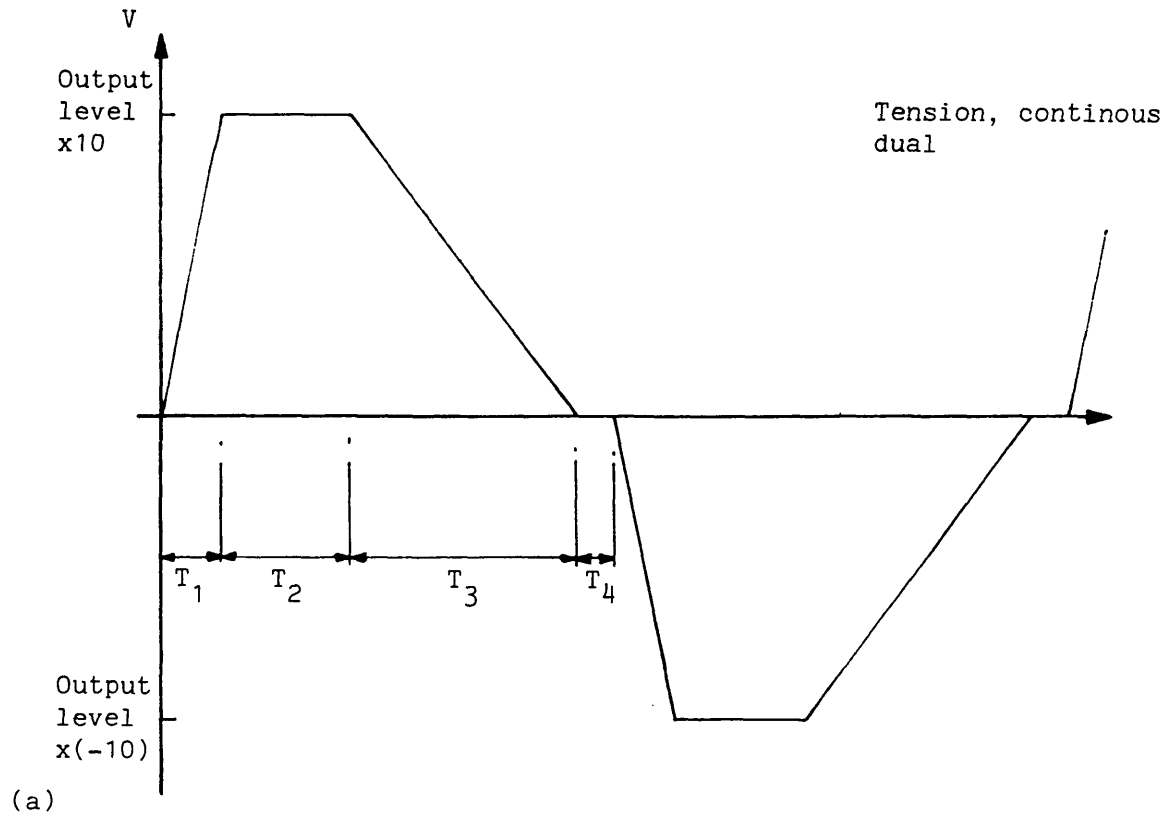

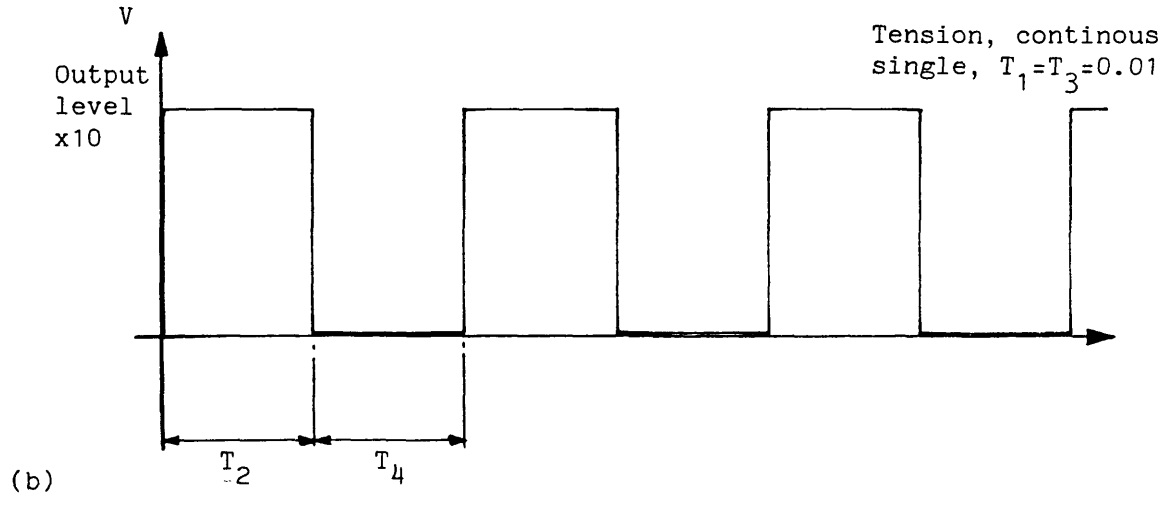

Fig. 4.6 Typical Ramp Generator wave forms

The system contains two Trip Units which may be connected to any two of the three control parameters. When the trip level, set on the front of the unit, is reached the system may be set either to shut down, or to switch to the parameter which tripped and to hold, or simply to indicate that the trip level has been reached.

The hydraulic oil is supplied by the Hydraulic Power Pack at a maximum pressure of 3600psi. and flow capacity of 19 litres/minute. The Power Pack is designed to be used either with the System 2000 Control Console or as a portable Power Pack. In the current tests it was controlled by the System 2000 Command Module which also included 'hidden legend' displays for any error conditions occurring within the Power Pack. The oil was fed to the actuator through a 19.25 litres/minute stainless steel servo-valve supplied by Moog Controls Ltd..

Three of the units shown in Figure 4.5, the Oscilloscope, the External Drive Signal and the Bypass Valve are not parts of System 2000 but were required to obtain sufficiently sensitive control of the system to perform the tests. Their use is described in the next section.

4.4.2.2 Control of the testing machine

4.4.2.2.1 Introduction

The combination of a large oil flow capacity both from the Hydraulic Power Pack and through the servo-valve, together with an actuator with small oil capacity, meant that the ram could move very rapidly. It had been hoped that this dynamic response might assist in obtaining stable failure (Section 3.2), however, this proved not to be the case. The drawback of the system is that it has a very high mechanical gain and consequently the electrical gain in the closed loop has to be low in order to avoid dynamic instability (Section 4.4.1). This limit on the allowable electrical gain caused several major problems with the

control of the machine. It can be seen that a machine, which is designed to move very quickly over a range of +/-50mm. might have a control problem when required to move at a rate of 2.5 micron per minute and to an accuracy of the order of 0.2 micron. Solutions were eventually found to the various apparently insurmountable problems encountered during the development of the test but it was not until 22 months after the assembly of the test frame for the 5T Actuator that the first successful test was completed. The majority of the problems which occured were directly related to the high physical gain of the machine and the consequent low electrical gain. This low electrical gain allowed too large a difference between demand and feedback signals to occur before a sufficiently large drive signal was sent to the servo-valve to correct the error. The problems are interrelated and often could only be solved by trial and error techniques. The difficulties in control are described in Section 4.4.2.2.2 and their solutions in Section 4.4.2.2.3.

4.4.2.2.2 Difficulties in testing machine control

The following difficulties in control were encountered, during the development of the test.

1. Spikes occurred on the extension signal. These spikes could be seen on an A3 plotter connected to the extension output signal of the Monitor Unit. With the extension plotted against time the spike was shown to be of extremely short duration (Fig. 4.7), the extension reading returning to near it's original value, often with some overshoot. The amplitude of the spikes might be up to 10 microns and they appeared to occur at random intervals. The amplitude of the spikes could also be observed as the difference between the 'Peak' and 'Trough' displays on the Monitor Unit. In order to check whether or not these spikes represented real movements of the ram or were just spikes on the electrical signal, a sensitive mechanical dial gauge was placed between the machine plattens. Unfortunately, due to the random nature of the spikes it was difficult to ensure that the gauge was being monitored when the

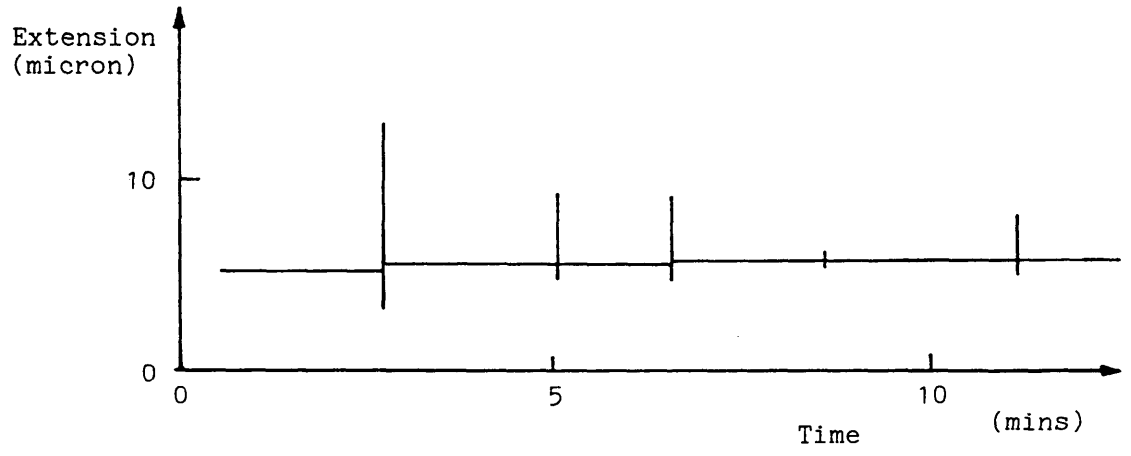

Fig. 4.7 Typical spike record

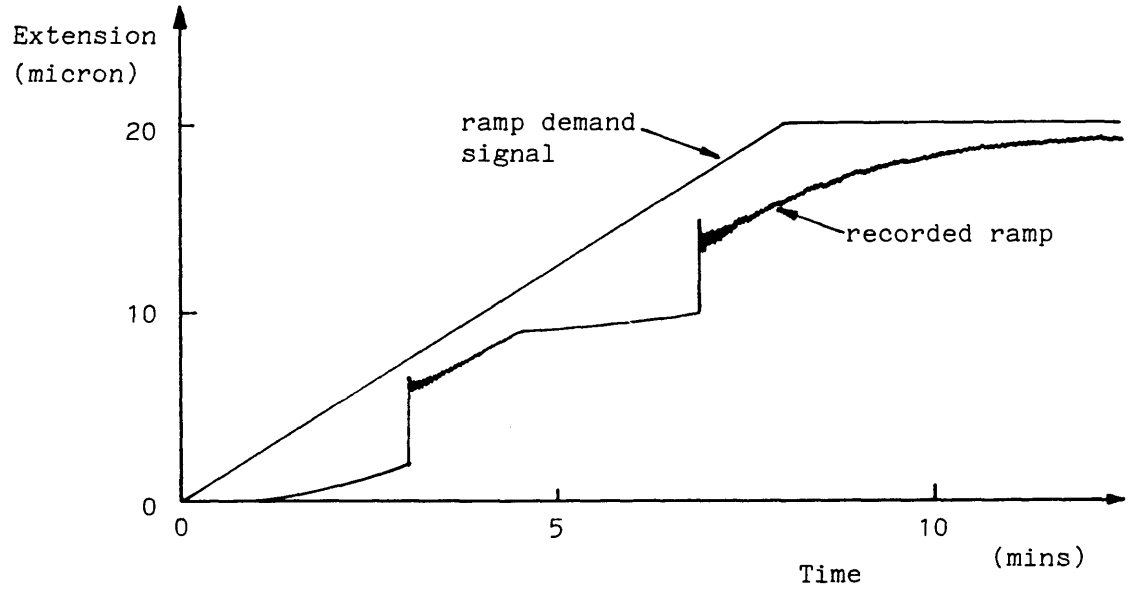

Fig. 4.8 Typical difficulty with ramping

spike occurred. However, it was discovered that the spikes could be created by turning on and off portable, mains powered, neon lights in the vicinity of the machine. Using the lights it was possible to show that the spikes corresponded to real ram movements and would cause significant damage to the specimen. Similar spikes occurred when the cooling fan for the Hydraulic Power Pack cut in or out, but it was not obvious which, if any, other equipment in the laboratory was able to cause spikes. It was concluded that the spikes were probably caused by either mains-borne or air-borne electrical interference. Two further possible causes of spikes were siltration or temporary obstruction of the servo-valve and electrical shorting across the output signals; these are discussed more fully in Section 4.4.2.2.3.

2. It was difficult to perform slight adjustments of the ram position. These adjustments, of the order of 0.5 micron, were necessary during the setting up of the test to limit the loads applied to the specimen. There were three basic causes of this difficulty. The first was that the Static demand control potentiometer on the Command Module was a small ten turn potentiometer. The ten turns corresponded to a ram movement range of +/- 1.0mm. consequently a rotation of the knob of only 1/40th. of a turn was required for a movement of 0.5 micron. This was physically difficult to achieve. The second problem was that due to the low proportional electrical gain allowed, the error signal had to be relatively large before the servo-valve would respond. The third problem was that of 'stiction' in the servo-valve and the actuator. The 'stiction' of the servo-valve should have been overcome by the Dither signal from the SDVA, although it may be that the fluttering of the valve ceased in some circumstances. It was, in practice, difficult to establish when the second or third problem caused the difficulty in fine control, or whether it was caused by a combination of the two.

3. The ram would sometimes not respond well to the Ramp Generator and occasionally the Ramp Generator itself would 'lock up' and not produce the required signal. The ram might take up to a minute to begin to respond after 'Run' had been pressed on the Ramp Generator and a similar period to stop again when 'Hold' pressed. The ramp speed was variable and often significantly less than that

programmed. The ramp might include sections of lower speed ramping followed by jumps and vibration. A typical extension/time plot showing these problems is given in Figure 4.8. The reason for the 'locking up' of the Ramp Generator is not clear but turning the machine off and then on again seemed to clear the condition. The poor response to the ramp signal was attributed to the latter two causes of the difficulty in fine control, ie. low gain and problems with 'stiction'.

4. The ram would sometimes jump up to 25mm. when the Power Pack was first turned on and often there were smaller jumps when changing between control parameters. The jump on start up was due to the fact that, in order not to have too large a gain in extension control, the displacement control gain was set very low so that the machine was not very well tuned in this control mode, it was sluggish and sometimes difficult to change from 'Standby' to 'Test' mode. The specification required that the jump when changing control parameters should be less than 1% of the maximum value of the new parameter. This could be up to 10 micron when changing to extension control which could damage the specimen significantly.

Although the control difficulties have been divided into the above four separate sections, it was often difficult to know which cause, or group of causes, could be attributed to any particular problem. During the course of test development, control systems were devised which dealt with most of the problems listed above. Some of the difficulties simply had to be accepted and the test technique designed to ameliorate their effects. The control systems devised are described in the next section.

4.4.2.2.3 Testing machine control systems

The difficulties experienced in testing machine control varied in their effects from those which caused slight problems during curing of the adhesive, to those which destroyed the specimen prior to the start of the test. In order to conduct a useful test series it was necessary either to reduce the likelihood of such difficulties occurring, or to ensure that, if they they did occur, then they would not affect the test adversly. Both of these approaches were used, however, it was inevitable that some tests would not provide usable data and the final test series was designed accordingly.

The problem of spikes was never completely solved but was diminished such that the spikes were less frequent and the maximum amplitude was reduced from 10 micron to 1.6 micron. Initially it was suggested by the manufacturer that the servo-value might be suffering from siltration which could have a pronounced effect when the ram was stationary or moving very slowly. Under these conditions the oil flow through the valve is very low and as it passes through the small opening of the valve it's temperature increases which may lead to degradation. It was suggested that small particles from the degraded oil might build up around the orifice and break off producing a surge of oil leading to a spike. In order to investigate this possible cause for the spikes a bypass valve was fitted between the servo-valve and the actuator. When the bypass was opened the oil flow through the servo-valve with the ram stationary, was greatly increased so that siltration could not take place. One disadvantage of the use of the bypass was that it affected the system mechanical gain by requiring the servo-valve to open further for a given movement of the ram, the amount of the effect depending on the oil temperature and applied load. It was found, however, that using the bypass valve did not eliminate the spikes and it was deduced, therefore, that siltration was probably not occurring and that the spikes were caused by electrical interference. It should be noted that symptoms very similar to the spikes were produced if the output points on the back of the Command Module were temporarily shorted. This happened in one test due to faulty wiring. The solution was simply not to use these outputs but to use those on the Monitor Unit which, if shorted, did not affect the

control of the machine.

The causes of electrical interference are very difficult to find and normally it is easier either to isolate the equipment from the interference or to prevent the response of the equipment to the interference. It should be possible to reduce mains-borne interference with a combination of radio frequency interference filters and mains transformers. Several mains filters were used but none was able to prevent spikes caused by the portable neon lights. This does not, however, prove that the interference was not mains-borne since there are many types of mains filter, none of which if fully effective over the full range of interference possible. Air-borne interference is even more difficult to isolate and would require an earthed metal cage to be built round the equipment. The control console itself is housed in an earthed cabinet but the leads to and from it are not fully protected. It proved impossible to isolate the equipment from the interference so various methods for reducing the response of the system to the interference were considered. It was thought best to avoid changing the components of the units and thereby creating a non-standard system. During the investigation the manufacture's service engineer updated the parameter amplifiers to the current specification. This was found to have a significant damping effect on the system response and the natural frequency was reduced from 40 Hz. to approximately 4 Hz.. The response to interference was also significantly reduced. When the neon lights were plugged into a ring main connected to a different phase of the power supply to that used for the control console, there was no noticable spike. When plugged into the same ring main the spike remained but it's size was reduced. In order to reduce the likelyhood of a significant spike during the critical portion of the test the following procedures were evolved:

1. The mains supply for the control console shall be taken from the ring connected to the yellow phase. This phase is less likely to be noisy than the red phase.
2. No other equipment shall be connected to this ring main during the test.
3. All neon lights throughout the laboratory shall be turned on prior to starting the test and left on until completion.
4. Overhead cranes and other similar equipment shall only be used

during the test if absolutely necessary.

5. The thermostat controlling the Hydraulic Power Pack cooling fan was adjusted so that the fan runs continuously.

When these procedures were followed it was found that the incidence of spikes and their amplitude were significantly reduced so that none of the tests in the final test series was adversely affected by a spike.

To avoid having to use the static demand potentiometer, which was too coarse, for fine control of the ram position, various other techniques were tried. The simplest solution was to adjust the zero offset of the extension amplifier. This applied an offset to the feedback voltage signal which was automatically compensated for by displacement of the ram such that the net change in this voltage was zero. Unfortunately, since the net feedback signal was unaltered, the extension reading did not change and it was not possible therefore to measure how far the ram had moved. If a separate D.C. signal was fed into the second input of the Command Module, this could be used as an auxiliary static demand signal. However, this second input was automatically de-selected when 'Hold' was pressed on the Ramp Generator causing the ram to jump by an amount equivalent to the voltage supplied. The servo-valve had two activating coils only one of which is normally used. If a D.C. voltage is applied across the second coil then it acts like a zero offset. The problem with this technique is that the effectiveness of the voltage changes with the gain of the SVDA. It is necessary to change the gain of the SVDA during setting up of the test and consequently the D.C. voltage also has to be altered. Finally, the solution adopted was to run the Ramp Generator in compression. It was found that the fine adjustments required were nearly always compressive so that the Ramp Generator could provide a means for controlled adjustments.

After a large number of trials it was found that the only way to make sure that the ram followed the Ramp Generator correctly was to overcome effects of 'stiction' by ensuring slight ram vibration and to use the maximum gain possible. The servo-valve dither can provide vibration of the ram, but, since the ram cannot follow the 200Hz. Dither signal the vibrations appear fairly random and may either die

out completely or grow to an unacceptable level. In order to observe the effects of varying the Dither frequency an external square wave generator was built and connected to the spare servo-valve coil (Fig. 4.9). With frequencies greater than 200Hz. the effects were similar to the 200Hz. signal. With low frequencies either the vibration would die out because the valve stiction was not being overcome or, as the amplitude was increased, the vibrations would become too great. The final solution was to use the 200Hz. Dither signal to ensure dither of the valve and an additional 2Hz. signal fed directly to the servo-valve, to ensure vibration of the ram. The amplitudes of these signals could only be set by trial and error and leaving the machine ramping for several days to check that the vibrations neither grew too large nor died out. A measurement of their amplitudes could be made with an oscilloscope across the terminals of the second servo-valve coil. Firstly, the square wave was measured with the System 2000 electronics turned off, then with the machine running the Dither could be measured due to the induction from the first coil to the second inside the valve. The optimum setting for the square wave was 1mV. amplitude and the Dither approximately 1.0V. amplitude. If during the test the vibrations were too great or too small then the Dither signal was adjusted accordingly. This adjustment was not very effective and sometimes took a few minutes to alter the vibration.

It is necessary for proper control for the SVDA gain to be set to the optimum for the particular test. Unfortunately it was found that the optimum gain was dependent on the applied load and probably also on the stiffness of the specimen. The technique used for setting the gain was to input a square wave from the Ramp Generator (Fig. 4.6b) and increase the Proportional gain until the optimum was achieved (Fig. 4.10). The optimum and maximum allowable Proportional gain settings for different loads applied against the parallel bars are given in Table 4.1. It was very difficult to obtain repeatable gain settings for loads applied against the bars and a concrete specimen but for the same load the optimum gain level was certainly increased. It was not clear what would happen to the optimum gain when the specimen began to fracture, some tests showed larger allowable gains at this stage than at the start of the test whilst others showed reduced allowable gain. What did become clear was that, with the Proportional gain set to the optimum at the begining of the test, it was still not sufficient to

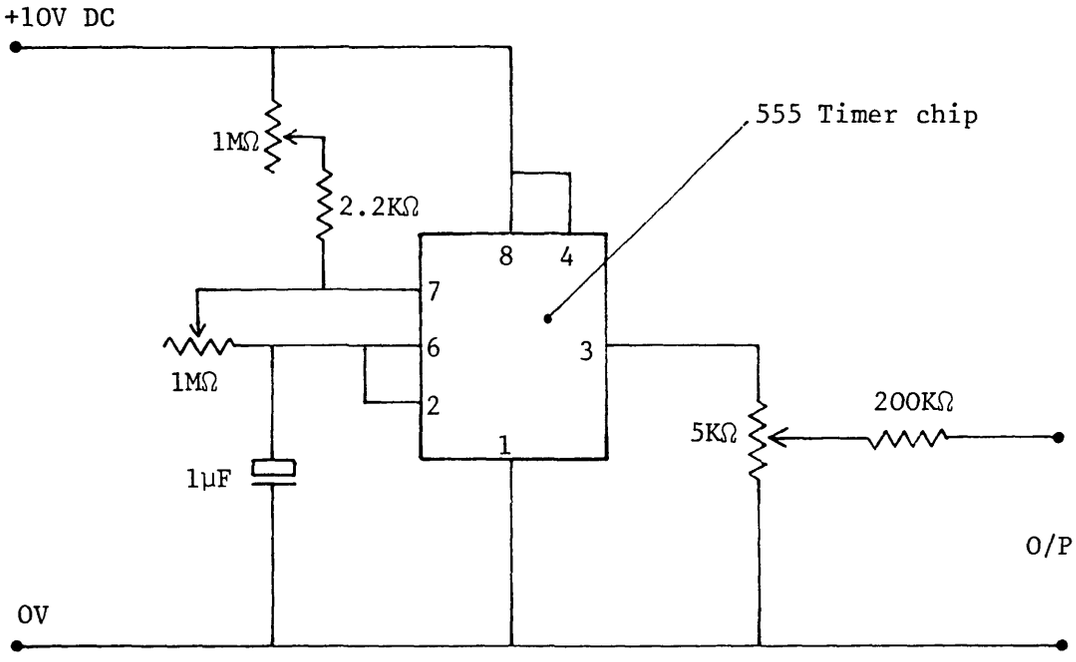

Fig. 4.9 Circuit diagram for external square wave generator

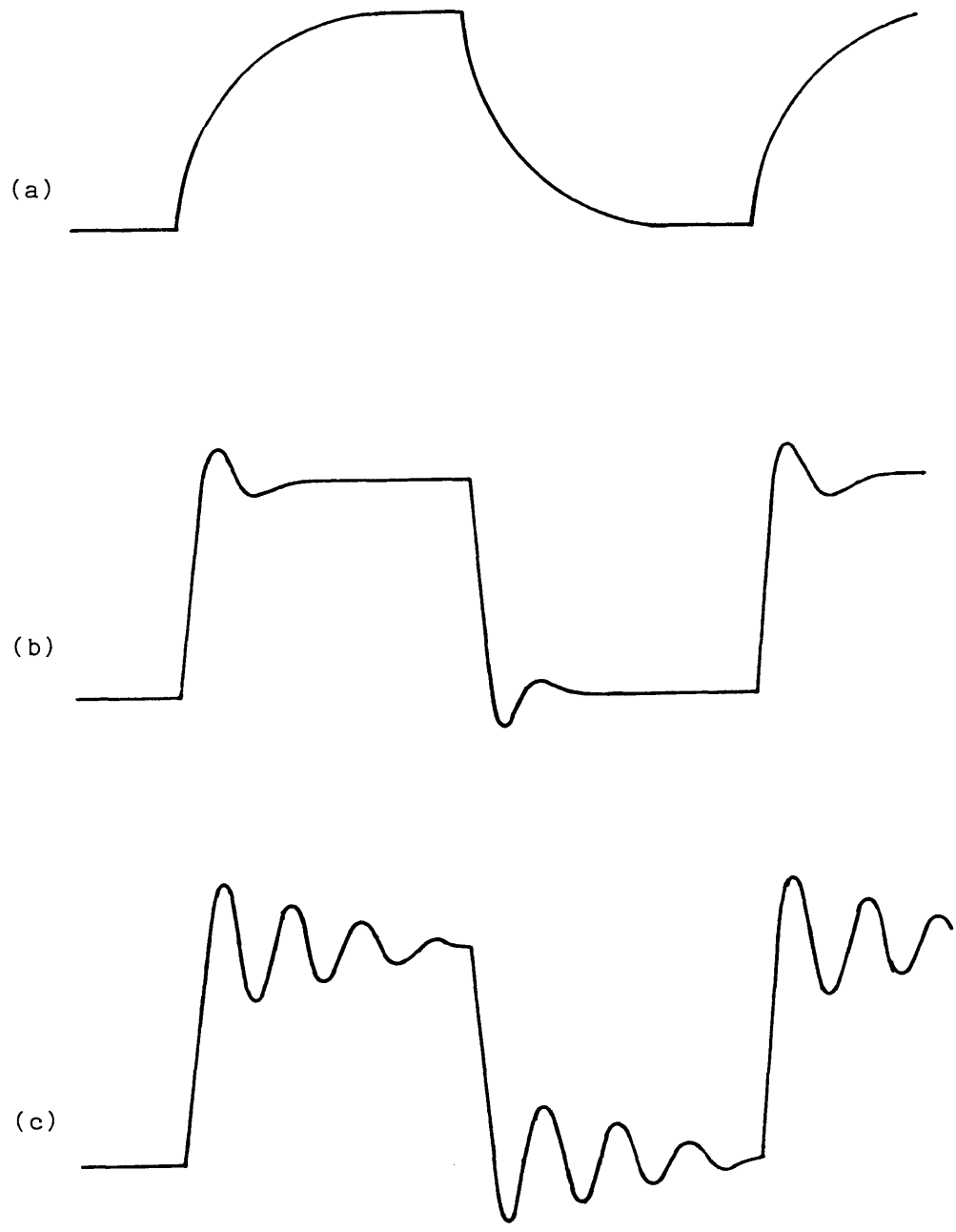

Fig. 4.10 Response to square wave input from Ramp Generator
(a) Gain too low, system over damped
(b) Optimum gain
(c) Maximum gain

ensure that the ram followed the Ramp Generator correctly. It should be noted, however, that at this stage of the development the external square wave signal had not been introduced and it may be that a combination of optimum Proportional gain with continual vibration of the ram might prove a suitable combination.

At this stage it was decided to attempt to use the Integral gain of the SVDA. This integrates the error signal over a time constant, which may be varied, to produce the drive signal and is used to increase the gain at lower frequencies. Integral gain cannot be used in displacement control since the response of the system in displacement control has a 90 degree phase lag behind the demand signal. When the response is integrated, a further 90 degree phase lag occurs with the result that the error signal has a 180 degree phase lag and causes the error to increase rather than decrease. The machine becomes unstable and will go out of control. In load control this does not happen because the first 90 degree phase lag does not occur. The extension control channel will act in the same way as displacement control until load is applied to the bars. When load is applied to the bars alone, their extension is proportional to the applied load and the extension signal acts in a manner similar to that which would be obtained from a load cell. In this case some Integral gain may be applied without causing machine instability. The maximum allowable Integral gain setting appears to be dependent on both the stiffness of the bars and the total applied load. The situation is less clear for a load applied to the bars and a specimen in parallel when the relationship between load and extension is non-linear. However, it was found that despite the apparent negative stiffness of the specimen after the peak load had been reached, there was no increased tendency towards unstablity and Integral gain could still be applied. This is probably due to the fact the any tendency to oscillate would have caused unloading of the specimen and then reloading along a path with a positive stiffness.

The setting up of Integral gain required more care than Proportional gain to avoid damage to the equipment. The basic steps are as follows:

1. Set Proportional gain for optimum. It was found most effective if this was done with no load applied to the bars.
2. Ensure that, if the ram does go unstable, then no damage can be

done. This can be achieved by having the ram very near the top of it's travel with sufficient load applied to the bars such that if the ram does go to the top of it's travel the bars do not become slack. The bars are strong enough to prevent the ram from going too far down. Ensure that neither the bars nor the extension transducer can be damaged if the ram moves up suddenly.

3. Increase the level of Integral gain (18-turn potentiometer, RV6 inside SVDA) by one turn.
4. Measure static demand signal by switching the Monitor Unit to 'Test' and connect the red test lead to the SVDA output point marked 'stat'.
5. Measure the feedback signal by connecting the test lead to the Extension Channel amplifier output point marked 'o/p'.
6. These two signals should be similar except for the sign which will be opposite. Increase the Integral gain setting (this affects the integral time constant) and monitor the feedback signal which will become closer to the demand signal. When the Integral gain is set too high the feedback will begin to 'wander' at a frequency of about 2Hz. When this occurs turn the Integral down until it stops.
7. Should it not be possible to obtain the wandering even with the Integral gain set to 100, turn it down, increase the setting of RV6 by 1 turn and try again.
8. The onset of wandering instability may alternatively be observed using an oscilloscope connected to the Extension output on the Monitor Unit.

Using the above technique the Integral gain may be correctly set for any value of the load applied to the bars. By applying a square wave from the Ramp Generator and monitoring the Extension output on the Oscilloscope it was possible to estimate the optimum and maximum Integral gain settings (Table 4.2). Interestingly, the change in optimum setting for a change in load from 12KN. to 24KN. is less for Integral gain than Proportional gain. It was found that, with a combination of Integral gain and Proportional gain, together with ram vibration, the ram would follow the Ramp Generator signal very well up to loads of about 40KN.. After this the ram lagged behind the demand signal but no sudden jumps occurred and this did not affect the tests.

There does not appear to be any simple way that the jump on turning

the Power Pack on and the jump when changing control modes can be avoided or reduced. It was necessary, therefore, to ensure that no damage could be done by either jump and the test procedure was adapted accordingly.

Load applied against parallel bars (KN)	Optimum Proportional gain setting	Maximum Proportional gain setting
0	050	080
12	320	450
18	370	500
24	400	540

Table 4.1 Proportional gain settings

Load applied against parallel bars (KN)	Optimum Integral gain setting	Maximum Integral gain setting
0	000	000
12	900	950
18	925	965
24	940	975

Table 4.2 Integral gain settings
Proportional gain setting = 050

4.5 Conclusions

In this chapter the development of a test technique to fulfil the loading requirements of Section 3.5 has been described. A specimen has been designed which will fail in a stable manner at a location remote from it's ends but without significant stress concentrations. The specimen size and moisture condition are considered suitable for direct tensile testing of concrete and the specimen shape enables the chosen strain measurement technique to be used. The connection of the specimen to the machine has been designed to restrain end rotations and can be made within an hour. The most difficult part of the test development has been the design of suitable control systems for the servo-controlled testing machine used. The equipment was not ideal for this type of test and it's capabilities had to be used to the limit in order to perform the tests successfully. The final test technique enables repeatable direct tensile tests to be conducted on concrete.

Chapter 5 Review of deformation measurement techniques

5.1 Introduction

It was shown in Chapters 2 and 3 that very little is known regarding the form, size and characteristics of the fracture process zone in concrete. None of the theories reviewed in Chapter 2 fully explains the initiation and propagation of cracks. The fracture process zone models described in Section 2.4 appear very promising but they suffer from one important limitation, namely, the assumption that, in the direct tensile tests conducted, the fracturing occurs simultaneously throughout the full cross-sectional area of the specimen. Despite the fact that there is no evidence to support this assumption, the load/extension curves for the tests are taken to be material properties ignoring any possible lateral localisation of strain within the cross-section (Section 2.4.4). One of the aims of the present project is to obtain more detailed information regarding both the longitudinal and lateral localisation of strain in concrete under tension.

All previous stable, direct tensile tests have utilised strain gauges, displacement transducers or similar devices to measure the strain in the specimen. These techniques can only yield the average strain across the gauge length and consequently give very little information regarding the progressive localisation of strain within that length. In order to obtain a more detailed appreciation of the localised deformations a full field strain measurement technique is required (Section 3.3.4).

There are several restrictions on the technique to be used as follows:

1. The strains to be measured are low, varying from approximately 100 microstrain to a maximum in the order of 1000 microstrain.

2. The strain gradients may be high requiring fine resolution of the strain field.
3. It is necessary for the concrete to remain moist before and during testing to ensure that no shrinkage stresses or cracking occur due to drying (Petersson, 1981b).
4. The results obtained must not be obscured by any solid body movement of the specimen during loading.
5. The strain field must be measured at several stages during the test in order to observe the development of the fracture zone.
6. The technique should not affect the loading or response of the specimen.

In addition, it would be convenient to measure the strains throughout the volume of the specimen and any measurements should be insensitive to vibration caused by the loading machine or transmitted through the points of attachment. If possible, the technique should cover a reasonably large area and be simple to operate, cheap, repeatable and yield real time visualisation of the strain field.

Several techniques have been considered but none of them fulfils completely the requirements set out above. The most difficult requirement is the measurement of strain throughout the specimen. All currently available techniques for measuring a strain within the body of a specimen affect it's response under loading and, therefore, cannot be used. Consequently, only surface strain measurement is possible and several relevant techniques are described below.

5.2 Photoelastic coatings

The first use of photoelastic coatings is reported to have been that by Mesnager in 1930, (Redner, 1980). However, the technique was not in widespread use until the 1950s. The theory of photoelasticity is well documented elsewhere (Post, 1979) and only a short summary will be given here.

When a ray of light enters a stressed birefringent material along one of the directions of principal strain, the light is divided into two component waves, each with it's plane of vibration parallel to one of the remaining two principal planes. The velocities with which these two component waves travel through the material are different and depend on the magnitudes of the two remaining principal strains. The waves emerge from the material with a new phase relationship or relative retardation, N. The emergent waves are recombined in a polariscope which permits interference. If N is a whole number of cycles the waves reinforce each other, whereas they tend to destroy each other if N is 1/2, 3/2, 5/2.... As a result, a series of fringes can be seen, light fringes where N is a whole number with dark bands between. These fringes form what is known as an isochromatic pattern. The difference between the two principal in-plane strains can be obtained from:

$$\varepsilon_1 - \varepsilon_2 = \frac{N \lambda}{K 1} \qquad (5.1)$$

where N is the relative retardation or ischromatic fringe order
λ is the wavelength of light
K is the material sensitivity
1 is the path length through the material.

Monochromatic light has been assumed in the above discussion, however, white light can be used giving a series of fringes of different colours. The interpolation between fringes of different colours is difficult and depends to a certain extent on operator skill.

Using the same equipment as required for the formation of isochromatic fringes it is also possible to obtain isoclinic fringes, these are lines along which the orientations of the principal strains are constant and known.

It can be seen that the above method (termed the normal incidence method) can yield the directions of the two principal strains and the difference in their magnitudes. In order to obtain their absolute magnitudes further information is required. Such data could be obtained from strain gauges but these suffer the problem of averaging the strain over the gauge length as previously mentioned and only yield information in discrete areas. An alternative, which utilises the photoelastic coating itself, is termed the oblique incidence method. The light beam is shone through the coating at some angle and reflected at the specimen surface. If the beam is aligned in one of the principal strain directions a second equation similar to Equation 5.1 is obtained, allowing solution of the two equations simultaneously, to yield the magnitudes of the two principal strains. McCreath (1968) attempted to use the oblique incidence method with photoelastic coatings on concrete specimens. However, he experienced great difficulty in obtaining good results. His measured strains were up to 200% different from those expected from the theoretical model. As a result the method was discarded in favour of strain gauges.

The accuracy with which strain can be measured depends on the coating material sensitivity and thickness. As an example, the sensitivity of a 2mm. thick epoxy coating is of the order of 1000 microstrain per fringe. This could be increased by fringe multiplication techniques whereby the light is made to pass through the coating several times. The practical limit for fringe multiplication for coatings is 5 times which would give a sensitivity of 200 microstrain per fringe. Fringe interpolation techniques can be used but they are not very successful up to the first fringe. Hence the first measurable strain difference would be 200 microstrain above which the measurements could be made to an accuracy 10 microstrain (Moore, 1983).

Apart from the lack of sensitivity to low strains the other main drawback with the use of a photoelastic coating is it's reinforcing

effect. The increase in stiffness by using a 2mm. coating on a 75mm. thick concrete specimen would only be of the order of 0.3% but the surface effects, which are important for fracture zone formation, would be much more significant. Since it is not possible to quantify these effects and due to the difficulty in obtaining full field strain measurements the photoelastic coating method is not considered suitable for the present project.

5.3 Brittle coatings

Brittle coatings have been in use for many years with varied degrees of success. A coating is applied to the specimen and when the specimen deforms the coating cracks, the cracks being approximately perpendicular to the principal tensile strain. The strain which causes first cracking, called the initial strain response, of the most sensitive untreated coating is of the order of 400 microstrain (Parks, Hofer & Durelli, 1962). This sensitivity can be increased by heat treatment to 300 microstrain (Rockey, 1951) and by cooling the strained coating with water to 100 microstrain (Parks et al. 1962). Theoretically the crack pattern is a reflection of the strain field and can be used to determine orientation and magnitude of the principal tensile strain.

Despite the volume of research into the use of brittle coatings, there is considerable uncertainty regarding the interpretation of data. Up to 34 variables affecting the sensitivity of one particular coating have been investigated (Durelli, Okubo & Jacobson, 1955; Durelli, Jacobson & Okubo, 1956). The variable of particular interest is the sensitivity to humidity and therefore presumably to the dampness of the substrate. Coatings are also susceptible to creep with up to 50% reduction in initial strain response during a test lasting 1000 sec. (Ellis, Stern & Baranowski, 1966). For these reasons brittle coatings cannot be used in the present project.

5.4 The moire method

If two similar sets of lines are superimposed they form a pattern known as the moire pattern. The word moire comes from the French name for a type of silk imported from ancient China which, when folded, forms patterns which are characteristic of the material. The moire effect can be used for several different forms of deformation measurement but the discussion presented below will be limited to in-plane surface deformation.

5.4.1 General principles

A grating of regularly spaced lines is made on the undeformed specimen. A second grating, called the reference grating, is superimposed on the specimen grating which produces a moire pattern. The change in the moire pattern as the specimen deforms is a measure of the deformation.

For example, suppose the reference and specimen gratings are initially of equal pitch and are superimposed as in Figure 5.1(a). The specimen grating is then strained in a direction perpendicular to the reference grating lines (this is known as the grating principal direction). In Figure 5.1(b) it can be seen that where the lines of one grating are halfway between the lines of the other grating the light is blocked and a dark fringe is formed, whereas, when the lines are superimposed, some light can pass through and a light fringe is formed. Denoting the centrelines of the reference grating lines as 0 to m, the specimen grating lines 0 to n and the light fringes 0 to N, (N is an integer unless otherwise specified and is known as the fringe order) it can be seen from Figure 5.1(b) that:

$$N = m - n \tag{5.2}$$

These fringes are called subtractive fringes.

Equation 5.2 can also be seen to be true for the case of pure rotation shown in Figure 5.2.

For the general case of extension and rotation, an analysis can be made by considering Figure 5.3. For simplicity it is assumed that the two gratings are identical prior to deformation. The grating lines are omitted for clarity and are represented simply by their centrelines. Let S be the fringe spacing, p the reference grating pitch and p' the specimen grating pitch. It can be seen that:

$$\overline{AB} = \frac{p}{\cos(\phi - \pi/2)} = \frac{p}{\sin\phi} \tag{5.3}$$

and

$$\overline{AB} = \frac{p'}{\cos(\phi - \pi/2 - \theta)} = \frac{p'}{\sin(\phi - \theta)} \tag{5.4}$$

Combining (5.3) and (5.4) we get:

$$p' = p\,\frac{\sin(\phi - \theta)}{\sin\phi} \tag{5.5}$$

Also:

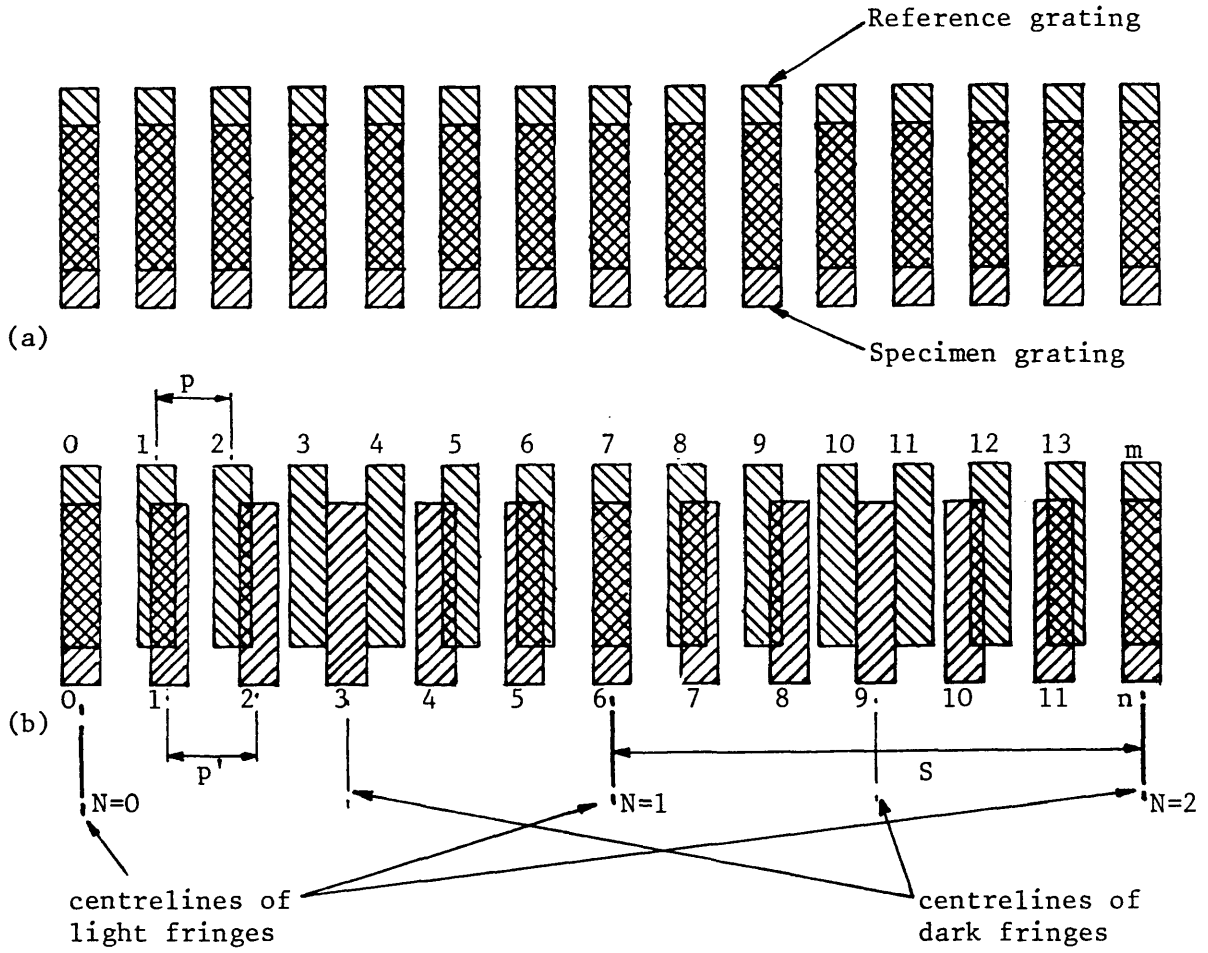

Fig. 5.1 Formation of moire fringes for pure uniaxial extension
(a) Before extension, no fringes
(b) After extension, fringes formed

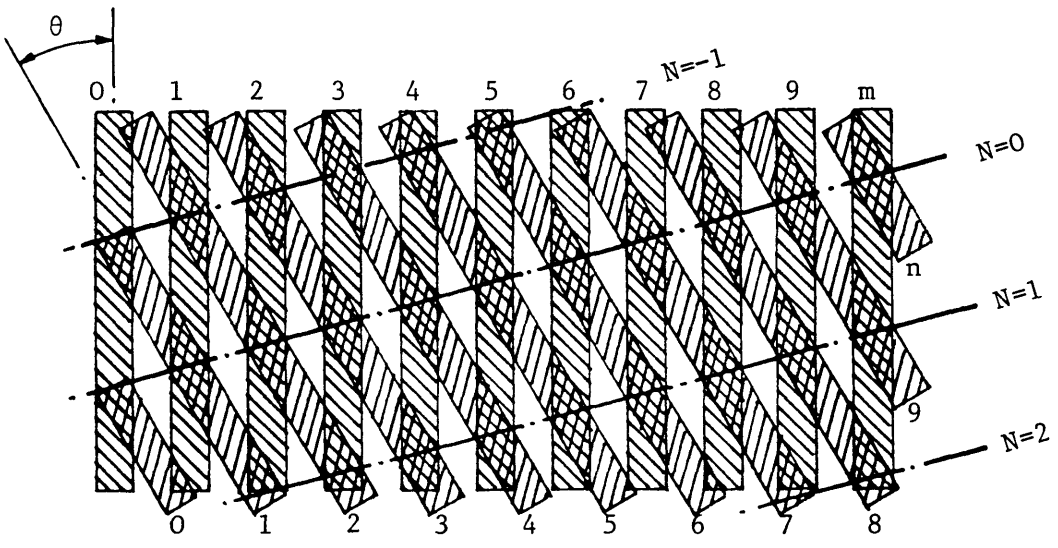

Fig. 5.2 Formation of moire fringes for pure rotational case

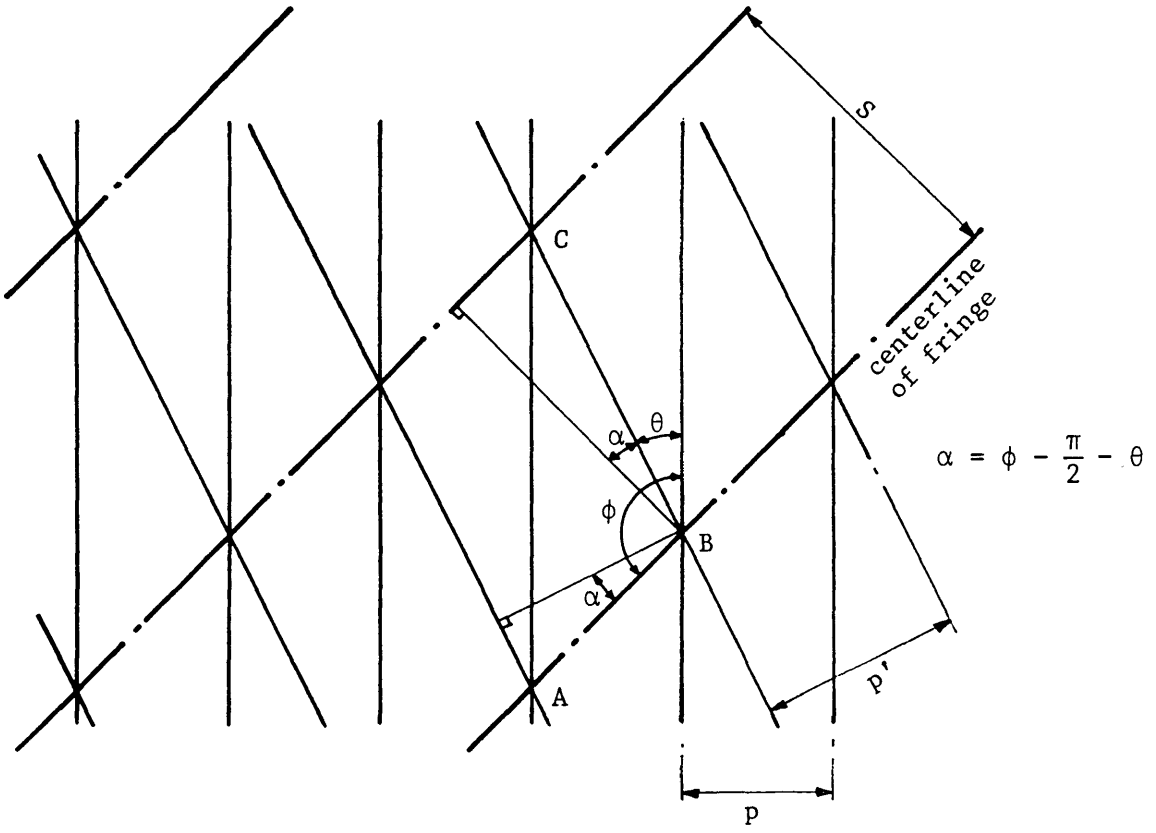

Fig. 5.3 Moire fringes produced by extension and rotation

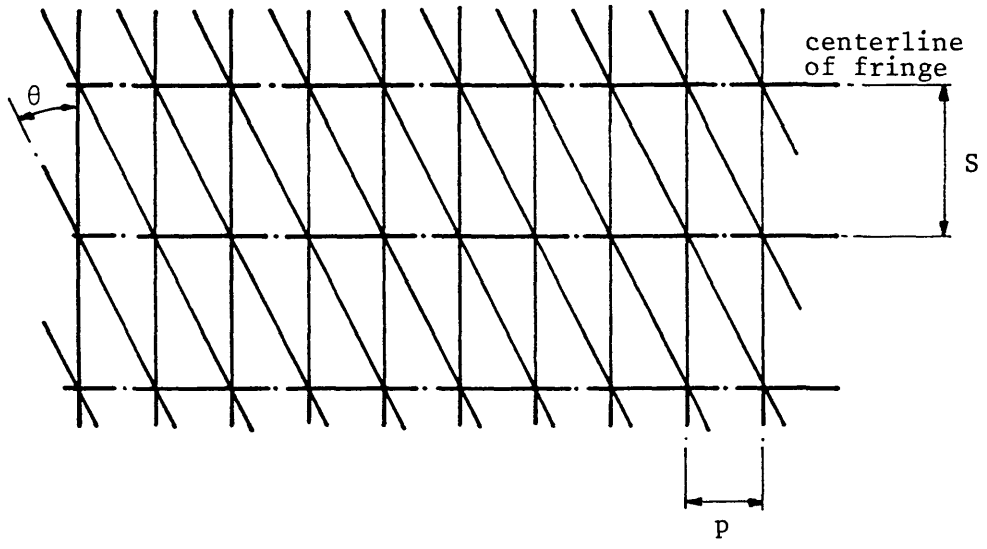

Fig. 5.4 Moire fringes produced by pure shear

$$\overline{BC} = \frac{p}{\sin \theta} \tag{5.6}$$

and

$$\overline{BC} = \frac{S}{\cos (\phi - \pi/2 - \theta)} = \frac{S}{\sin (\phi - \theta)} \tag{5.7}$$

By combination of these equations it can be shown (Chiang, 1979) that:

$$\theta = \tan^{-1} \left(\frac{\sin \phi}{S/p + \cos \phi} \right) \tag{5.8}$$

and

$$p' = \frac{S}{\sqrt{\left(1 + (S/p)^2 + 2 (S/p) \cos \phi\right)}} \tag{5.9}$$

Hence by measuring S, p and ϕ, θ and p' can be deduced. It should be noted that neither solid body translation nor extension in the direction of the grating lines affects the fringe spacing or orientation.

As an alternative, moire fringes may be considered as isothetics i.e. contours of displacement component. Considering again the unaxial extension situation in Figure 5.1, and denoting displacement as u we have:

$$u = N.p \tag{5.10}$$

The fringes are shown to be contours of displacement in the principal

direction, spaced at intervals of displacement of p. For small longitudinal strain:

$$\varepsilon_x = \frac{\partial u}{\partial x} = \frac{\partial}{\partial x}(Np)$$

$$\therefore \quad \varepsilon_x = p\frac{\partial N}{\partial x} \tag{5.11}$$

It should be noted that the moire technique is not restricted to small strains, however, the mathematics is simplified if this assumption is made.

For the case of pure shear strain shown in Figure 5.4, fringes are formed in the principal direction, hence $\partial N/\partial x = 0$ so that Equation 5.11 is still valid. The fringe spacing is now a function of the shear strain. It can be seen that:

$$\frac{\partial u}{\partial y} = \frac{\partial}{\partial y}(Np)$$

$$\therefore \quad \frac{\partial u}{\partial y} = p\frac{\partial N}{\partial y} \tag{5.12}$$

In order to obtain the full two-dimensional strain field, two orthogonal gratings are required. This is normally achieved using a crossed grating on the specimen and interrogating it with two orthogonal reference gratings one after the other. If we denote the fringe order obtained using gratings whose principal directions are x as N, those obtained with gratings whose principal directions are y as N' and the displacements in x and y directions as u and v respectively, we can obtain the strain field as follows:

$$\varepsilon_x = \frac{\partial u}{\partial x} = p\frac{\partial N}{\partial x}$$

$$\varepsilon_y = \frac{\partial v}{\partial y} = p\frac{\partial N'}{\partial y} \qquad (5.13)$$

$$\gamma_{xy} = \frac{\partial u}{\partial y} + \frac{\partial v}{\partial x} = p\left(\frac{\partial N}{\partial y} + \frac{\partial N'}{\partial x}\right)$$

It should be noted that in the normal application of moire methods Eulerian rather than Lagrangian strain is used.

The above method, sometimes known as coarse or mechanical moire, is the simplest form of in-plane moire measurement. The sensitivity is inversely proportional to the grating pitch, hence the sensitivity can be increased by using finer gratings. There is, however, a limit on the pitch which can be obtained. This limit for normal gratings is of the order of 40 lines/mm. This is insufficient for the present project, for which a sensitivity equivalent to a grating of 1000 lines/mm is required. However, there are several techniques to improve the sensitivity and, using interferometry, it is also possible to produce gratings with much greater line densities.

5.4.2 Mechanical moire - Increased sensitivity techniques

5.4.2.1 Fringe interpolation

As has been shown, the difference in the component of displacement, in the principal direction, between two adjacent fringes is equal to one grating pitch. If the reference grating is shifted by a small proportion of the grating pitch, the relative displacement will be modified by the amount shifted and new fringes will be formed between the original fringe positions. Displacement information is now available for non-integral fringe order positions. Durelli & Parks (1970) state that by this technique the sensitivity can be increased five fold, however, this depends on very accurate grating shifts.

5.4.2.2 Grating mismatch

The discussion in Section 5.4.1 was limited to the situation where the specimen and reference gratings were identical prior to loading so there were no fringes in the no-load field. Fringes can be obtained in the no-load field either by modifying the pitch or the orientation of one of the gratings. The displacement (or strain) is then related to the difference between the initial and final patterns. In this case there are more fringes so that the displacement is known at more positions which results at greater resolution of the displacement field. A fuller description of grating mismatch techniques may be found in Chiang (1979).

5.4.2.3 Fringe multiplication

So far light has been considered as rays moving in straight lines. When light passes through a small aperture diffraction effects become significant and it is more helpful to consider light as waves. The gratings used for sensitive mechanical moire work are sufficiently fine to cause significant diffraction. In physical optics (as this approach is termed) light is treated as continually emanating from every point in all directions, in a similar way to the ripples caused by a stone dropped in water (Fig. 5.5). This is known as Huygen's principle and has certain limitations (Longhurst, 1973). However, it provides a useful visualisation of the diffraction effect.

Before discussing diffraction the terms constructive and destructive interference must be understood. A plane wave may be described mathematically as:

$$\psi = A \cos \left(\omega t - \frac{2\pi x}{\lambda} + \phi\right) \qquad (5.14)$$

where ψ is the disturbance at a point.
A is the amplitude.
ω is the circular frequency.
t is time.
x is the distance in the direction of travel.
ϕ is the phase when $t = x = 0$.

It can be seen that ψ can vary from A to -A depending on the phase at the given values of x and t. When two waves are superimposed their disturbances are additive and are said to interfere with each other. When the phases are equal or are an even number of π apart the disturbances reinforce each other. This is constructive interference. Destructive interference occurs when the phases are an odd number of π apart with the result that the disturbances detract from one another.

Figure 5.6 shows the diffraction which occurs at a grating. For

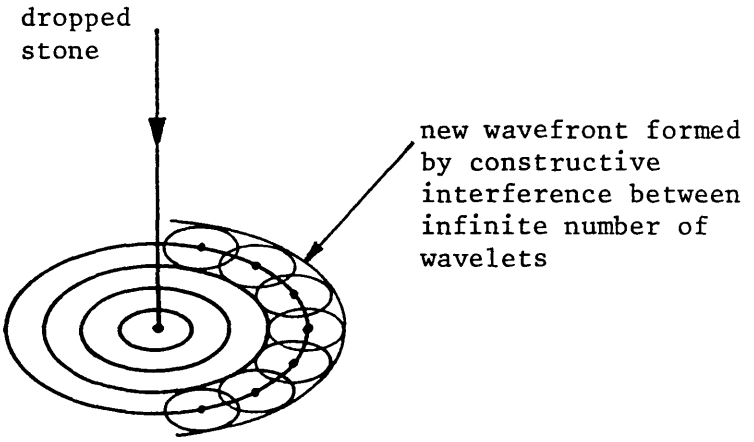

Fig. 5.5 Huygen's principle - illustration of stone dropped in water

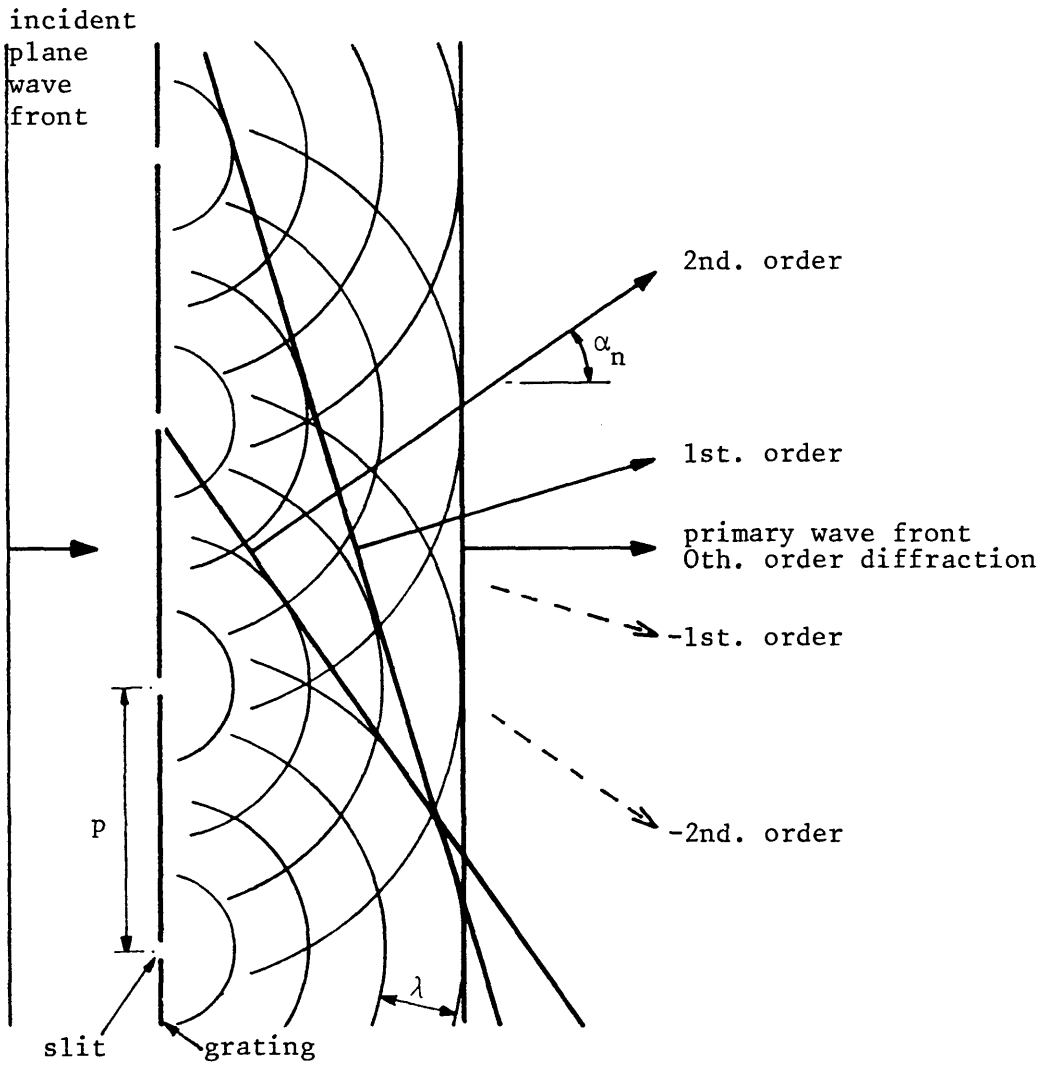

Fig. 5.6 Diffraction at a grating

simplicity we assume a monochromatic incident plane wave front. Each slit in the grating can be considered to be a new light source in phase with all other slits. From the Figure it can be seen that several wave fronts leave the grating at various angles α_n to the normal. The wave fronts are caused by constructive interference between the waves emanating from the slits. The values of α_n are given by:

$$\sin \alpha_n = \frac{n \lambda}{p} \tag{5.15}$$

where n is an integer known as the diffraction order.

For further discussion of diffraction effects refer to Smith & Thompson (1971) or Longhurst (1973).

If these wave fronts are focused by a lens, an array of dots in the focal plane of the lens will result. These dots correspond to the different diffraction orders and, for small α, will be spaced $f\lambda/p$ apart. The light from the dots can then be recombined to form an image of the grating as shown in Figure 5.7.

The amplitude of a wave front is modified as it passes through a grating. The resultant amplitude is a function of the position across the grating which is dependent on the grating transmittance. This function can be expanded in a Fourier series:

$$A(x) = A_0 + A_1 \cos\frac{2\pi x}{p} + A_2 \cos\frac{4\pi x}{p} + \ldots\ldots + A_n \cos\frac{2n\pi x}{p} \ldots\ldots \tag{5.16}$$

Each term corresponds to a diffraction order (Sciammarella, 1982). If, instead of allowing the light from all the dots to be focused by the second lens, a filter which only passes light of selected orders is placed in the plane of the dots, then the image of the grating will only consist of light from these orders. For example, if only light from the +2 and -2 orders is allowed to pass (Fig. 5.8), then the light focused by the second lens will be $A_2 \mathrm{Cos}(4\pi x/p)$. This modified

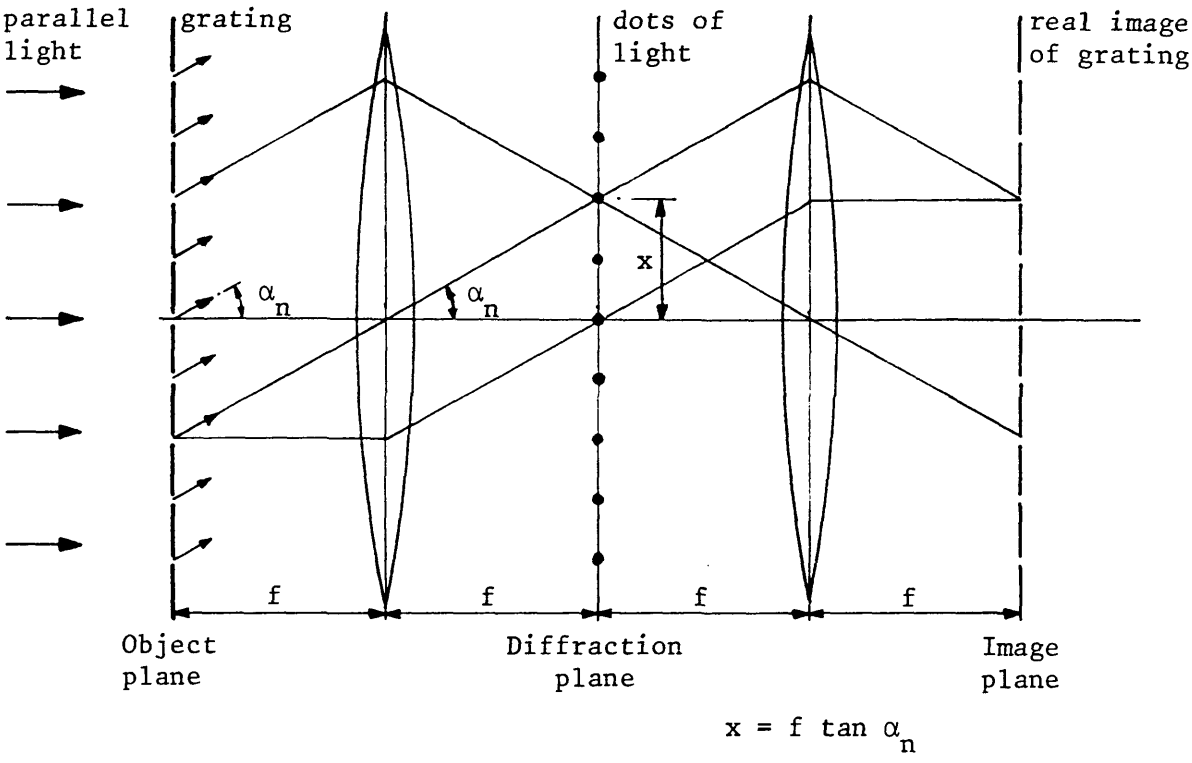

Fig. 5.7 Optical filtering arrangement

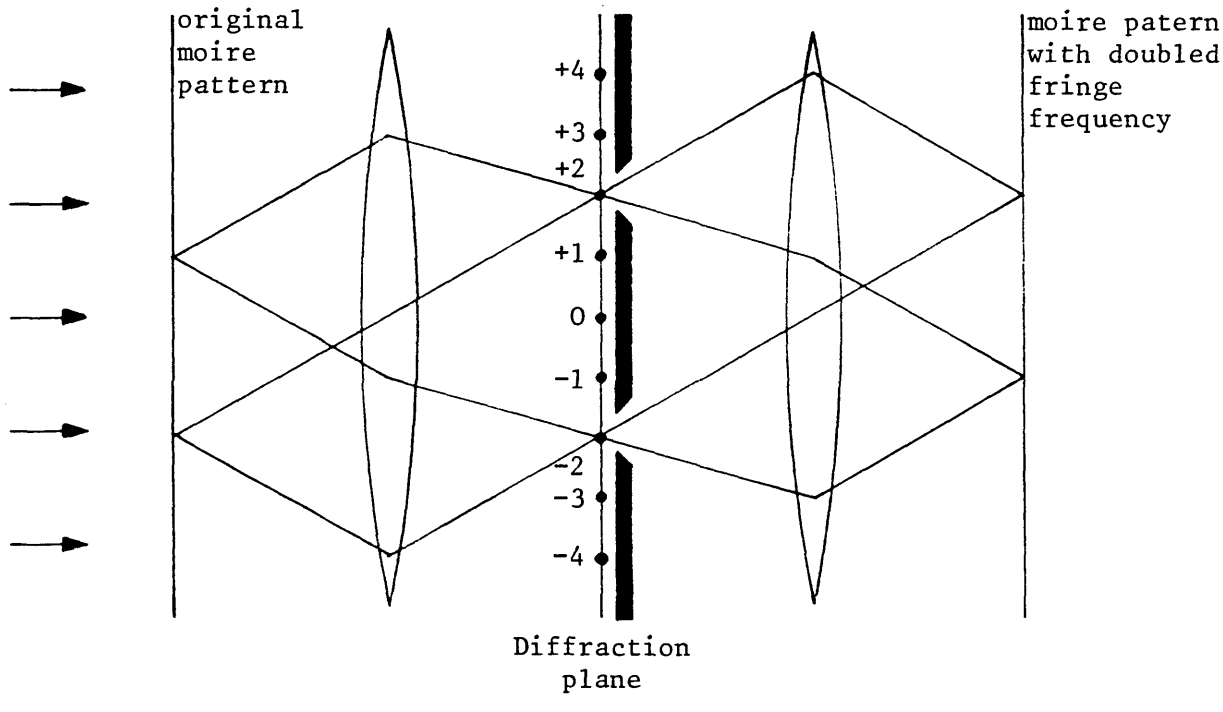

Fig. 5.8 Arrangement for fringe multiplication by a factor of 2

function shows that the amplitude still varies cosinusoidally but with a frequency twice that of the original grating. This is the principle of fringe multiplication by optical spatial filtering. If the grating is replaced by a high density moire pattern the frequency of the fringes can also be increased by selection of light only in the higher orders.

The level of fringe multiplication possible depends on the light available in the higher orders. For instance, if the transmittance of the object varies cosinusoidally with x then, when expanded in a Fourier series, this would consist of only the first two terms, i.e. there would be no diffraction orders greater than 1. On the other hand a step function light amplitude yields a significant proportion of light in the higher orders. In theory the multiplication factor could be as great as 50 however 25 is more common (Walker & McKelvie, 1978).

A further technique, sometimes mistakenly referred to as fringe multiplication, is the use of a reference grating finer than the specimen grating. It can been seen from Figure 5.1 that the use of a reference grating of double the frequency of the specimen grating yields a moire pattern similar to that which would be obtained if both gratings had the higher frequency. Post (1968) used a combination of this technique and fringe multiplication by optical spacial filtering to produce multiplication factors of up to 30.

Optical filtering can also be use to filter out a high density mismatch or to optimise fringe contrast (Durelli & Parks, 1970). A fuller description of optical filtering may be found in Chiang (1969).

5.4.3 Moire interferometry

The term moire interferometry has been givern to a form of the moire method which depends on the interference between two coherent light beams to set up one or both of the gratings. The basic theory is the same as for mechanical moire, however, the grating frequencies are much higher allowing greater sensitivity.

The technique, invented by Boone (1971a), involved setting up two coherent light beams and recording their interference pattern in a photographic emulsion on the specimen surface. Figure 5.9 shows the interference pattern set up. It consisted of closely spaced 'walls' of destructive and constructive interference. The distance between two adjacent constructive interference 'walls', p, is given by:

$$p = \frac{\lambda}{2 \sin \theta} \tag{5.17}$$

The specimen was strained and a second recording of the interference pattern was made on the emulsion. The emulsion was developed and the two gratings produced which, when illuminated, formed the moire pattern corresponding to specimen deformation. Boone showed that if the bisector of the two light beams was perpendicular to the specimen surface then the fringes are contours of the in-plane displacement component in the grating principal direction. The technique can also be used to measure out-of-plane displacement. Boone (1971b) extended the method to determine strains directly using optical rather than mathematical differentiation of the displacement field.

Similar techniques have been used by several researchers. Lehmann (1972) produced metallic gratings for spectroscopy of up to 1100 lines/mm.. Wadworth, Billing & Marchant (1972; Wadsworth, Marchant & Billing, 1973) and Marchant & Bishop (1974) used gratings recorded on a photo-resist, or photo-sensitive layer, to measure deformation of aluminium and carbon-fibre specimens. The photo-resist was of the positive working type, that is to say the developer dissolves those parts which have been exposed to light leaving a phase type grating.

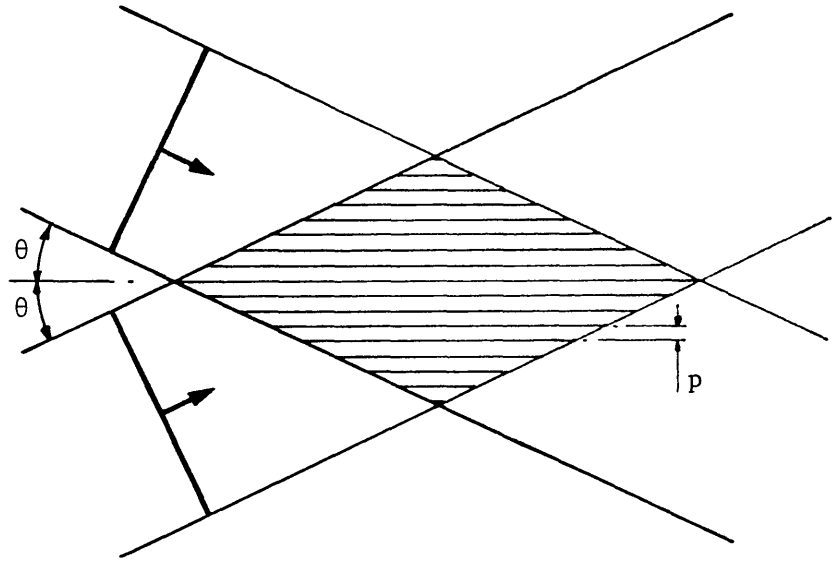

Fig. 5.9 Virtual grating formed by interference between two coherent light beams

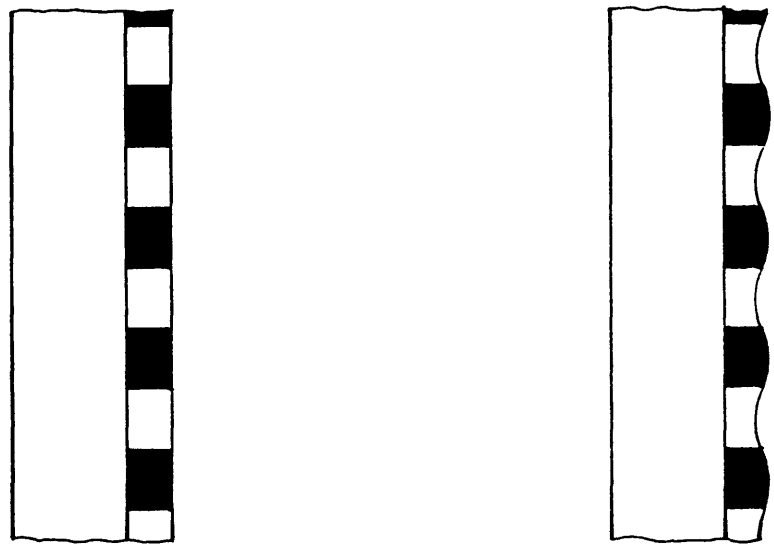

(a) Developed plate, wet

(b) Dry, gelatin shrinkage

Fig. 5.10 Manufacture of mold using a photographic plate

In this case, as in all subsequent uses of the method using a photo-resist, only one grating was recorded on the specimen which was then developed. Live fringes were visible during deformation of the specimen when it was illuminated by the same interference pattern used to form the specimen grating. This type of reference grating is known as a virtual grating.

If live fringes are not required then the double exposure technique can be used. A photograph is taken of the undeformed specimen grating. A second exposure is made of the same film, to the deformed specimen grating. The moire pattern is formed when the negative is illuminated.

Fringe multiplication and grating mismatch are both applicable to moire interferometry. However, fringe interpolation is impractical due to the small grating shifts required.

More recently the scope of moire interferometry has been extended through a method originally devised by Post and others at the Virginia Polytechnic Institute and State University. In this case, the specimen grating is formed using a mould. A high resolution photographic plate is exposed to a virtual grating. When developed, the plate contains metallic silver in the bands exposed to constructive interference while the silver is leached out of the gelatin in the bands exposed to destructive interference. On drying, the gelatin tends to shrink but is restrained by the silver which results in the undulated surface shown in Figure 5.10. This surface can then be used as a mould for a phase-type grating on the specimen. To form the grating, Post & Baracat (1981) used a film of liquid silicone rubber on the specimen surface onto which the mould was clamped until the rubber had cured. In later work, an epoxy resin or an acrylic cement was used instead of the silicone rubber (Post, 1982). The grating reflectance can be significantly improved by evaporating a layer of aluminium onto the surface of the mould which subsequently sticks to the adhesive. The greater reflectance is important since it means that either a less powerful laser may be used or the area under examination may be increased.

Several optical arrangements are possible for this form of moire interferometry and two are shown in Figure 5.11. They have in common,

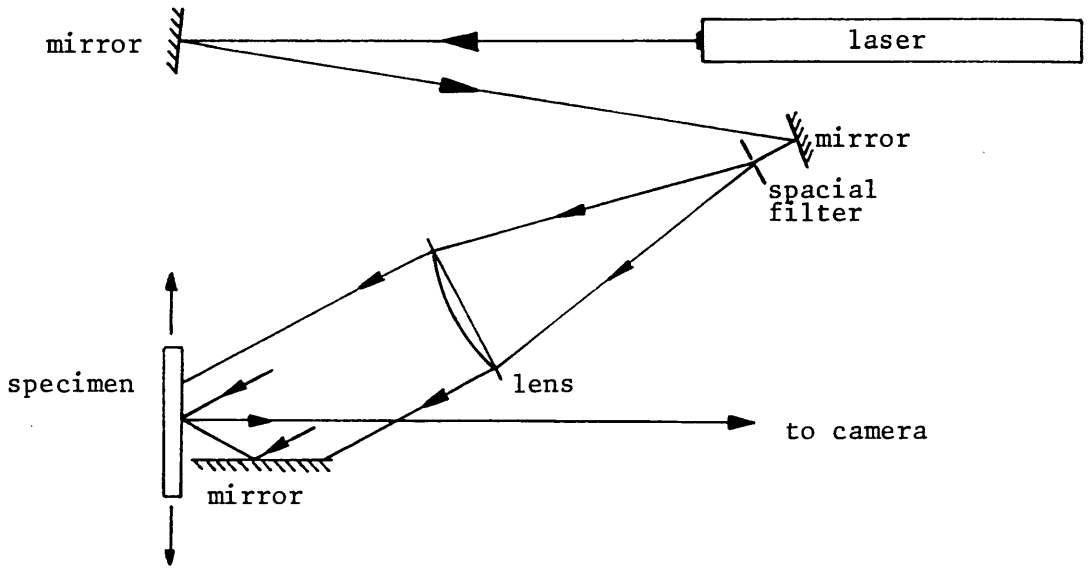

(a) Arrangement 1, mirror at right angles to specimen

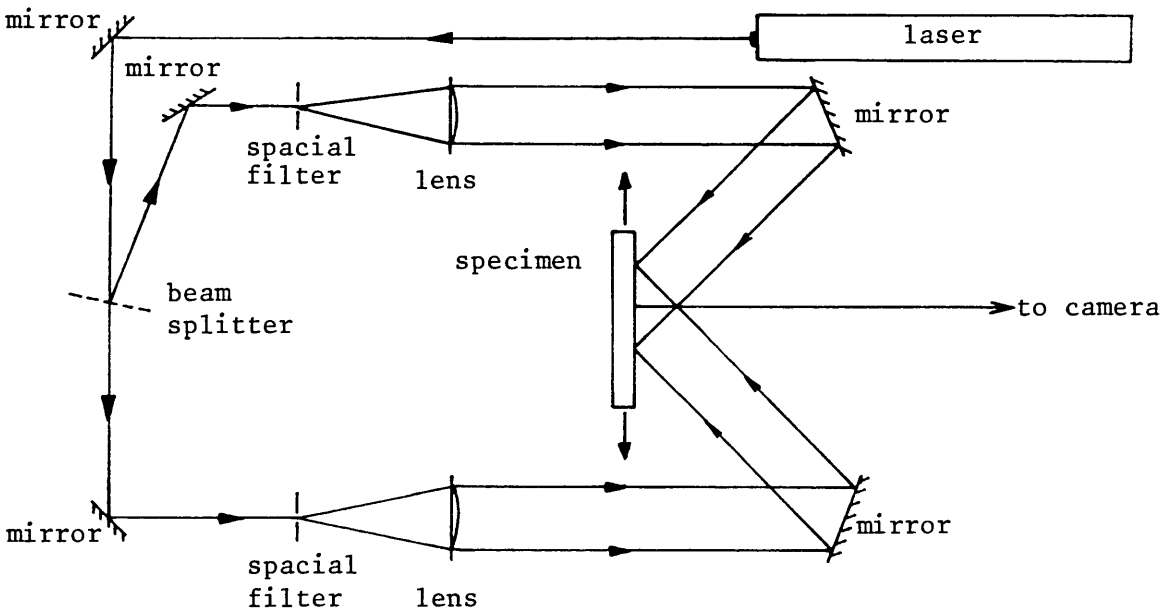

(b) Arrangement 2, double expanded beam illumination

Fig. 5.11 Two optical arrangements for moire interferometry

two incident coherent light beams at equal angles either side of the normal to the specimen surface. The angles of incidence of the two beams are arranged such that their first order diffraction beams are aligned along the normal. The recording system is located along the normal. It should be noted that in this technique the frequency of the reference grating is twice that of the specimen grating giving an apparent fringe multiplication by a factor of 2. The theoretical upper limit for sensitivity is approached when the grating pitch approaches half the wavelength of the light used (Weissman & Post, 1982a). This is more than sufficient for the present project.

In order to obtain the full, surface strain field two illumination directions are required (Weissman & Post, 1982b). In this case a crossed specimen grating is used. The mould is manufactured by twice exposing the photographic plate to the virtual grating, rotating the plate by 90 degrees between exposures. This technique has been used to measure the deformation of several materials; graphite-polyimide composite sheet (Post et al., 1981), polymethylmethacrylate (Basehore & Post, 1981,2) and metals (Nicoletto, 1983). A similar technique using a real reference grating has been used to determine coefficients of thermal expansion of graphite-epoxy laminates (Bowles, Post, Herakovich & Tenney, 1981).

The main disadvantage with this technique is that, in order to observe an area of 100mm.x100mm. with an arrangement which is not sensitive to vibration (ie. sufficient light to have short exposures for the mould), it is necessary to have a powerful laser and large costly optics. The majority of the work so far has been done using small observation areas.

This problem can be circumvented using a system called the Optecord Live-fringe Interferometer (McDonach, McKelvie, MacKenzie & Walker, 1983), which has been developed at the Centre for Industrial Innovation, University of Strathclyde. In place of the 'home-made' moulds of the 'Post' technique, a ready made master grating, 100mm.x100mm., was purchased from the National Physical Laboratory from which submasters could be taken to form the specimen grating moulds. This means that, instead of having to illuminate the whole of the area of interest at one time, a patchwork of observations of

smaller parts of the area may be made. In practice the interferometer has an observation area of 50mm. diameter so that 9 observations would be required to cover the whole of the largest possible specimen grating.

The other difference between the 'Post' technique and Optecord is in the choice of diffraction orders. The 'Post' technique considers the crossed grating as two superimposed gratings and uses the +1 and -1 orders for one grating followed by the +1 and -1 orders for the second grating. This entails using four illumination directions. Optecord makes use of the fact that a two dimensional grating has diffraction orders which are a combination of the diffraction orders of both principal directions (Longhurst, 1973). This can be visualised by considering the diffraction orders shown in Figure 5.12. The 'Post' technique uses the (1,0) and (-1,0) orders to obtain displacements in the x-direction and (0,1) and (0,-1) orders to obtain displacements in the y-direction. Optecord uses (-2,-2) and (2,-2) to obtain the x displacements and (2,2) and (2,-2) to obtain the y displacements, hence using only three directions of illumination. If the (2,2) and (-2,-2) orders are used the displacements in the 45 degree direction are obtained (McDonach, McKelvie & Walker, 1980). The profile of the specimen grating has been optimised to give the maximum possible light in these orders. The main disadvantage with Optecord is that it is necessary to take several photographs at each load level, for each displacement direction.

The only known application of moire interferometry to concrete is that being undertaken at Politecnico di Milano (Cedolin, Dei Poli & Iori, 1981 & 1983; Iori, Lu, Marozzi & Pizzinato, 1982a & b). The specimen grating is recorded on photoresist in a similar method to that used by Wadsworth et al.. Due to the poor reflectance of the grating a large laser (500mW) is used. Considerable difficulty has been experienced in obtaining a sufficiently smooth surface on the concrete, also, the best exposure time for the photoresist is dependent on the ambient conditions.

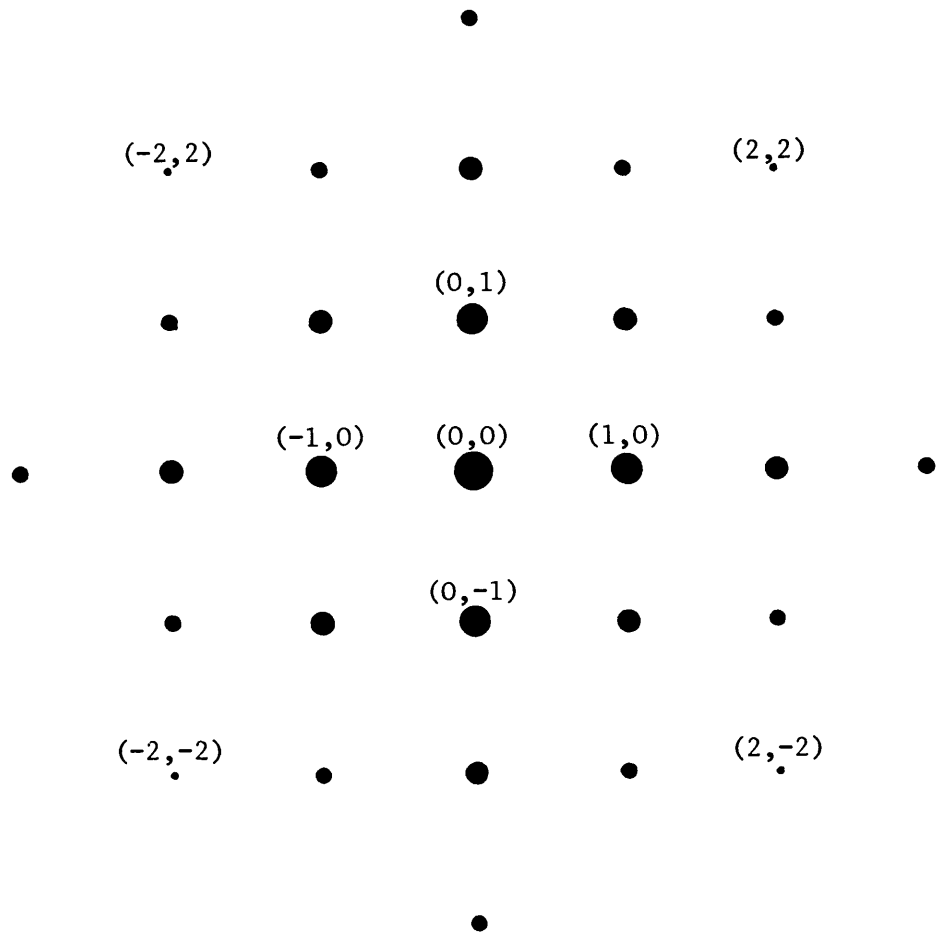

Fig. 5.12 Diffraction orders for crossed grating

5.4.4 Summary

Both mechanical moire with increased sensitivity and moire interferometry could be used to measure the strains in concrete specimens. However, the increased sensitivity techniques used with mechanical moire all suffer the drawback that live fringes cannot be obtained and post-processing is always required.

Three moire interferometry techniques have been described, the main differences between them being the formation of the specimen grating and the choice of diffraction orders. The photoresist technique is not easy to use. The 'Post', home-made mould technique would require expensive optics and a large laser. The Optecord Live-fringe Interferometer can only observe an area 50mm. in diameter and would require a patchwork of observations to cover a larger area.

5.5 Non-contact optical techniques

The main disadvantage associated with the moire method described in Section 5.4 is that it requires the formation of a grating on the surface of the specimen. The non-contact techniques described below rely on imaging the surface itself rather than imaging a superimposed grating. When a rough object is viewed in coherent light, the surface is seen to be covered by a random pattern of small speckles. This phenomenon is due to the multiple interference of the reflected light caused by random division of the incident beam at the object surface. The size of the apparent speckles depends on the resolution of the imaging system and is given approximately by Archbold, Burch & Ennos (1970) as:

$$b_s \simeq 1.2 \lambda F \tag{5.18}$$

where λ is the wavelength of the light.

F is the 'f' number of the aperture of the imaging system.

Typical imaging systems vary from about f/1.4 to f/32, consequently if, for example, a Helium-Neon laser is used, (λ = 632.8nm) then the speckle size can be varied from 1 to 24 microns. It is this speckle field which can be used to measure the displacement of the surface.

In conventional photography only the intensity of the light is recorded. Referring again to the mathematical description of a light wave given in Equation 5.14, it can be seen that for a full recording of the wave, it is necessary to record both amplitude and phase. This is the basis of holographic interferometry in which recordings in both amplitude and phase of the speckle fields before and after straining are compared. Speckle interferometry and speckle photography compare recordings in intensity only of the speckle fields.

5.5.1 Holographic interferometry

The word hologram comes from the Greek word 'holos' meaning 'the whole', because it contains the whole of the information, i.e. both amplitude and phase, of the incident light wave. The optical set up used to create 'off-axis' holograms using reflected light is shown in Figure 5.13. A coherent light source is used so that the path lengths of the object and reference beams need not be identical. It is convenient to consider the light beams as a series of wavefronts along which the phase angle is constant. Light from the one source is split into the object and reference beams. The object beam wavefronts reflected from the surface of the object become distorted and when they are recombined with the reference beam in the plane of the hologram, form a series of very fine interference fringes. These fringes are recorded on a high resolution photographic plate. When the developed plate is reilluminated by the reference beam it acts as a diffraction grating, the main emergent beams being the 0, -1 and +1 diffraction orders (Fig. 5.14). The true image beam (1st order diffraction) is a reproduction of the original object beam so that the image appears to be three dimensional. The -1 diffraction order forms a conjugate image.

Gabor (1948,9), the inventor of holography, used it as a means of increasing the magnification of optical microscopes. He used an electron beam source to create the hologram which was subsequently re-illuminated using a visible light source. The magnification comes about due to the ratio of the wavelengths of the electron and visible light beams.

In order to measure the deformation of an object we need to compare, interferometrically, the deformed object beam with the object beam as it was before the deformation took place. This can be done by recording on the same plate the holograms of the object both before and after deformation. When the developed plate is re-illuminated the original and deformed image beams are seen superimposed. Since the phase of the deformed image beam will have changed from the original by an amount dependent on the change in path length the object is seen to be covered by a series of interference fringes. This is known as

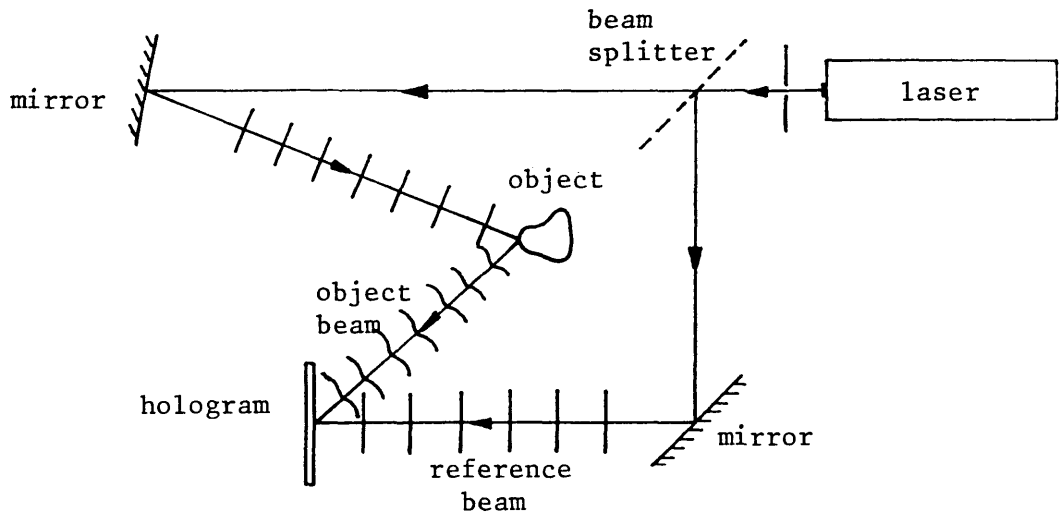

Fig. 5.13 Arrangement for making holograms using reflected light (Taylor, 1979)

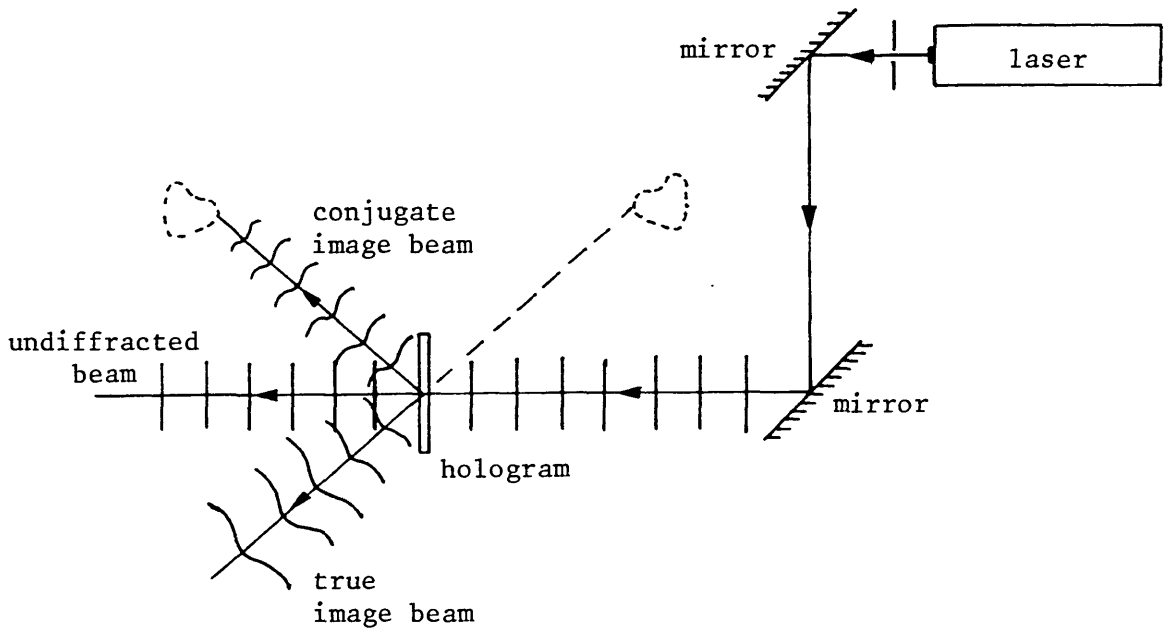

Fig. 5.14 Arrangement for reconstruction of wavefronts (Taylor, 1979)

double exposure holographic interferometry. Real time holographic interferometry may also be carried out and in this case a hologram is made of the undeformed object which, after processing, is returned exactly to its original position. Now, the deformed object beam interferes with the image beam emerging from the hologram and the object is seen to be covered by a series of fringes which move as the object is deformed.

Consider a point P on the surface of the object, which moves a distance d to a new position P' (Fig. 5.15). The angle between the directions of illumination and observation is 2α and their common bisector makes an angle of β with the direction of movement. The total increase in path length, Δ, is given by:

$$\begin{aligned} \Delta &= \overline{AP'} + \overline{P'B} \\ &= d\,(\cos(\alpha + \beta) + \cos(\alpha - \beta)) \\ &= 2d \cos\alpha \cos\beta \end{aligned} \tag{5.19}$$

It can be seen that the system is only sensitive to displacement in the direction of the common bisector of the illumination and observation directions. The path difference can be related to the wavelength as follows:

$$\Delta = N\lambda \tag{5.20}$$

where N is the fringe order.

λ is the wavelength.

Hence:

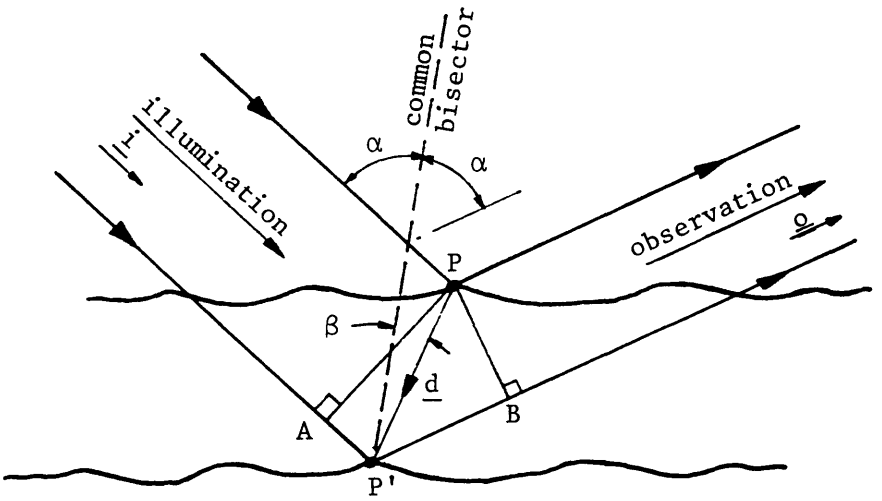

Fig. 5.15 The geometry of holographic displacement fringe formation (Robertson & King, 1983)

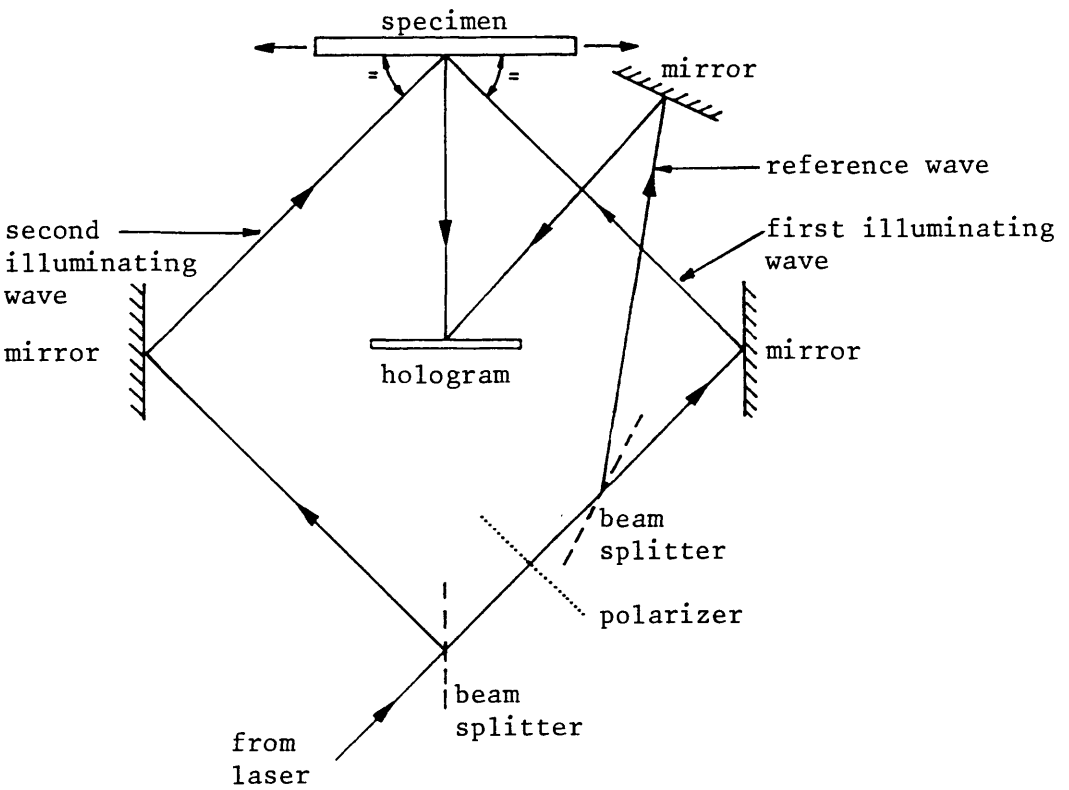

Fig. 5.16 Holographic measurement of in-plane deformation (Boone, 1970)

$$N\lambda = 2d \cos\alpha \cos\beta \qquad (5.21)$$

This is the simplified case in which the movement is in the plane of the illumination and observation directions. In the general, three dimensional case, Ennos & Archbold (1976) use the following equation:

$$N\lambda = \underline{d} \cdot (\underline{i} - \underline{o}) \qquad (5.22)$$

where $\underline{d}$ is the vector of displacement of point P.
$\underline{i}$ is the unit vector in the illumination direction.
$\underline{o}$ is the unit vector in the observation direction.
(Note, the nomenclature has been modified from the original).

The sum of $\underline{i}$ and $\underline{o}$ is sometimes denoted $\underline{s}$, the sensitivity vector along the common bisector. In general, $\underline{s}$ is not a unit vector (Boone, 1976).

Holographic interferometry is shown, therefore, to be most easily usable for the measurement of out-of-plane displacements and that only the component of displacement along the sensitivity vector is available for each fringe pattern. It follows that, in order to obtain the full displacement field, three non-coplanar sensitivity vectors must be used. In the present project only in-plane displacement is required which cannot be measured directly since that would require a sensitivity vector in the plane of the surface. Ennos (1968) used two holograms to obtain in-plane displacement. The first hologram had a sensitivity vector which was nearly parallel to the specimen surface making use of partially retroreflective paint. The second hologram was a reflective hologram with an out-of-plane sensitivity vector normal to the specimen surface. The difference in the fringe orders of the two holograms yielded the in-plane displacement fringe orders. An improved method for the determination of in-plane strain was proposed by Butters (1970) and used by Boone (1970) to determine the in-plane displacements of a stretched foil. The test set up used by Boone is

shown in Figure 5.16 The specimen is illuminated by two beams at equal angles on either side of the normal and viewed along the normal. The two reflected object beams are combined with a reference beam at the holographic plate and the two holograms simultaneously recorded. Since the sensitivity vectors are at equal angles on either side of the normal the resultant sensitivity vector (a subtraction of the two separate vectors) is parallel to the surface of the specimen. The fringes formed are contours of equal in-plane displacement and can be thought of as a type of moire fringe. For this reason the technique is sometimes known as holographic-moire. It should be noted that the fringe spacing, in the case of two beam illumination, is not affected by small solid body movements. Boone obtained poor fringe contrast but this was improved by Sciammarella & Gilbert (1976) and Sciammarella & Chawla (1978) by using an initial high density pattern which was subsequently filtered.

There are two disadvantages with the use of holographic interferometry for the present project. The first is that any change in the phase difference between the object and reference beams during exposure will obliterate the fine interference pattern on the photographic plate. It is necessary, therefore, to isolate the equipment as well as the object from any relative vibration. This would require a large spring-supported heavy mass on which all the equipment could be mounted.

The second disadvantage is that holographic interferometry is sensitive to total movement and the maximum measurable movement is of the order of 20 microns (Jacquot & Rastogi, 1983). It is expected that significantly larger displacements will occur in the central area of the specimen. In this case it would be necessary to follow the movement using several double exposure holograms one after the other. This was the technique used by Luxmoore (1973,4) when applying out-of-plane holographic interferometry to detect cracks in concrete specimens loaded under compression. An alternative is to arrange that the no-load hologram be shifted by an ammount equal to the solid body displacement of the specimen during the loading (Boone, 1976). The relative displacement between the specimen and no-load hologram could then be limited to a maximum of 20 microns, however, this this does not seem to be practical in the present project.

5.5.2 Speckle interferometry

The in-plane holographic interferometry arrangement used by Butters and Boone (Fig. 5.16) records more information than is actually required to obtain the displacements. Leendertz (1970) used the same arrangement except that he omitted the reference beam and in this case the photographic plate records two superimposed speckle fields rather than two superimposed holograms. A displacement in the x-direction (Fig. 5.17) produces a relative phase change between the two speckle fields which is recorded on the plate. When the plate is developed the surface is seen to be covered by fringes which are contours of equal displacement in the x-direction. The interpretation of the fringes is similar to that for two beam illumination holographic interferometry. It can be seen that displacements in the y- and z-directions produce no relative phase change and do not, therefore, affect the fringe pattern. Also, small solid body movements in the x-direction do not affect the fringe spacing (Jones, 1974). For full plane strain measurement, two illumination directions are required (Jones, 1976).

Real time fringe patterns may be obtained by developing the photographic plate after the first exposure and returning it to it's original position. Alternatively pseudo real time fringes can be formed using the Electronic Pattern Speckle Pattern Interferometer developed at Loughborough University (Denby & Leendertz, 1974; Butters, 1976 & 1983). In this case the two superimposed speckle fields are recorded using a television camera and then compared with the deformed object speckle fields electronically rather than optically.

The main advantage of speckle interferometry over holographic interferometry is that the high resolution requirements of the recording medium can be relaxed and for this reason a television camera can be used. The optical set up is also slightly simpler, however, the sensitivity to external vibration and the limits on measurable displacement are unchanged. The reason for the upper limit

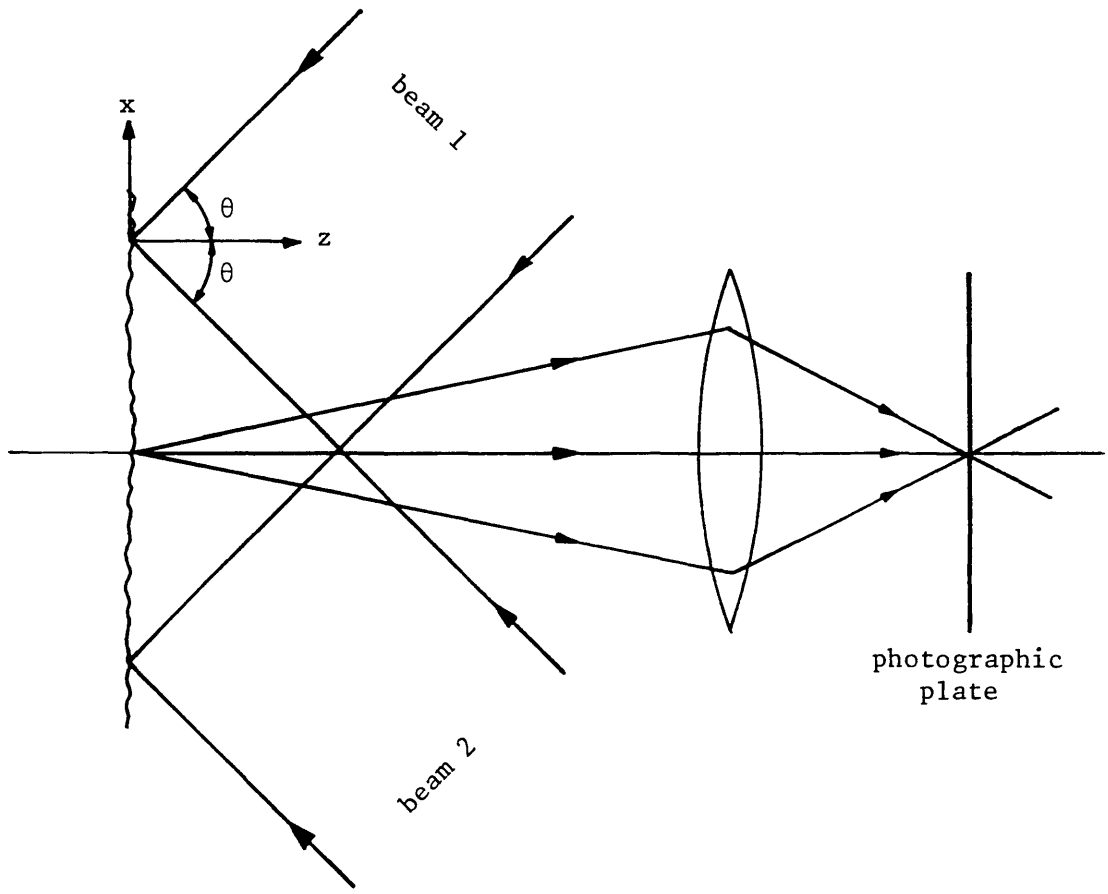

Fig. 5.17 Measurement of in-plane displacement using the speckle effect

on the measurable displacement is that as displacement increases correlation of the speckle fields decreases. Archbold et al., (1970) show that the fringe visibility falls to less than one third of its original value when the displacement is equal to the apparent speckle diameter. For measurement of displacements greater than the apparent speckle diameter an alternative technique known as speckle photography can be used.

5.5.3 Speckle photography

Burch & Tokarski (1968) investigated the effects of recording two identical speckle fields on a photographic plate with a short transverse shift between the fields. When the processed plate was illuminated by a narrow coherent light beam the diffraction halo so produced contained a pattern of parallel straight fringes similar to Young's fringes. This resulted from the combined effects of interference between each of the speckle pairs. If the speckle patterns are images of a surface before and after displacement, the magnitude and direction of that displacement may be found from the spacing and orientation of the fringes (Jacquot et al., 1983; Archbold et al., 1970) Conveniently, the lower limit of displacement which gives rise to fringes in the diffraction halo is approximatly equal to the apparent speckle diameter. This means that the technique becomes usable when speckle interferometry cannot be used. It should be noted that, if the two speckle fields within the area of the image illuminated by the narrow light beam are not identical, then the fringe contrast will be reduced. This can happen when the strain is very large or when the nature of the surface changes due to the presence of a crack. Giglio, Musazzi, Perini & Rossi (1983) have made use of this de-correlation of the speckle fields to detect cracks in concrete beams.

Analysis of the processed plate by a narrow coherent light beam gives point-by-point information on the displacement from which the strains can be calculated. Archbold & Ennos (1972) describe an alternative method involving a type of spatial filtering which yields contours of

displacement in a given direction across the whole of the image.

Speckle photography has been used to measure displacements in several different materials. Luxmoore, Amin & Evans (1974) and Evans & Luxmoore (1974) used the technique on Araldite and aluminium specimens, Archbold & Ennos (1975) located cracks in steel welds and Ennos et al., (1976) studied the deformation of polymers. De Backer (1975) was the first to make use of speckle photography to detect cracks in concrete. He was also able to measure the opening of cracks under load. Pflug (1979) used speckle photography for the detection and monitoring of cracks in concrete beams.

Despite this fairly widespread use, there remains some doubt over the quantitive accuracy of speckle photography. Archbold, Ennos & Virdee (1978) and Allison & Ennos (1981) have responded with a critical assessment of the technique. Their initial studies on the effect of out-of-plane movements indicated that significant errors of the order of 300 microstrain could occur unless a telecentric imaging system was used. Even under the best conditions, uncertainties of up to 100 microstrain, or 20% of the value being measured occurred which were attributed to lens aberration effects. Greater errors are to be expected when applying the technique to concrete specimens due to the surface not being flat. Pflug (1979) compared the use of speckle photography with microscopic and holographic techniques and concluded that it can only be conveniently used for the detection of cracks in concrete and not for any precise measurement.

5.5.4 Summary

The three non-contact optical measurement techniques described have the advantage that no special surface preparation is required, however, they all have drawbacks which make them unsuitable for the present project. The main disadvantages with holographic and speckle interferometry are their sensitivity to external vibration and an upper limit to the measurable displacement of the order of 20 microns. Both these problems could be overcome but only with difficulty.

Speckle photography is an inexpensive, adaptable technique, but the accuracy to which the strains can be evaluated is insufficient.

5.6 Conclusions

In this chapter several full-field surface strain measurement techniques have been reviewed. In Section 5.1 the requirements for strain measurement in the direct tensile testing of concrete specimens were outlined.

Photoelastic coatings, which have previously been applied to concrete specimens, are not considered suitable for the present project due to the surface reinforcing effects which may inhibit the localisation of strain in the specimen. Similarly brittle coatings may not be used since they lack sufficient sensitivity and accuracy.

Three non-contact optical techniques have been reviewed, namely, holographic and speckle interferometry and speckle photography. The interferometric techniques suffer two main drawbacks which prevent their use in the present project. Firstly, due to their high sensitivity to displacements they must be isolated from any vibration and secondly, they can only be conveniently used when the displacement of the surface from it's original position is less than approximately 20 micron. Speckle photography has been shown to be insufficiently accurate.

The only technique considered suitable is the moire method and in particular moire interferometry. Mechanical moire is not sensitive enough unless post-processing techniques or grating mismatch are used which means that live fringes cannot easily be obtained. Three different techniques for moire interferometry have been outlined. The selection and full description of the technique to be used is given in Chapter 6.

Chapter 6 Adopted deformation measurement technique

Various full field strain measurement techniques were reviewed in Chapter 5 and it was concluded that moire interferometry was the most suitable for the present project. Three different moire interferometry techniques were described. The selection of the technique to be used is discussed in Section 6.1; the technique itself is described in detail in Section 6.2. The analysis of the results and the limitations of the technique are discussed in Sections 6.3 and 6.4 respectively.

6.1 Selection of moire interferometry technique

Three possible moire interferometry techniques were outlined in Section 5.4.3. All three techniques are capable of producing similar results and consequently the selection of the technique to be used depended on the following considerations:

1. The cost of the technique. This includes both the cost of the equipment and the cost of the consumable materials required.
2. The ability of the technique to be used on a damp substrate.
3. The development time and expertise necessary to set up the technique in the laboratory.
4. The amount of specimen preparation required.
5. The ease of use of the technique.
6. The ease of relocation of the equipment for use on other projects in the laboratory.
7. The safety requirements, particularly when using lasers.
8. Whether or not the technique could be tried out prior to capital outlay on equipment.

In order to assess the relative merits of the techniques, contact was established with various researchers who had used each of the techniques. To evaluate the photo-resist technique, the writer spoke to M. Marchant (see Marchant & Bishop, 1974) at the Royal Aircraft Establishment, Farnborough, and also visited the Politecnico di Milano, where the photo-resist technique had already been used on concrete (Cedolin, Dei Poli & Iori, 1981,3; Iori, Lu, Marozzi & Pizzinato, 1982a&b). There were several major drawbacks some of which were described by Cedolin during the visit, and these are highlighted below.

1. In order to produce a good specimen grating a very flat surface was required, many gratings had to be re-made since they were not of sufficient quality.
2. The optimum exposure time for the photoresist was dependent on ambient conditions.
3. It was necessary to mount all the equipment on a marble slab

supported on springs to eliminate vibration during exposure.

4. Due to the poor reflectance of the grating a large laser (500mW) was required, with the associated safety hazard and high capital cost.
5. The technique had not been applied to damp concrete and it was expected that the moisture would adversely affect the photoresist.

For these reasons, and on Cedolin's recommendation, the photo-resist technique was discarded.

The 'Post' technique has been used by several researchers and whilst in Italy, the writer took the opportunity to discuss the technique with Dott. Ing. Nicoletto at Instituto di Meccanica Applicata alla Macchine, Bologna, who had applied it to the fracture of metals (Nicoletto, Post & Smith, 1982; Nicoletto, 1983). The two main extensions of the technique that would be required for it to be used in the present project were the need to find a moisture tolerant material for the specimen grating and the need to increase the area of observation to approximately 140mm. diameter. The laser power necessary for the manufacture of gratings of this size was not known but would be of the order of 25mW.. Due to the size of the specimen grating required, Professor Post, in a private communication, suggested the use of the Optecord L.F. Interferometer.

The Optecord L.F. Interferometer works on the same basic principle as the 'Post' technique, however, the main difference is that a master grating can be supplied with the Interferometer. The laser power and sizes of the optical components required for the 'Post' technique are dependent on the size of the specimen grating, whereas in Optecord they depend only on the area of observation. In order to use this latter technique the only developments required were the formation of the grating on a damp substrate and the manufacture of a carriage which would allow easy positioning of the Interferometer in front of different parts of the specimen grating. Tests at the University of Strathclyde identified a suitable epoxy resin for use as the first layer of the grating to seal the concrete surface. It should be noted that this resin might also have been useful for the 'Post' technique.

The main advantages of Optecord were that the equipment was already

built, housed in an easily transportable box, and that the technique could be proved at the University of Strathclyde before purchase. On the other hand, the 'Post' technique might take several months to set up. The Optecord laser power was only 5mW. with only the expanded beam emerging from the housing. This made it particularly suitable for general laboratory use. The processes involved in the manufacture of gratings, using the Optecord master grating, were simpler and less time consuming than the 'Post' technique. The main disadvantage of Optecord was the need to take several photographs to observe the full area of the grating. The total cost of the Optecord L.F. Interferometer and associated master grating was £10,400. The estimated cost for the components of the 'Post' technique was £7,500. The running costs per test were very similar for the two techniques, Optecord needing a larger number of photographs of the fringe patterns, the 'Post' technique requiring a holographic plate to manufacture the grating mould.

It was decided to conduct trials using the Optecord L.F. Interferometer. Two tests were carried out at the University of Strathclyde on damp concrete specimens. The first specimen failed outside the field of view, restricted as it was, to an area of 50mm. diameter. A notch was introduced into the second specimen to force the failure to occur at the centre. Significant localisation in the strain field was observed ahead of the notch, the magnitude of which could be measured from the photographs of the fringe patterns. Due to the ease of use and the lack of development time required it was decided to purchase an Optecord. The writer and a technician from Imperial College were trained at the University of Strathclyde in the manufacture of gratings, the use of Optecord and the analysis of the resultant fringe patterns.

6.2 Optecord L.F. Interferometer

The Optecord L.F. Interferometer is an instrument for the measurement of full field strain employing the moire interferometry technique. The theory of the technique is given in Section 5.4.3. In this section the use of Optecord in the present project is described.

An epoxy resin master grating, on a glass substrate, was supplied with the Interferometer. From this grating silicone rubber replica gratings could be made which were then used as moulds for the final specimen grating. The specimen grating was built up in three layers, the first two in a moisture tolerant epoxy resin and the last layer in a suitable epoxy for casting the fine specimen grating. The overall grating thickness was approximately 0.3mm.. The detailed techniques for the manufacture of gratings are given in Appendix D.

The Interferometer consists of a vertical metal plate on which are mounted a 5mW. He-Ne laser, a beam expander, two beam splitters and several mirrors. The Interferometer is shown in Figure 6.1 with the front cover removed. Three, 50mm. diameter expanded laser beams are produced which are directed such that they intersect at the specimen surface. Three shutters are provided to allow choice as to which beams are shone onto the specimen. The rear of the Interferometer is shown in Figure 6.2. Three different virtual gratings can be created. The intersection of Beams 1 and 2 forms a grating whose principal direction is horizontal (Fig. 6.3a). Beams 2 and 3 combine to give a grating whose principal direction is vertical (Fig. 6.3b) and Beams 1 and 3, a grating with the principal direction in the 45 degree direction (Fig. 6.3c). The specimen grating is a crossed grating with horizontal, vertical and 45 degree principal directions. When illuminated with any one of the virtual gratings the fringe pattern formed is related to strain in the principal direction of the virtual grating. The laser beams are diffracted by the specimen grating in many directions; the diffracted beams of interest are those which are perpendicular to the grating. These pass back through a lens in the centre of the Interferometer and may then be recorded on the film of a still camera or by a video camera.

Fig. 6.1 Optecord LF Interferometer

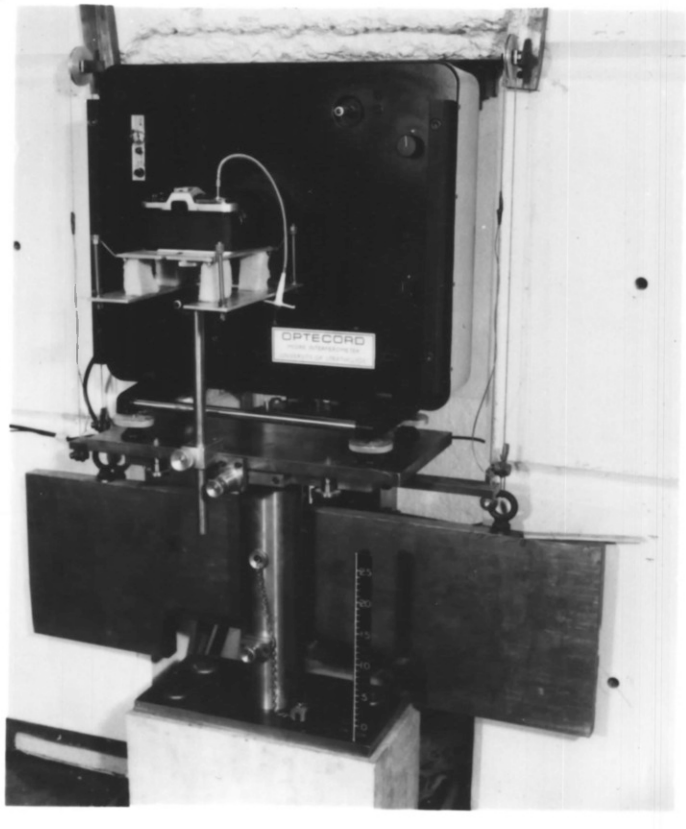

Fig. 6.5 Interferometer in position on carriage

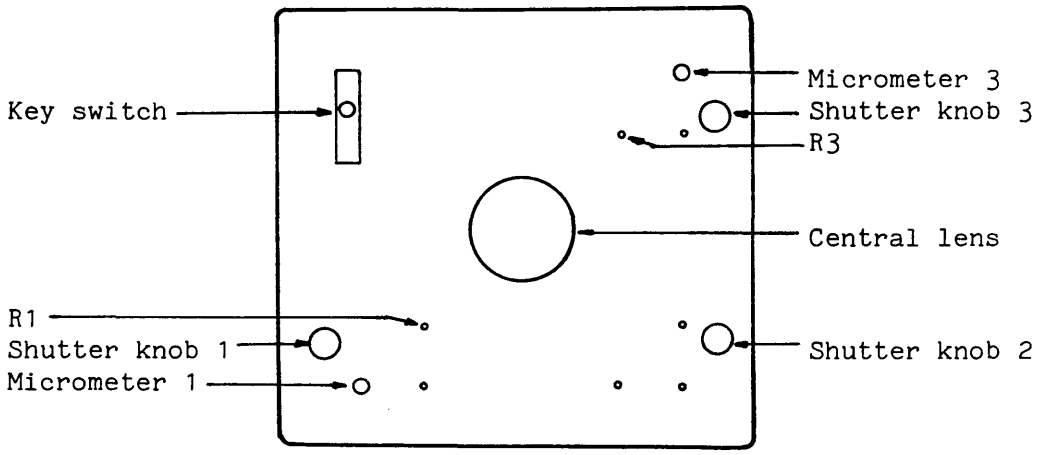

Fig. 6.2 Optecord backplate

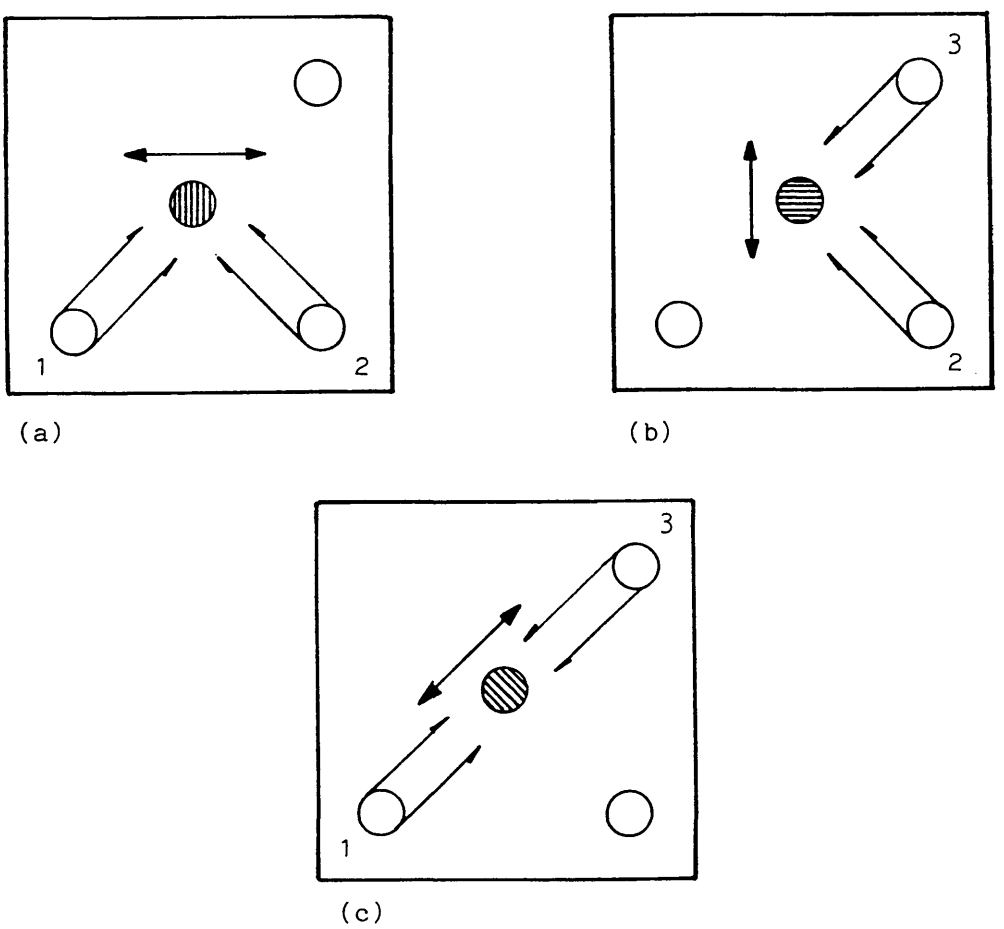

Fig. 6.3 The three possible virtual gratings
(a) Grating principal direction horizontal
(b) " " " vertical
(c) " " " at 45 degrees

The final mirrors which control the directions of Beams 1 and 3 can be adjusted. The micrometers allow adjustment of the pitches of the virtual gratings whilst the Allen screws marked R_1 and R_3 in Figure 6.2 are used to rotate the horizontal and vertical gratings respectively. Once set up, R_1 and R_3 should not need to be altered, provided that the specimen grating is always placed on the specimen in the same orientation and not rotated through 90 degrees. The reason why the grating may not be rotated is that the vertical and horizontal gratings on the master are not perfectly at right angles and R_1 and R_3 need to be set up to align the virtual gratings with the specimen gratings. If rotated through 90 degrees one or other of the gratings would appear to be out of alignment. The other Allen screws on the Interferometer backplate must not be altered since they result in more complicated changes in the fringe patterns.

The alignment of the Interferometer in front of the specimen is a simple procedure taking 5 to 10 minutes. The Interferometer is placed on its carriage, parallel to the specimen and with the beams overlapping fully at the specimen grating. Care must be taken to ensure that the Interferometer is indeed approximately parallel to the specimen so that only the intended diffracted beams pass through the central lens. It is now necessary to align the virtual gratings with the specimen gratings. If properly set up it is sufficient to align one grating for all three to be correct. All three rotational degrees of freedom of the Interferometer must be adjusted. Adjustment using the grating with vertical principal direction will be described but in principle any of the three gratings could be used. The steps required for adjustment are as follows:

1. Ensure that the Interferometer is supported by only 3 of the 4 feet. This is necessary to prevent any change in support conditions after setting up, leading to bending of the back plate and misalignment of the optics.
2. Open the shutters for Beams 2 and 3.
3. Place an opaque screen with crossed hairs in the focal plane of the central lens; the two beams are seen as dots on the screen.
4. If the dots are separated in the vertical direction, the pitches of the specimen and virtual gratings are not identical and the

virtual grating pitch must be adjusted by means of the micrometer for Beam 3.

5. If the dots are separated in the horizontal direction then the Interferometer is rotationally out of alignment along an axis perpendicular to the specimen. This can be corrected by adjustment of the height of the feet using the knurled discs fitted.
6. If the dots are not centred on the crossed hairs then rotation about either or both of the Interferometer in-plane axes is required. This can be achieved by adjusting the position of the Interferometer on the carriage top plate for the vertical axis and adjustment of the height of the feet for the horizontal axis.
7. Final adjustment of the Interferometer must be made by observation of the fringes. The opaque screen is removed and a camera mounted behind the Interferometer through which the fringes may be seen.
8. If the fringes are not horizontal the Interferometer must be rotated about the axis perpendicular to the specimen grating by adjustment of the height of the feet.
9. If there are a large number of fringes they can be removed by adjustment of the micrometer for Beam 3.
10. It is now necessary to check that the spots are still centred on the opaque screen crossed hairs and that the beam overlap is still on the correct portion of the specimen. If not the Interferometer must be moved and the adjustments repeated from step 2.
11. It should also be possible to observe the fringes for the grating with a horizontal principal direction. This can be checked by opening the shutters for Beams 1 and 2 only. The fringes observed through the camera should be vertical, if not then the Interferometer is out of adjustment and it will be necessary to adjust the allen screws, R_1 and R_3. If there are a large number of fringes they can be removed by adjustment of the micrometer for Beam 1.
12. The Interferometer is now set up. If mismatch is required this can be achieved by adjusting one or both of the micrometers. A clockwise rotation of the micrometer for Beam 3 or the micrometer for Beam 1 results in a fictitious tensile strain field in the vertical or horizontal directions respectively. The mismatch in the 45 degree field will be a function of the mismatch in the other two directions.

The Interferometer is supported on a specially built carriage with a counterweight (Fig. 6.5), designed to allow the Interferometer to be moved vertically and horizontally in a plane parallel to the specimen surface so that various parts of the specimen grating may be examined. Registration dowels on the carriage ensure that the Interferometer is correctly positioned. The registration positions are at the centre of travel and also 17mm. either side of the centre, both vertically and horizontally. During testing, normally only four of these positions are used as shown in Figure 6.4 giving a patchwork of photographs of the fringe patterns covering an area of approximately 75mm.x75mm.. The carriage has been designed to reduce any unwanted rotation of the Interferometer to a minimum. Rotation about an axis perpendicular to the specimen grating causes rotation of the fringe pattern but the spacing in the principal direction is unaltered so that the measurements are not affected. Rotation about either of the two in-plane axis would cause an error in the measurements, this is discussed in Section 6.4.1.

The fringe patterns are recorded using an Olympus OM-10 35mm. camera fitted with a Tamron 80-210mm. zoom lens, mounted just behind the central lens of the Interferometer. The camera mounting is supported by the carriage so that the camera follows the translation of the Interferometer. The only problem with this arrangement is that vibrations caused by the camera shutter are transmitted to the Interferometer causing the fringes to vibrate so rapidly that they can become invisible to the naked eye. This could be allowed for by using ultra-high speed film, however, it was found that, by supporting the camera on a combination of springs and foam rubber pads, the photograph could be taken before vibration affected the fringes (Fig. 6.5). The film used was 400 ASA, black and white, and was uprated to 1600 ASA in the development. The shutter speed is set to 1/250th. and the aperture to f/3.8. It is necessary to use a shutter release cable.

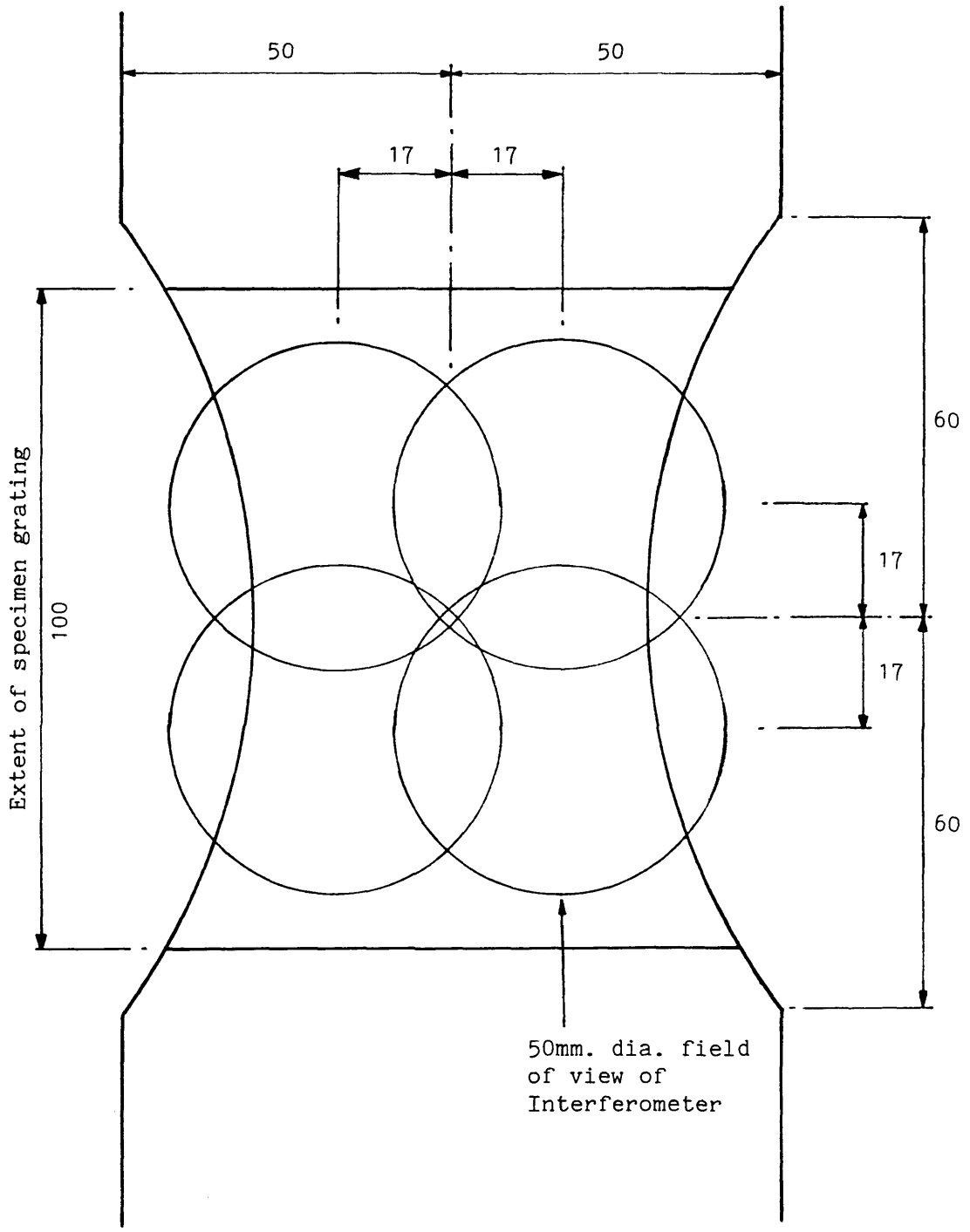

Fig. 6.4 Patchwork of observation positions for Interferometer
Dimensions in mm.

6.3 Analysis of fringe patterns

The theoretical analysis of moire fringe patterns was described in Section 5.4.1; the axial, transverse and 45 degree strains are analysed in accordence with Equ. 5.11, using the three available grating principal directions. The three strains so obtained can be used to calculate principal strains and their orientation if required. Equ. 5.13 would enable the full strain field to be obtained from just two fringe patterns, however, this technique is not used due to the difficulties in determining the shear strain. Rotation of the Interferometer about an axis perpendicular to the specimen surface introduces fictitious shear strains which, although they are self-cancelling in Equ. 5.13 lead to a reduction in accuracy of the measurement.

The specimen grating contains defects and consequently the zero strain field may contain one or two fringes. These fringes may loop in and out of the field of view making assessment of the fringe order very difficult. It is convenient to introduce a limited amount of mismatch (Section 5.4.2.2) into the zero field by adjustment of the two micrometers. The introduction of mismatch has the following advantages:

1. Ease of assessment of the fringe orders.
2. Elimination of doubt regarding the sign of the strain for low strains.
3. Greater discrimination in the strain field due to the larger number of fringes.
4. Simplified location of the centre of the fringe during analysis due to the reduced width of each fringe.

The only drawbacks with the use of mismatch are that the localisation of strain is less obvious during the test and that it is necessary to analyse the zero strain field and subtract it from all subsequent strain fields to obtain the true strain field. Mismatch equivalent to approximately 500 microstrain in tension has been used during the

tests, the exact level of mismatch depending on the clarity of the zero field.

The photographs of the fringe patterns are analysed using a digitising tablet connected to the College main frame computer running a purpose-written suite of programs. The theory behind these programs is given in Appendix F. The zero field mismatch is subtracted from the strain fields and the programs interpolate the results to provide strain contours. Several vertical sections of the strain field are analysed to enable strain contour plots to be drawn.

6.4 Limitations of technique

6.4.1 Accuracy

The sources of inaccuracy in moire interferometery may be subdivided into those which change the observed fringe spacing and those which occur due to analysis of the fringe pattern. The observed fringe pattern will be affected by errors in the initial specimen grating, errors in the virtual grating and some of the possible relative displacements of the two gratings. The effects due to local errors in the grating will be circumvented if the zero strain field is subtracted from the final strain field as has been done in this project. Overall errors in the grating pitch are deemed to be insignificant compared with analysis errors. In-plane translation of the Interferometer has no effect on the virtual grating pitch and consequently, although the fringes may be displaced their spacing is unaltered. Displacement of the Interferometer along a line perpendicular to the specimen grating has no effect except to change the area of overlap of the laser beams. In-plane rotation of the Interferometer has the effect of rotation of the fringes without changing their spacing in the grating principal direction and therefore does not affect the results. Rotation of the Interferometer about an axis parallel to the grating principal direction does not affect the fringe pattern. The only relative displacement of the two gratings which effects the fringe spacing in the principal direction is out-of-plane rotation about an axis perpendicular to that direction. A small relative rotation of $\Delta\alpha$ may be considered to increase the virtual grating pitch by a factor of $\cos^{-1}(\Delta\alpha)$. For small $\Delta\alpha$, this factor becomes $(1+\Delta\alpha^2/2)$ and results in an apparent compressive strain of $\Delta\alpha^2/2$. If a relative rotation of 0.2 degrees occurs between photographing the zero strain and final strain fields, the error in strain measurement is only 6.1 microstrain. If the Interferometer is set up initially with an angular misalignment of $\Delta\alpha$, then no inaccuracy occurs, simply a slight reduction in fringe quality. The Interferometer carriage allows repositioning within an angular misalignment of 0.2 degrees and it is considered that

inaccuracies arising from errors in the fringe pattern are insignificant.

The main stage for introduction of any inaccuracy in the strain measurements is in the analysis of the photographs of the fringe patterns. This stems from the difficulty in identifying precisely the centre of the fringes. For a 500 microstrain mismatch the fringes are at 2mm. centres. The widths of the dark fringes vary from approximately 0.1mm. to 1.0mm. on the specimen, being magnified by a factor of 3.5 in the photographs used for digitising. An error in location of the centre of one fringe by 0.2mm. on the specimen would lead to a 50 microstrain error. In order to reduce errors due to digitising, all digitising runs were repeated and, if the maximum percentage difference between the two runs was greater than 10%, for strains of up to 1500 microstrain, then the data was discarded and the digitising repeated. This limit was reduced to 5% for zero fields. The accuracy achieved on subtraction of the zero field is, therefore, probably similar to the manufacturers quoted accuracy of the greater of +/- 50 microstrain or +/- 5%. The accuracy may be improved by increasing the gauge length. This may be achieved by digitising only every second, third or fourth fringe but results in a reduction in discrimination. In order to achieve the limits on errors stated above it was normally necessary to digitise alternate fringes only.

6.4.2 Discrimination

The discrimination available is selected by the level of mismatch. For example, if no mismatch is used then at 100 microstrain the fringes would be at 10mm. centres giving data also at 10mm. centres. However, for the same strain level with 500 microstrain mismatch, the fringes would be at 1.67mm. centres with correspondingly increased discrimination. The discrimination available with 500 microstrain mismatch is considered sufficient for the present project even if alternate fringes only are digitised, and still allows the localisation to be observed during the test.

6.4.3 Application to concrete

It has been necessary to make some modifications to the grating manufacturing techniques to enable them to be used on damp concrete surfaces (Appendix D), but otherwise the application of the Interferometer is similar to that for other substrate materials. The only difference occurs at high strain levels when the grating becomes debonded and bridges over the highly microcracked concrete. The Interferometer now yields strain in the grating which does not reflect true strain in the concrete but an average strain over the debonded width. The fringes may be considered to be contours of equal displacement and the opening over the debonded width can be calculated. This may, at first, seem to be a limitation, however, the concept of strain has little physical meaning in a material which is largely damaged and may contain a discrete crack; 'crack opening' may be a more useful parameter. The debonding is also convenient from another point of view in that, if it did not occur, the local strain in the grating would be very much greater possibly leading to local strengthening of the specimen. Debonding is obvious in the fringe pattern when the fringes become close, parallel and equally spaced, indicating uniform, high strain. This normally occurs at between 1000 and 1500 microstrain.

Chapter 7 Experimental programme

7.1 Scope and objectives

At the outset of the project, it had been intended to divide the programme into two distinct phases. The first phase included the test development and was designed to validate the test method, obtain initial results and assist in the planning of the second phase of the work. This second phase was to be an investigation of the effects on the fracture characteristics of changes in the material used. These changes would have been related to the mix constituents as well as the age of the specimen. In practice, due to the extended development time, only the first phase has been completed. The majority of the work which would have been covered by the second phase is included in the recommendations for further research given in Section 11.3.

The objectives for the experimental work undertaken can be summarised as follows:

1. To develop a stable tensile test which could allow the observation and measurement of fracture process zones.
2. To demonstrate the suitability and repeatability of such a test.
3. To obtain initial results which would provide sufficient information to allow the definition of objectives and detailed planning of further work.

The development of the test took place over a period of approximately 2 years, during which 56 direct tensile tests were conducted. Initially only 55% of the tests failed in the central portion of the specimen with only 20% of the failures being stable. These figures were improved to 100% and 80%, respectively, using the techniques described in Chapter 4. Even after the significant improvements made in refining the test procedures, it was not possible to ensure that all tests were completely successful. The complexities of the testing

machine control systems and specimen preparation provided many sources for potential problems which could result in unsuccessful tests. It also seemed inevitable that some specimens would fail in an unstable manner. It was decided, therefore, to allow a reserve in planning the testing and to conduct a greater number of tests than were strictly necessary for the validation of the techniques in order to allow for some unsuccessful tests. In the event, 23 tests were conducted in the final test series with 17 being fully successful, 3 failing in an unstable manner and 3 more considered to be unsuccessful in other ways (Section 8.1).

In order to assess any unwanted effects of the interference grating on the response of the specimen, specimens were cast in pairs. Each pair was tested during one day and, in the majority of cases, a grating was applied to only one of the specimens. The specimens without gratings were a control sample by which the effects of the gratings on specimen response could be assessed (Section 8.2.7).

7.2 Specimen casting

7.2.1 Moulds

The specimens were cast vertically in steel moulds. The need for vertical casting was established in Section 3.3.1. Initially, shaped steel inserts were used in the mould to form the specimen neck. However, it was found that when the neck was reduced to 60mm.x60mm., cracking occurred in the more curved parts of the specimen surface. This was due to restraint to the autogenous concrete shrinkage occurring during the first 24 hours, provided by the steel inserts. One specimen was demoulded after 5 hours and the cracks were found already to have formed. The solution was to make the inserts out of a material which was sufficiently flexible and yet could maintain dimensional accuracy. Several different techniques were tried, the final choice being wooden inserts covered with a thin layer of foamed plastic material. This material was absorbent and was sealed by lacquered tissue paper and finally protected by a self-adhesive plastic film. These moulds were used approximately 15 times each without showing significant signs of deterioration.

7.2.2 Casting procedures

Pairs of specimens were to be tested on the same day. Therefore, to ensure that they could be tested at an age of 28 days, they were also cast in pairs. This meant a large number of castings and possibly a variation between the different batches of concrete. As a check on the concrete quality all batches were tested for slump, Vebe and air content in accordance with BS1881 (1983) (Parts 102, 104 and 106). In addition, three 4-inch cubes were made for each batch and tested for the 28 day cube strength in accordance with BS1881 (1983) (Parts 108 and 116). The results of these tests, together with the mix proportions used, are given in Appendix B. The results indicate that

the concrete quaility was sensibly uniform throughout the test series.

The specimens were cast on a vibrating table in 3 layers. In some specimens a certain amount of segregation occurred. This segregation would not normally have been important. However, in these tests a weak layer adjacent to the adhesive interface could not be permitted so that it was necessary to remove the 'fat' at the top of the specimen and replace it by concrete.

7.2.3 Curing regime

It was essential to prevent moisture loss from the specimen from the time of casting until after the test (Section 3.3.1). It is normal practice to allow the surface moisture in a specimen to evaporate before covering and curing. It was considered that, in the dry atmosphere of the laboratory, this process might result in weakening of the upper end of the specimen due to shrinkage. It was noticable that the majority of specimens which failed away from the central portion, failed at the upper end, as cast. The reason for this was not entirely clear. The weakness was probably due to segregation, although moisture loss at the end may have made some contribution. In order to reduce the moisture loss to the minimum, the specimens were covered by wet hessian and polythene immediately after casting. The hessian was supported just above the concrete until the initial set had occurred after which it was lowered onto the concrete surface.

The specimens were de-moulded after 24 hours, the surfaces dampened to counteract any tendency for moisture loss, and then placed in re-sealable polythene bags. Excess air was removed from the bags, before they were sealed, to reduce air circulation. The seals on the bags were not perfect and, in order to prevent any loss of moisture from the bag containing the specimen, it was placed inside a second bag. A piece of wet absorbent material was placed between the two bags so that the air in this gap was kept at 100% Relative Humidity. The specimens were cured in these bags for approximately 3 weeks after which they were prepared for testing (Section 7.3).

7.3 Specimen preparation

7.3.1 End plates

As described in Section 4.2, steel end plates were stuck onto the specimen using a filled moisture tolerant epoxy resin, Sikadur 31 (Rapid Grade). The adhesive was supplied in two parts, which were combined in the proportions by weight of 3 parts of resin to 1 part of hardener. The adhesive has a 10 minute pot life at laboratory temperature and hardens sufficiently for handling after 12 hours and for testing after 24 hours. The adhesive can be applied to damp surfaces, provided that standing water is removed and that the adhesive is properly worked into the surface.

The ends of the specimen were prepared by grinding, under a continuous flow of water, to remove the laitence and expose the aggregate. Any residue left on the surfaces after grinding was removed by gentle rubbing with a wire brush, again under running water.

The end plates were mechanically abraded to remove any adhesive from previous tests. The surfaces were roughened using emery cloth and then thoroughly cleaned and de-greased. Small perspex spacers were required to ensure the correct adhesive thickness. These spacers (4.7mm. thick) were all cut from the same part of a perspex sheet to ensure uniformity. Four spacers were stuck onto one side of each of the end plates using Multibond 330 adhesive. Small aluminium strips were stuck to the edges of the plates to ease the alignment of the plate and specimen.

The surface moisture on the ends of the specimen was removed by compressed air whilst ensuring that the bulk of the specimen remained damp. The adhesive was spread onto the ends of the specimen as well as the end plates, making sure that both interfaces were properly 'wetted'. The specimen together with the end plates was clamped in a special alignment jig which ensured that the plates were parallel. Once assembled in the jig, excess adhesive was removed and the

specimen was ready for sealing (Section 7.3.2)

7.3.2 Surface sealing

It would have been possible for the specimens without gratings to have been maintained in an atmosphere of 100% Relative Humidity until the time of testing so that their surfaces would only have needed sealing during the test. However, those specimens, which were to be monitored using the interferometer, required sealing whilst the grating was being manufactured. This took at least 3 working days and it was decided to seal all specimens at the same time as the end plates were attached. Various different techniques have been used for moisture retention of specimens by previous researchers. In this instance, there was also the additional requirement to be able to prepare a portion of the specimen for the grating whilst the rest of the specimen remained sealed. It was decided to use a curing agent which could be painted onto the specimen surface. This could then be removed in the area of the grating when required. Tests were conducted on three different curing agents (Appendix C). None of them gave a perfect seal; however, three coats of Cormix CM90 was very effective in limiting moisture loss. Another advantage of this material was that it was water based rather than spirit based. It was considered that the water based material was less likely to have any damaging side effects on the surface of the specimen. Three coats of Cormix CM90 were applied to the specimens as soon as they were assembled in the lining up jig. Each coat was painted on as thickly as possible and left to dry for approximately 20 minutes.

7.3.3 Grating manufacture

The gratings were manufactured in a separate room off the main laboratory in order to be in as dust free an atmosphere as possible. Any dust or dirt on the final grating would reduce the clarity of fringes and occasionally introduce spurious fringes into the zero strain field. The specimen preparation was as described in Sections 7.3.1 & 2 with the additional surface treatment described in Appendix D. The detailed techniques for grating manufacture are also described in the appendix.

7.4 Load and extension measurement

7.4.1 Data logger

The experimental data of applied load and extension were recorded by a Hewlett Packard data logging system. The system consisted of an HP-85 microcomputer, an HP3497A Data Acquisition/Control Unit and an HP3456A Digital Voltmeter. The data recording was controlled by programing the microcomputer. During the reading cycle, readings were taken of seven different voltages. These were the total applied load and extension signals from the R.D.P.Howden System 2000 Monitor Unit, together with the energizing voltage for the bars in parallel with the specimen and the signal voltages for the loads in the bars. The load applied to the specimen was calculated by subtracting the loads in the parallel bars from the total applied load. Readings were taken at regular intervals and loads calculated and displayed on the microcomputer screen without any data storage.

The data storage was restricted to only 700 sets of readings so that the program was designed only to store readings and print out the load and extension, when it was required to do so. Reading storage could be selected manually or on given changes in the extension reading. There was also a 'Fast' mode which allowed the reading and data storage cycle to be reduced from 4 seconds to 3 seconds; the readings themselves were taken during a period of 0.7 seconds. The short time taken for the readings was achieved by storing all 7 readings in the Data Acquisition Unit before transferring them to the microcomputer memory. It was necessary to limit the reading time as far as possible so that changes in the readings during that time became insignificant. This is particularly important in this test, where the load applied to the concrete is calculated by the difference between two relatively large values. A proportionately small error in one of these values, due to the readings not being simultaneous, leads to a larger error in the calculated specimen load. The data were stored on a magnetic tape and also printed out by the microcomputer printer together with the graph of load applied to the specimen vs. extension.

One drawback of the use of the microcomputer to calculate the load applied to the concrete is that the load is only known at 3 second intervals and another is that the load is printed out with a time lag of about 2.5 seconds. This means that identification of the peak load is difficult. In one of the modified techniques suggested in Chapter 11 for future application, the parallel bars would not be required and consequently the output signal from the R.D.P.-Howden System 2000 Monitor Unit would be the load applied to the specimen. This could be displayed on an X-Y Plotter for convenience of identification of peak load with the purpose of holding the 'Ramp Generator' and taking photographs of the moire fringe patterns at this critical stage.

7.4.2 Load measurement

The parallel bars were calibrated in a 44001b. Amsler testing machine. The bars were subsequently used to calibrate the load channel amplifier, of the R.D.P.-Howden System 2000. The bars were fixed in place in the testing machine and loaded. The amplifier gain and zero were adjusted to obtain the best equality of the load in the bars and the applied load. It was found that any bending of the bar gave fictitious axial load readings and that this could occur due to imperfect seating of the nut on the underside of the lower platen. To overcome this problem, spherical washers were used. The loads applied to the bars were now more even and the average difference between the load measured by the differential pressure transducer and that applied to the bars was adjusted to be less than 0.05KN.. That did not mean that any single reading during a test would be accurate to +/- 0.05KN., since the vibration of the ram that was required (Section 4.4.2.2) also introduced errors. The accuracy of any individual reading was very difficult to estimate and depended on the level of vibration occurring but was probably of the order of +/- 0.2KN..

7.4.3 Extension measurement

The extension of the specimen was measured using a +/- 1mm. linear variable differential transformer (LVDT) mounted between the platens adjacent to the specimen. Strictly speaking, the extension measured included the deformation of the adhesive layer, however, assuming that this deformation was elastic, it would not have affected the fracture energy measured. The LVDT (Type D5/40G8, R.D.P. Electronics Ltd.) was of B.S.I. Grade A quality with a repeatability of better than 0.3 micron.

7.5 Test procedure

As described in Section 4.4 considerable difficulty was encounted in the control of the testing machine which required extremely careful operation for successful testing. To this end, a detailed check list of required operations was produced and followed for each test. The check list is reproduced in Appendix E and only general comments will be made here.

The outer surfaces of the specimen end plates and the top and bottom platens were mechanically abraded to remove any traces of adhesive, roughened with emery cloth and thoroughly degreased. All but two of the specimens were stuck to the bottom platen the day before the test using Multibond 330 Adhesive. The adhesive was spread on the bottom end plate and the activator sprayed onto the platen. The bottom plate was then placed on the raised portion of the platen, which was used to ensure correct positioning of the specimen, and held there for 5 minutes. After 15 minutes the assembly could be carefully handled and after 45 minutes the joint was strong enough to be tested. Two specimens, on which the grating final layer had to be repeated, were stuck onto their lower platens during the morning of the day on which they were tested in the afternoon. All specimens were tested in the same orientation as they were cast.

The upper platen was bolted to the testing machine using the parallel bars. The bars were tightened as much as possible with a normal spanner to limit the flexibility of this bolted joint. When the bottom platen was bolted to the actuator ram, these bolts were tightened in a similar manner.

During the setting up of the test, the Ramp Generator was run twice before the specimen was finally stuck in position. This was to check that the Ramp Generator had not 'locked up' (Section 4.4.2.2.2). If it had, it could be freed by simply turning the electronics off for a few seconds and then turning them on again. This could not be done once the specimen was in position because of the tendency of the ram to jump (Section 4.4.2.2.2) when the machine was turned on.

The Ramp Generator was used for fine control of the position of the ram due to the problems described in Section 4.4.2.2.2. This was required at four stages during the preparation of the test. The first was to raise the specimen slowly, squeezing the upper adhesive out into a thin layer. The second was to counteract the movements caused by the increase in the Integral gain, after having tightened the nuts on the parallel bars. The third was to raise the ram occasionally whilst the adhesive was setting and hardening, to follow the shrinkage of the adhesive and prevent the concrete going into tension. The fourth requirement was a repeat of the second one as the Integral gain was increased to it's final level, just before beginning to load the specimen.

The vibration of the ram was monitored on a X-Y Plotter, plotting extension versus time. The level of vibration could, to a certain extent, be altered by the dither signal (Section 4.4.2.2.3). It was necessary to monitor these vibrations throughout the test.

During the loading of the specimen the Ramp Generator was programmed to increase the extension at a rate of 2.5 micron per minute. This gave initial stress and strain rates at the centre of the specimen of approximately 0.33 N/mm^2 per minute and 14 microstrain per minute respectively. The programmed rate was achieved until near the end of the test where, due to problems with the electrical gain, the rate reduced. From zero load up to a specimen load of 4KN. readings were recorded at intervals of 0.5 micron extension after which the data logger fast reading storage rate was selected. The reading interval was increased again after the peak load first to 0.5 micron extension and then 2.0 micron extension.

For the specimens which did not have a grating the Ramp Generator was simply run until the end of the test. For specimens with gratings the Ramp Generator was held at certain points of the test to allow the fringe patterns to be photographed. The first set of photographs was taken at zero load after which photographs were taken at given loads until either localisation in the strain field was observed or the maximum load was reached. From this point on, in the stable tests, photographs were taken at suitable intervals to show the fracture

process zone propagation. One final set of photographs was taken at the end of the test to monitor the unloading of the material outside the fracture process zone.

Chapter 8 Experimental results

8.1 Introduction

The experimental results obtained during the current project are described in this chapter. The results may be broadly sub-divided into two areas. The first area concerns the results available from the measurement of load and extension. These results are similar to those published by previous researchers and are described in Section 8.2. The data of primary importance in the present project are those obtained from the surface strain measurement. These data form the second main sub-division of results and are described in Section 8.3. The fracture surfaces are described in Section 8.4. Comments on the results and comparisons with the results obtained by other researchers are given in Chapter 9.

The final test series consisted of 23 tests of which 17 may be considered to be fully successful, 3 failed in an unstable manner just after the peak load had been reached and the remaining 3 tests were unsuccessful. The tests are listed in Table 8.1 which also indicates those tests in which the surface strain was measured. The letter in the test number denotes the batch from which the specimen was taken. The specimens were tested at the age of 28 days and, with the exception of Test D1, two specimens from each concrete batch were tested on the same day. The fresh concrete properties of the different batches may be found in Appendix B.

Three of the tests (D1, F2, I2) which failed in an unstable manner provide data regarding tensile strength and Young's modulus but could not be used to calculate the fracture energy. Localisation in the strain field prior to unstable failure was observed for two of these three tests (F2, I2) in which the surface strain was measured. Of the three tests which were considered to be unsuccessful, two (A2, H2) failed at substantially lower loads than were obtained for the

remainder of the test series, whereas in the third test (B2), failure occurred suddenly prior to controlled loading of the specimen due to accidental shorting of the electrical output points on the testing machine (Section 4.4.2.2.3). The causes for the premature failure of Tests A2 and H2 are unknown but are probably related to damage of the specimen prior to controlled loading. This damage may have resulted from either undetected spikes in the testing machine control signal or excessive compression applied when gluing the specimen to the testing machine platens. It is also possible that the specimens contained defects, however, an examination of the fracture surfaces showed no large voids or other obvious causes for premature failure. Of the 17 fully successful tests two (F1, G2) exhibited a rapid drop in load in the descending portion of the load/extension curve indicating that they were on the stable/unstable limit. The fracture energy for both of these tests (calculated up to an extension of 100 micron) was found to be only slightly greater than the average of all the stable tests and it was concluded that they were not adversely affected by the rapid drop in load.

Test	Strain measurement	Comments
A1	None	Stable failure
A2	Uniaxial	Unstable, low strength
B1	None	Stable failure
B2	Uniaxial	Uncontrolled loading
C1	None	Stable failure
C2	Uniaxial	Stable failure
D1	None	Unstable failure
E1	None	Stable failure
E2	Uniaxial	Stable failure
F1	None	Stable failure
F2	Uniaxial	Unstable failure
G1	None	Stable failure
G2	Uniaxial	Stable failure
H1	None	Stable failure
H2	Uniaxial	Stable, low strength
I1	None	Stable failure
I2	Full field	Unstable failure
J1	None	Stable failure
J2	Full field	Stable failure
K1	Full field	Stable failure
K2	Full field	Stable failure
L1	Full field	Stable failure
L2	Full field	Stable failure

Table 8.1 Final test series. 'Uniaxial' and 'Full field' denote strain measurement in one and three directions respectively.

8.2 Data obtained from load/extension curves

8.2.1 Introduction

Determination of the load/extension curve for each test allowed values to be obtained for Young's modulus, tensile strength and fracture energy. The curves represent the overall response so that no information can be obtained regarding localisation of strain within the specimen. The form of the curves obtained is discussed in Section 8.2.2 while values of the measured properties are given in Table 8.2 and discussed more fully in Sections 8.2.3 - 5. The measured value of the characteristic length proposed by Petersson (1981b) (Section 2.4.2.1) is also included in the table and is discussed in Section 8.2.6. One of the main reasons for conducting tests without interference gratings is to be able to evaluate the effects of the grating on the specimen. This is discussed in Section 8.2.7.

Test Number	Cube Strength f_{cu} (N/mm^2)	Tensile Strength f_t (N/mm^2)	Young's Modulus E (KN/mm^2)	Fracture Energy* G_f (N/m)	Character-istic length l_{ch} (mm)
A1	34.36	2.11	21.64	73.14	356.1
A2	34.36	1.27	-	-	-
B1	36.72	2.16	29.02	62.78	391.1
C1	34.39	2.29	27.66	67.94	359.5
C2	34.39	2.05	24.09	64.36	367.8
D1	36.33	2.73	25.92	-	-
E1	35.07	2.44	34.45	66.03	383.3
E2	35.07	1.94	29.62	68.97	540.4
F1	35.59	2.44	26.14	81.83	359.6
F2	35.59	2.69	27.87	-	-
G1	34.52	2.35	25.60	68.22	315.5
G2	34.52	2.07	21.57	78.50	394.4
H1	37.10	2.25	23.05	98.28	448.5
H2	37.10	0.96	-	-	-
I1	37.43	2.01	20.79	85.50	439.6
I2	37.43	2.99	24.84	-	-
J1	37.52	2.58	27.19	82.69	338.3
J2	37.52	2.57	19.61	93.94	279.0
K1	36.75	2.51	22.79	83.03	299.4
K2	36.75	2.63	25.11	79.61	288.2
L1	36.52	2.62	27.25	80.44	320.2
L2	36.52	2.10	24.36	75.61	418.8
Mean	36.01	2.38	25.43	77.11	370.6
Coeff. of Variation	4.2%	12.1%	13.7%	13.2%	17.9%

Table 8.2 Results obtained from load/extension curves

* G_f has been calculated up to an extension of 100 micron only. This value of G_f has been used in the calculation of l_{ch}. Tests A2 & H2 are not included in the calculation of the mean properties.

8.2.2 Shape of load/extension curves

The load/extension curves for 22 tests are shown in Figure 8.1 (For convenience, separate graphs are given for the different concrete batches and numbered such that the suffix on the figure number corresponds to the batch designation, i.e Fig. 8.1h contains the curves for the two specimens of batch H). The curves can be seen to be qualitatively similar to the curves obtained by other researchers (see for example, Figure 3.1). In order to photograph the fringe patterns for those tests in which moire interferometry was used, it was necessary to hold the extension at certain levels. This allowed some relaxation of the load which was largely regained when loading re-commenced (see for example, Test J2).

The ascending portion of the curves is initially linear wih some non-linearity prior to the attainment of peak load. The non-linearity sometimes takes the form of a sudden change in slope (Tests E2 and F1) but more often is a gradual change in stiffness. Due to the gradual nature of this change, it is not possible to state precisely at what level the non-linearity starts, however, it may be seen to occur at a load of as little as 45% of the maximum in Test B1. In other tests, such as Tests K1 and K2, the non-linearity is barely discernable.

After the peak load is reached, the curves for the stable tests are typified by a rapid fall in load followed by a curve of reducing descending slope tending to become asymptotic to the extension axis. The shapes of the descending portions vary from smooth curves (Tests G1 and J1) to those which include sections where the rate of decrease in load is significantly reduced such as Tests B1, H1 and I1. The curves for the unstable tests (D1, F2 and I2) exibit a sudden fall in load followed by some load recovery.

All the tests, with the exception of I2, were continued until the full load capacity of the actuator was applied to the combination of the parallel bars and the specimen. This limited the value of the maximum extension obtained to between 92 micron (Test C2) and 182 micron (Test H1). The extension obtained depended on the load applied to the parallel bars at the beginning of the test.

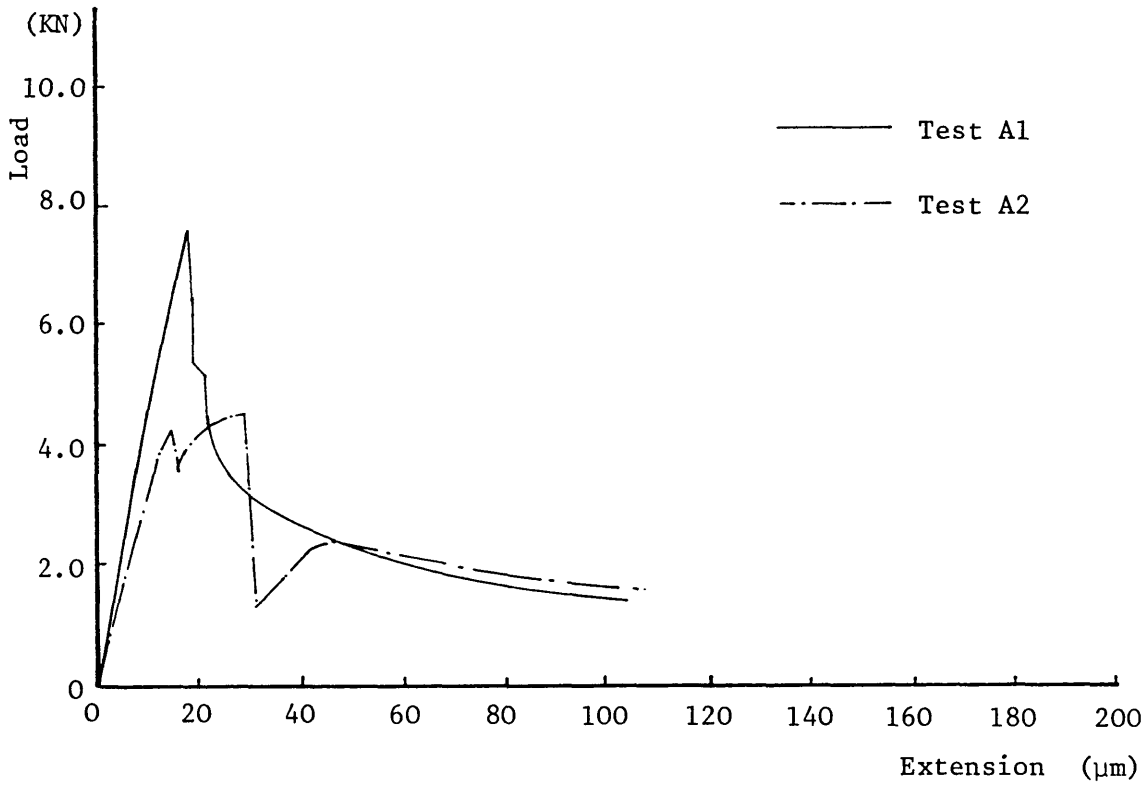

(a) Tests A1 & A2

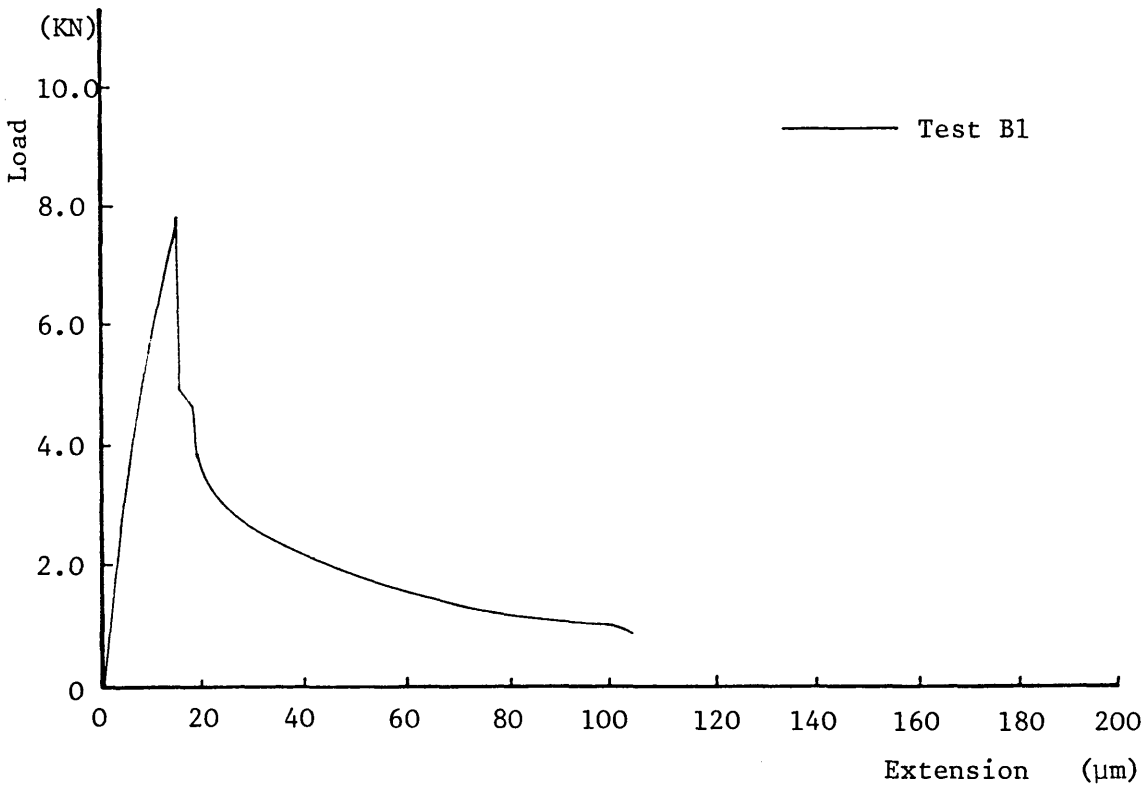

(b) Test B1

Fig. 8.1 Load/extension curves

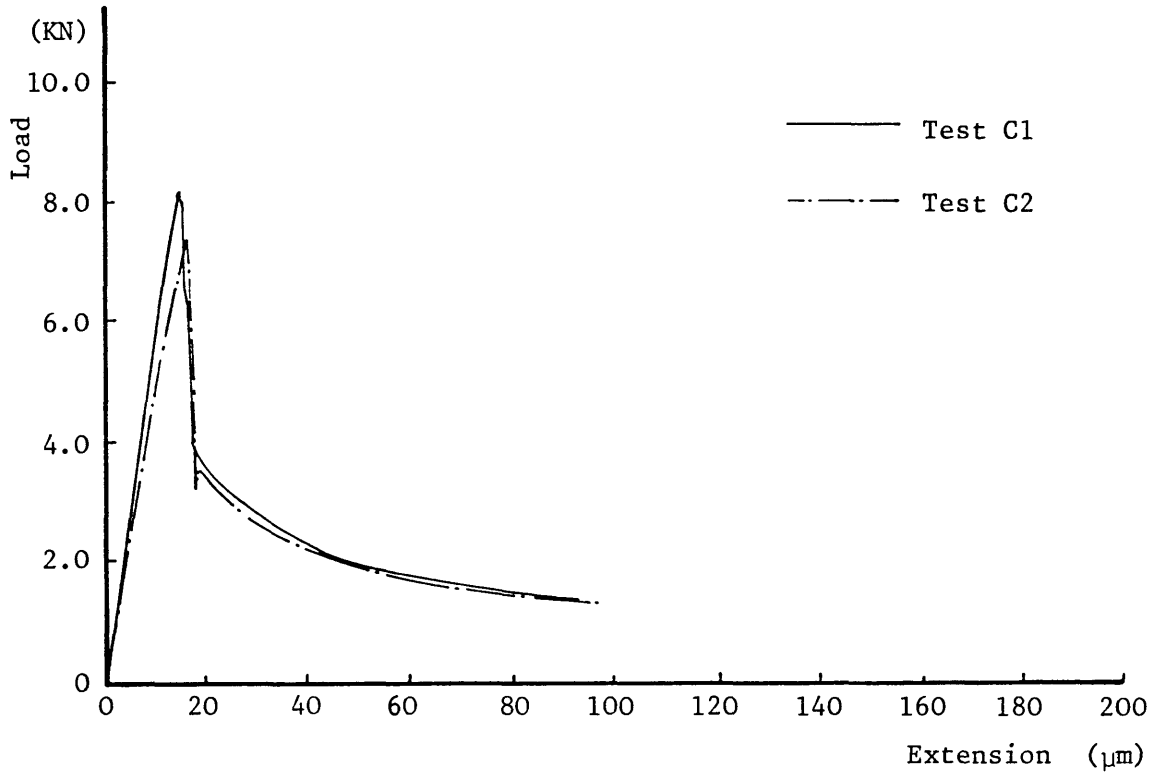

(c) Tests C1 & C2

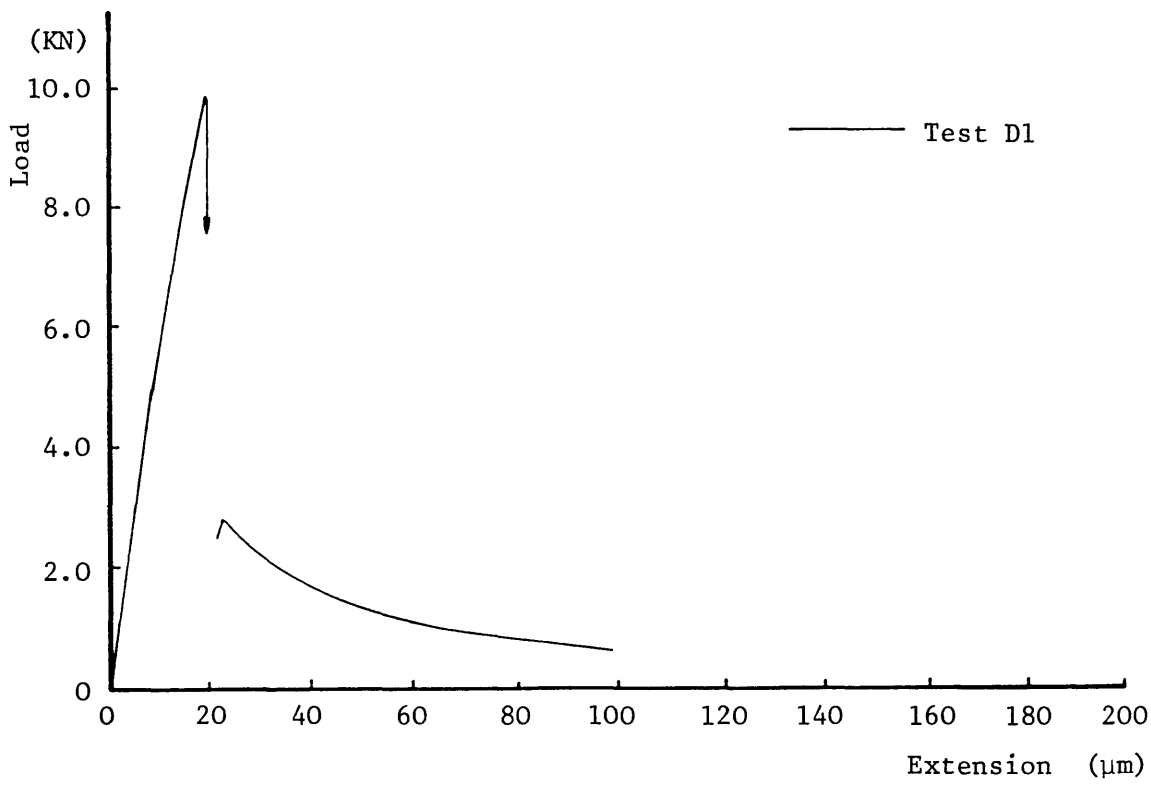

(d) Test D1

Fig. 8.1 Load/extension curves (cont)

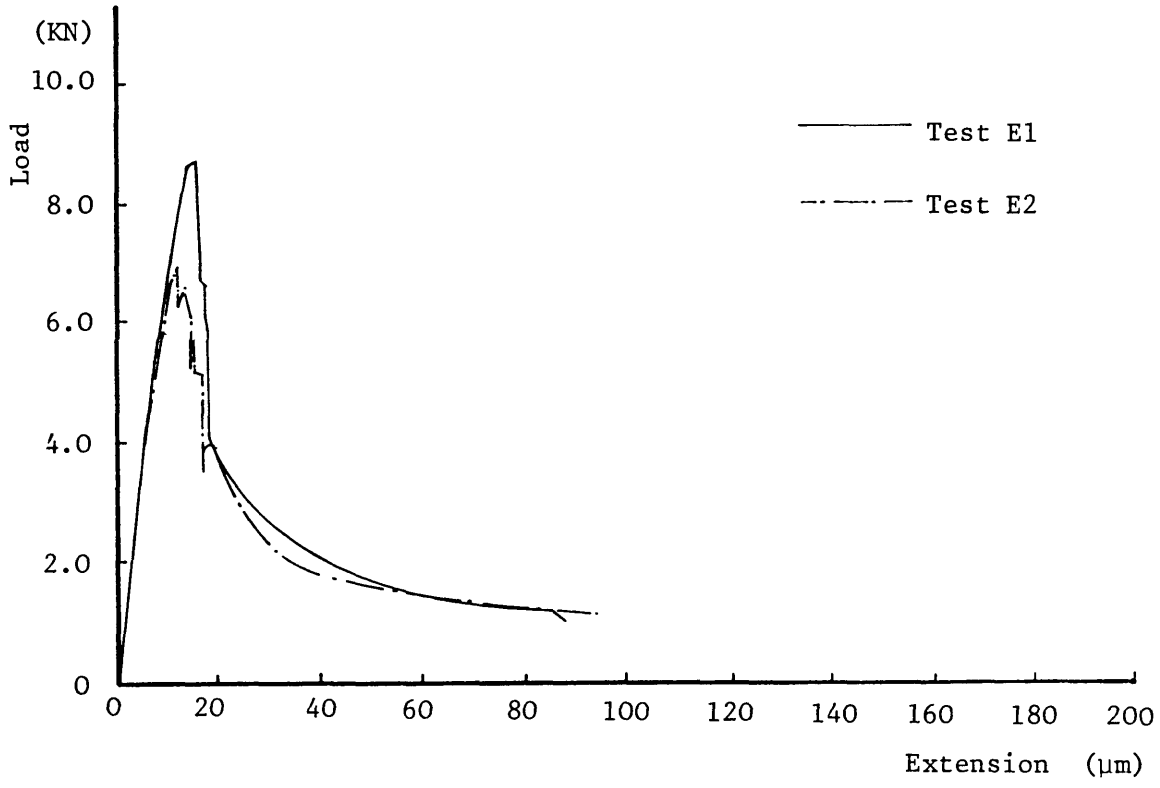

(e) Tests E1 & E2

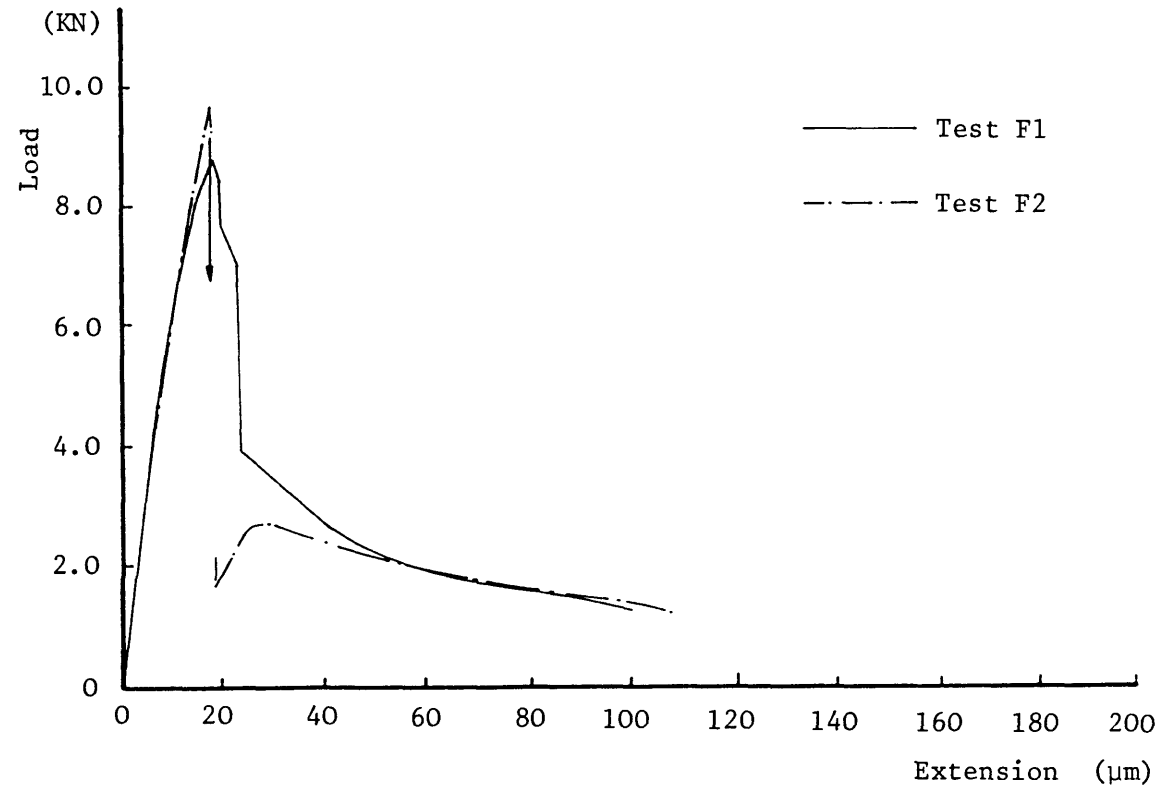

(f) Tests F1 & F2

Fig. 8.1 Load/extension curves (cont)

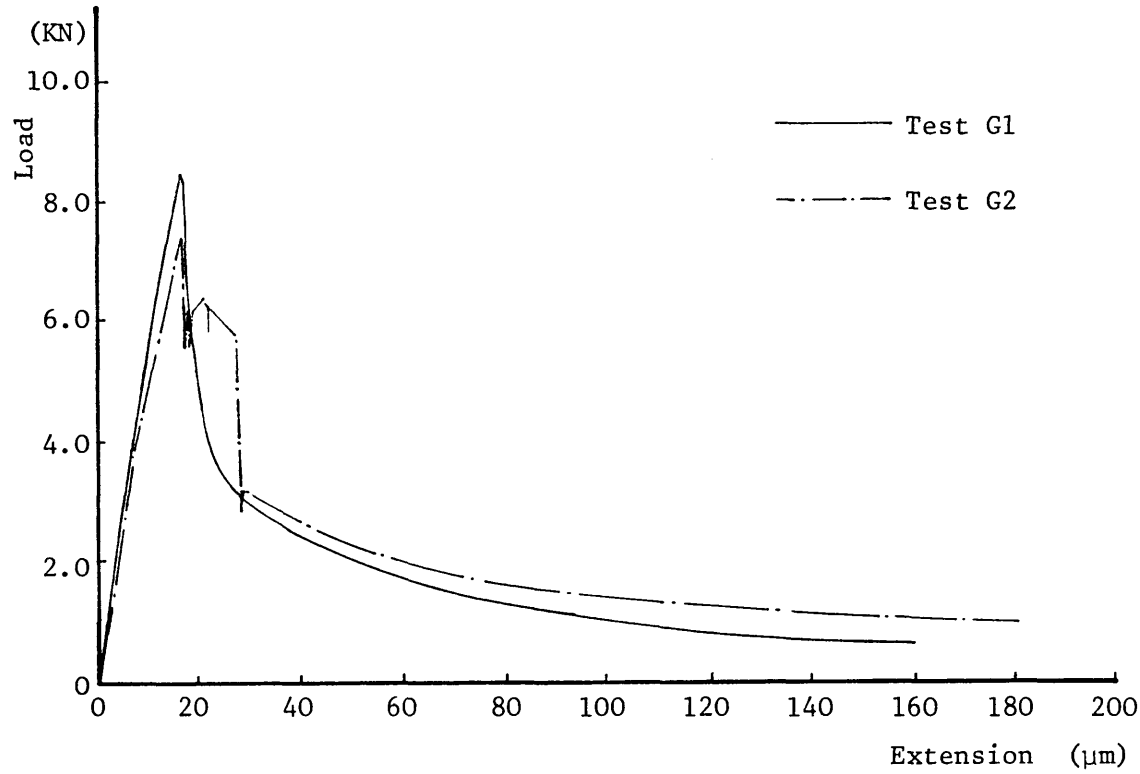

(g) Tests G1 & G2

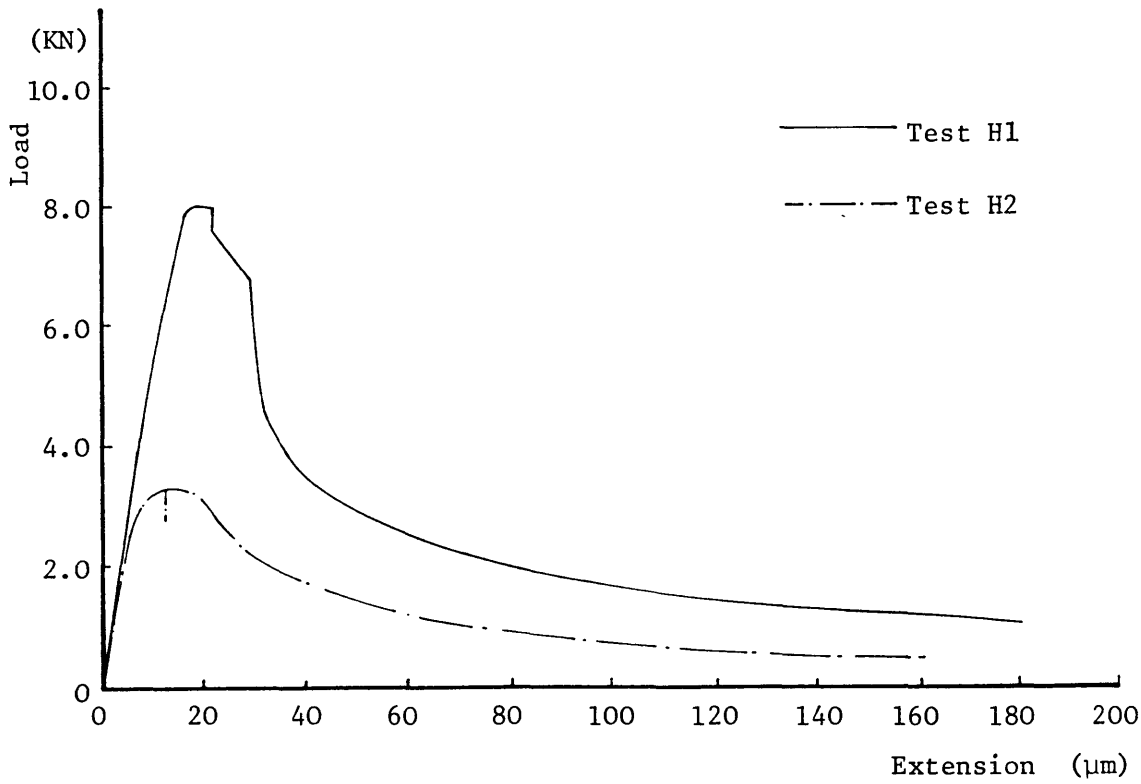

(h) Tests H1 & H2

Fig. 8.1 Load/extension curves (cont)

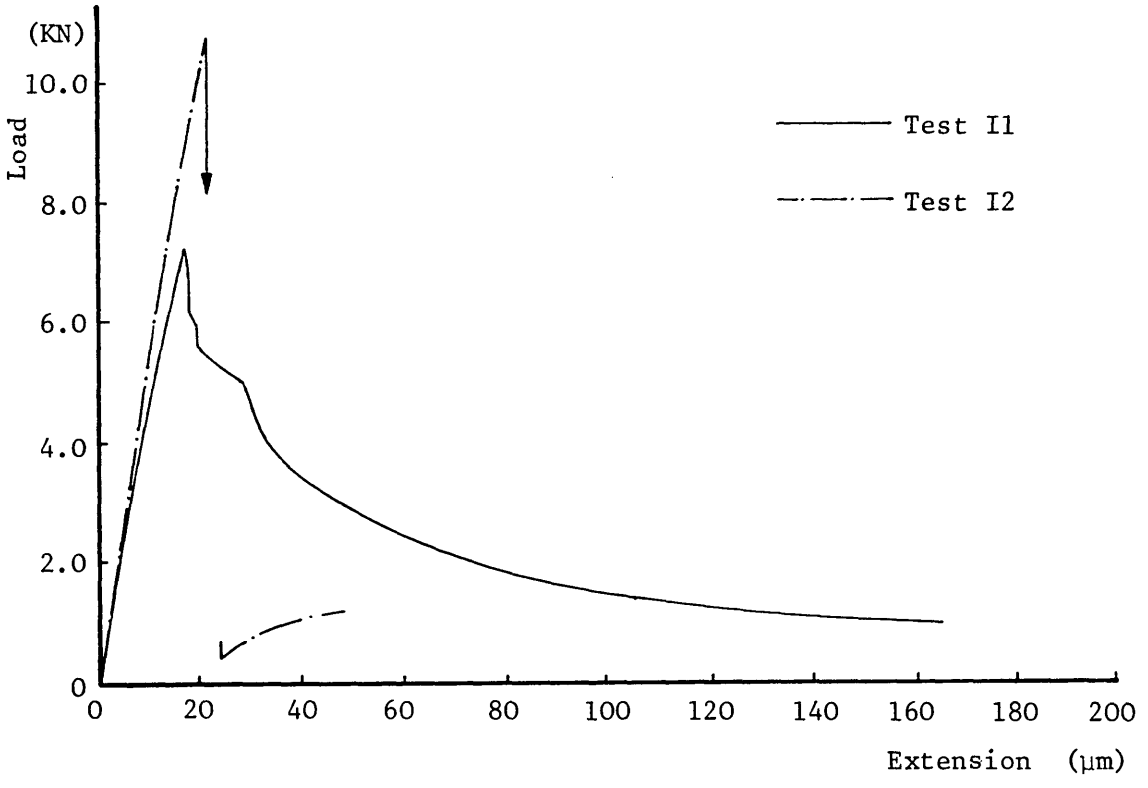

(i) Tests I1 & I2

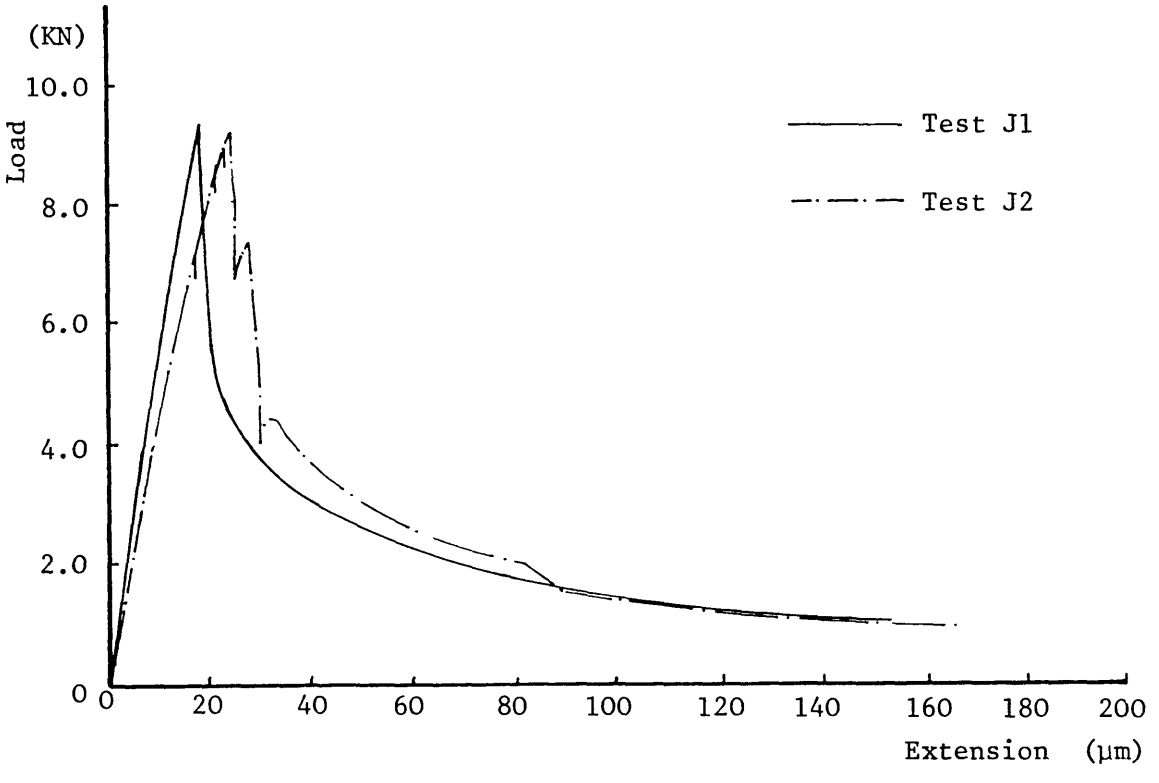

(j) Tests J1 & J2

Fig. 8.1 Load/extension curves (cont)

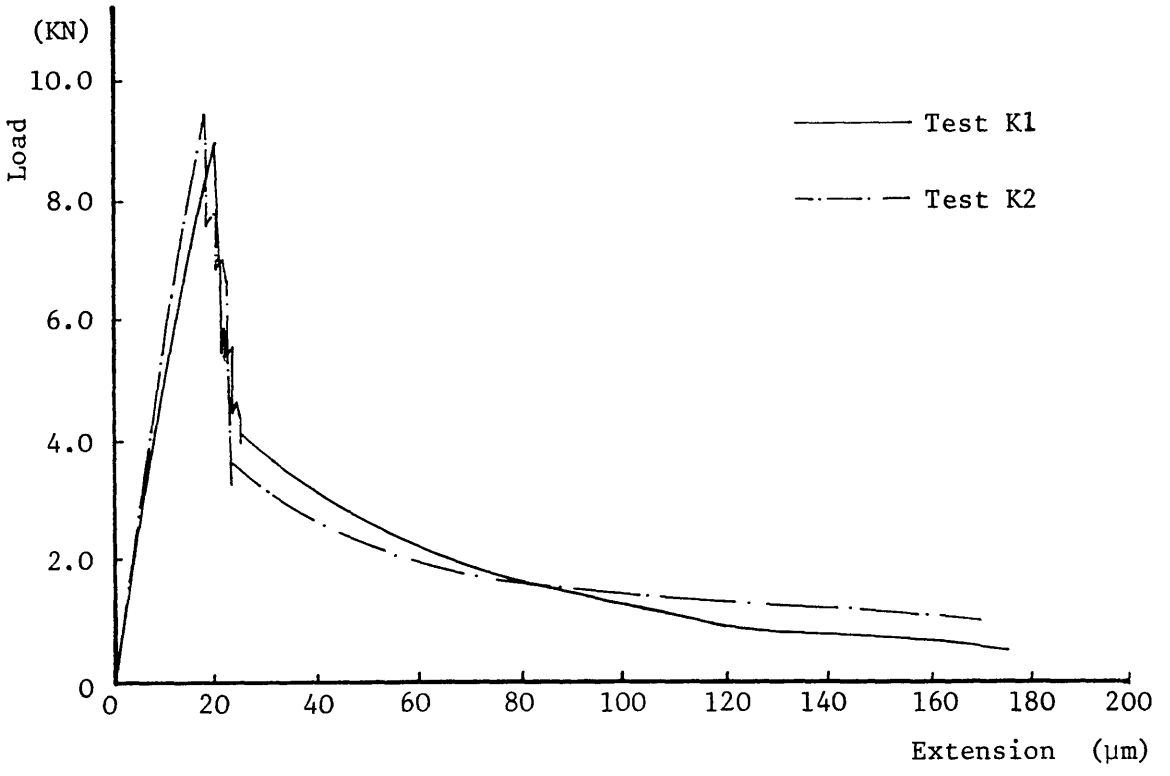

(k) Tests K1 & K2

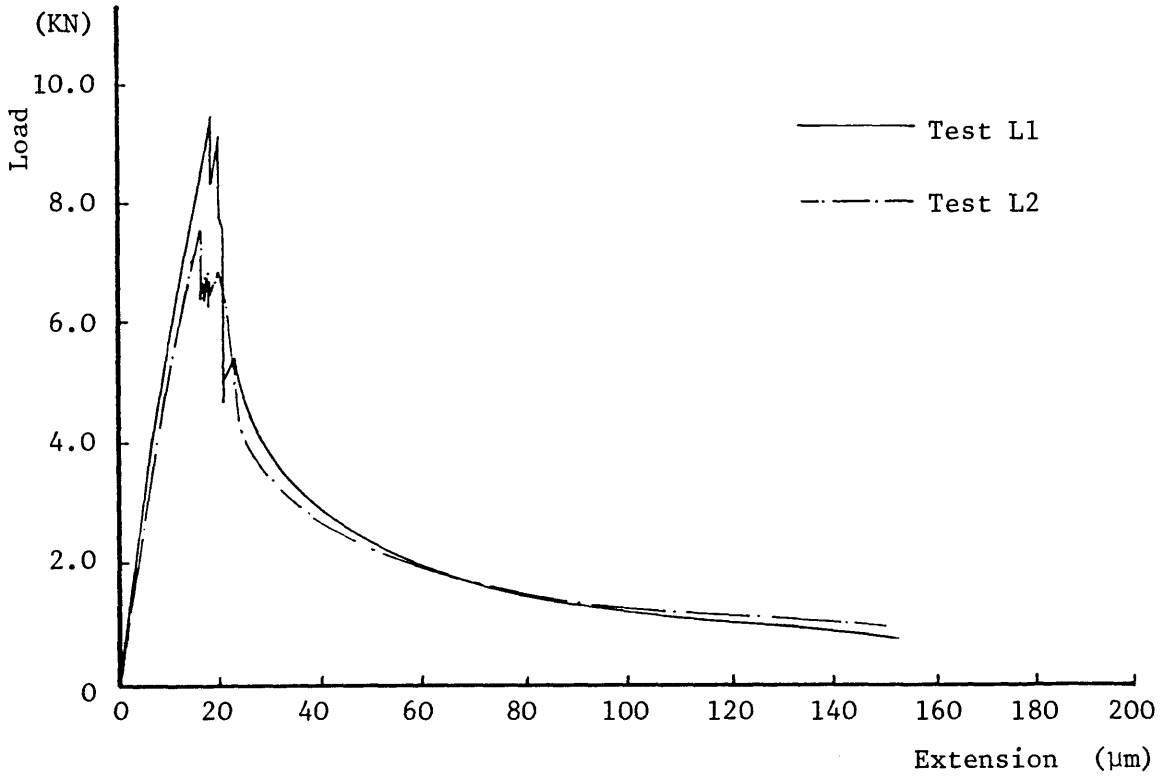

(l) Tests L1 & L2

Fig. 8.1 Load/extension curves (cont)

The shapes of the curves for Tests A2 and H2 can be seen to be significantly different to those obtained in the other tests and, as described in Section 8.1, these are not considered to be successful tests and are not included in the calculation of mean properties in Table 8.2.

8.2.3 Tensile and compressive strengths

The 28 day cube strengths and tensile strengths are given in Table 8.2. The cube strengths are the mean of three 4 inch cubes tested in accordance with BS 1881 (1983) for each batch with the exception of batch L for which only two cubes were available. The mean and coefficient of variation of the cube tests are based on the individual cube results rather than the averaged values. Due to the irregularity of the fracture surfaces it would not have been possible to define a suitable cross-sectional area related to each fracture surface, and consequently the tensile strengths are based on the maximum load sustained divided by the cross-sectional area of the neck of the specimen.

The coefficients of variation of the cube and tensile strengths are 4.2% and 12.1% respectively. The variation of cube strength is within the range expected for well controlled laboratory conditions and greater variation in the tensile strength is to be expected and is due largely to the sensitivity of tensile strength to localised defects in the material. Two other factors contribute to the variability in tensile strength. The first is a true variation in material properties such that all the batches were not identical. This is demonstrated by the slight reduction in the coefficient of variation to 11.0% when the tensile strengths are divided by the associated cube strengths. The second is the uncertainty in the measured peak load which results from the fact that readings were only taken at 3 second intervals (Section 7.4.1) and that the accuracy of load measurement was only of the order of +/- 0.2 KN. (Section 7.4.2). These latter effects might be expected

to contribute approximately 1% to the coefficient of variation.

8.2.4 Young's modulus

The Young's modulus quoted for each specimen in Table 8.2 has been calculated from the initial stiffness of the load/extension curve. However, this curve relates to the extension of the whole of the necked specimen together with the adhesive layers and the steel end plates. The extensions of the adhesive and the steel were assumed to be elastic with Young's moduli of 7.0 KN/mm^2 and 200.0 KN/mm^2 respectively. The extension of the specimen was assumed to be equal to that obtained for a specimen of varying cross-section but subjected to uniaxial stress throughout it's length. The extension of such a specimen is given by:

$$\delta = \frac{P}{E} \int_0^1 \frac{1}{A} \, dl \qquad (8.1)$$

where P = applied load
E = Young's modulus of concrete
A = cross-sectional area of specimen
1 = length of specimen.

For the specimen geometry used in the current project:

$$\int_0^1 \frac{1}{A} \, dl = 0.04452 \ mm^{-1} \qquad (8.2)$$

The initial stiffness was calculated from linear regression of the load and extension readings up to an applied load of 3KN. If the upper limit for the regression had been increased it would have extended into the non-linear portion of some of the sets of readings. If it had been lowered then the variability of the results would have been

increased. For example, if the regression was calculated up to 1KN. then the mean of the stiffnesses would have altered by less than 1%, however, the coefficient of variation would have increased from 12.6% to 19.4%.

8.2.5 Fracture energy

The fracture energy, G_f, as defined in Section 2.2.2.3.2 is the energy required, per unit area, to cause complete separation. In the analysis of the current test series, this is taken to be the area under the load/deformation curve divided by the cross-sectional area of the neck of the specimen. This assumes that all the energy absorbed by the specimen contributes to the fracture processes and that there are no bulk dissipative effects. In order to measure the full fracture energy the test should have continued until full separation occured, however, in the current test series, the maximum extension of the specimen was limited by the capacity of the actuator (Section 8.2.2). For comparison purposes, the values of G_f quoted in Table 8.2 have all been calculated up to an extension of 100 micron. Those tests in which the final extension was just less than 100 micron (C1, C2, E1 and E2) have been extrapolated to 100 micron for the calculation.

The values for G_f calculated up to the end of the test are given in Table 8.3. The maximum extension obtained was 182 micron. (Test H1). Although this is greater than any of the tests in the published literature, complete separation had not yet occurred and the contribution to G_f of the portion of the curve beyond 100 micron extension is significant. There is, as yet, insufficient data regarding the length and shape of the final part of the load/extension curve for an accurate analysis of the complete value of G_f to be made. The mean value for G_f calculated up to the end of the test for those tests where the extension exceeded 160 micron. is 110.0N/m, which would suggest that the full fracture energy may be at least 120N/m. Extrapolation either of the curves obtained during the present project or of those published in the literature cannot be relied upon. Further

experimental data is required before a more accurate estimate of the fracture energy can be made.

Test Number	Extension at end of test (mm)	G_f for ext. = 100 micron (N/m)	G_f up to end of test (N/m)
A1	102.8	73.14	74.28
B1	104.8	62.78	64.03
C1	92.3	67.94	65.03
C2	96.0	64.36	62.89
E1	92.5	66.03	64.03
E2	96.0	68.97	67.89
F1	100.1	81.83	81.89
G1	159.4	68.22	80.92
G2	179.4	78.50	105.50
H1	181.6	98.28	128.58
I1	164.9	85.50	106.92
J1	150.6	82.69	99.92
J2	164.0	93.94	114.03
K1	173.1	83.03	100.64
K2	169.1	79.61	103.42
L1	152.0	80.44	94.64
L2	149.7	75.61	91.56

Table 8.3 Fracture energy results

8.2.6 Characteristic length

Based on the fictitious crack model (Section 2.4.2.1) and the corresponding interpretation of the tensile test, Petersson (1981b) defined a characteristic length l_{ch}, which, when taken together with the shape of the stress/fracture zone opening curve, was a measure of the brittleness of the material. The value of l_{ch} is related to the measured values of Young's modulus, tensile strength and fracture energy and the results for the current tests are included in Table 8.2. It should be noted that l_{ch} has been calculated using the value of G_f up to 100 micron extension.

8.2.7 Effect of interference grating on response

The main reason why photoelastic coatings were not used in the current project was that the effect of a thick plastic layer on the surface of the specimen was unknown (Section 5.2). Although the grating required for moire interferometry is relatively thin (approximately 0.3mm. thick) it was still necessary to check whether it had any effect on the specimen. Tests were conducted on specimens without gratings as a control sample against which the tests with gratings could be evaluated. The envelopes enclosing the successful, stable load/extension curves for each of the two types of test are shown in Figure 8.2. The mean values of the three properties obtained from the load/extension curves for specimens with and without gratings, together with their coefficients of variation, are given in Table 8.4.

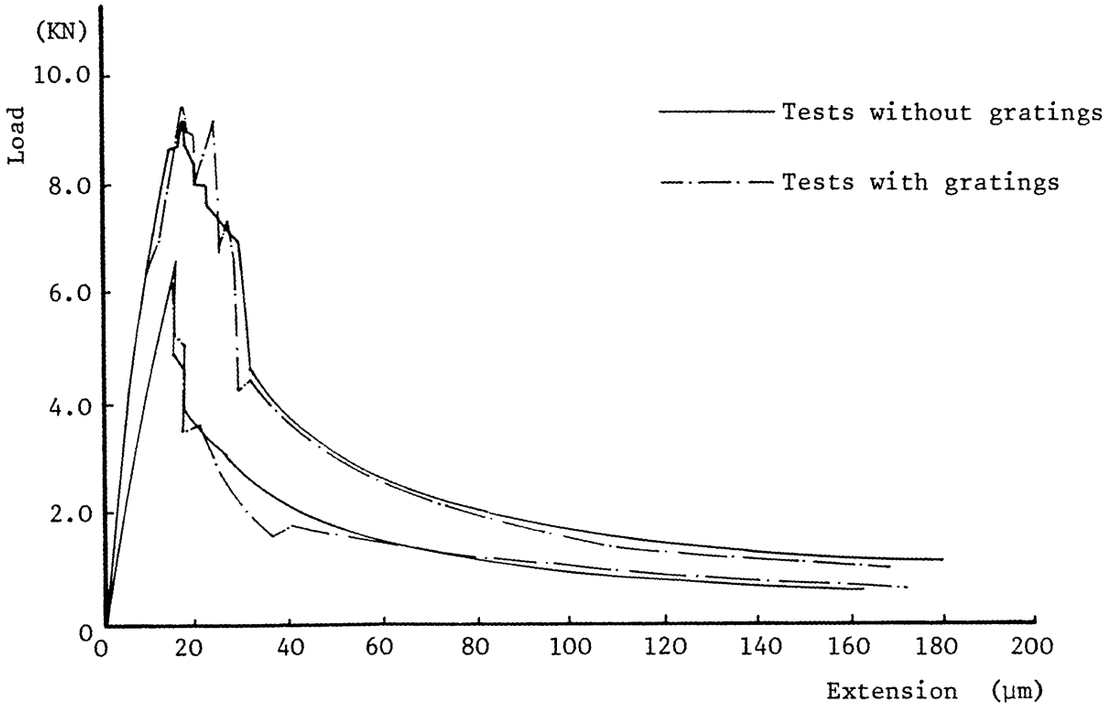

Fig. 8.2 Envelopes for load/extension curves of tests with and without interference gratings applied

	Tensile strength f_t (N/mm^2)	Young's modulus E (KN/mm^2)	Fracture energy* G_f (N/m)
Tests without gratings:			
Mean value	2.29	26.17	76.28
Coeff. of variation	7.9%	16.0%	15.2%
Tests with gratings:			
Mean value	2.31	24.30	78.06
Coeff. of variation	12.8%	13.0%	11.5%

Table 8.4 Mean measured properties for tests with and without gratings

* G_f calculated up to an extension of 100 micron only.

8.3 Data obtained from strain measurement

8.3.1 Introduction

Examples of typical axial strain fringe patterns are given in Figures 8.3 and 8.4. The photographs in these figures are in overlapping pairs covering the upper half of the specimen grating. The strain is inversely proportional to the fringe spacing so that, as may be seen in the figures, the fringes become more closely spaced in the fracture zone. Alternatively, the fringes may be thought of as contours of axial displacement spaced at approximately 1 micron intervals. In that case, the number of fringes concentrated together in the fracture zone may be considered as approximately equal to the opening of the fracture zone in micron.

In Figure 8.3 the fracture zone may be seen to develop at the left hand edge and to propagate across the specimen with increasing axial extension. In Figure 8.4a two separate fracture zones may be seen to be just developing, one in the upper left hand corner of the left hand photograph and the other in the lower right hand corner of the right hand photograph. In Figure 8.4b & c the lower zone continues to grow but the upper zone develops more rapidly and dominates until, as shown in Figure 8.4d, it has propagated across the whole width of the specimen. This last figure is particularly interesting since not only are two zones shown to develop but also a third zone branches off the upper zone at the top right hand corner of the left hand photograph, reappearing at the centre of the top of the right hand photograph. An examination of the fracture surface revealed a conglomeration of several aggregate particles at the point where the fracture zone branched.

Photographs of the moire fringe patterns have been analysed as described in Section 6.3. In the majority of tests only axial strain was analysed. In this case, the photographs were analysed along vertical lines spaced at 5mm. intervals across the width of the specimen. The data output from the computer programs included the positions of strain contour levels. These were plotted along the

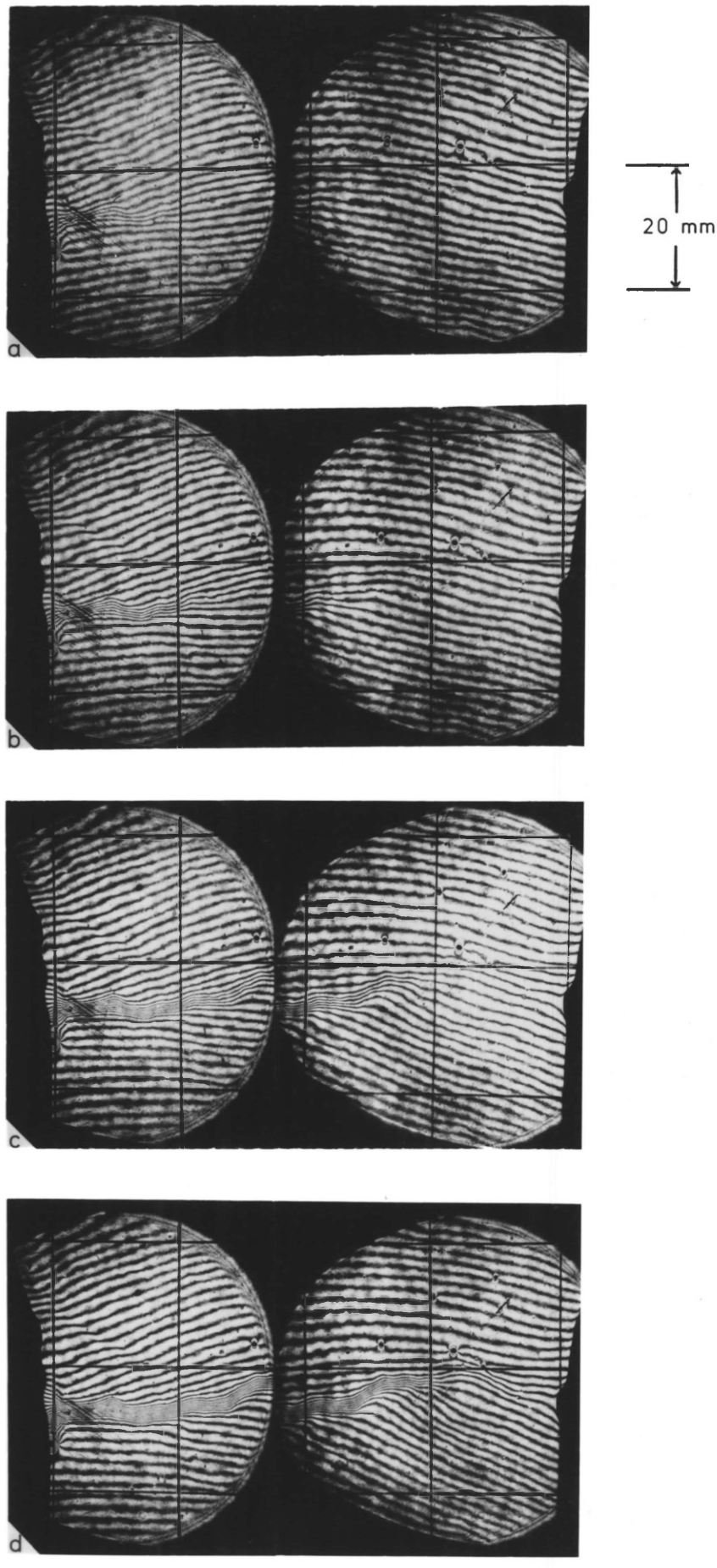

Fig. 8.3 Axial strain fringe photographs — Test G2
Pairs a, b, c & d correspond to
Fig. 8.8 d, f, h & i respectively

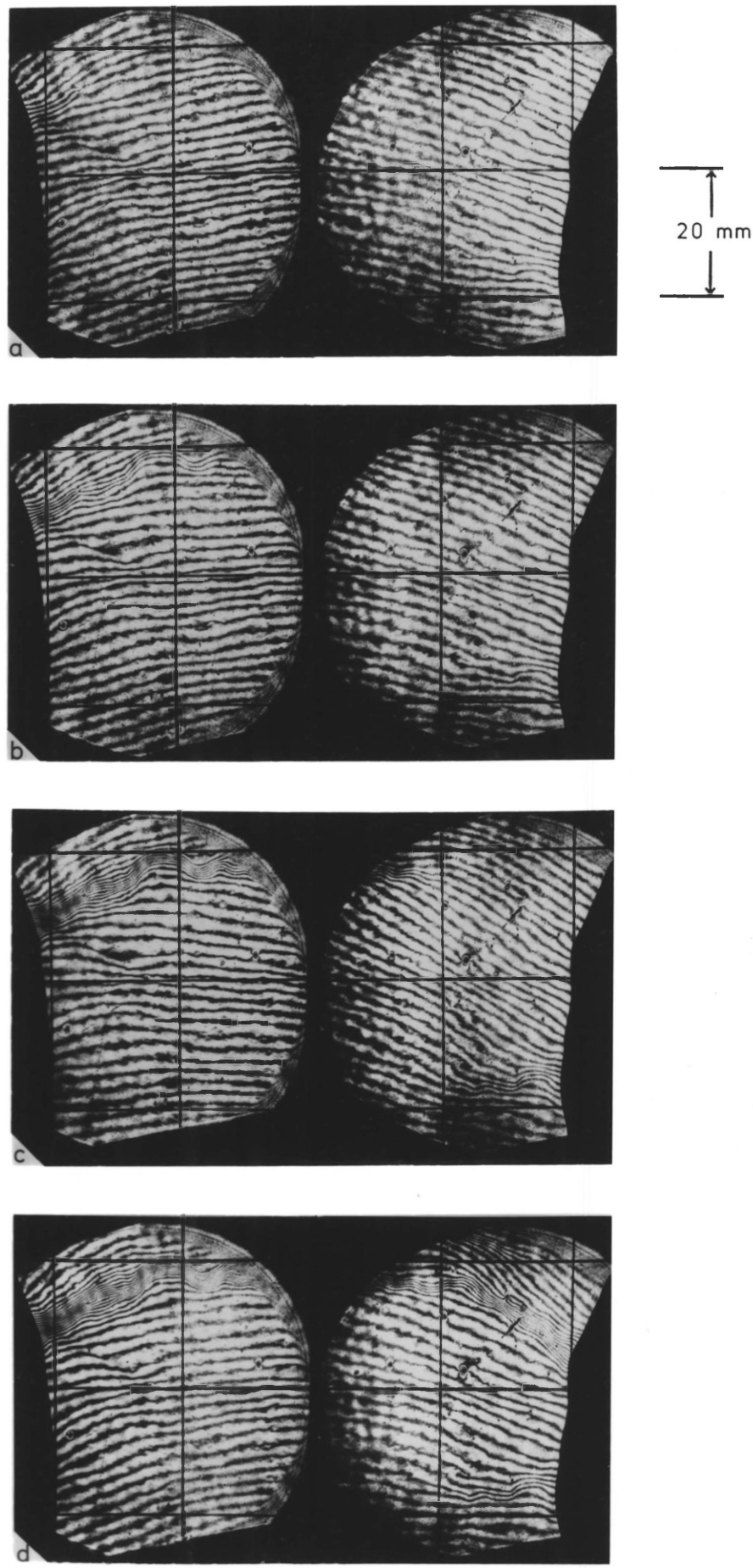

Fig. 8.4 Axial strain fringe photographs — Test K2
Pairs a, b, c & d correspond to
Fig. 8.12 d, e, g & h respectively

vertical lines to enable the contour plots in Section 8.3.2 to be drawn.

The effects of gauge length and position when calculating strains from the fringe patterns are discussed in Section 8.3.3. The relationship between local field strain and fracture zone opening is described in Section 8.3.4. Transverse strain and displacement effects are described in Section 8.3.5.

8.3.2 Axial strain contour plots

The axial strain contour plots for the 10 successful tests in which the strain was measured are given in Figures 8.5 - 8.14. When considering the results shown in these figures, the limitations of the moire interferometry technique detailed in Section 6.4 should be borne in mind. In particular, strains greater than 1000 microstrain cannot be considered to be representative of the concrete beneath the grating and, similarly, the distribution of measured strains within a region of high strain gradient is a function of de-bonding of the grating rather than a true concrete strain gradient. In the figures, the intermediate strain contours in regions of this type are omitted.

In several of the tests a large number of small areas exhibited strains of slightly greater than 100 microstrain, however, for clarity only those areas which subsequently develop into fracture zones or those areas which are adjacent to such zones are shown. Care must be exercised in the interpretation of the computer output. The curve fitting algorithm between data points may cause a large compressive strain to be attributed to the material in a thin band adjacent to a zone of very high strain gradient. This compressive strain is fictitious and is not included in the figures. However, compressive strains in areas between 10 and 20mm. from the centre of developed fracture zones and running parallel to the zones, did occur in several specimens. These true compressive strains are relatively low and only in one test (Fig. 8.10) do they exceed 100 microstrain.

The levels at which significant localisation in the strain field was first observed and also at which it appears across the full width of the specimen are given in Table 8.5.

Test Number	Percentage of maximum load at first observed localisation	Percentage of maximum load for localisation across full width	Strain contour figure number
C2	95% Pre-peak	49% Post-peak	8.5
E2	78% Post-peak	57% Post-peak	8.6
F2	68% Pre-peak	(Unstable failure)	8.7
G2	96% Pre-peak	79% Post-peak	8.8
I2	38% Pre-peak	(Unstable failure)	8.9
J2	76% Pre-peak	61% Post-peak	8.10
K1	67% Post-peak	62% Post-peak	8.11
K2	91% Pre-peak	47% Post-peak	8.12
L1	85% Pre-peak	75% Post-peak	8.13
L2	73% Pre-peak	95% Post-peak	8.14

Table 8.5 Levels for first observed strain localisation and localisation across full width

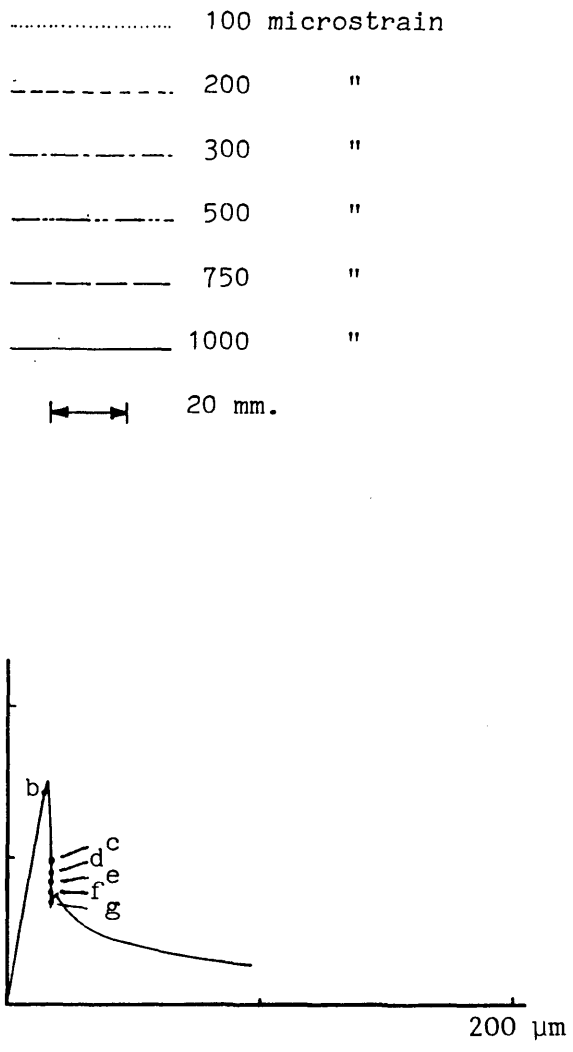

(a) Load/extension curve showing strain contour plot positions

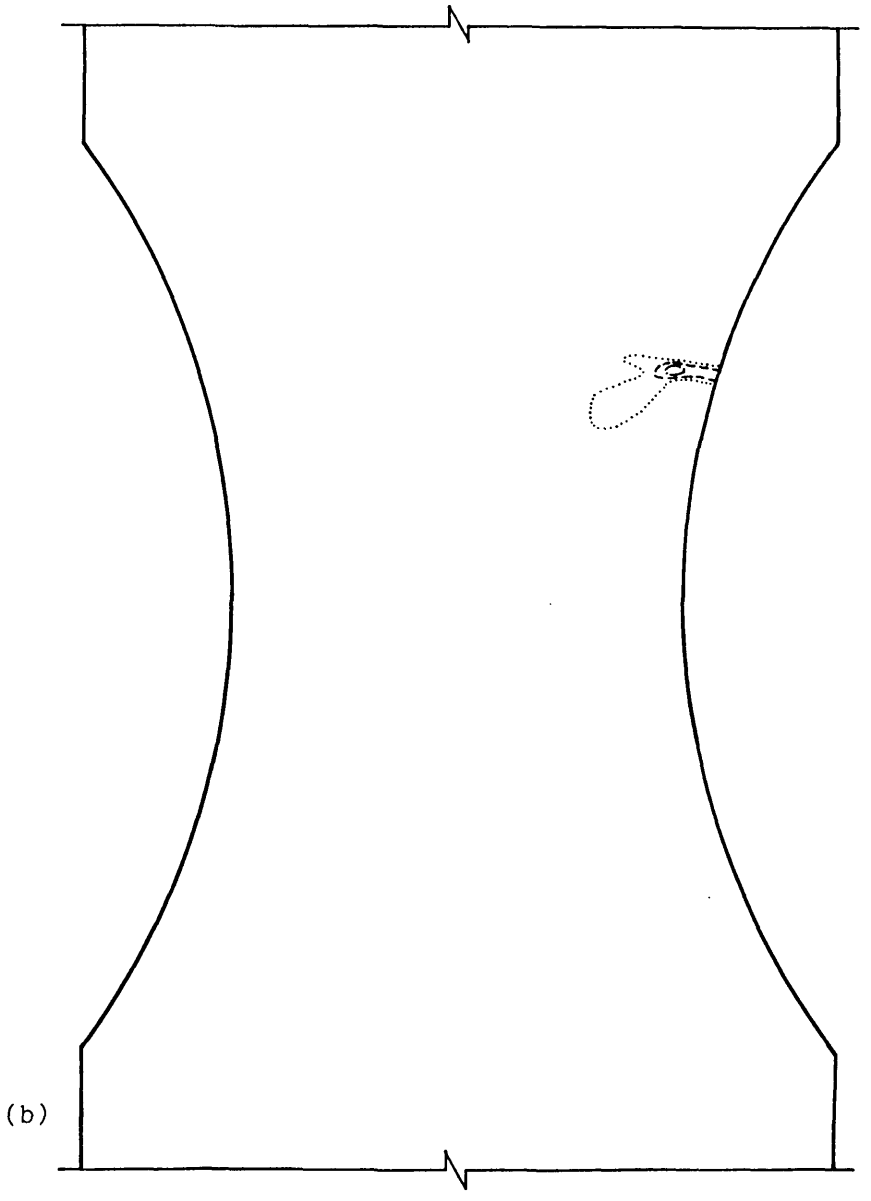

Fig. 8.5 Test C2, strain contour plots

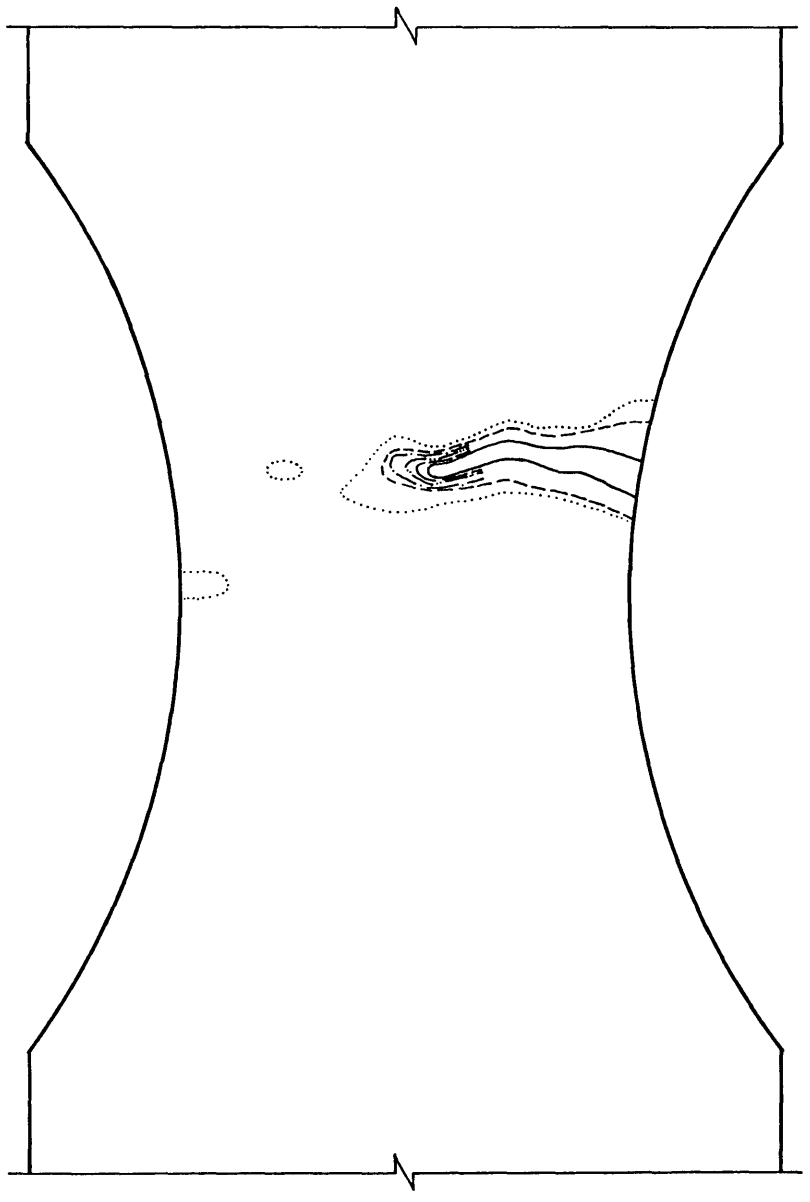

(c)

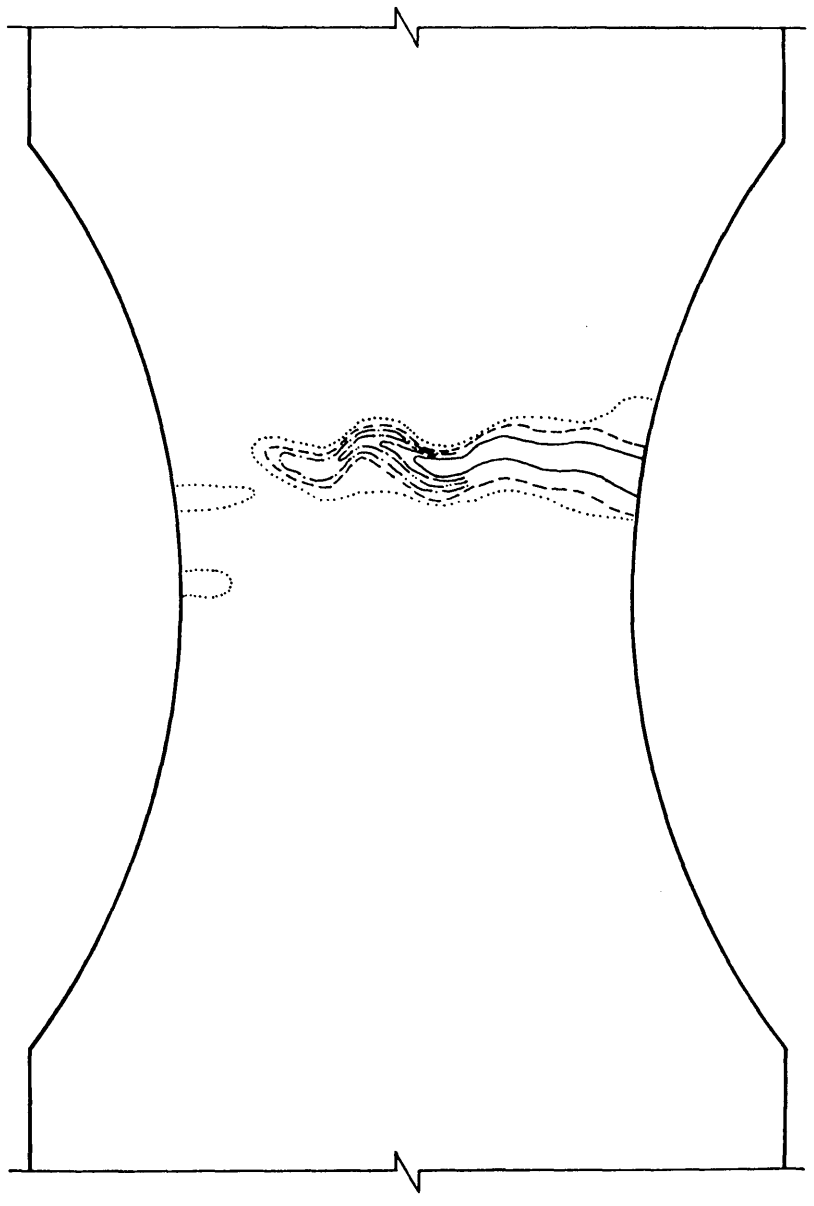

(d)

Fig. 8.5 Test C2, strain contour plots (cont)

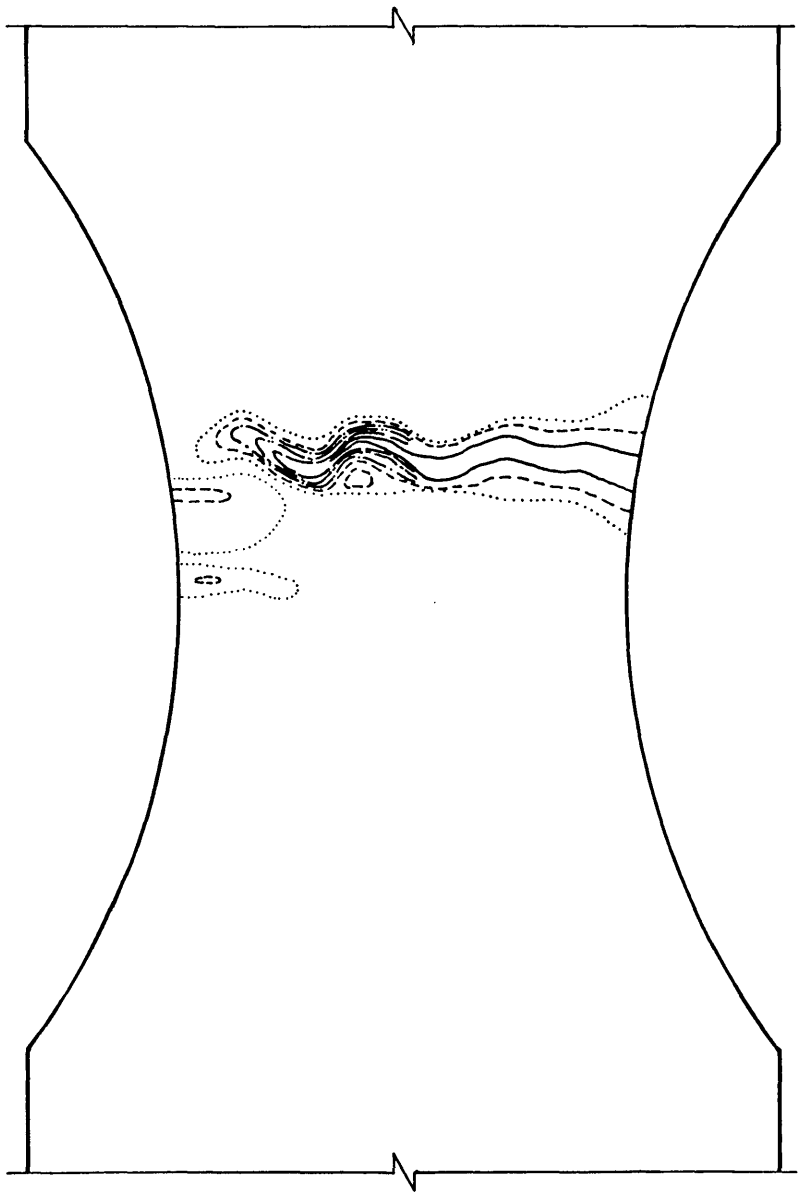

(e)

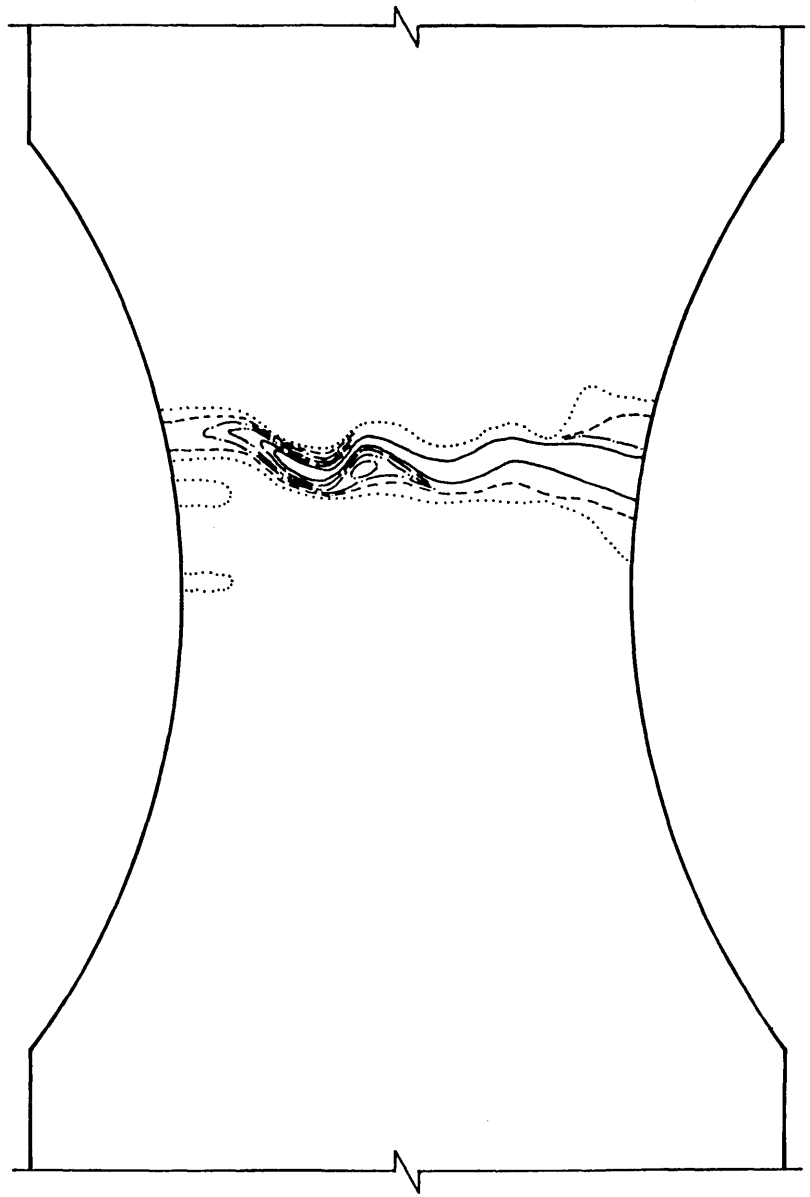

(f)

Fig. 8.5 Test C2, strain contour plots (cont)

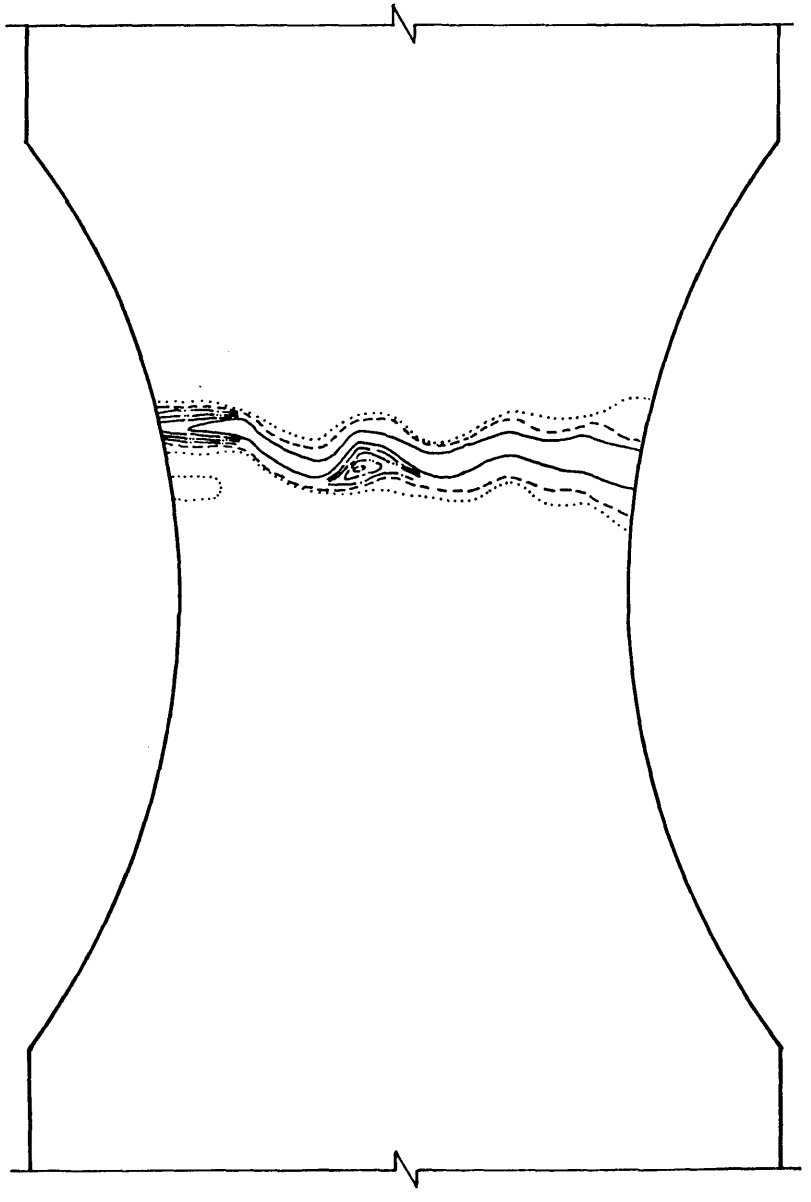

(g)

Fig. 8.5 Test C2, strain contour plots (cont)

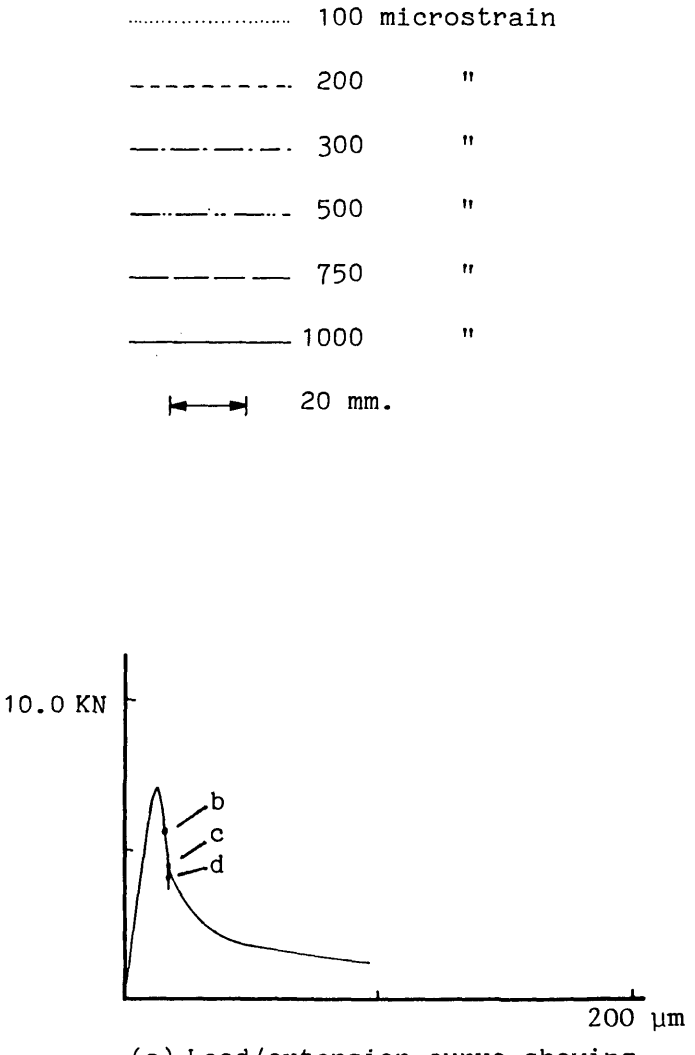

(a) Load/extension curve showing strain contour plot positions

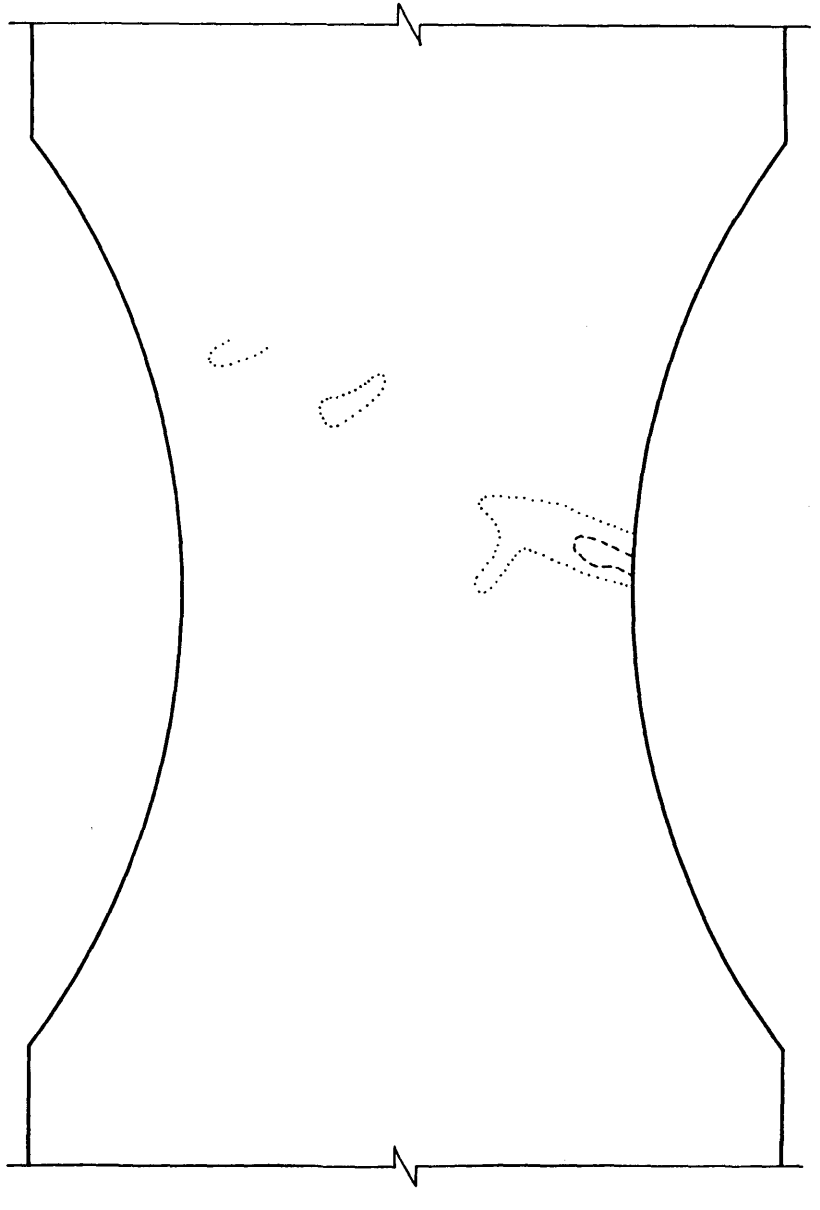

(b)

Fig. 8.6 Test E2, strain contour plots

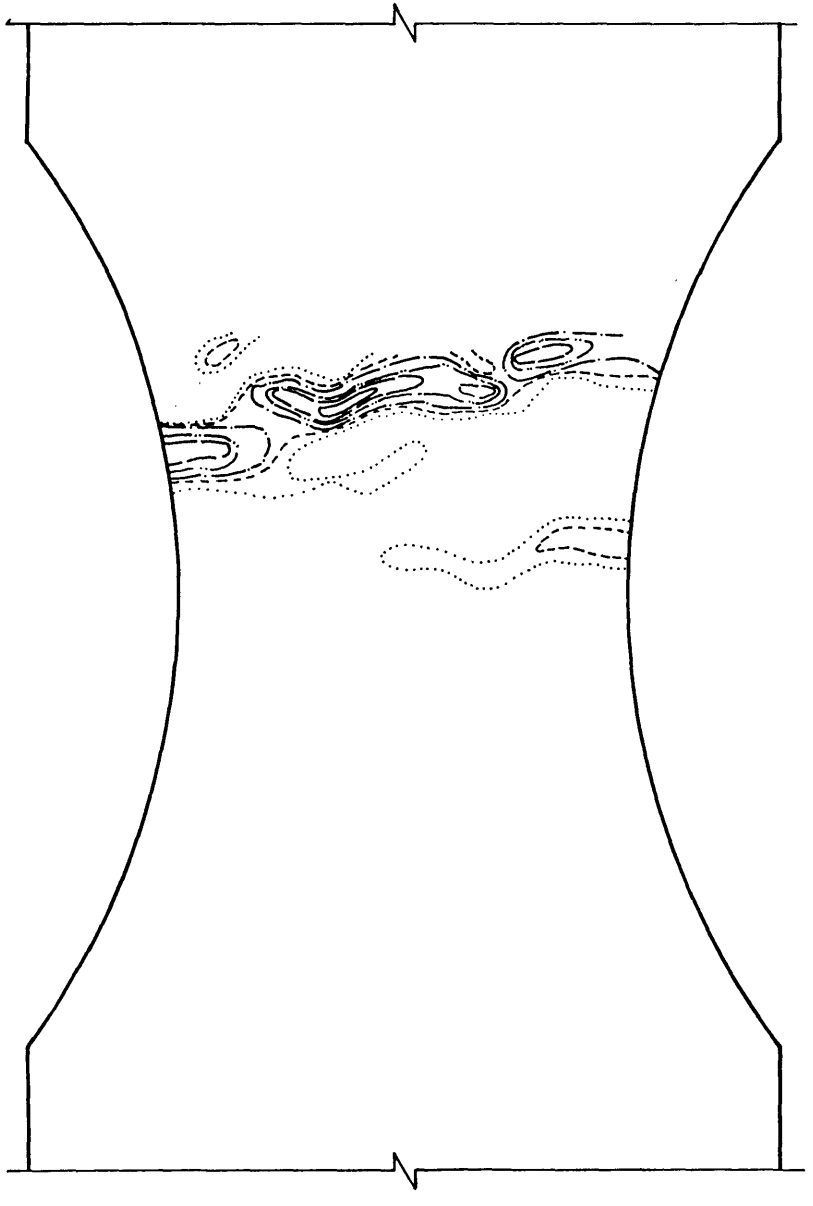

(c)

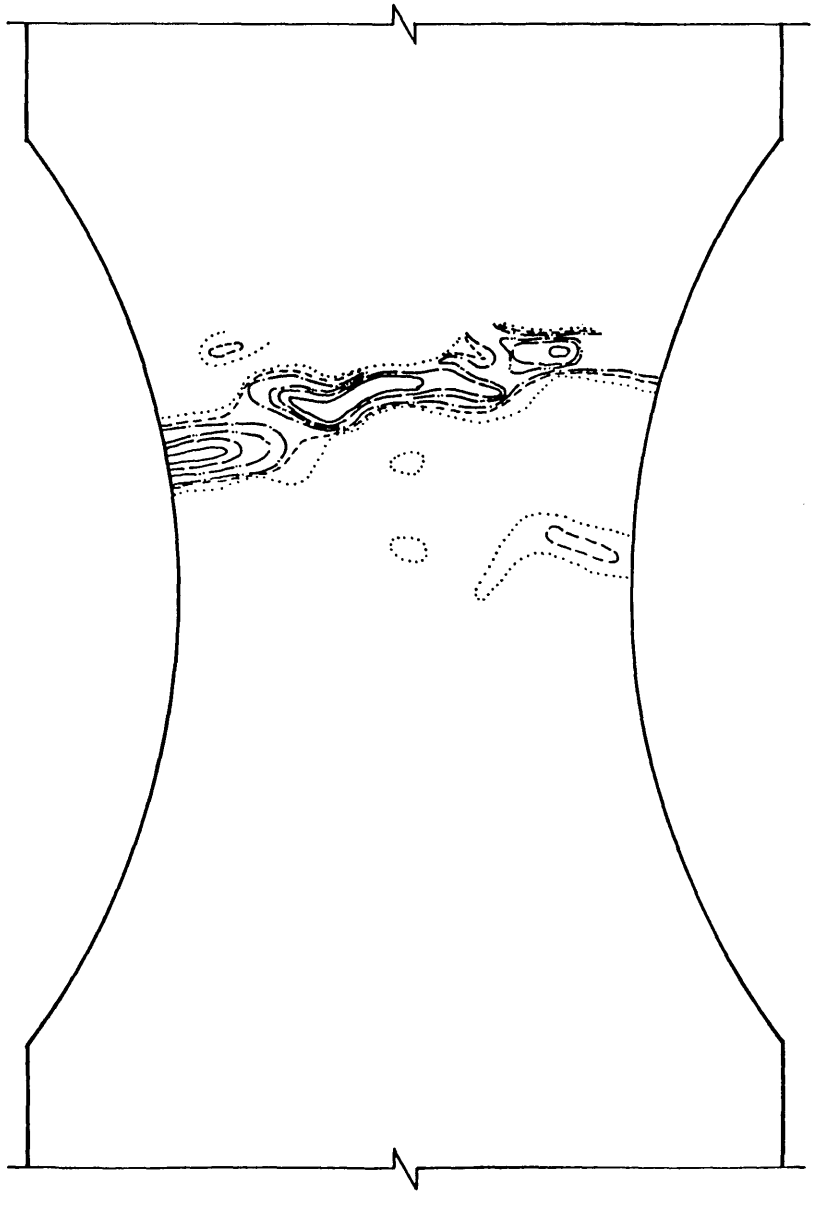

(d)

Fig. 8.6 Test E2, strain contour plots (cont)

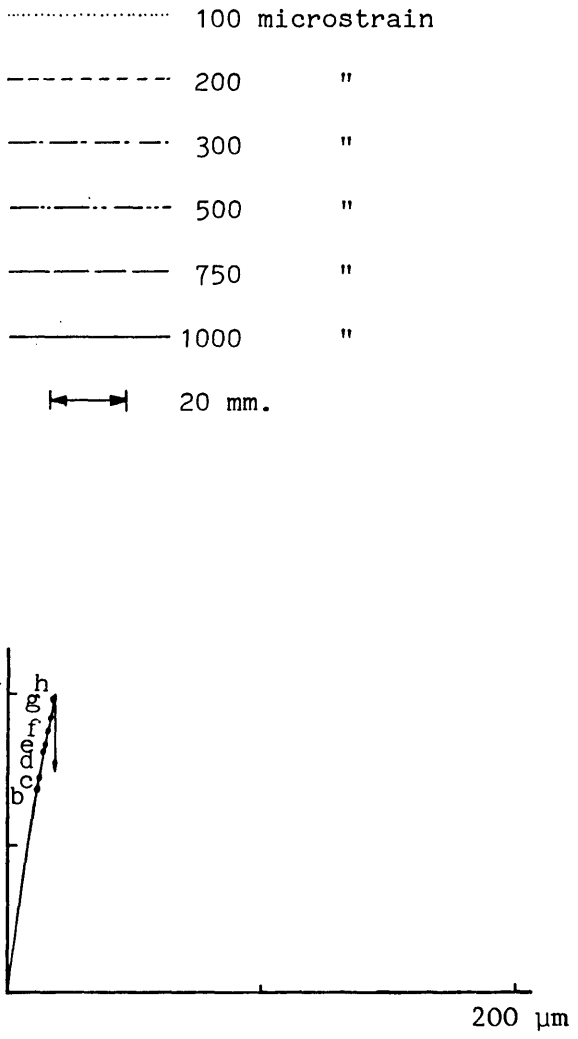

(a) Load/extension curve showing strain contour plot positions

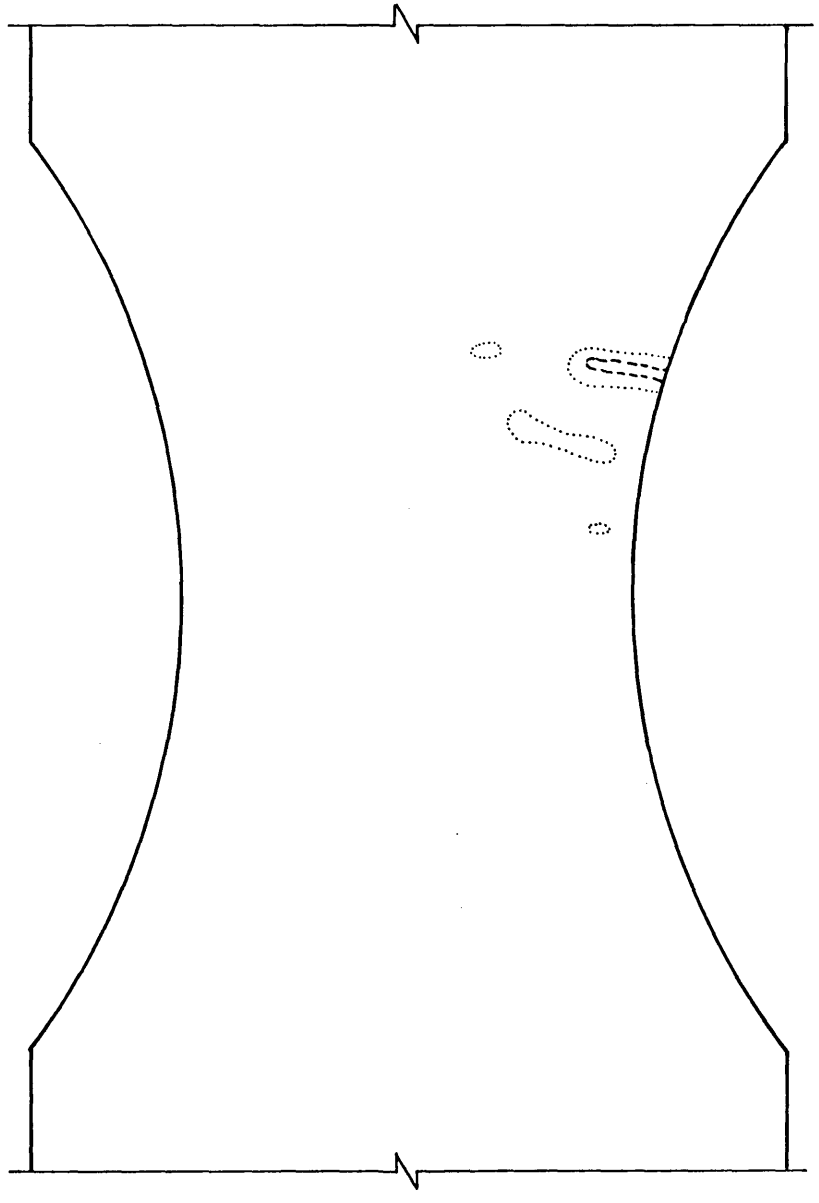

(b)

Fig. 8.7 Test F2, strain contour plots

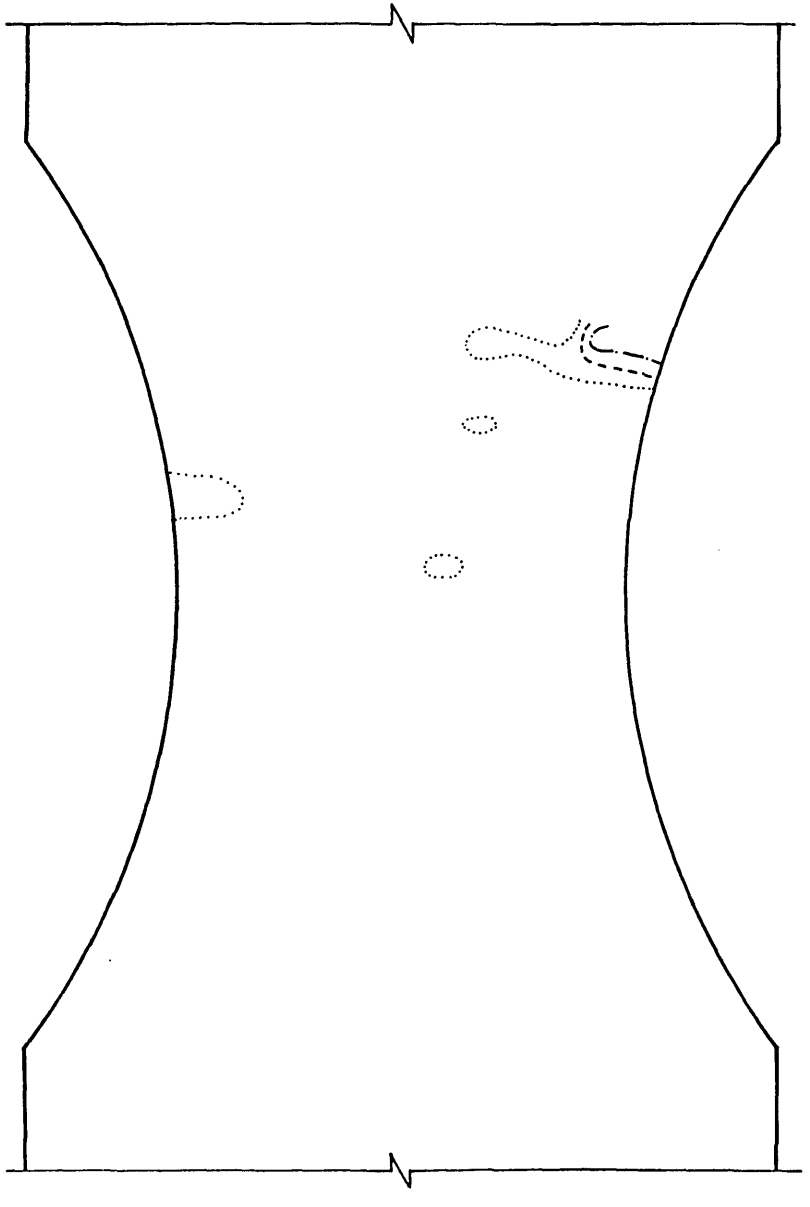

(c)

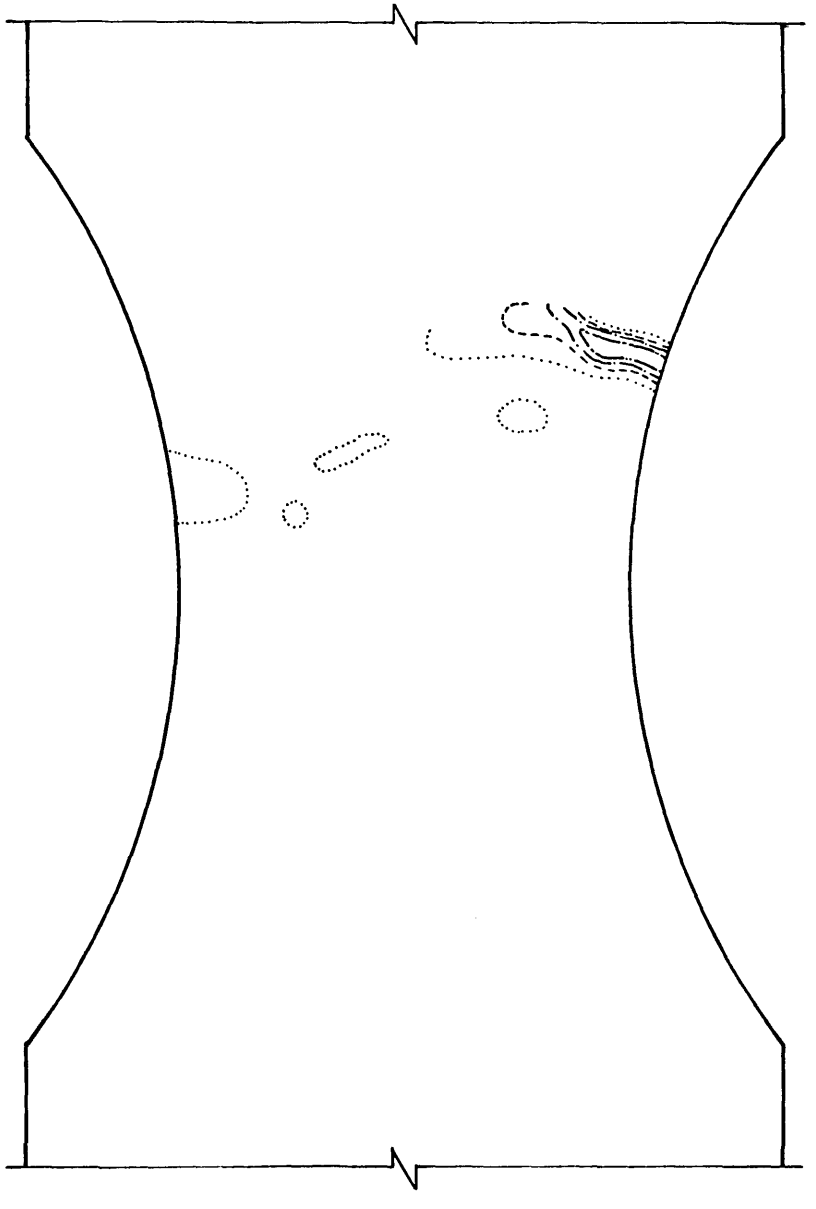

(d)

Fig. 8.7 Test F2, strain contour plots (cont)

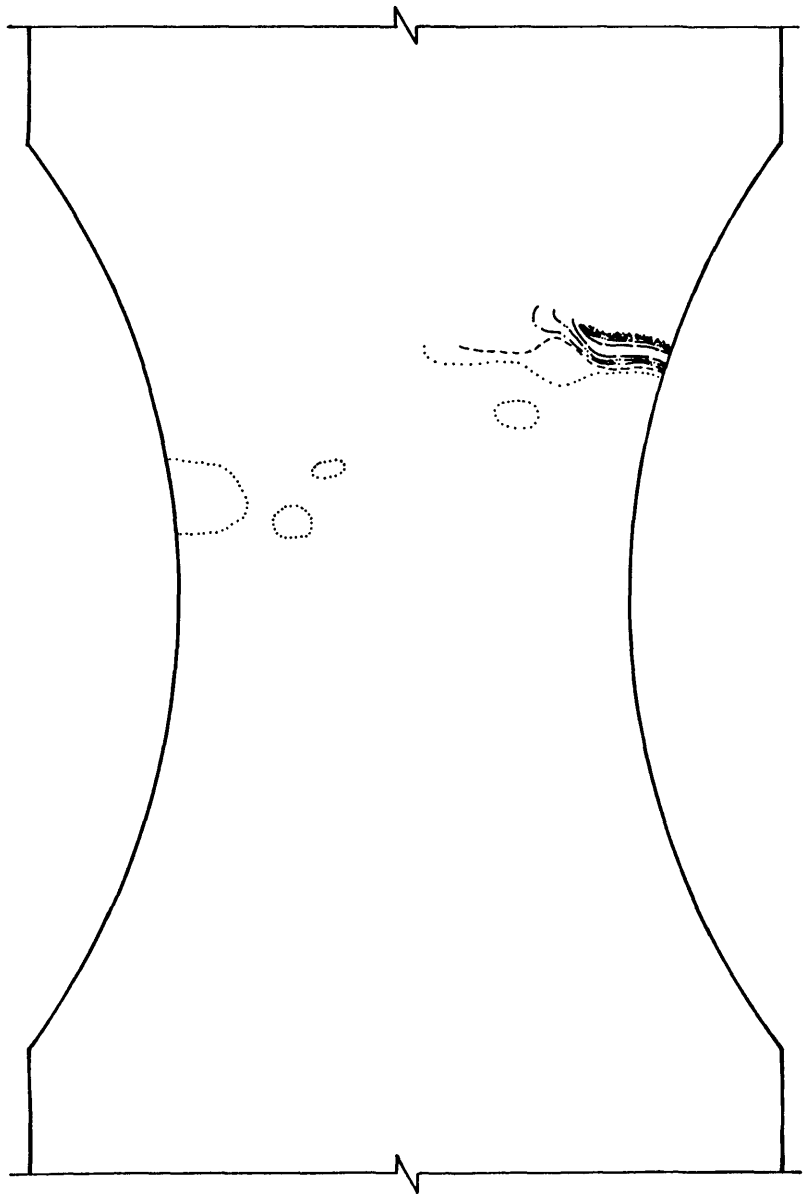

(e)

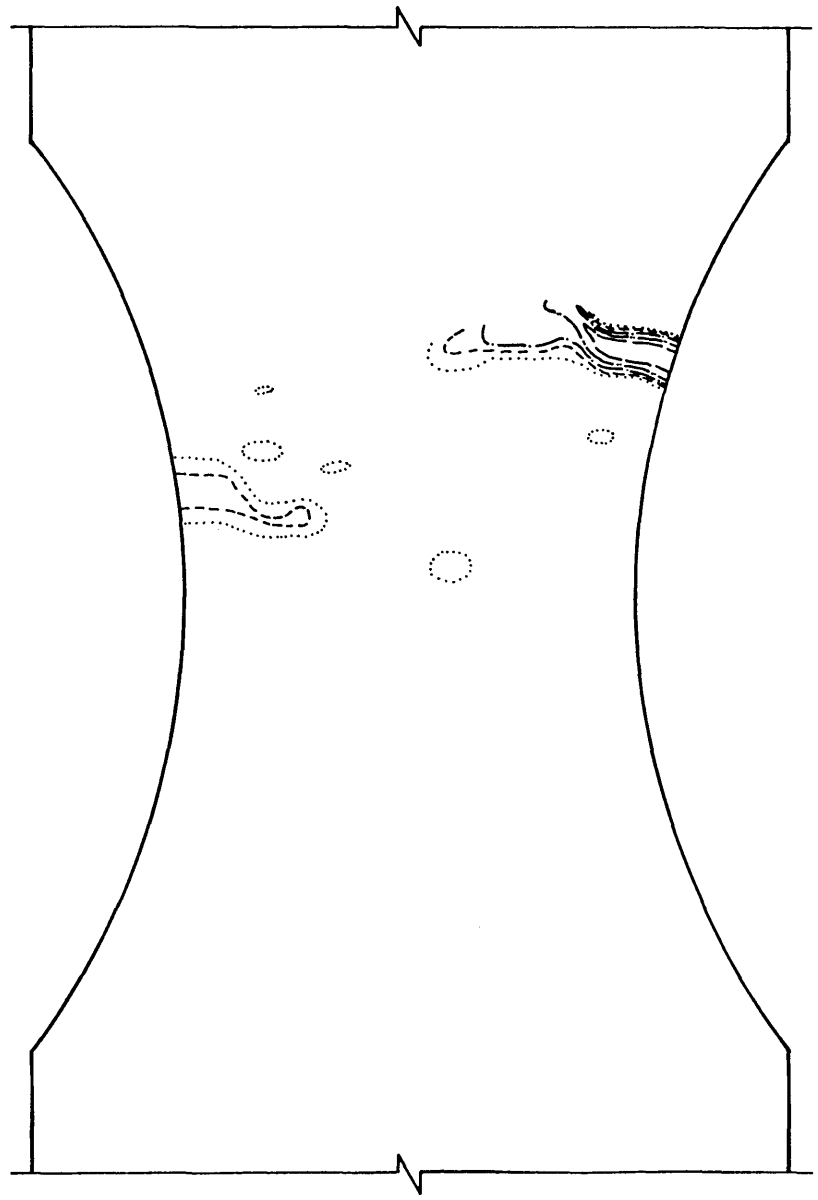

(f)

Fig. 8.7 Test F2, strain contour plots (cont)

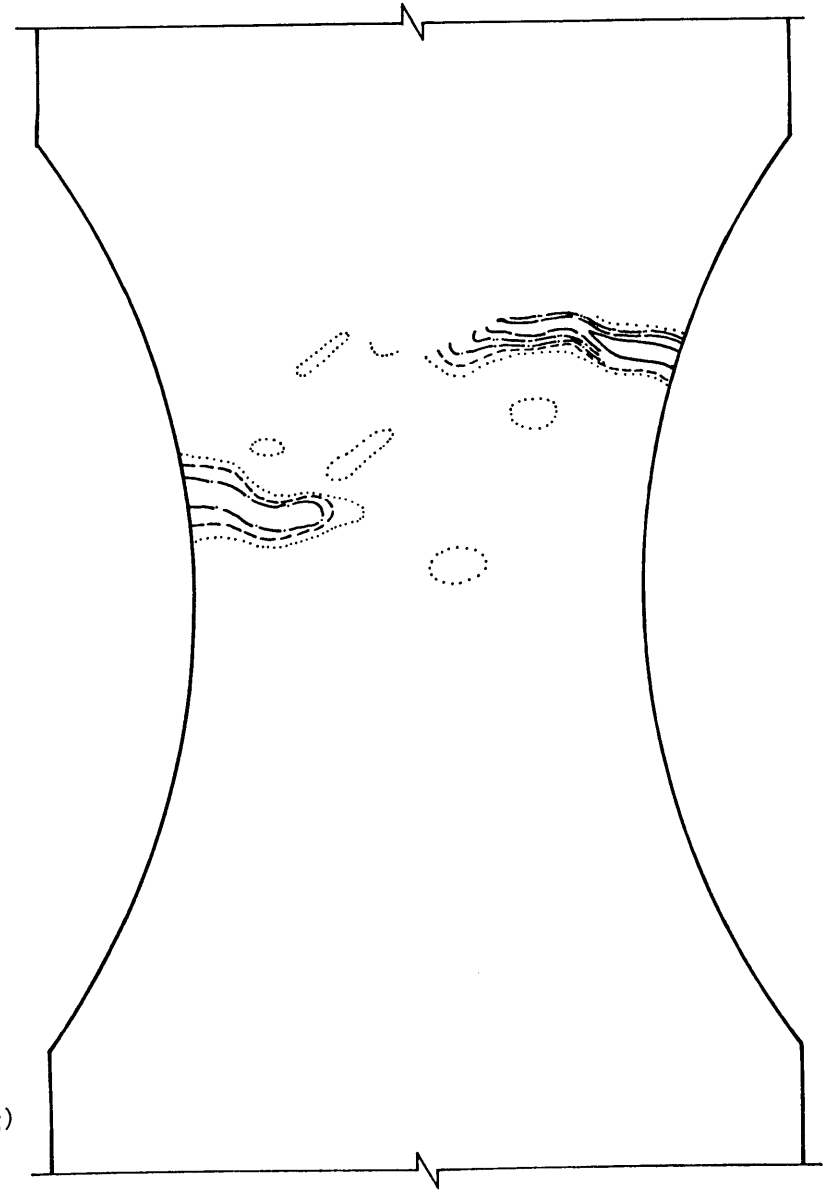

(g)

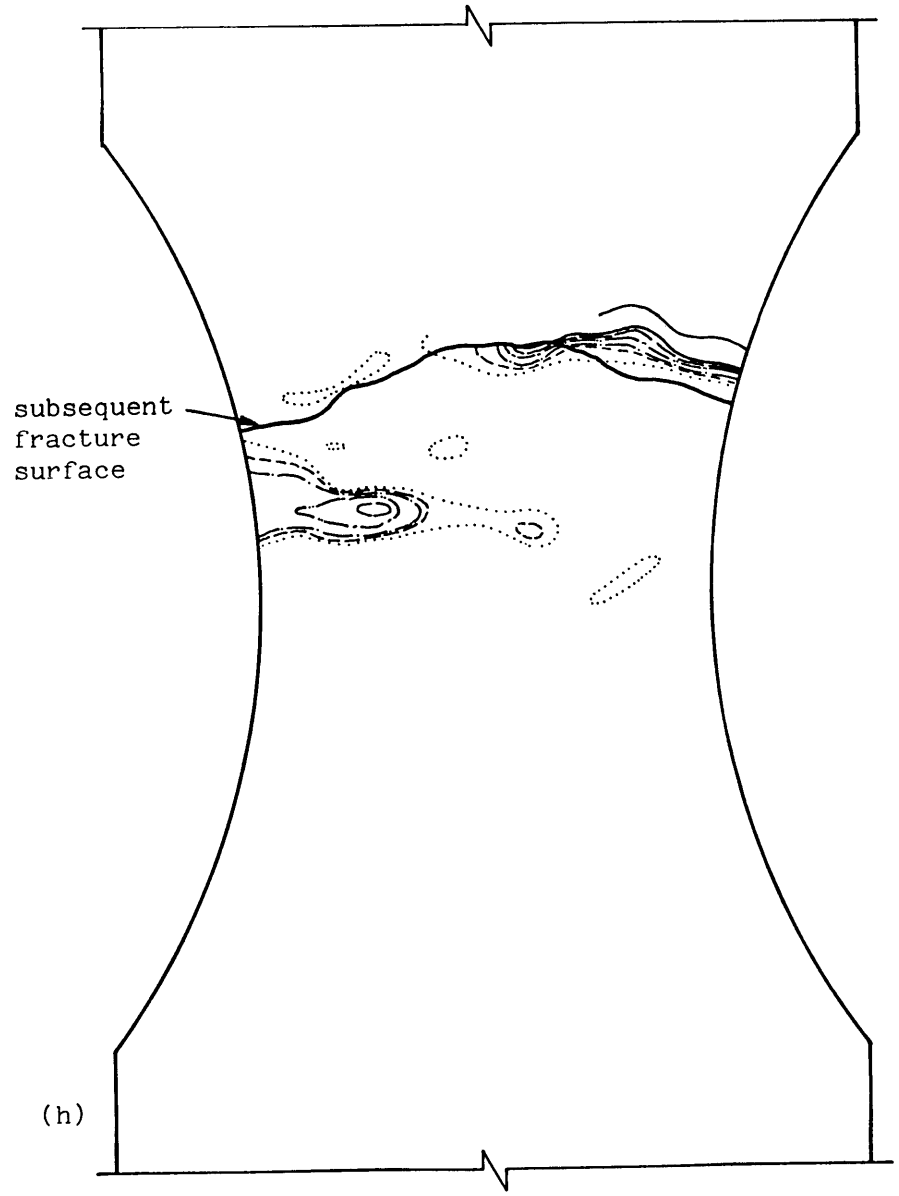

(h)

Fig. 8.7 Test F2, strain contour plots (cont)

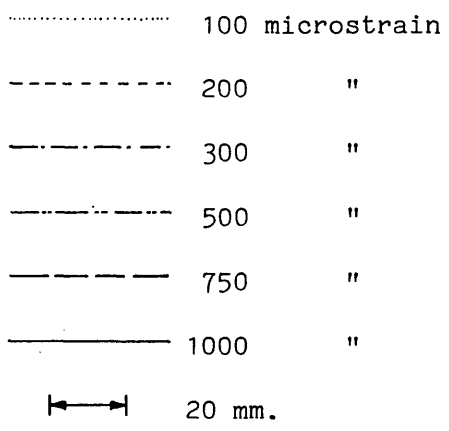

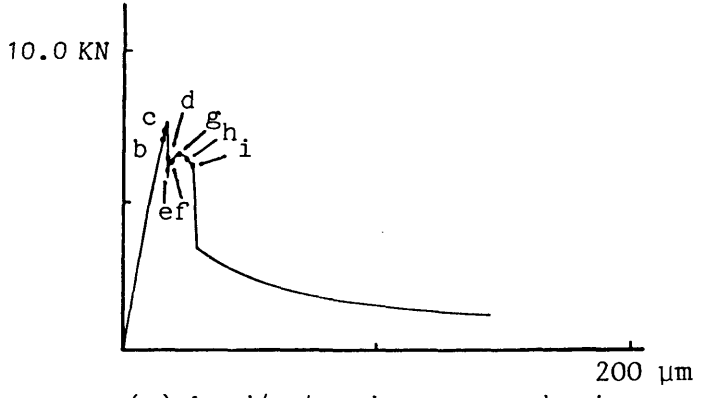

(a) Load/extension curve showing strain contour plot positions

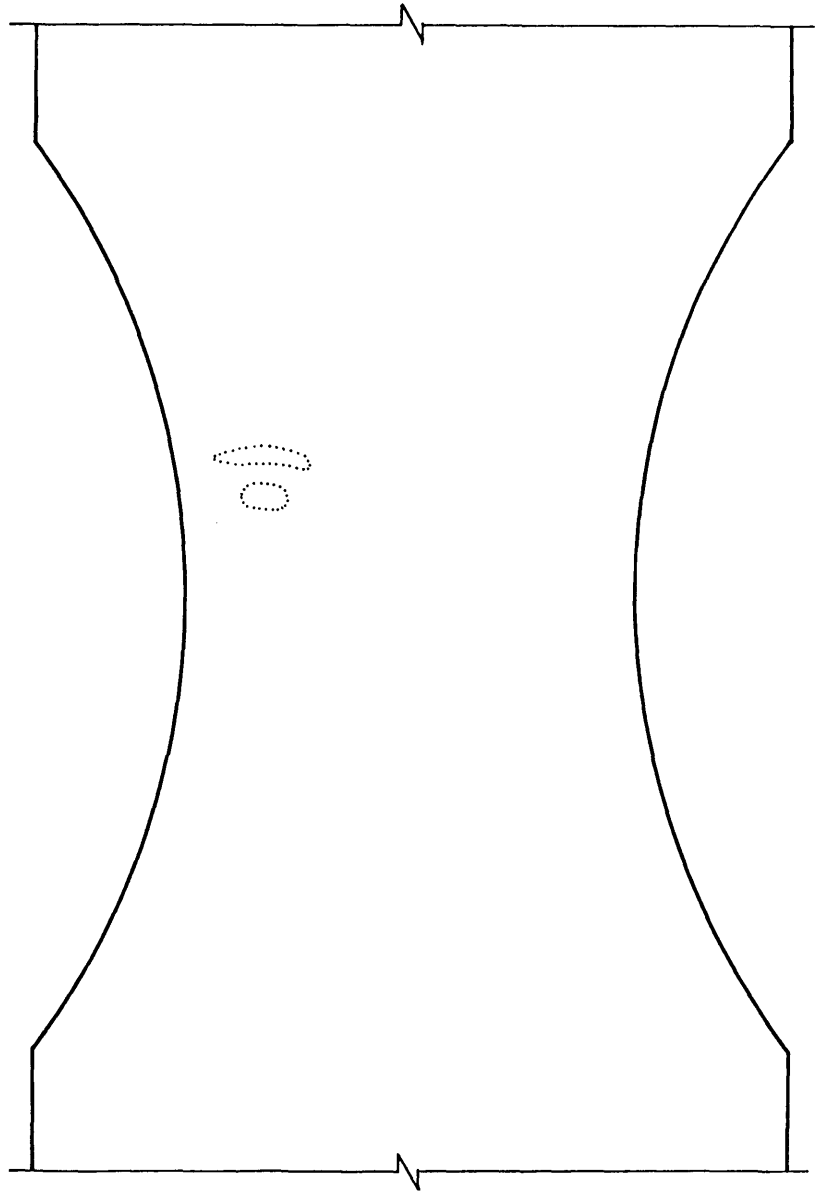

(b)

Fig. 8.8 Test G2, strain contour plots

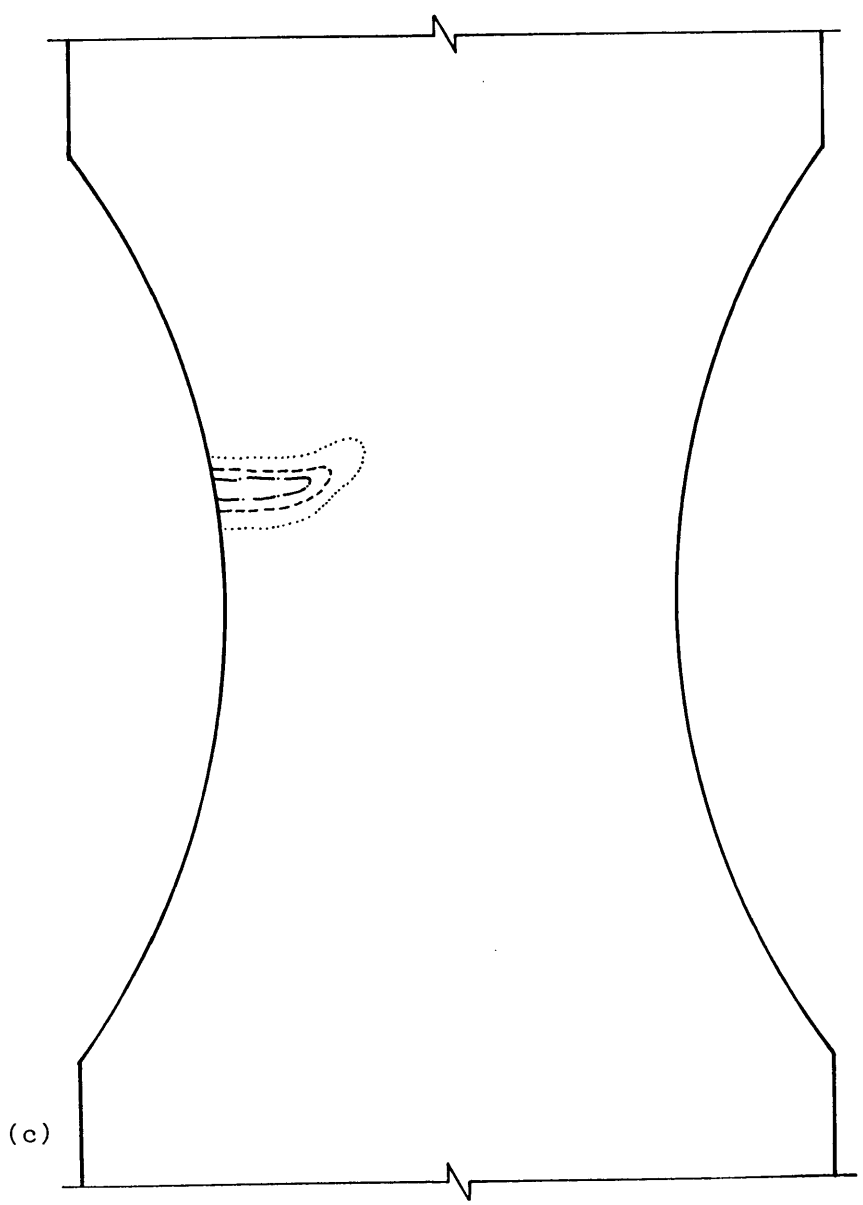

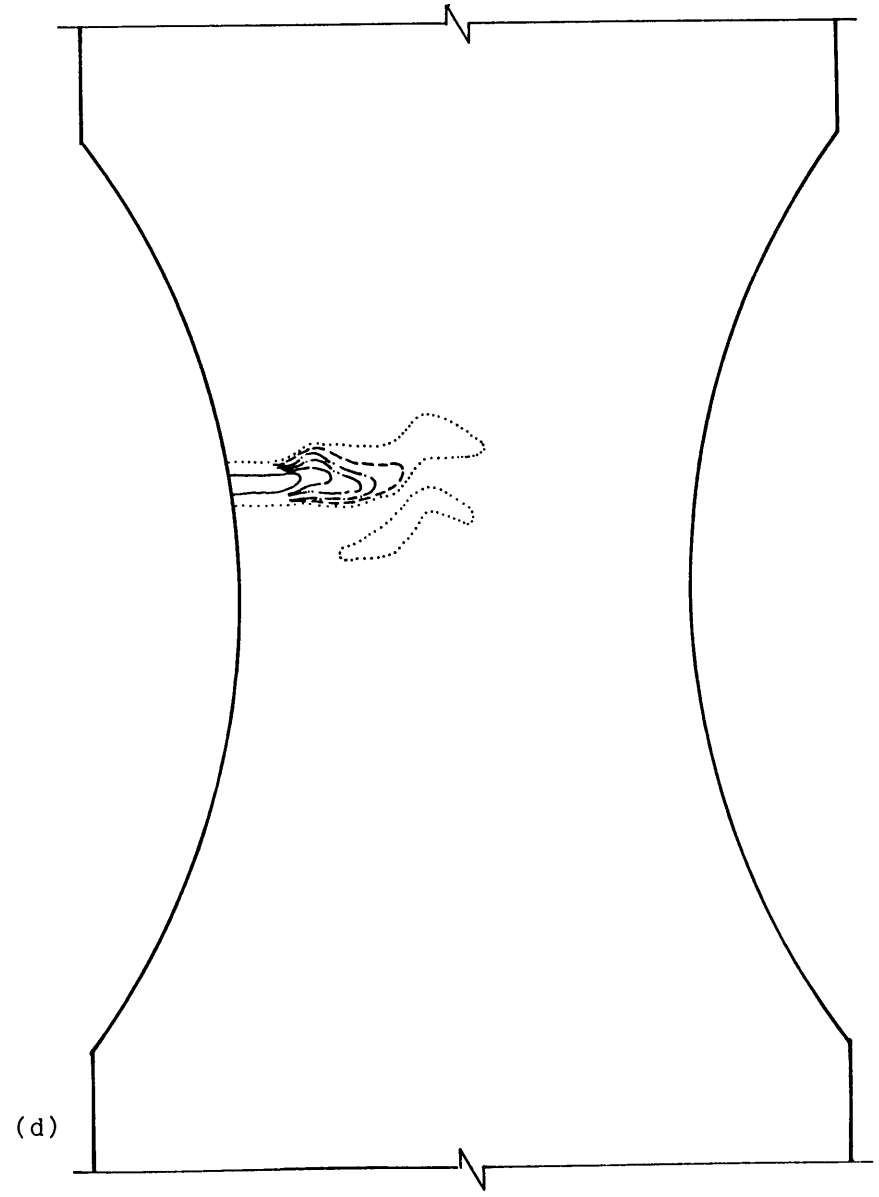

Fig. 8.8 Test G2, strain contour plots (cont)

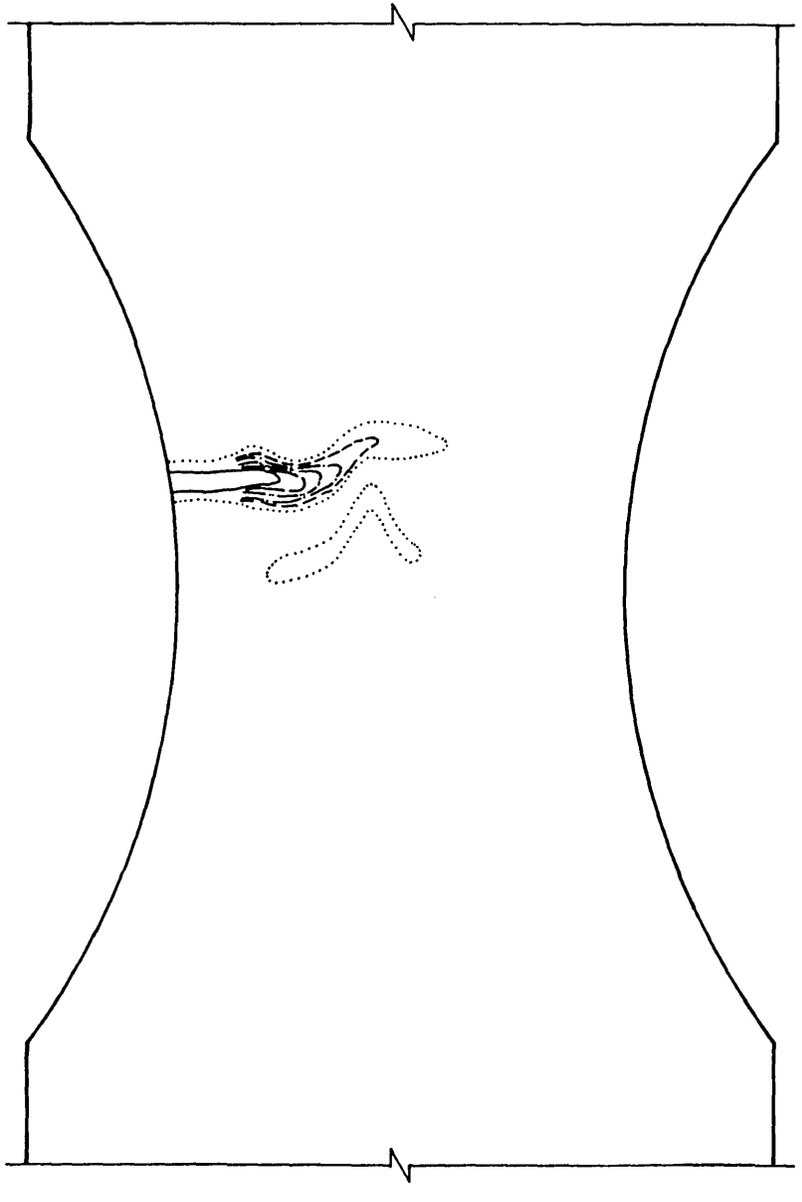

(e)

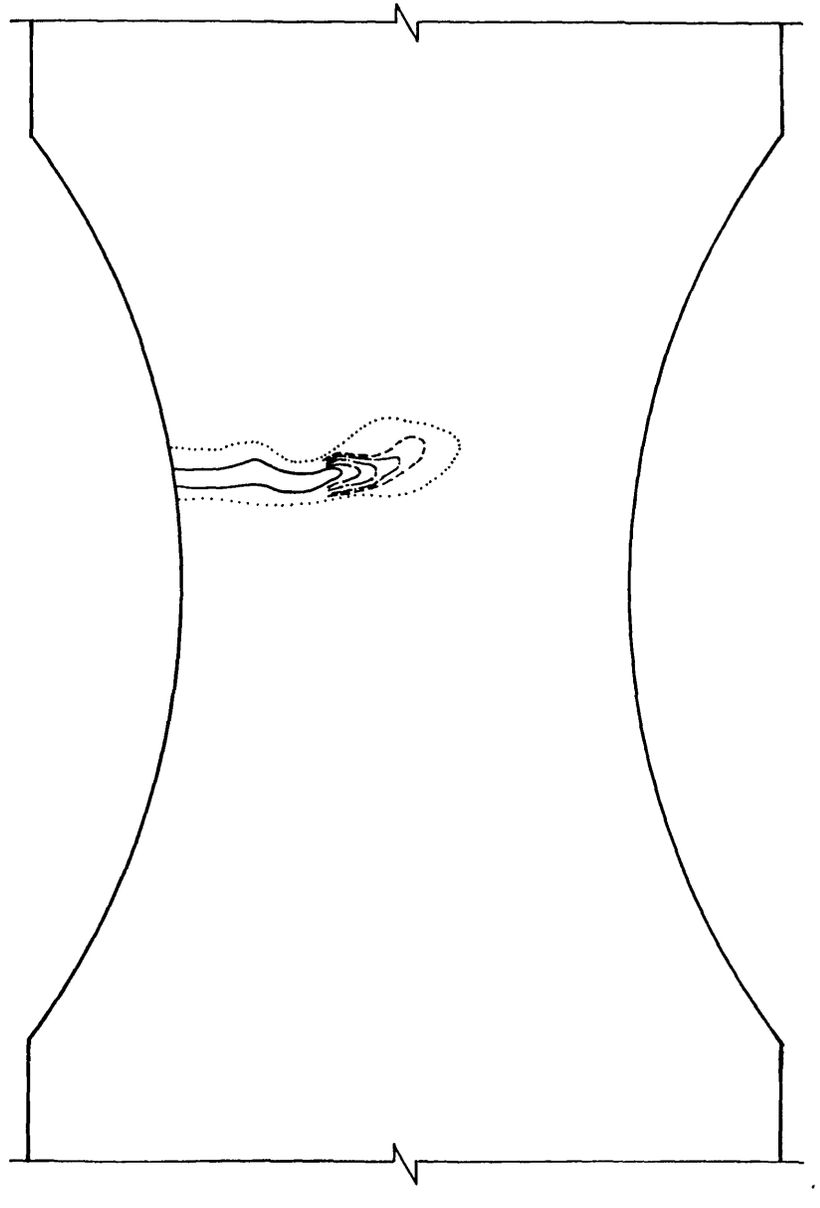

(f)

Fig. 8.8 Test G2, strain contour plots (cont)

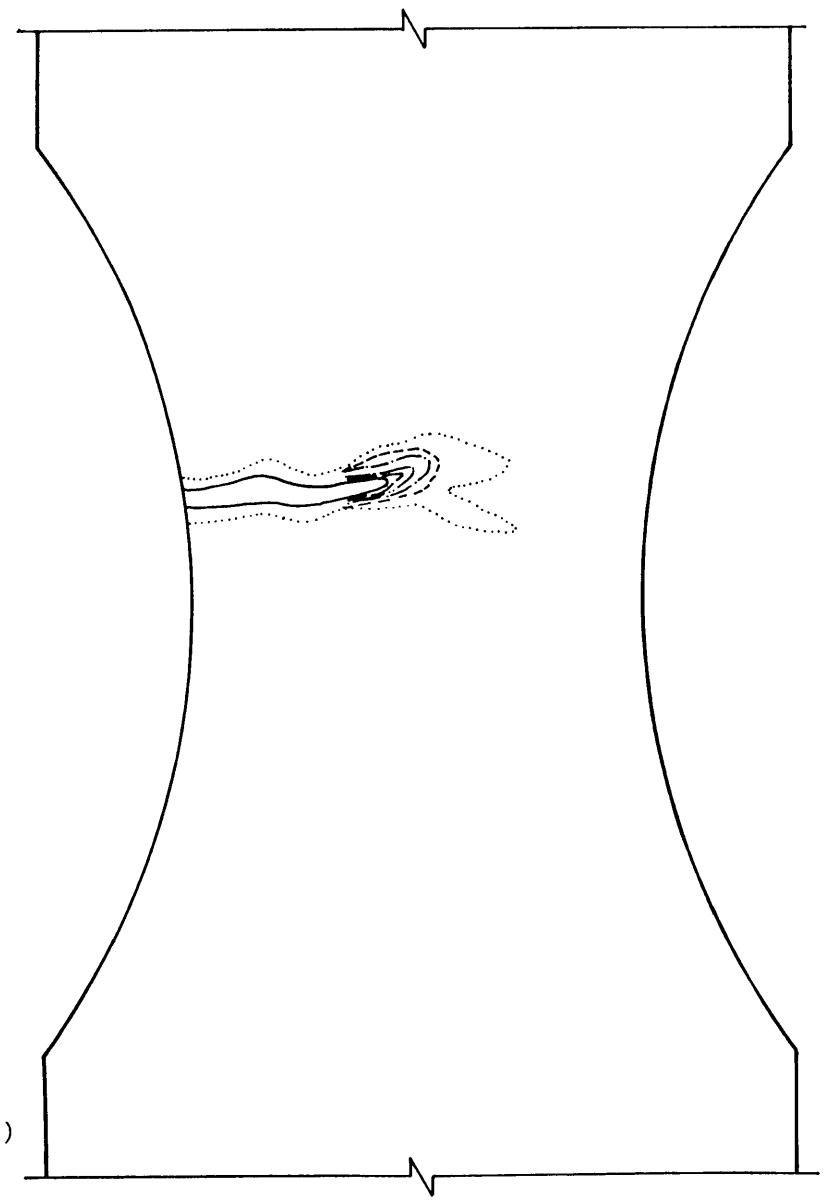

(g)

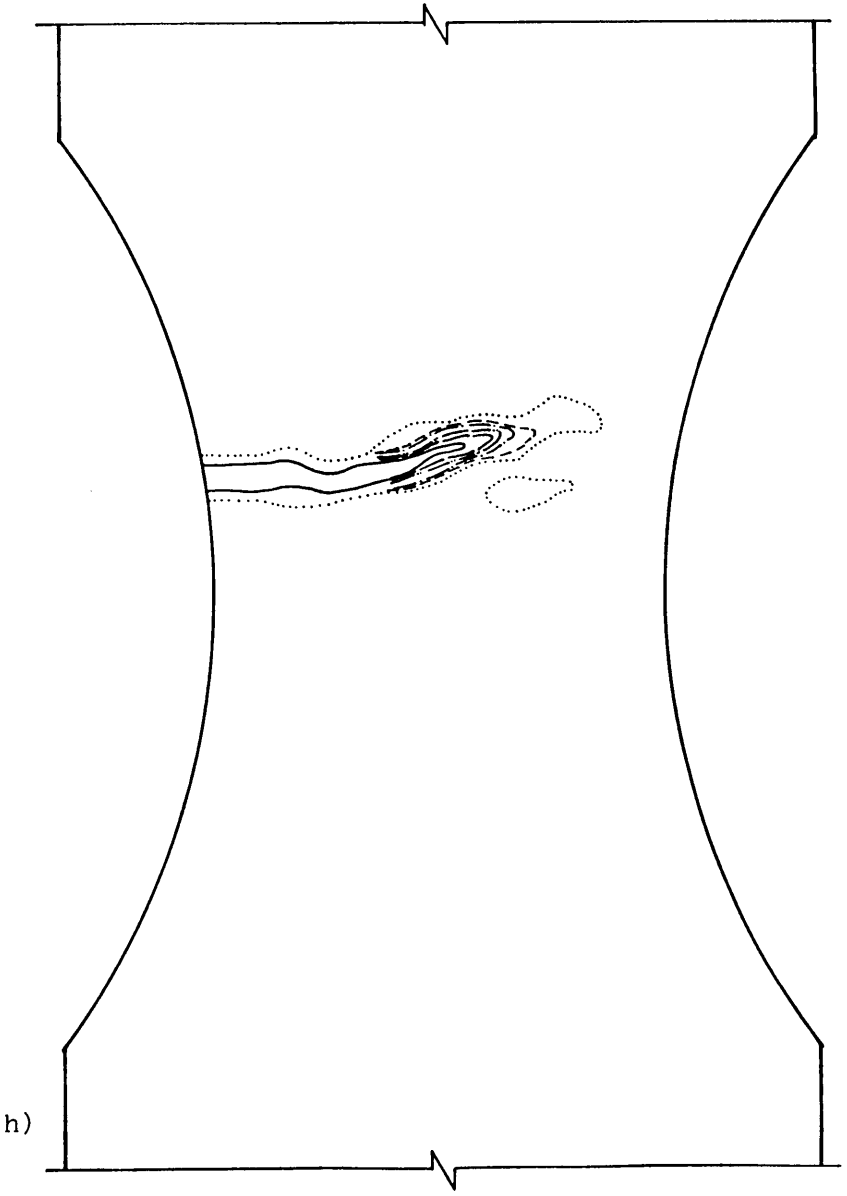

(h)

Fig. 8.8 Test G2, strain contour plots (cont)

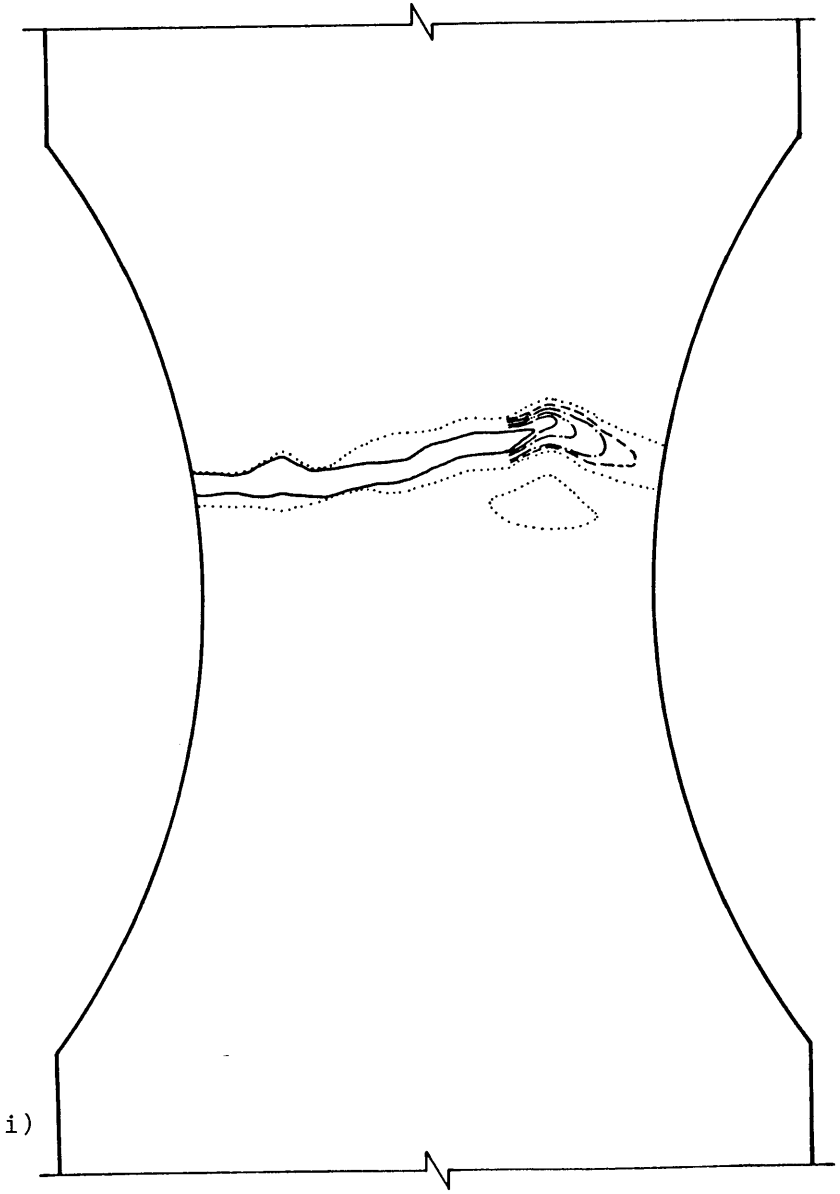

(i)

Fig. 8.8 Test G2, strain contour plots (cont)

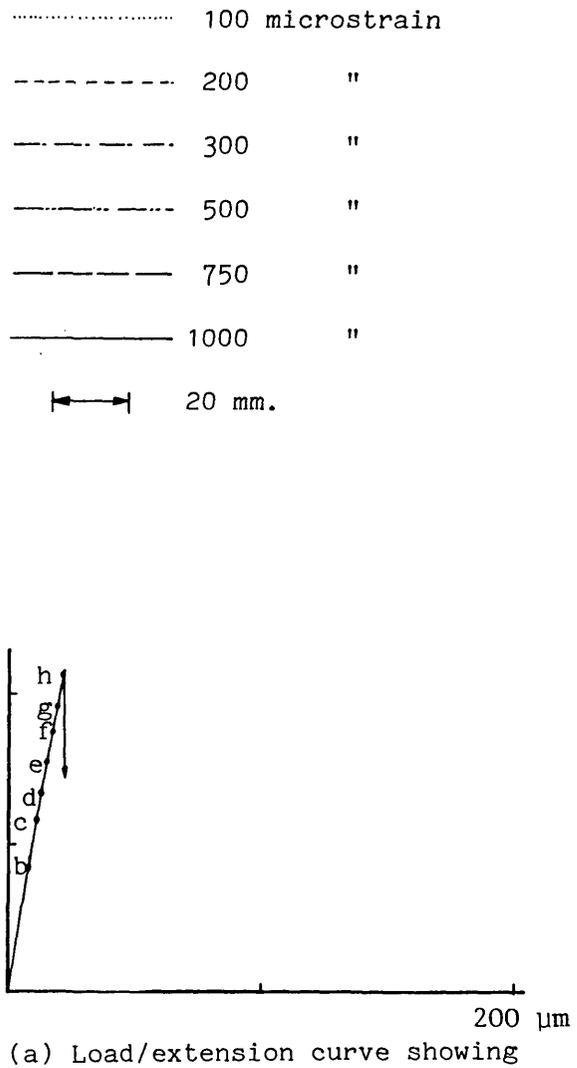

(a) Load/extension curve showing strain contour plot positions

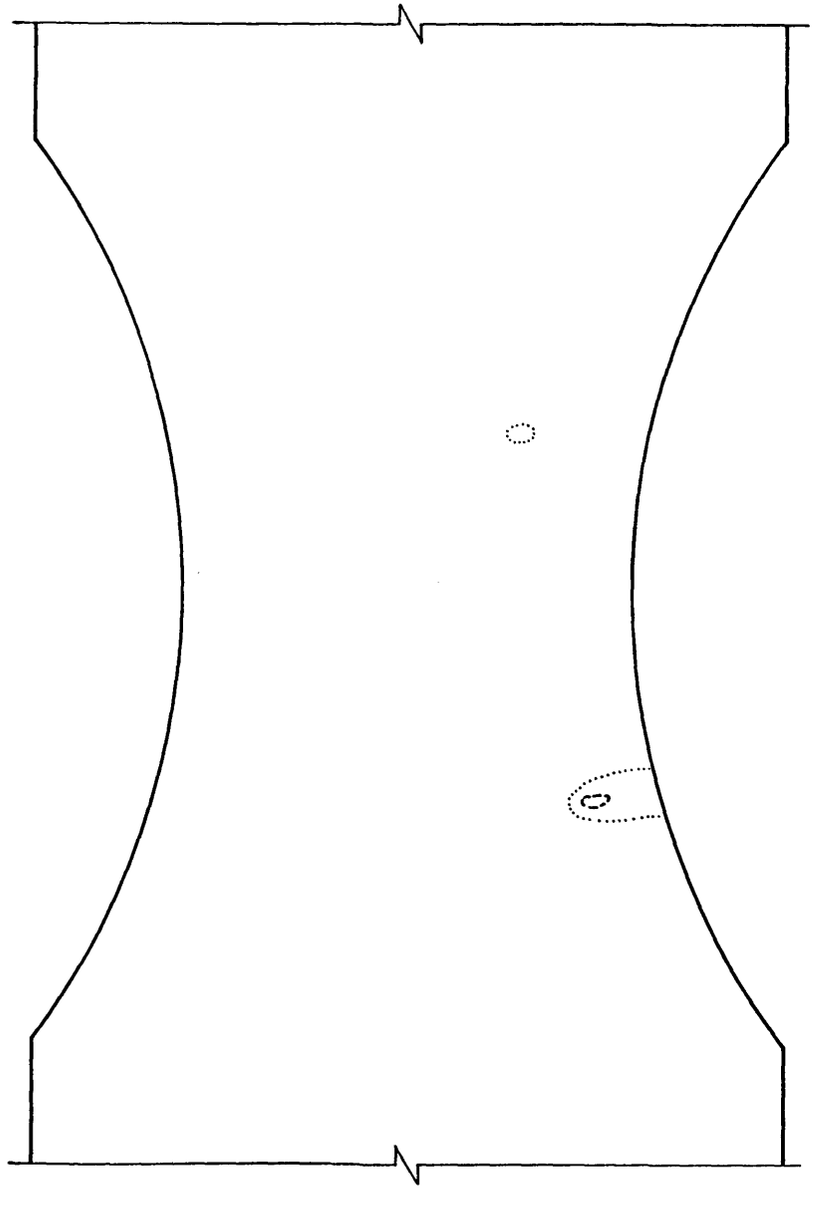

Fig. 8.9 Test I2, strain contour plots

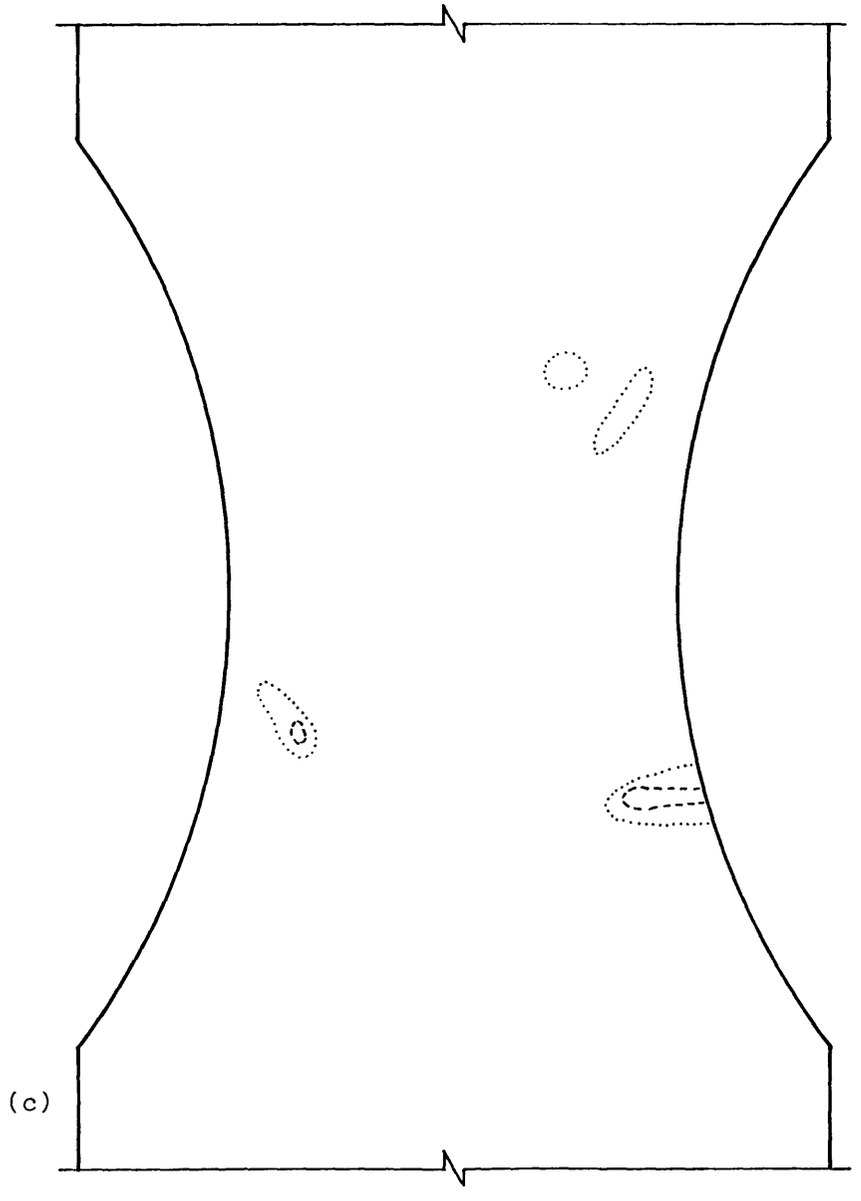

(c)

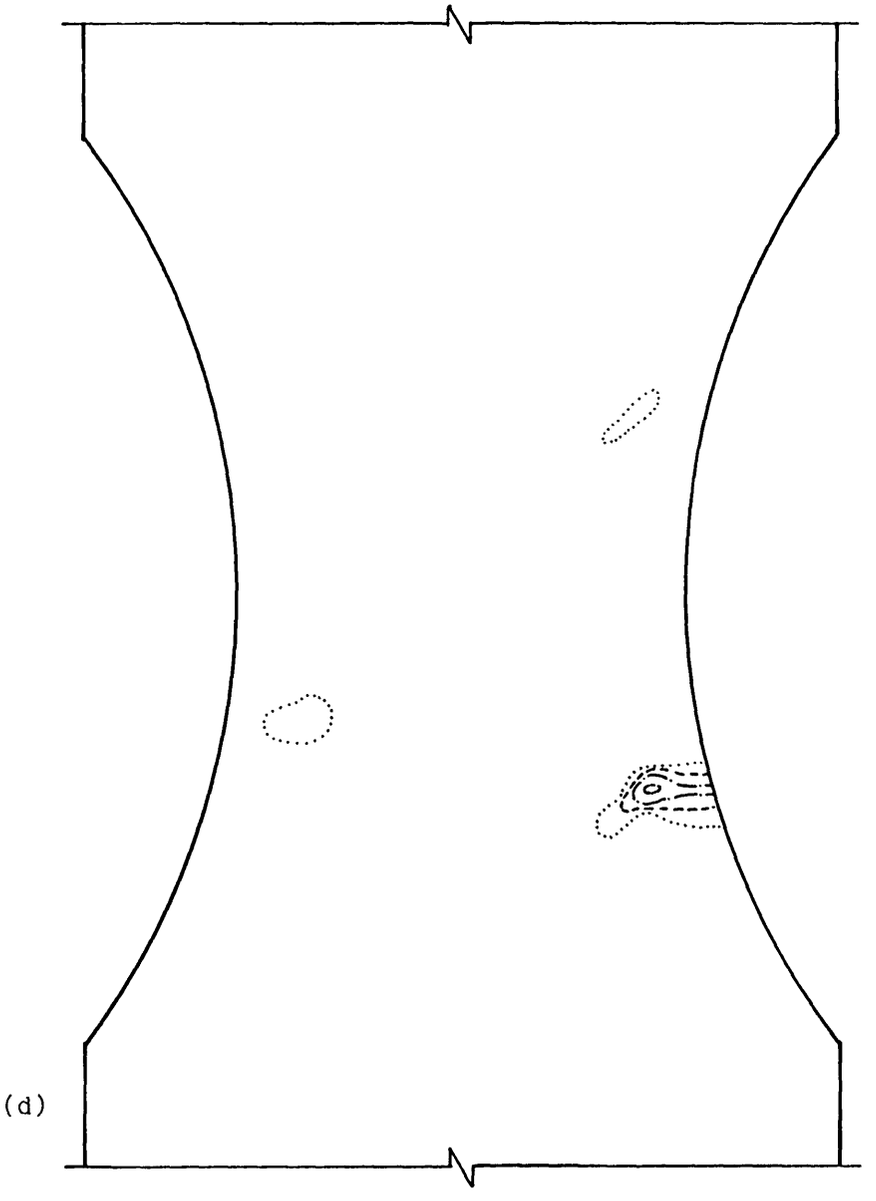

(d)

Fig. 8.9 Test I2, strain contour plots (cont)

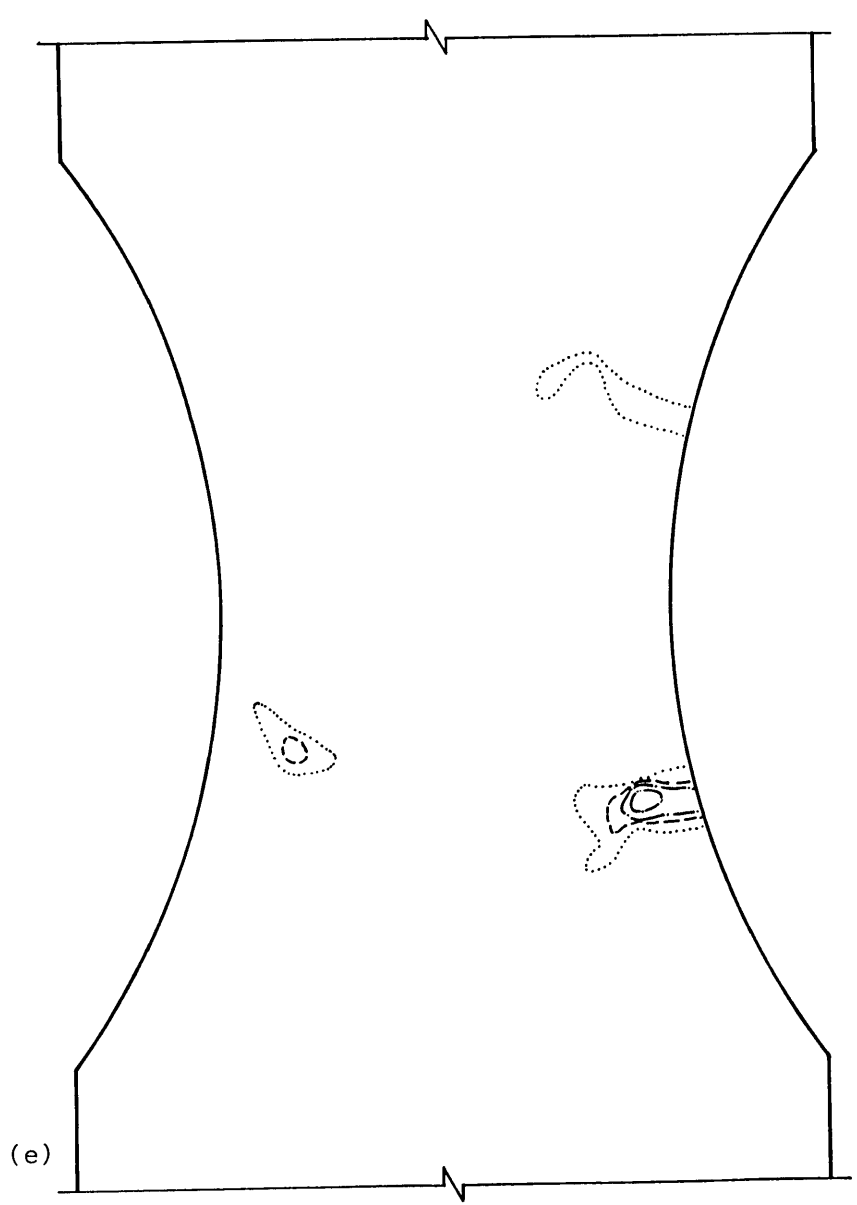

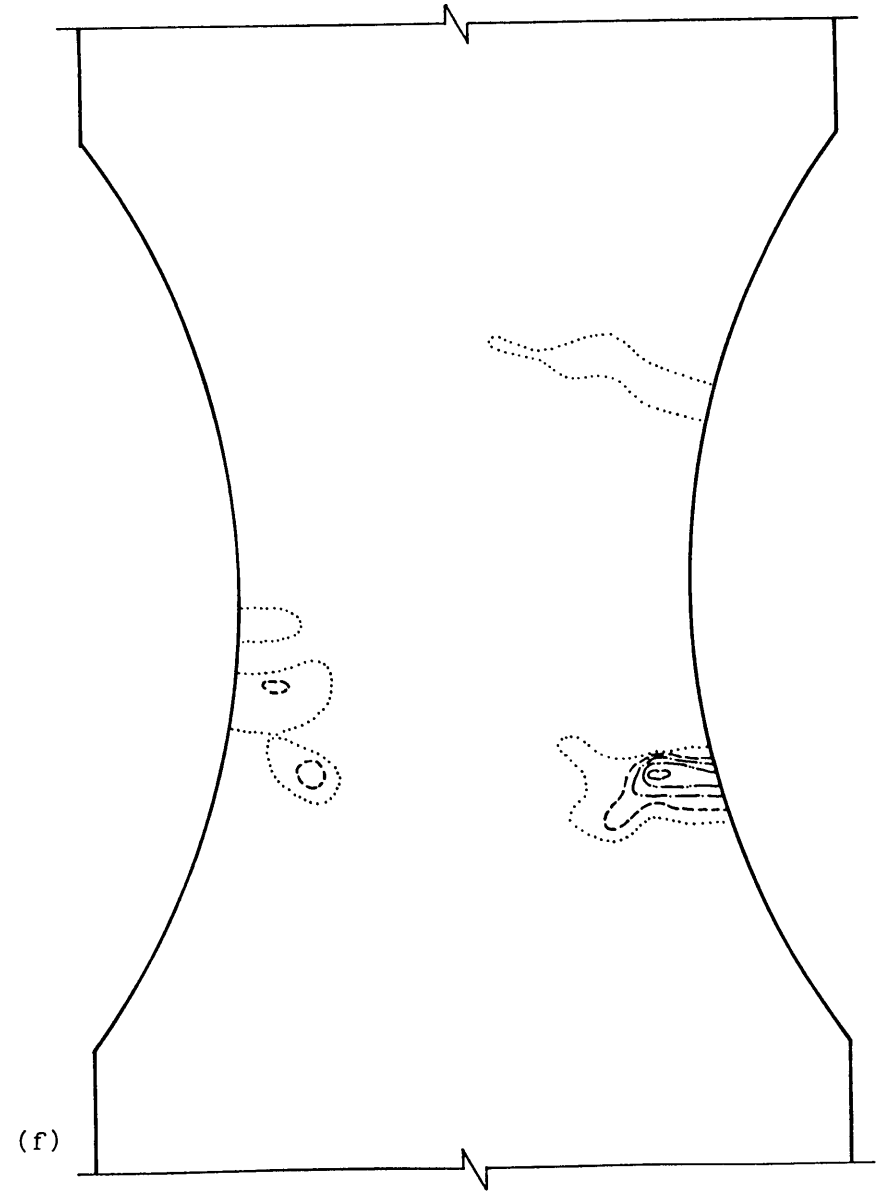

Fig. 8.9 Test I2, strain contour plots (cont)

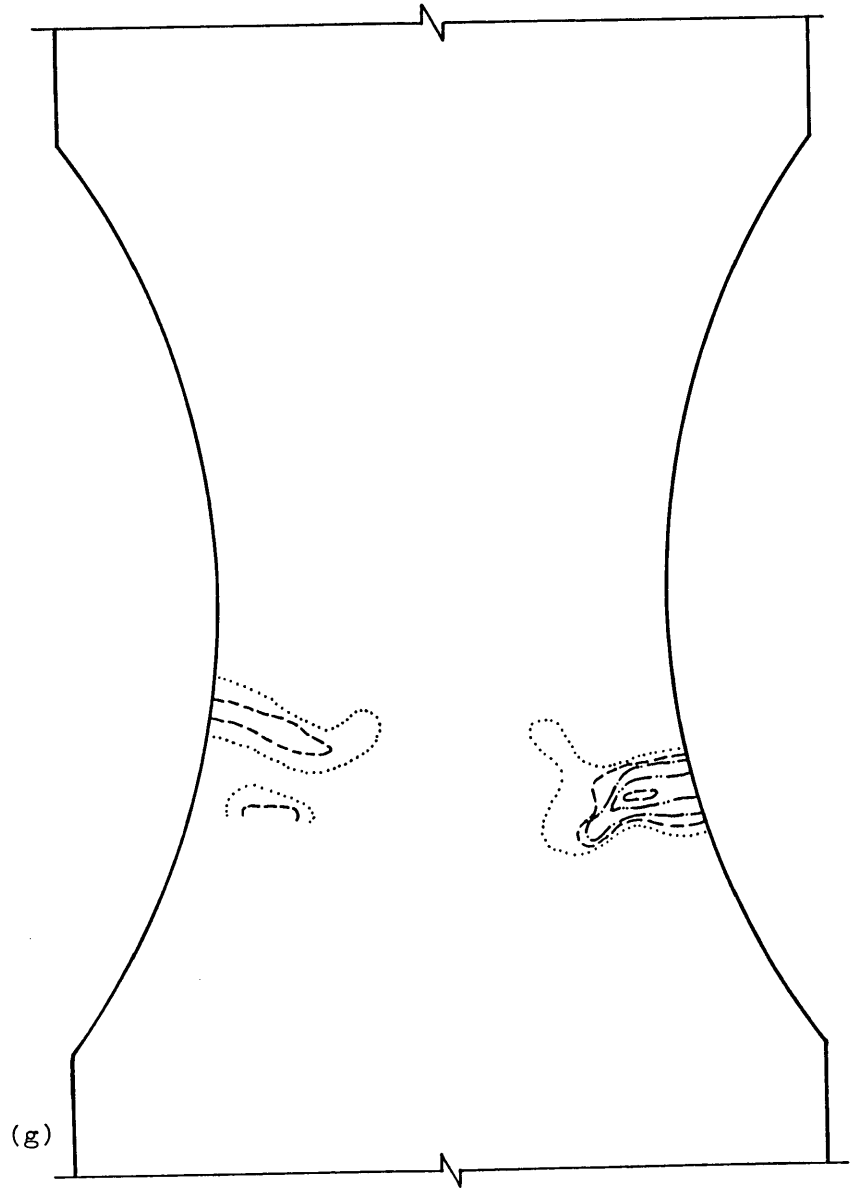

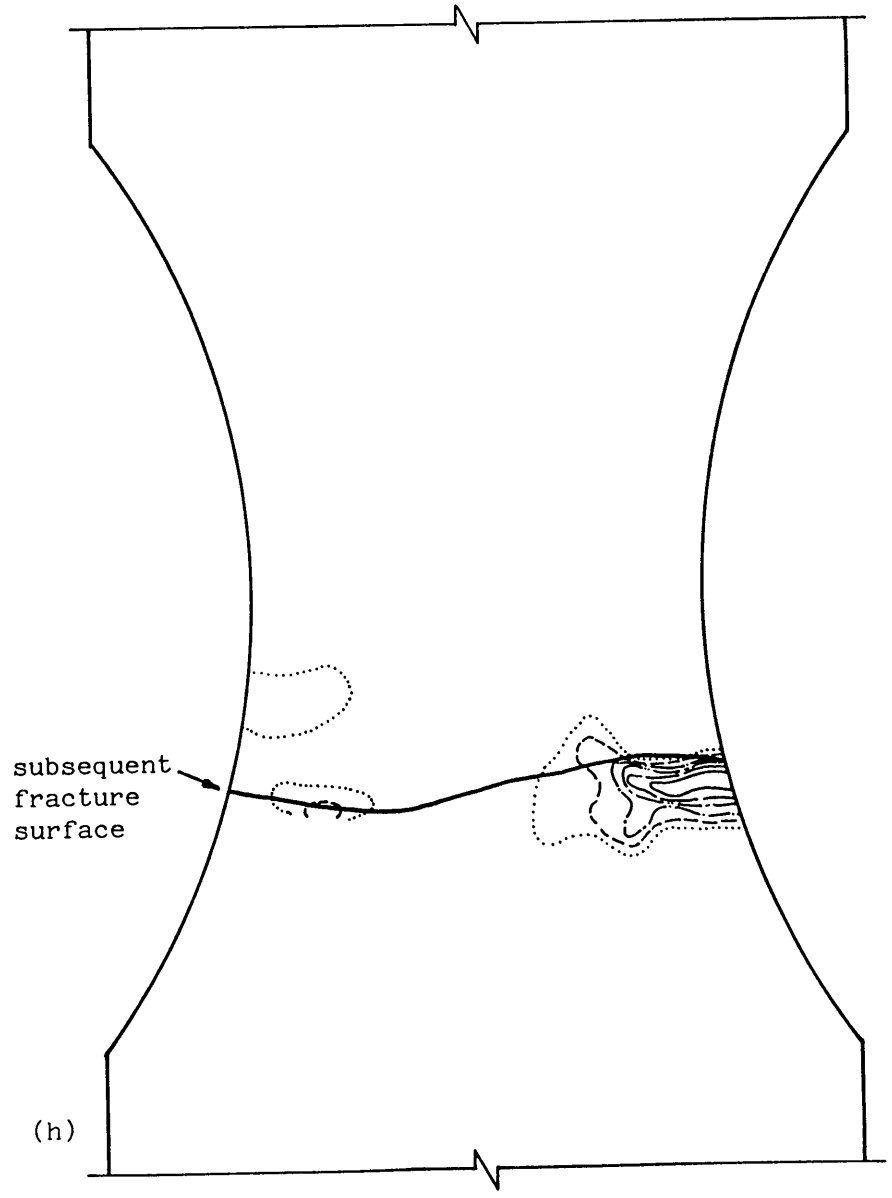

Fig. 8.9 Test I2, strain contour plots (cont)

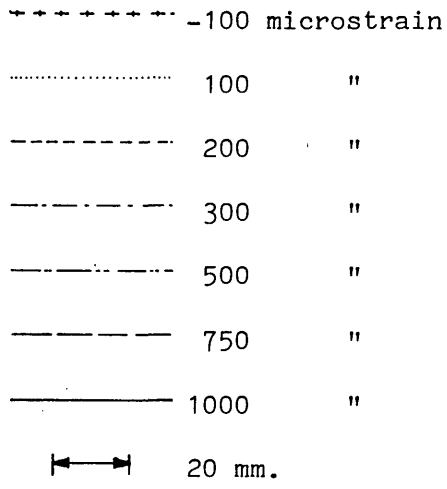

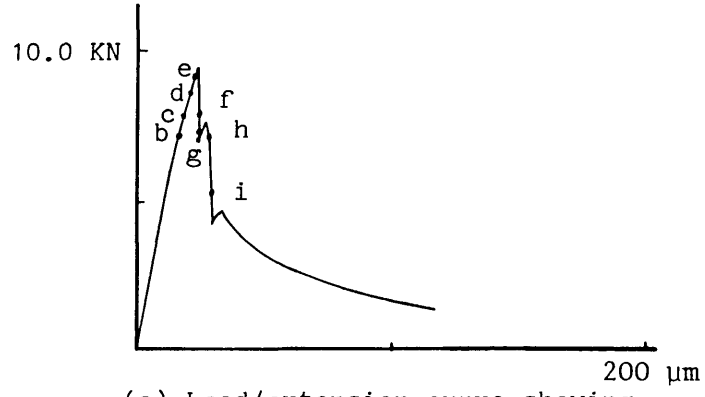

(a) Load/extension curve showing strain contour plot positions

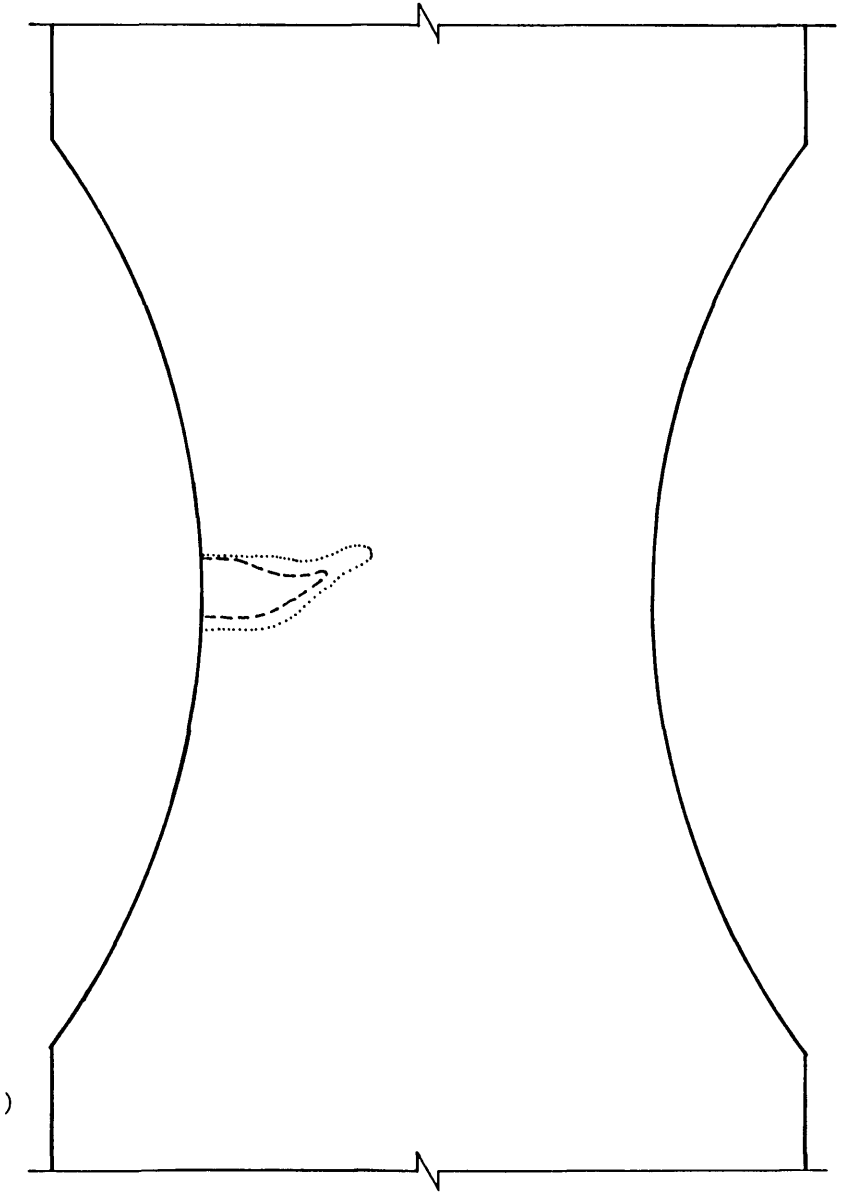

(b)

Fig. 8.10 Test J2, strain contour plots

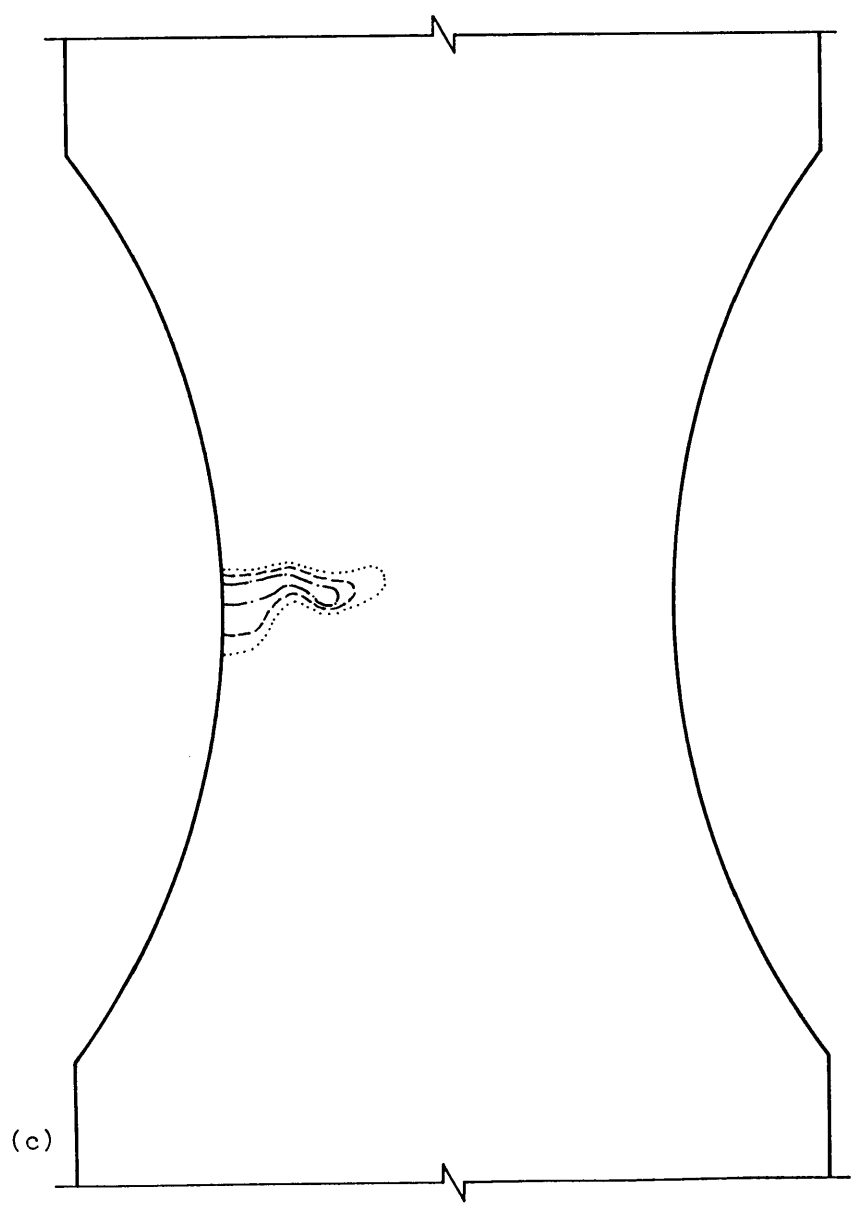

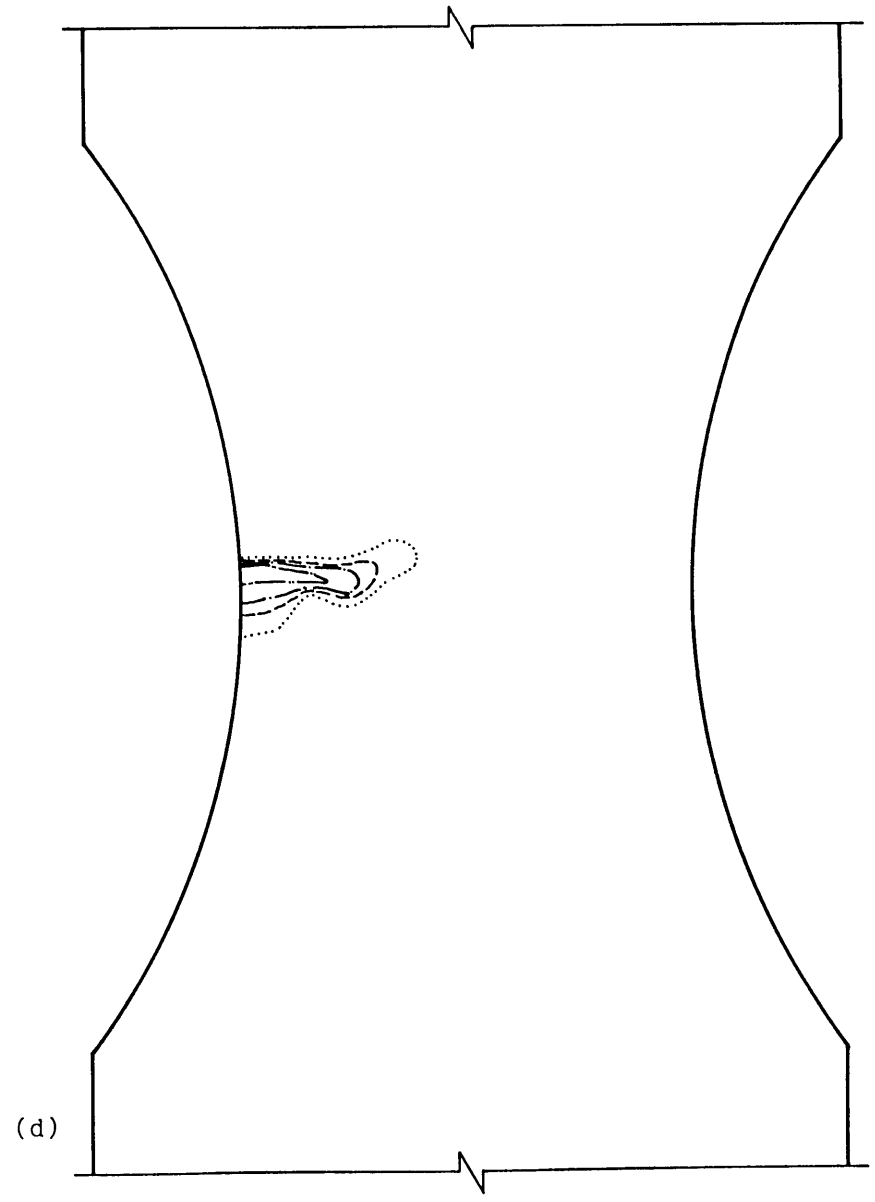

Fig. 8.10 Test J2, strain contour plots (cont)

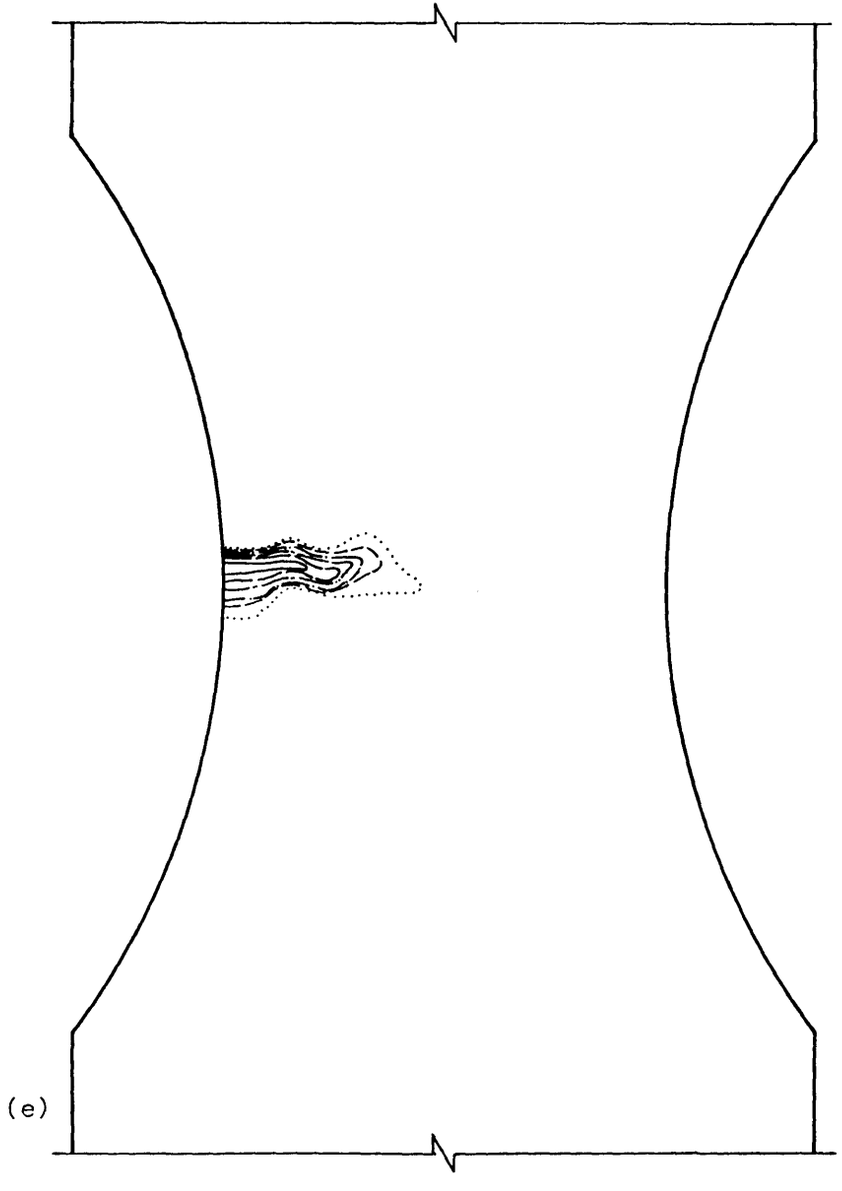

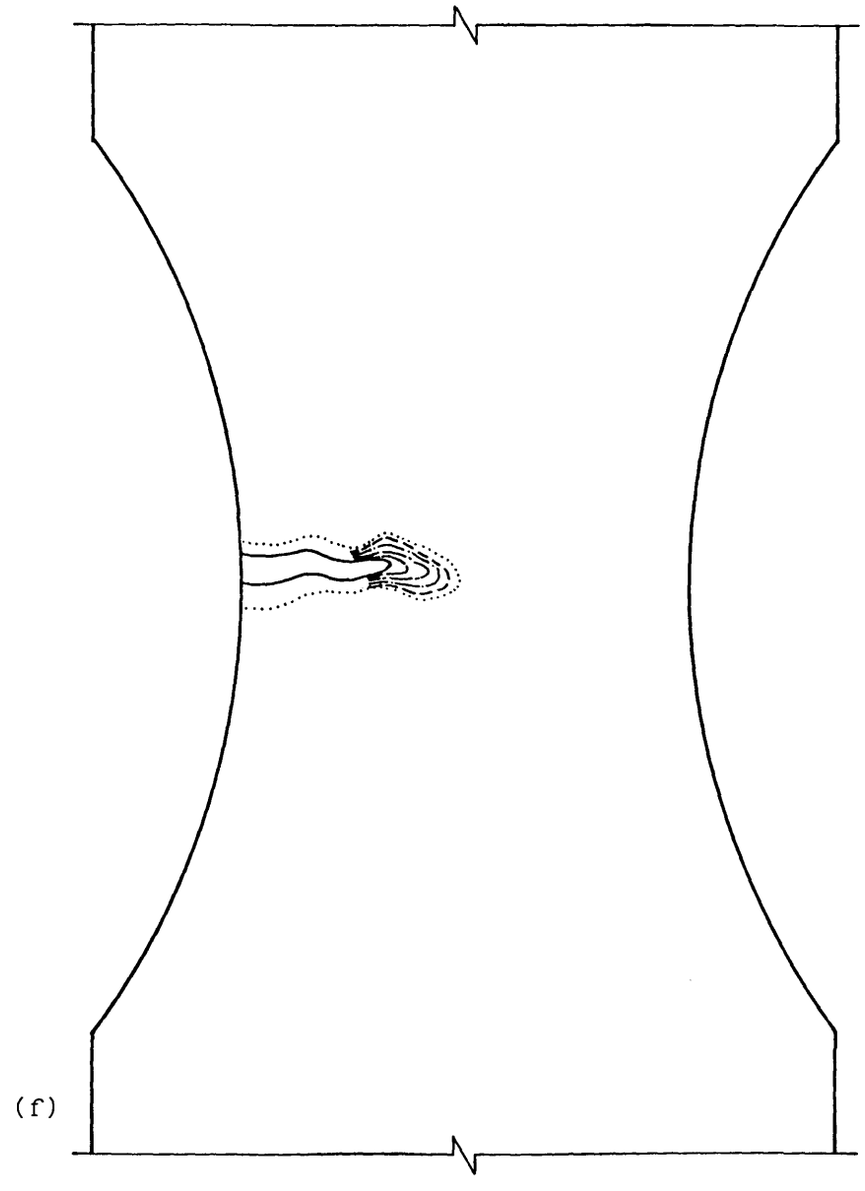

Fig. 8.10 Test J2, strain contour plots (cont)

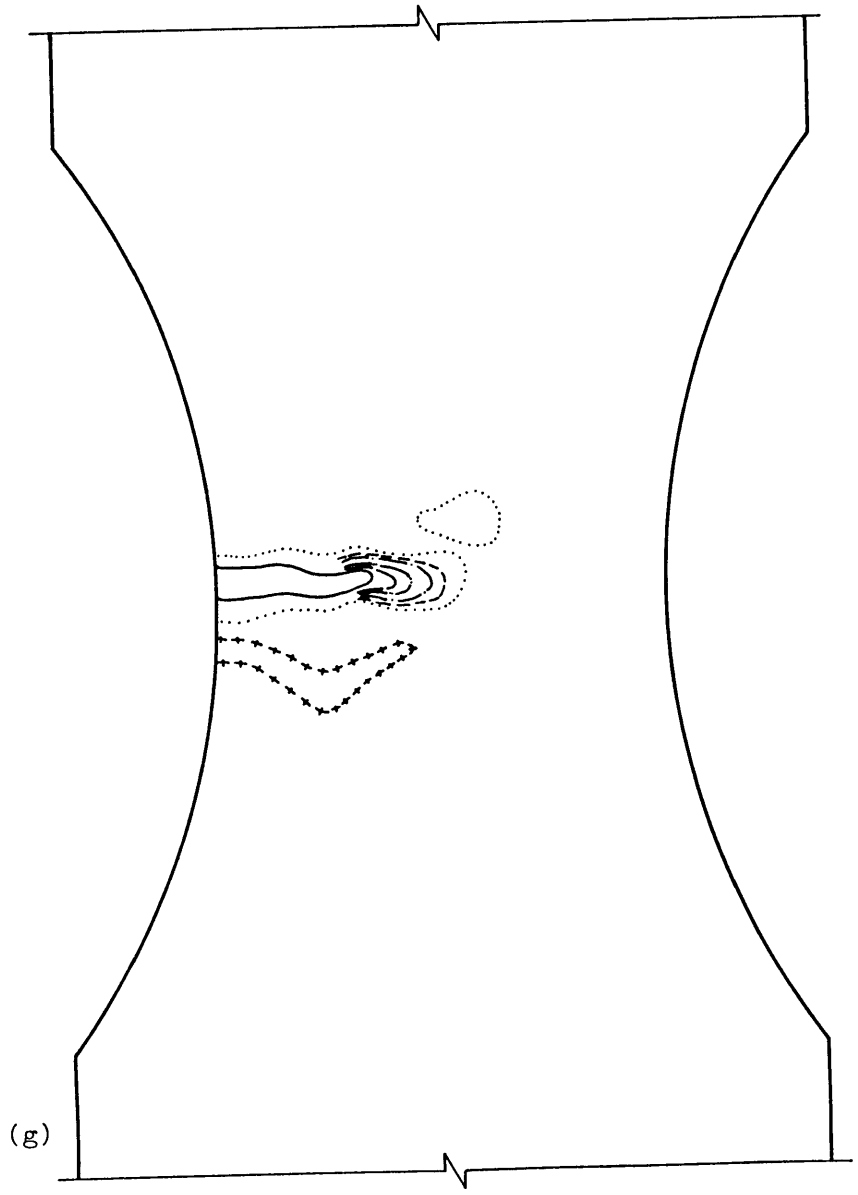

(g)

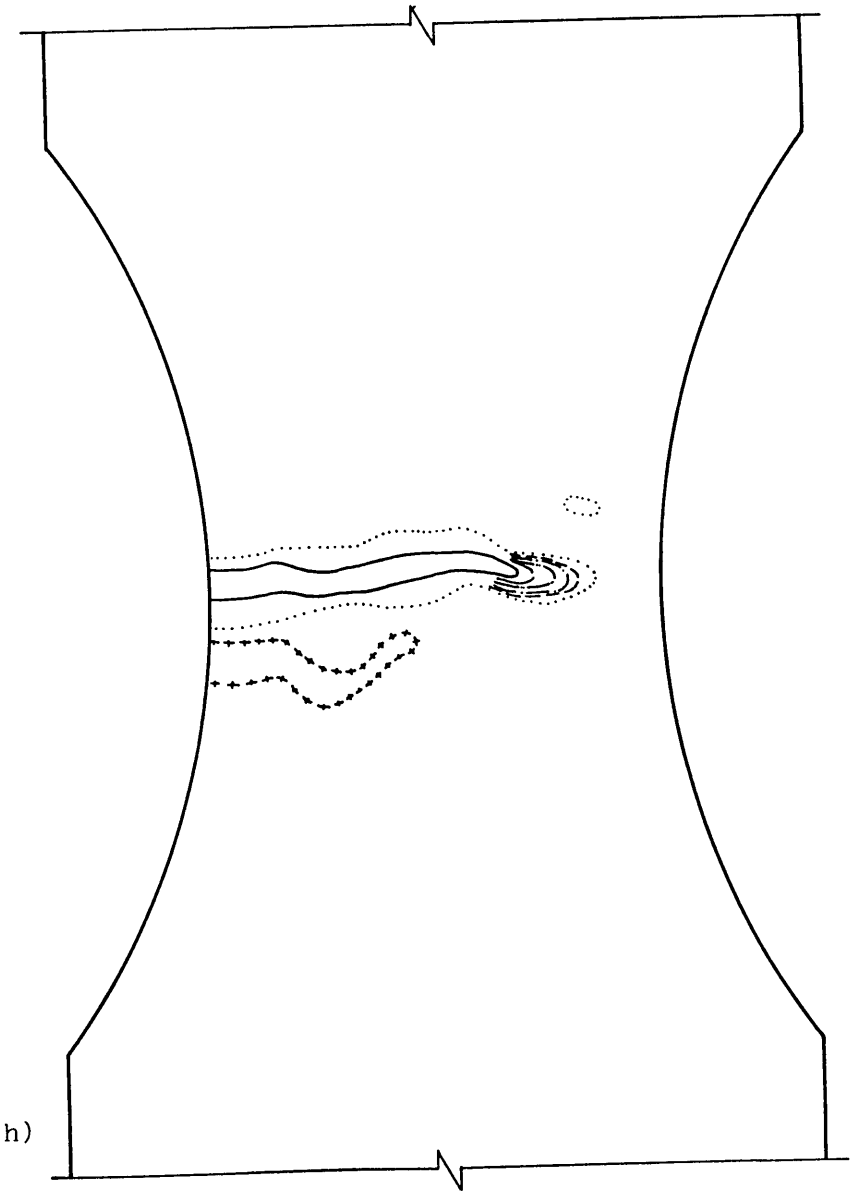

(h)

Fig. 8.10 Test J2, strain contour plots (cont)

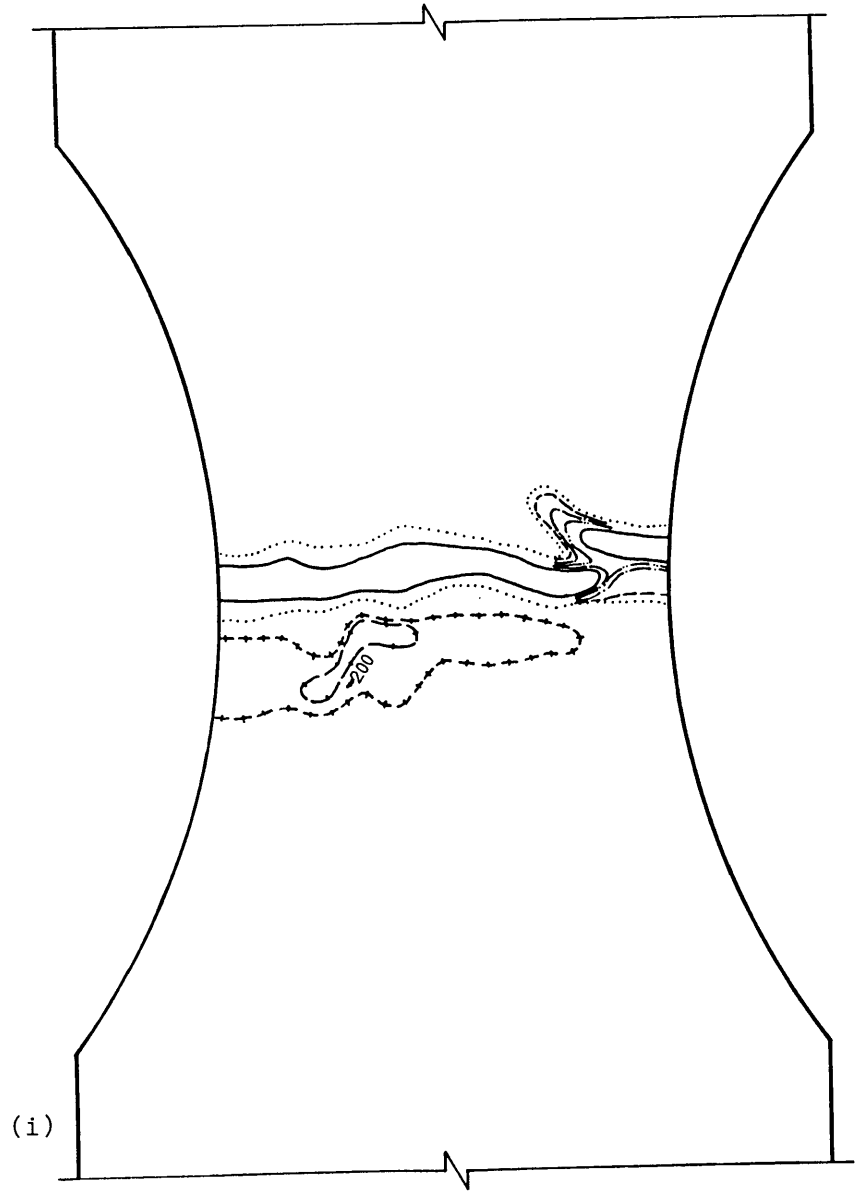

Fig. 8.10 Test J2, strain contour plots (cont)

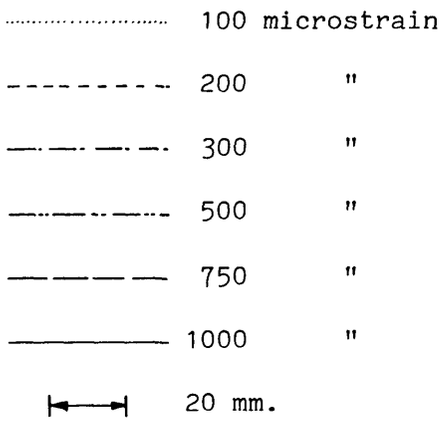

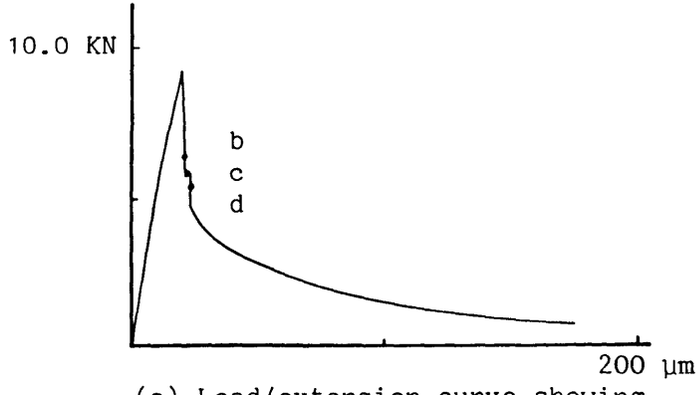

(a) Load/extension curve showing strain contour plot positions

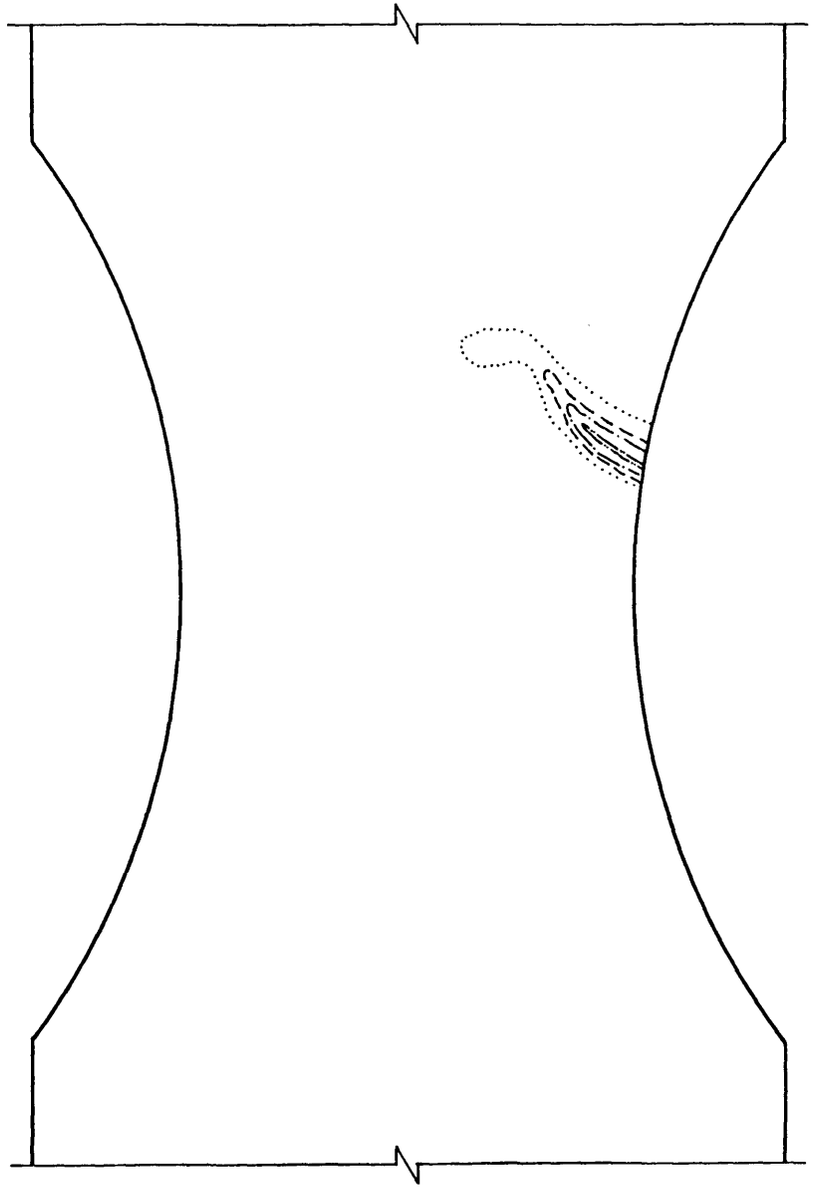

(b)

Fig. 8.11 Test K1, strain contour plots

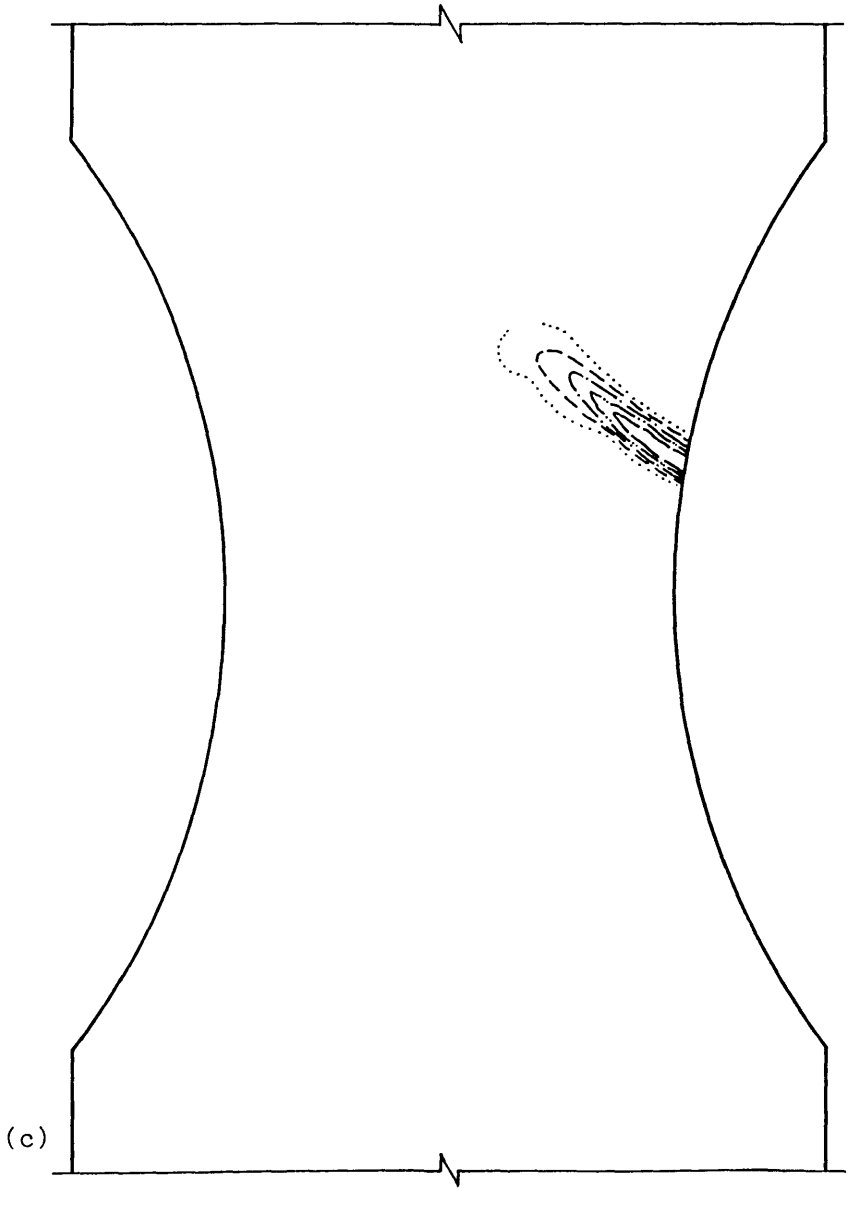

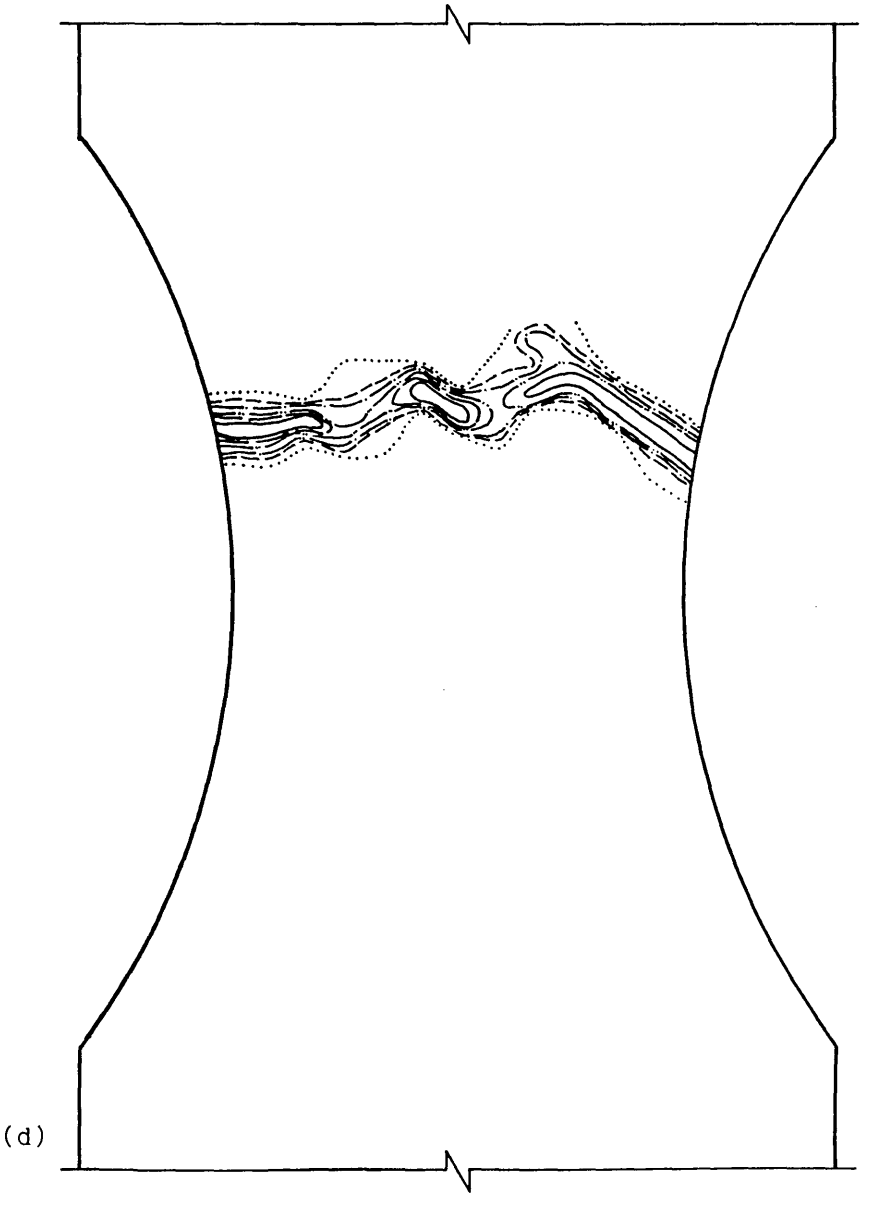

Fig. 8.11 Test K1, strain contour plots (cont)

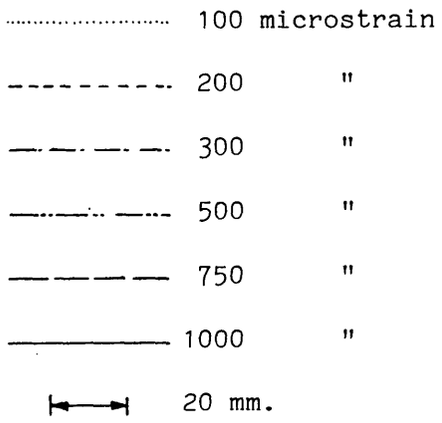

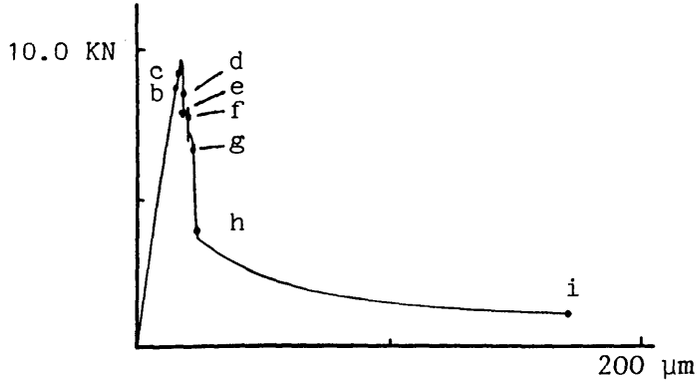

(a) Load/extension curve showing strain contour plot positions

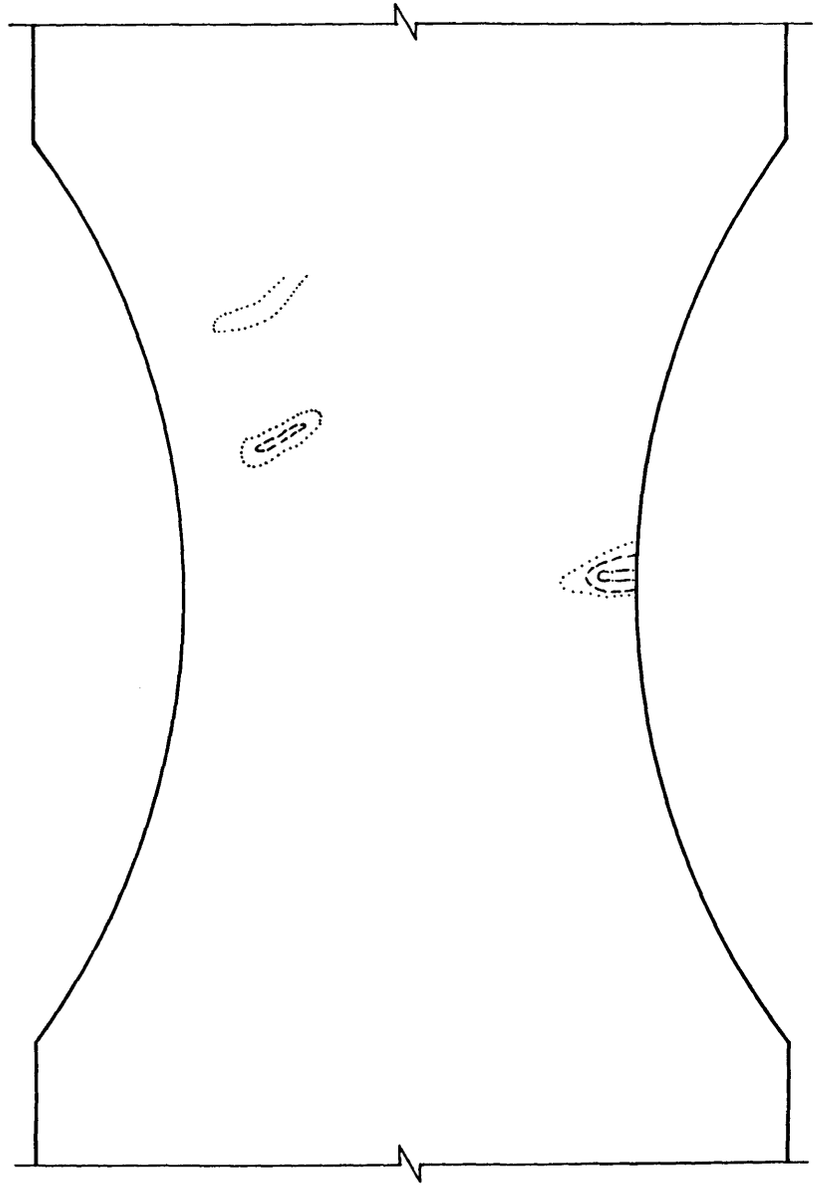

(b)

Fig. 8.12 Test K2, strain contour plots

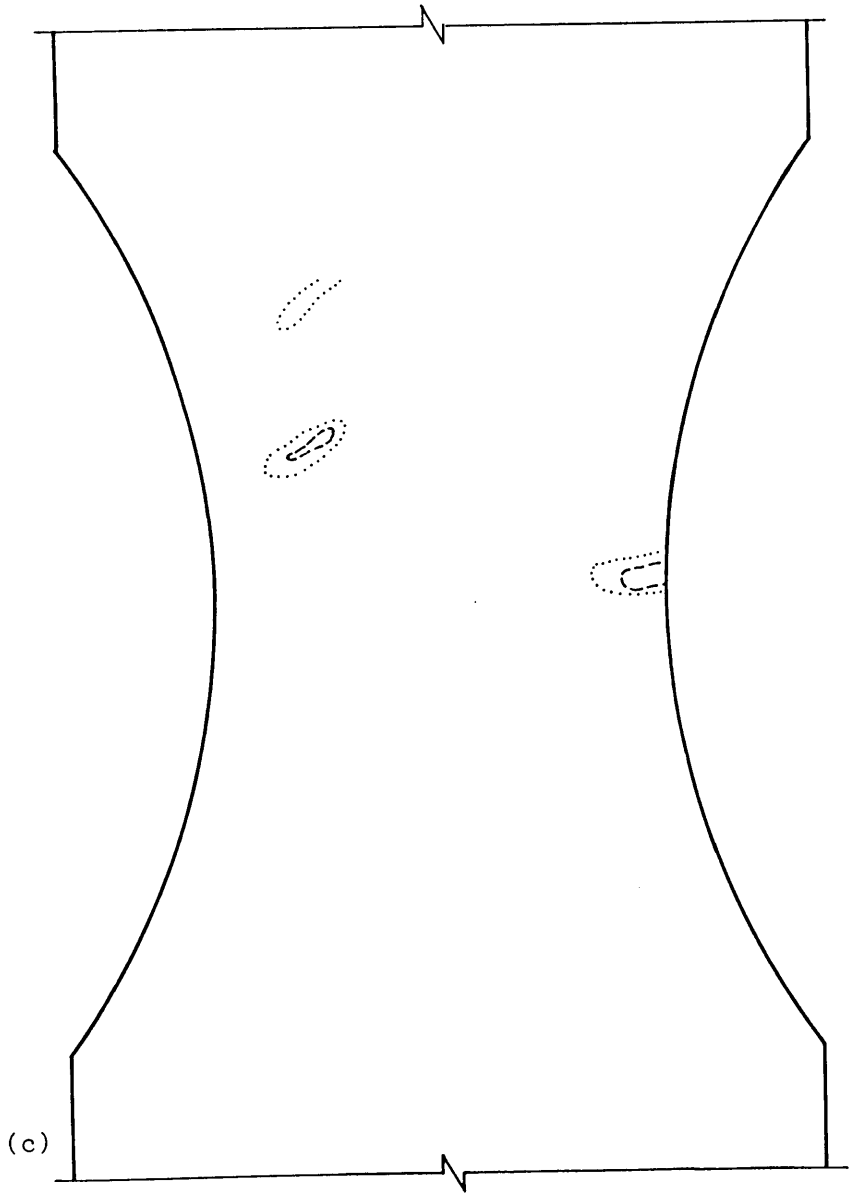

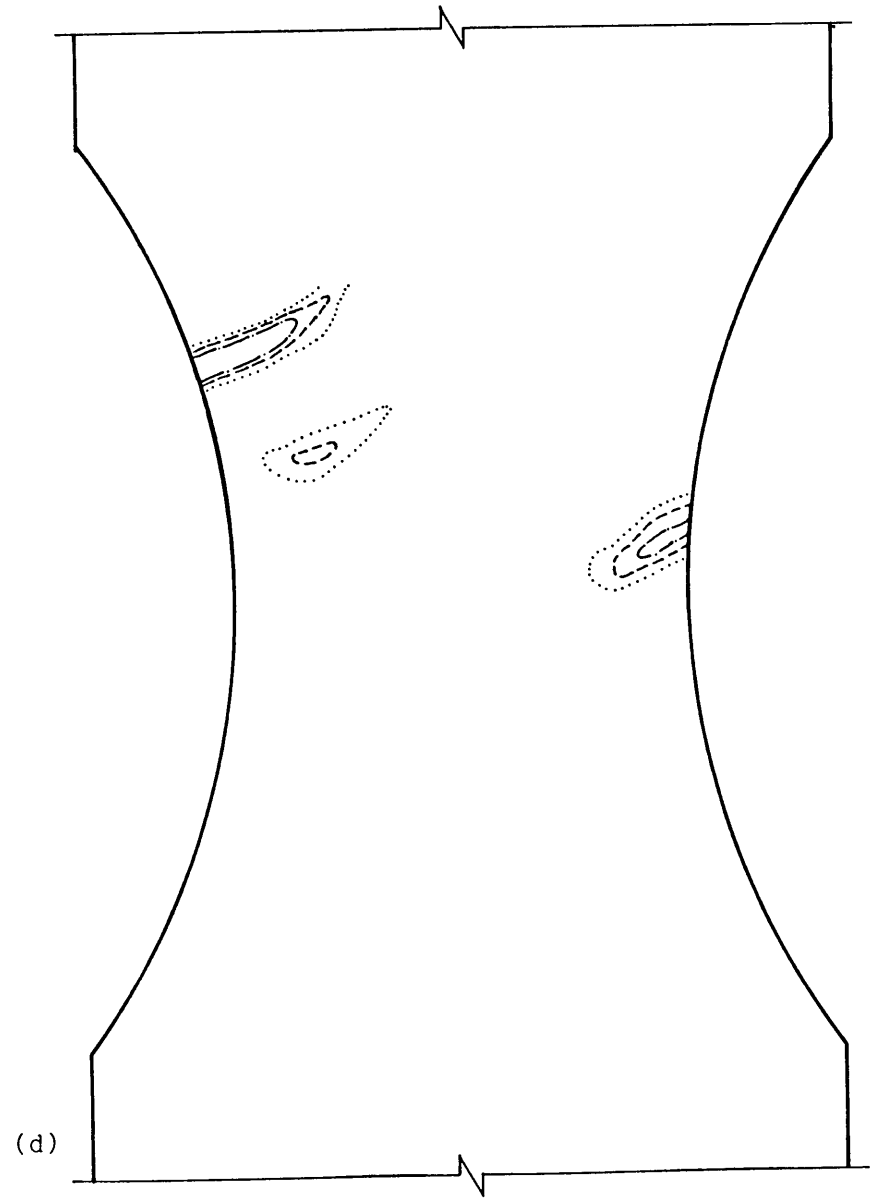

Fig. 8.12 Test K2, strain contour plots (cont)

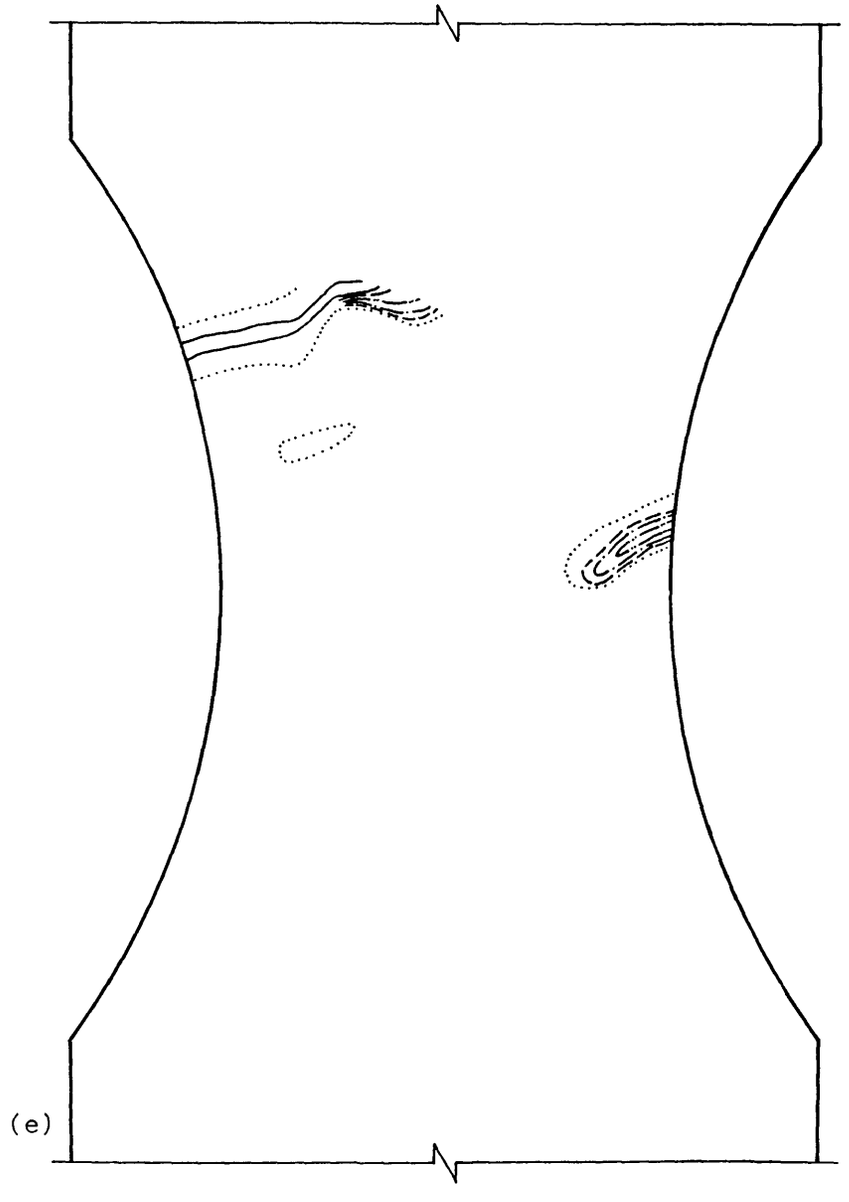

(e)

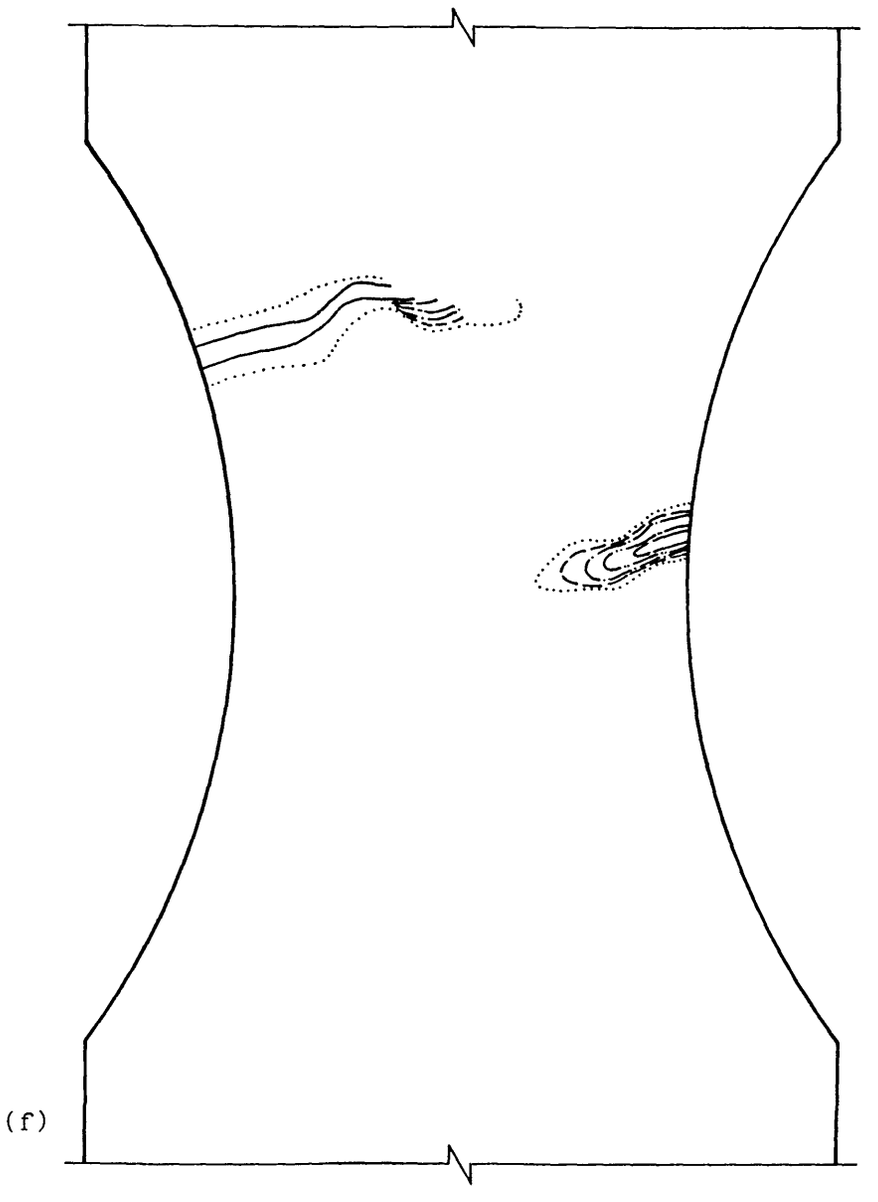

(f)

Fig. 8.12 Test K2, strain contour plots (cont)

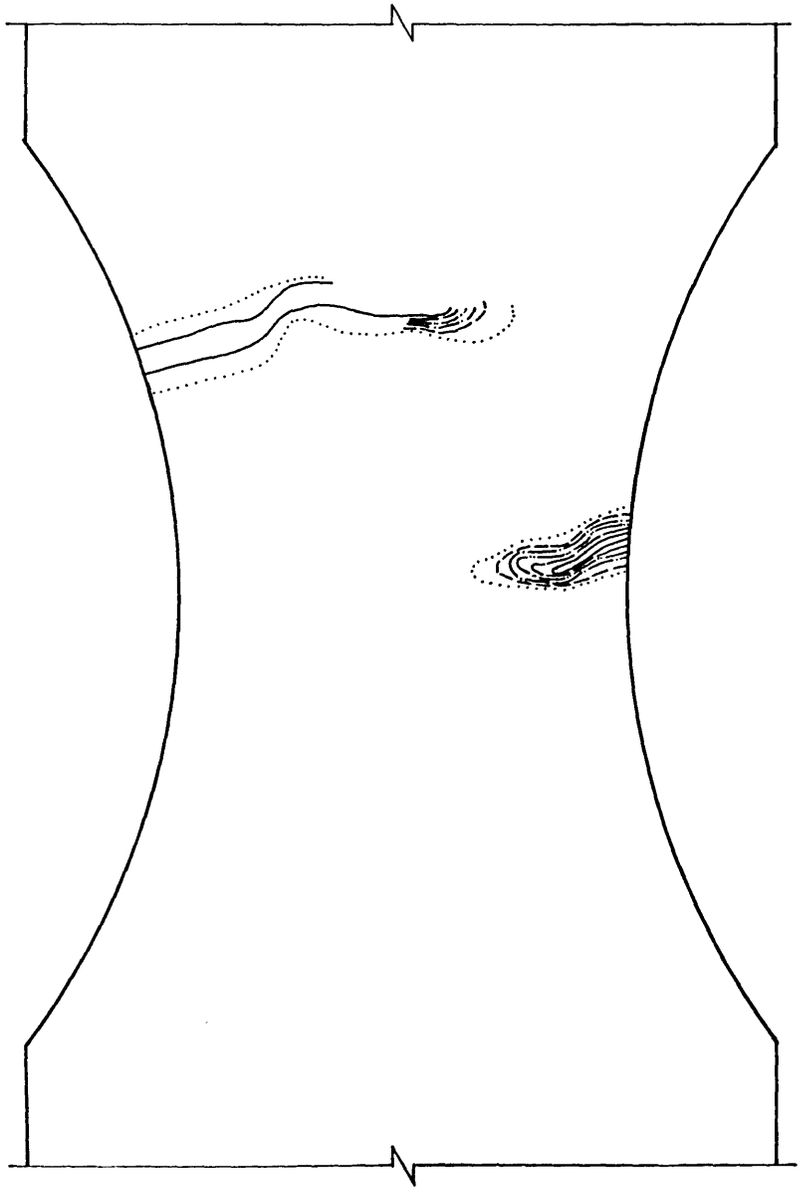

(g)

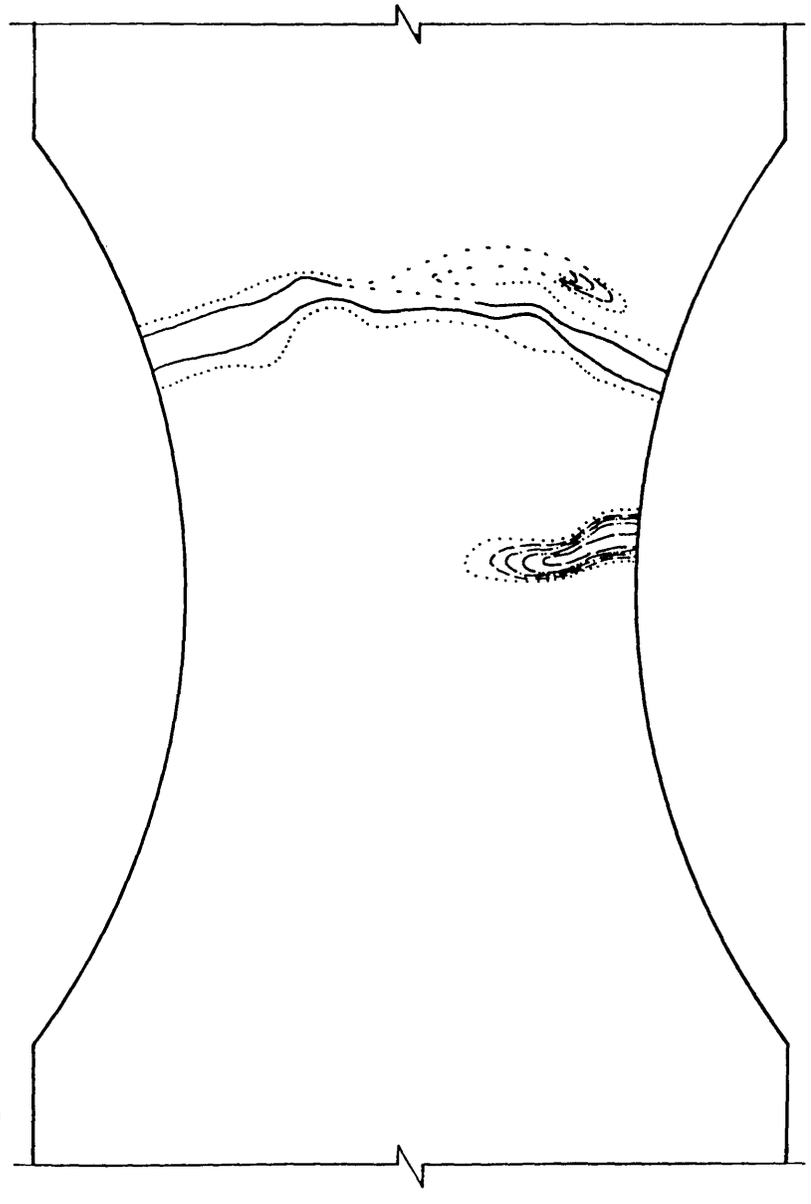

(h)

Fig. 8.12 Test K2, strain contour plots (cont)

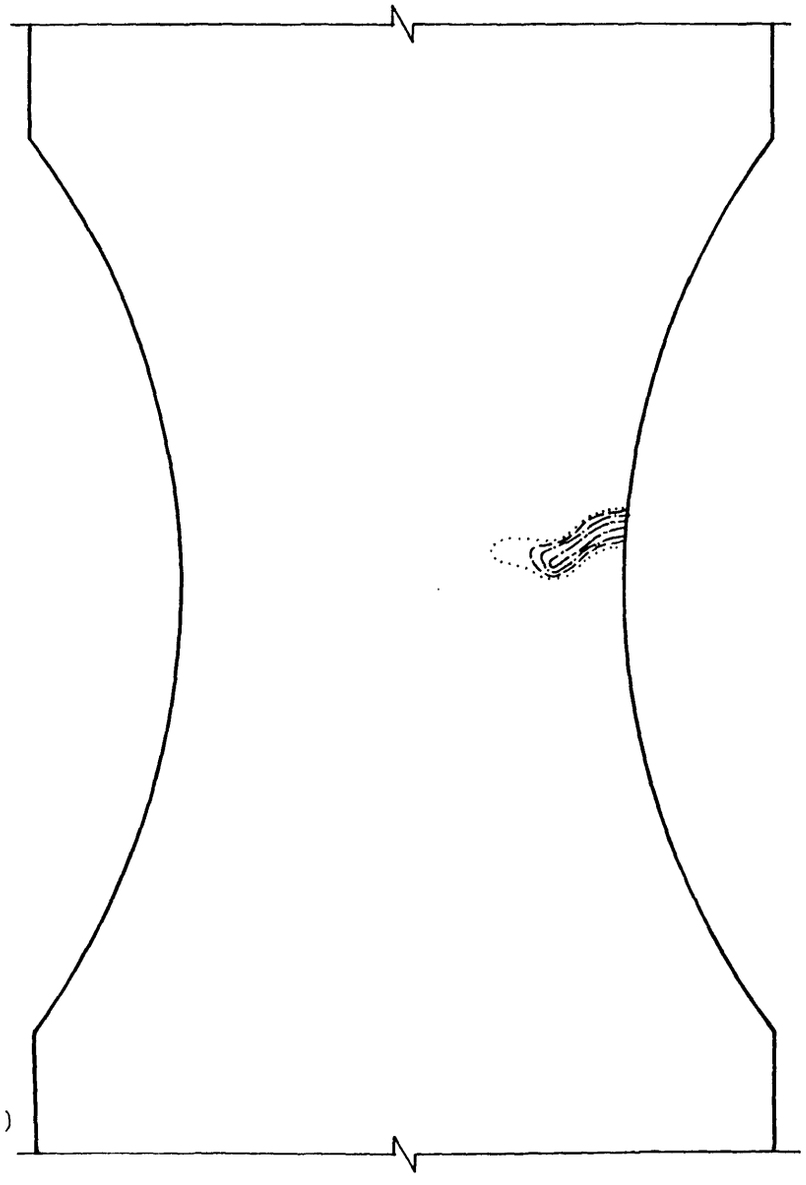

(i)

Note: primary fracture zone not shown

Fig. 8.12 Test K2, strain contour plots (cont)

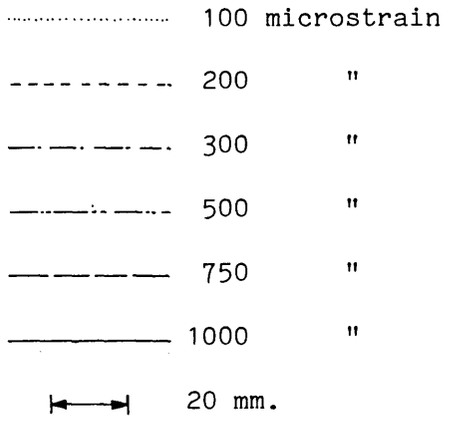

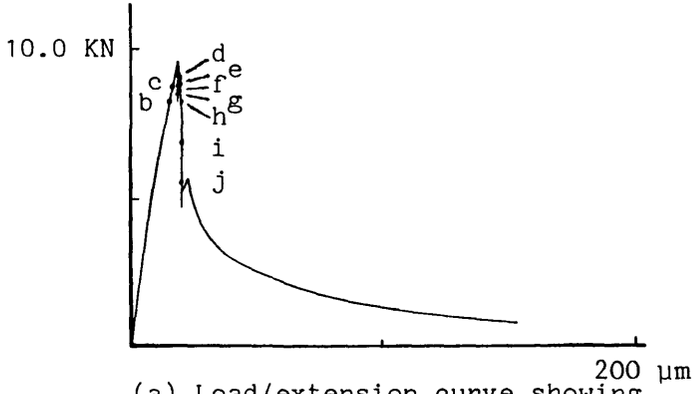

(a) Load/extension curve showing strain contour plot positions

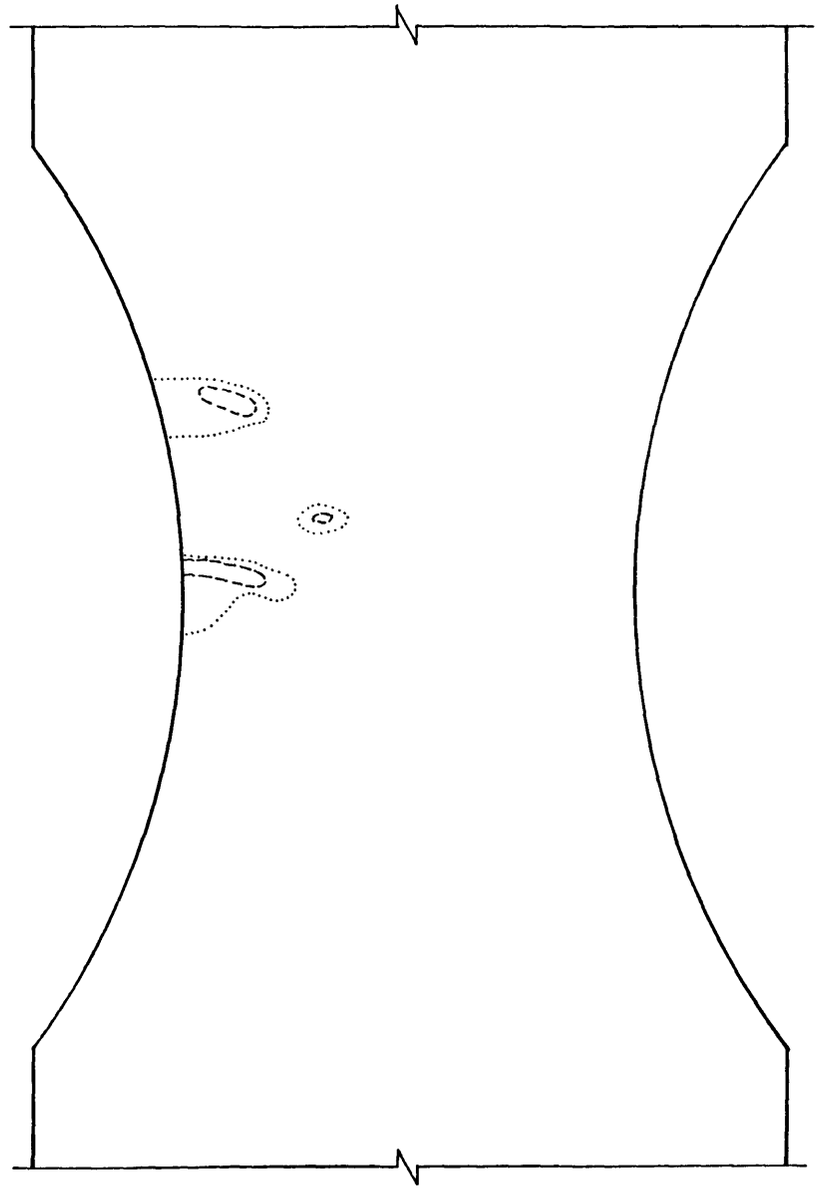

(b)

Fig. 8.13 Test L1, strain contour plots

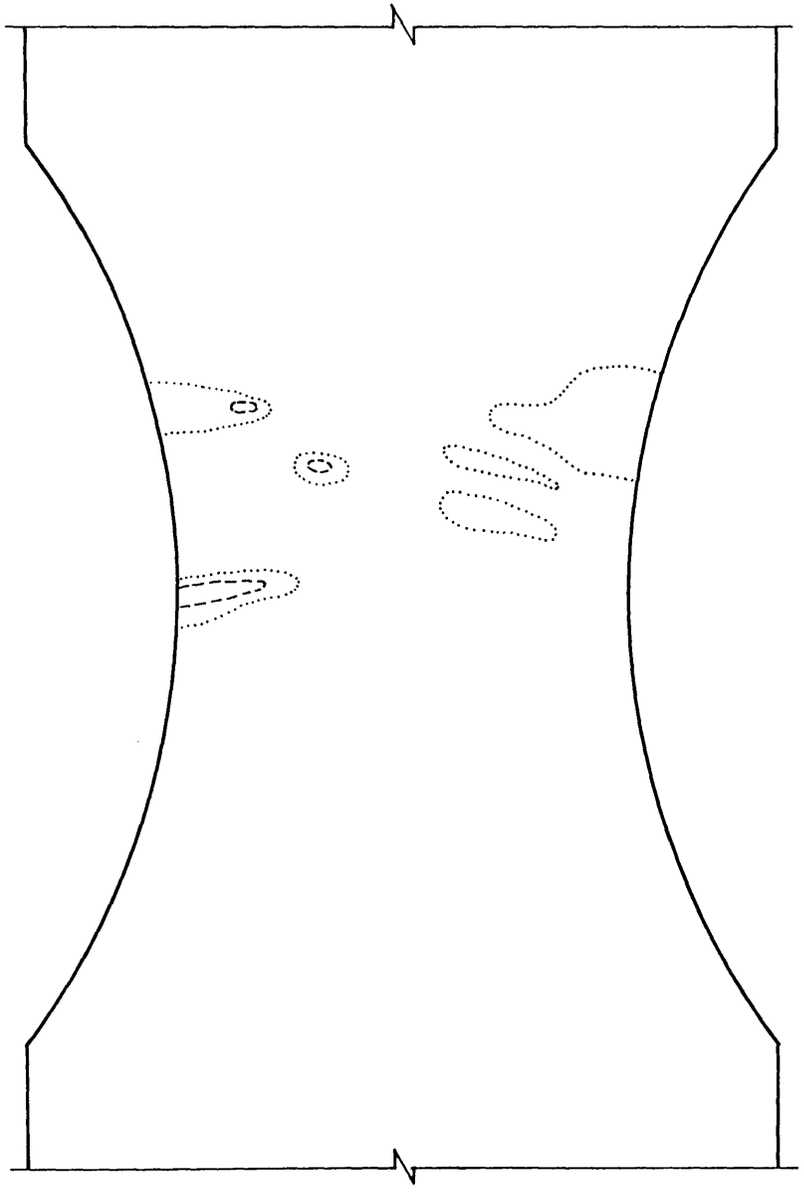

(c)

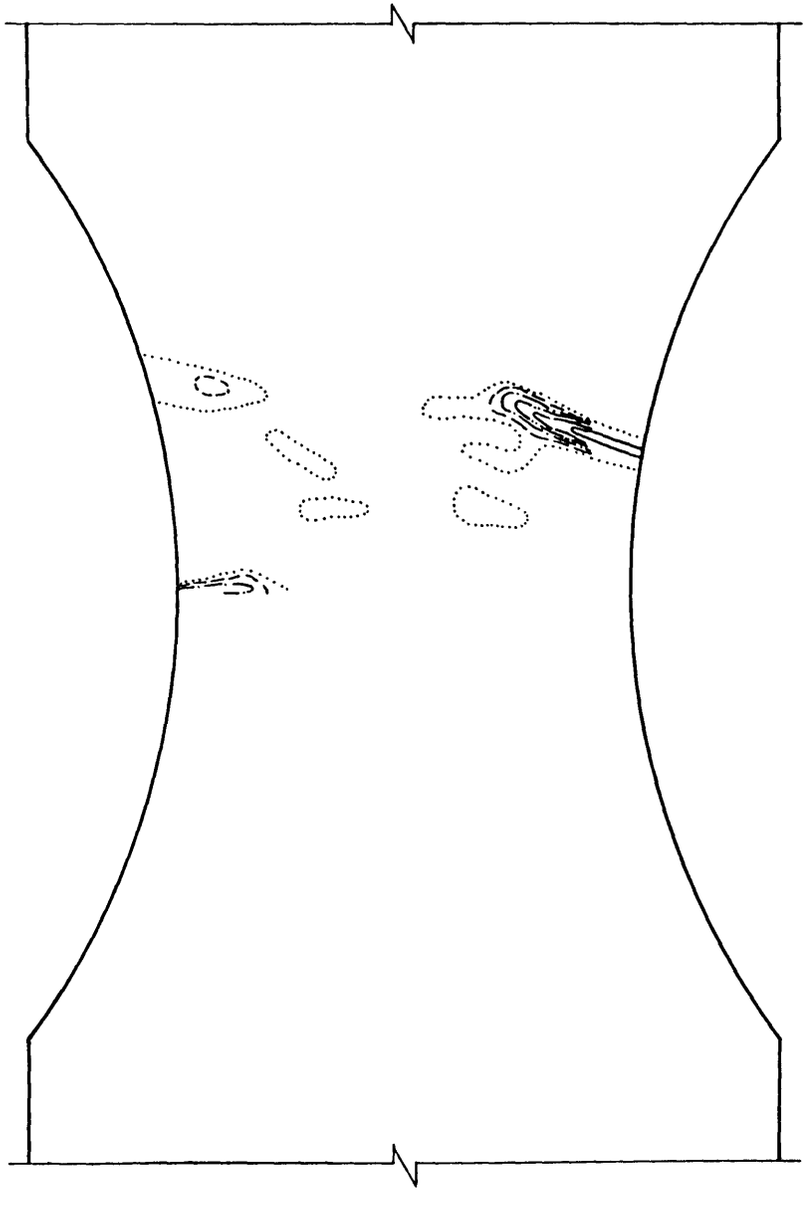

(d)

Fig. 8.13 Test L1, strain contour plots (cont)

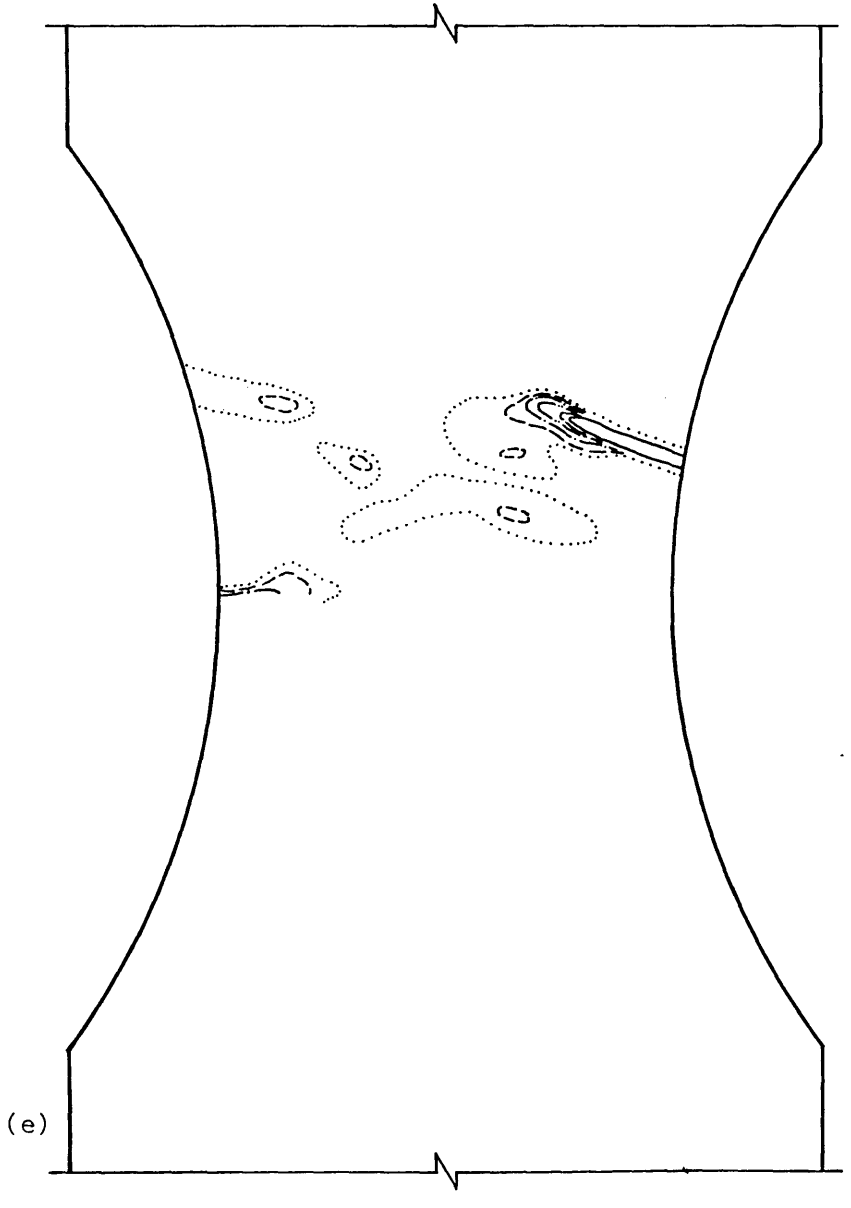

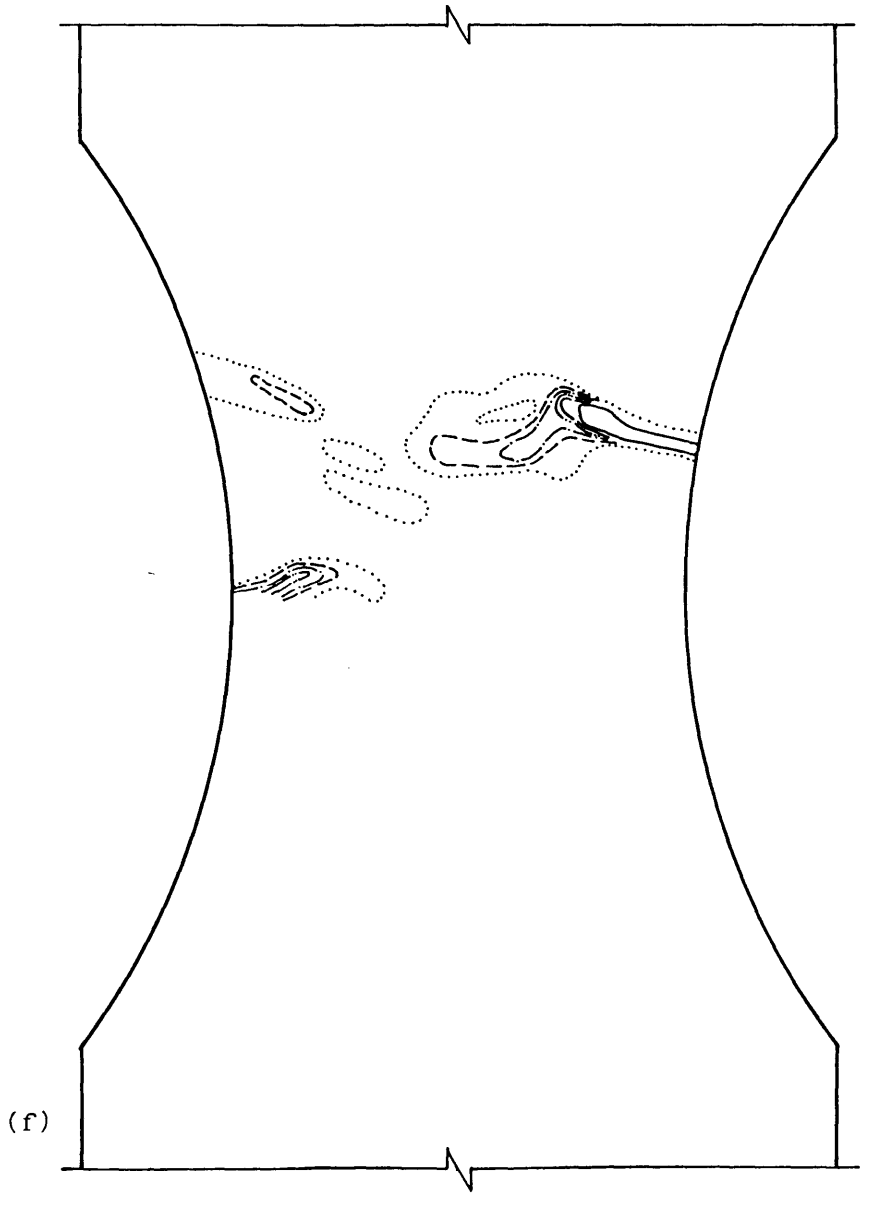

Fig. 8.13 Test L1, strain contour plots (cont)

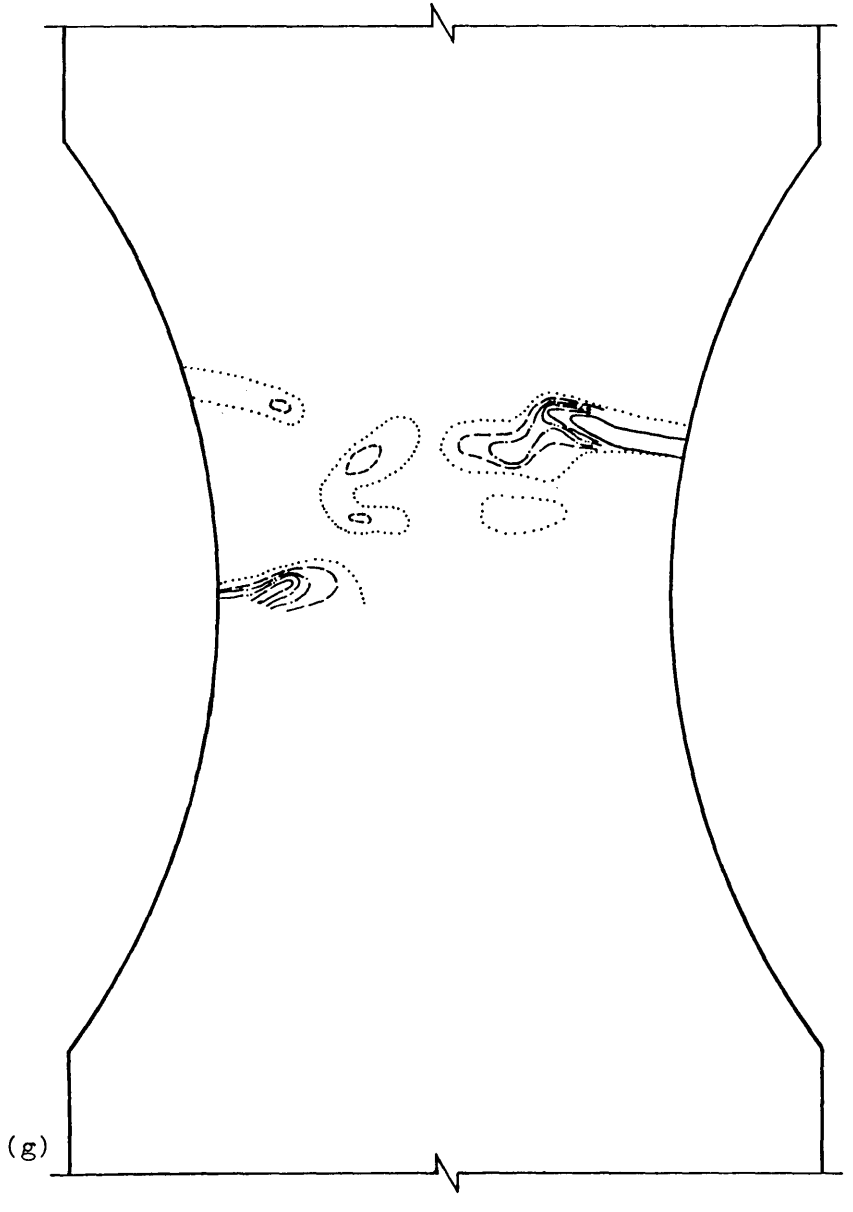

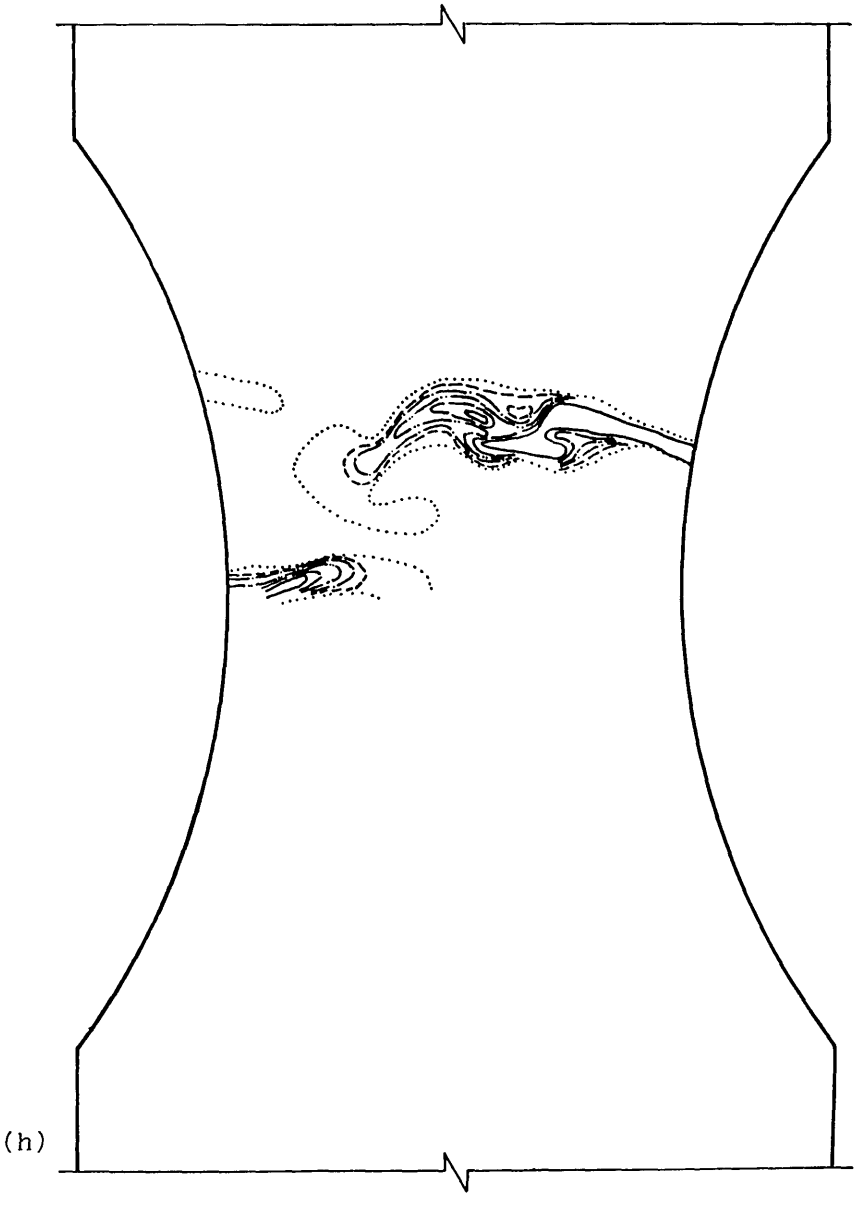

Fig. 8.13 Test L1, strain contour plots (cont)

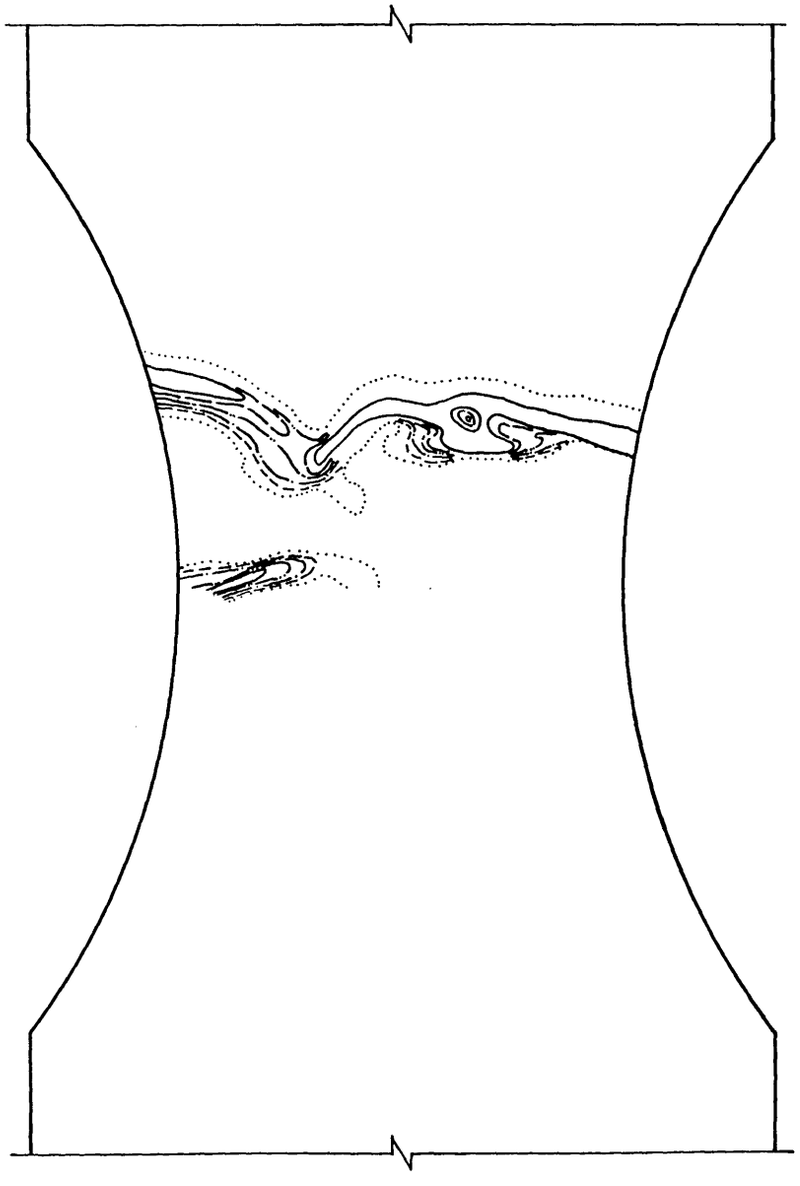

(i)

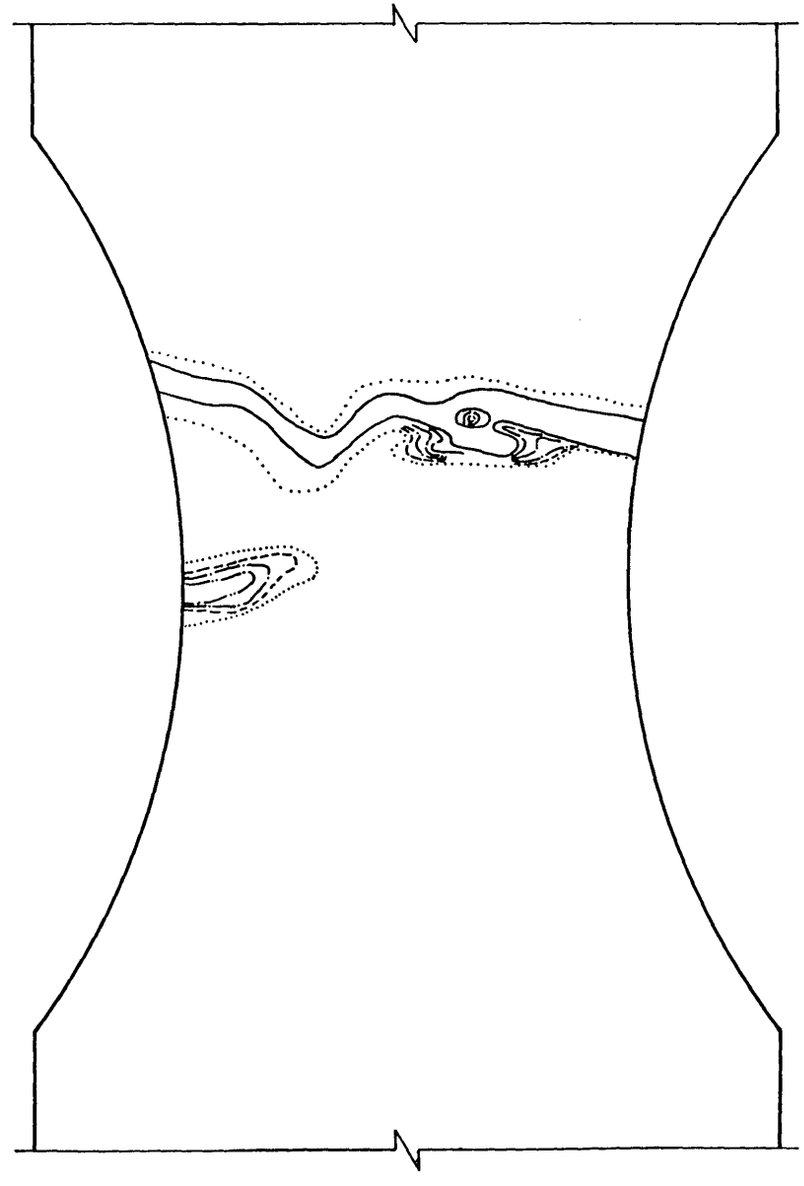

(j)

Fig. 8.13 Test L1, strain contour plots (cont)

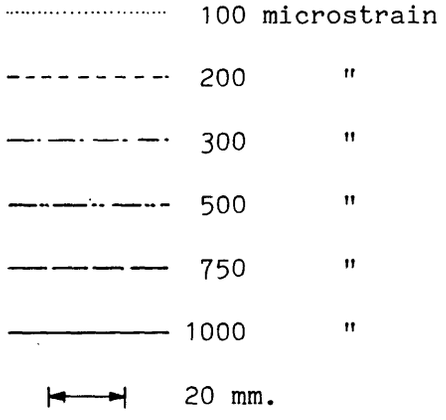

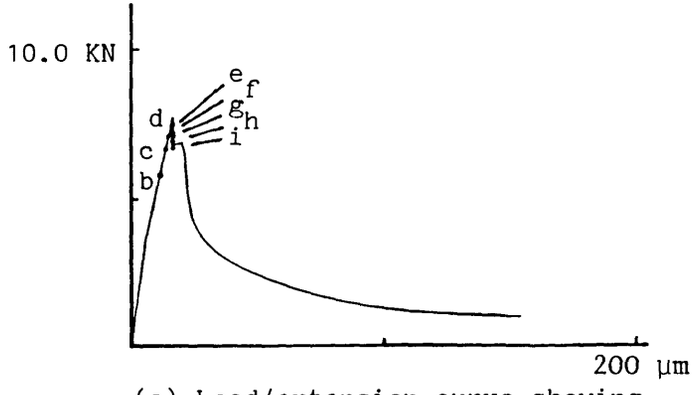

(a) Load/extension curve showing strain contour plot positions

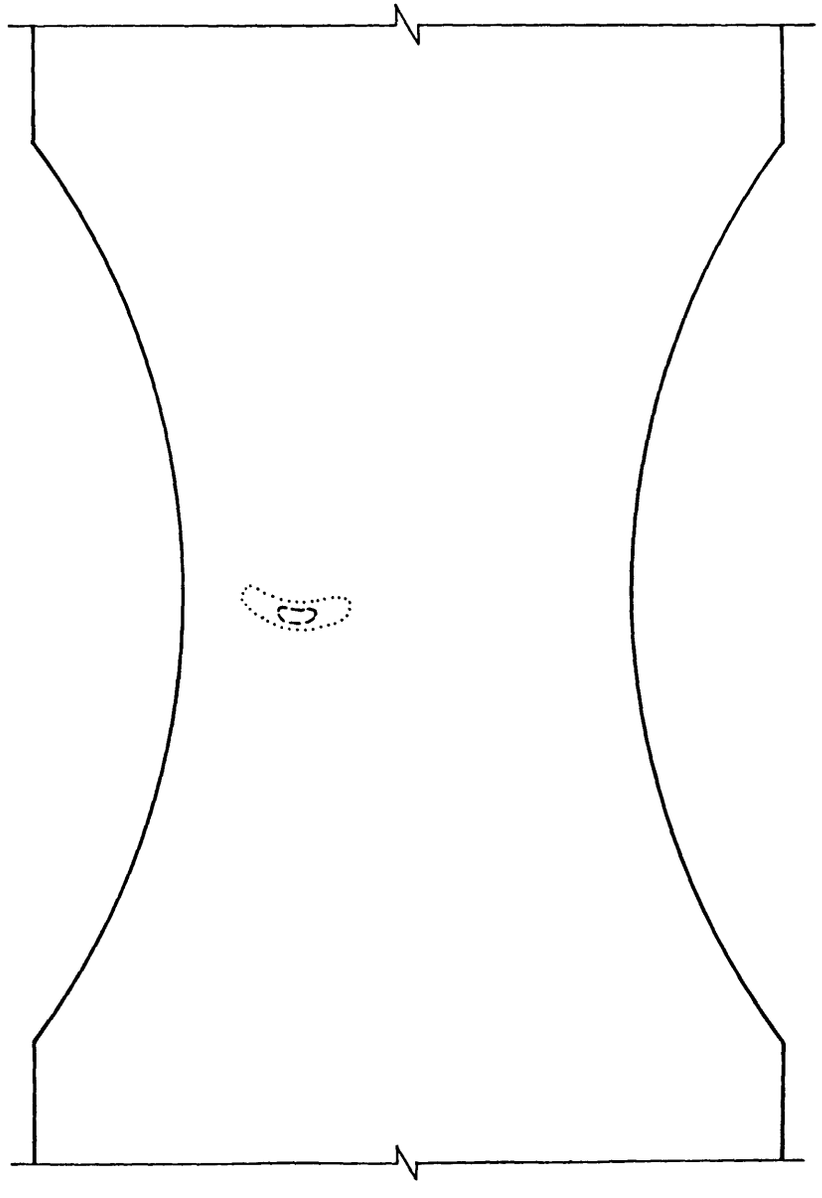

(b)

Fig. 8.14 Test L2, strain contour plots

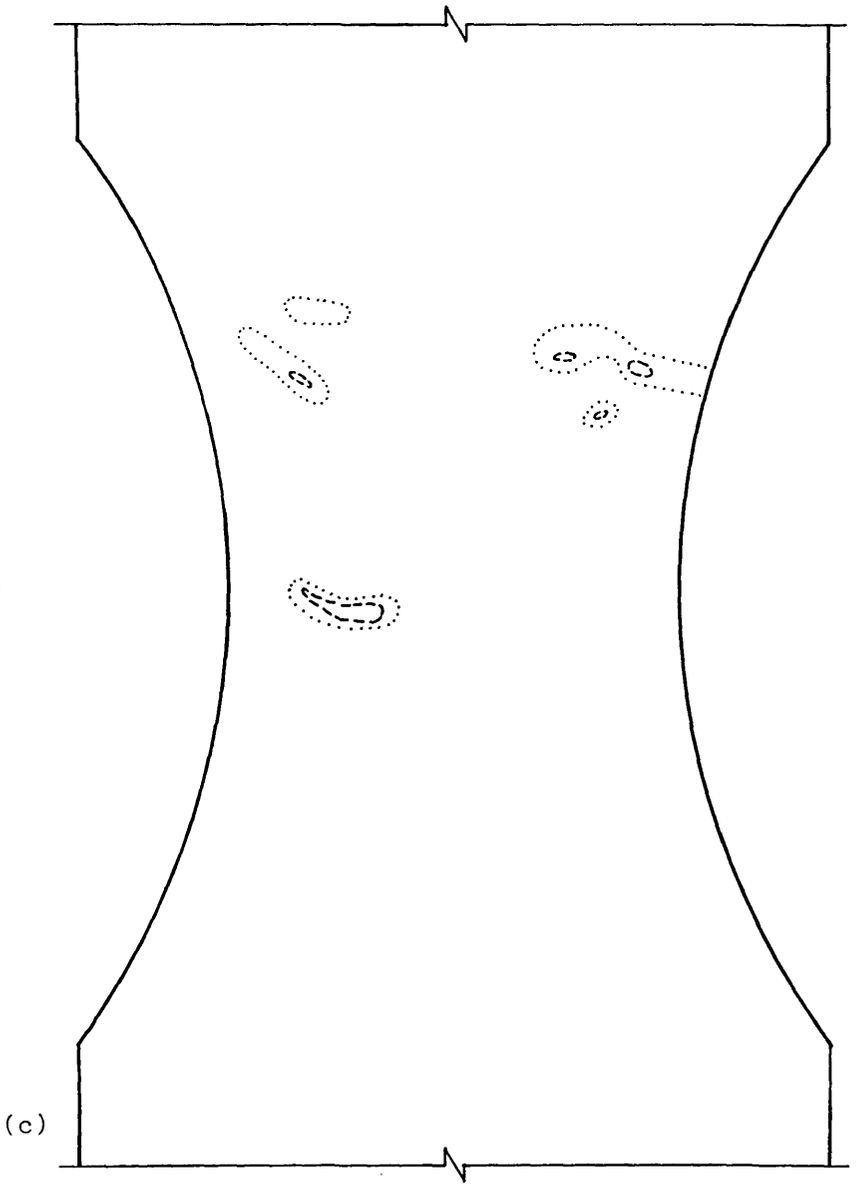

(c)

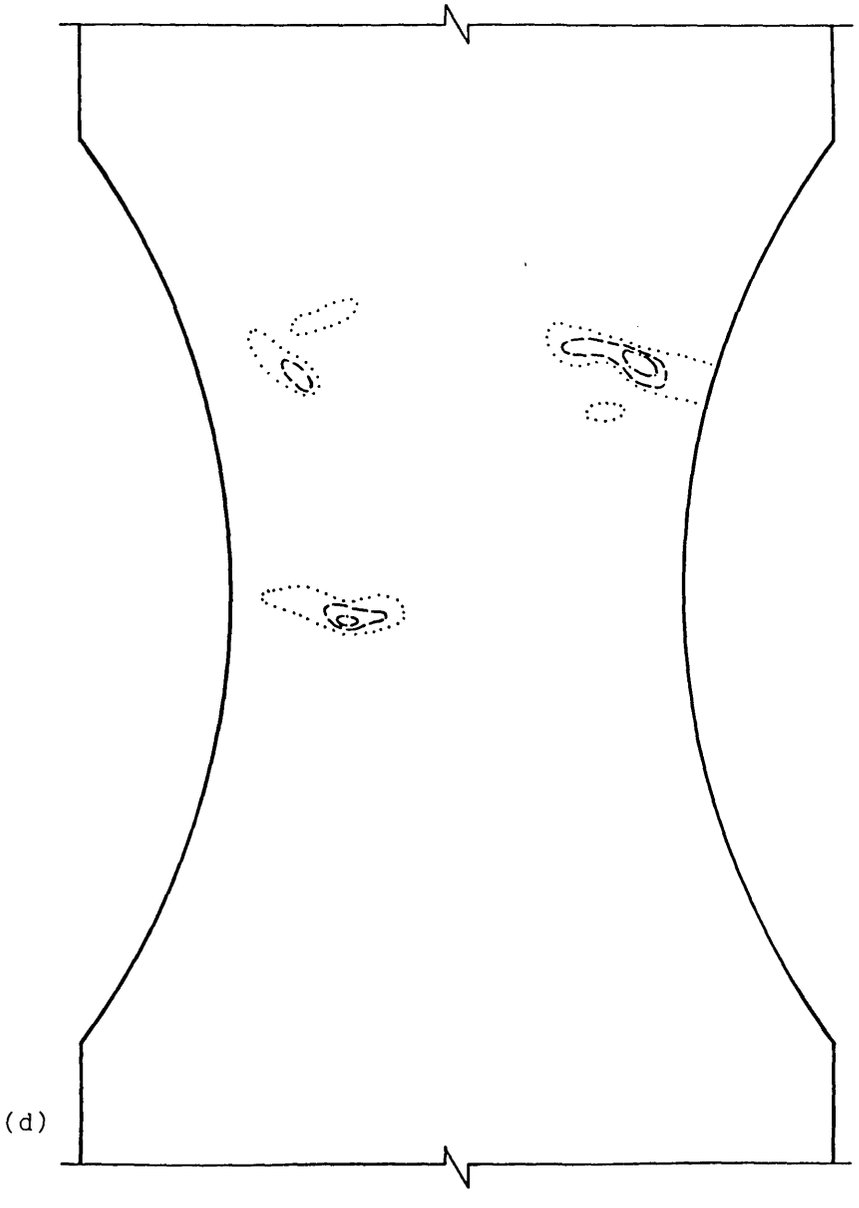

(d)

Fig. 8.14 Test L2, strain contour plots (cont)

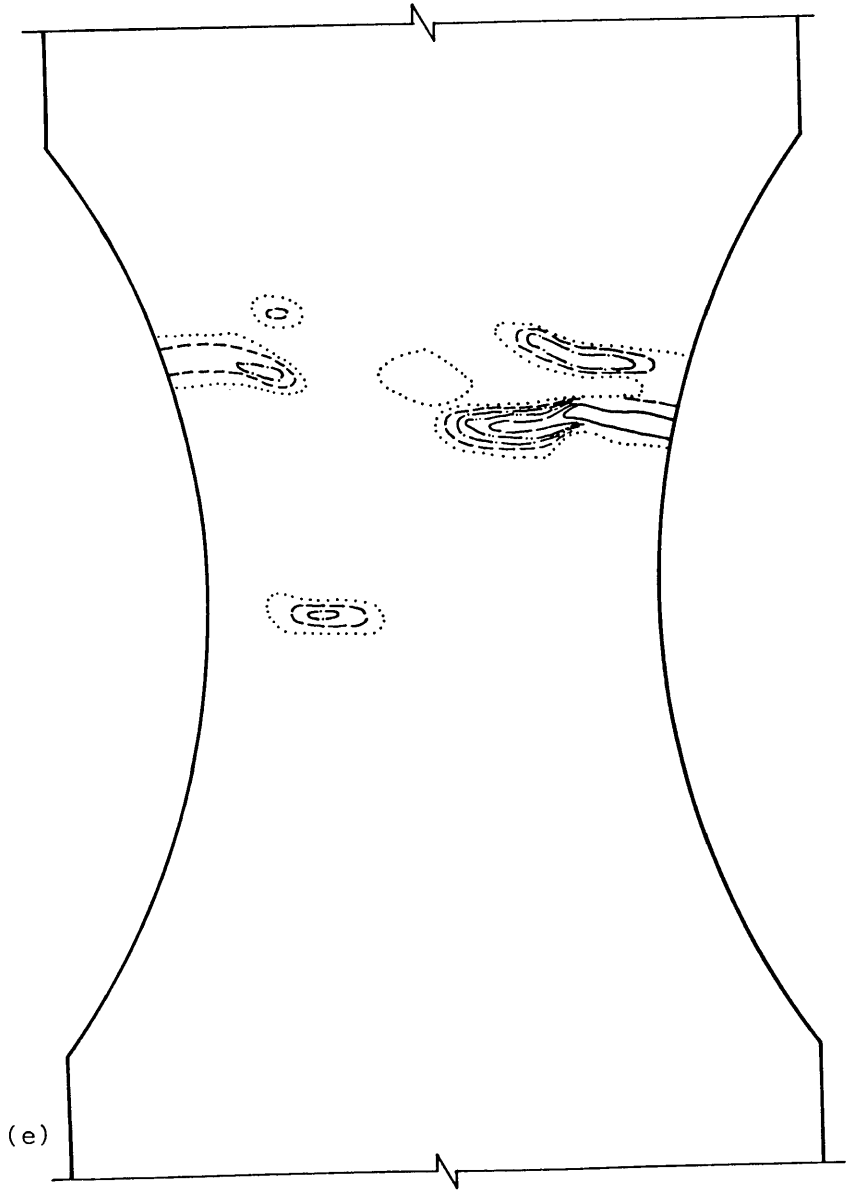

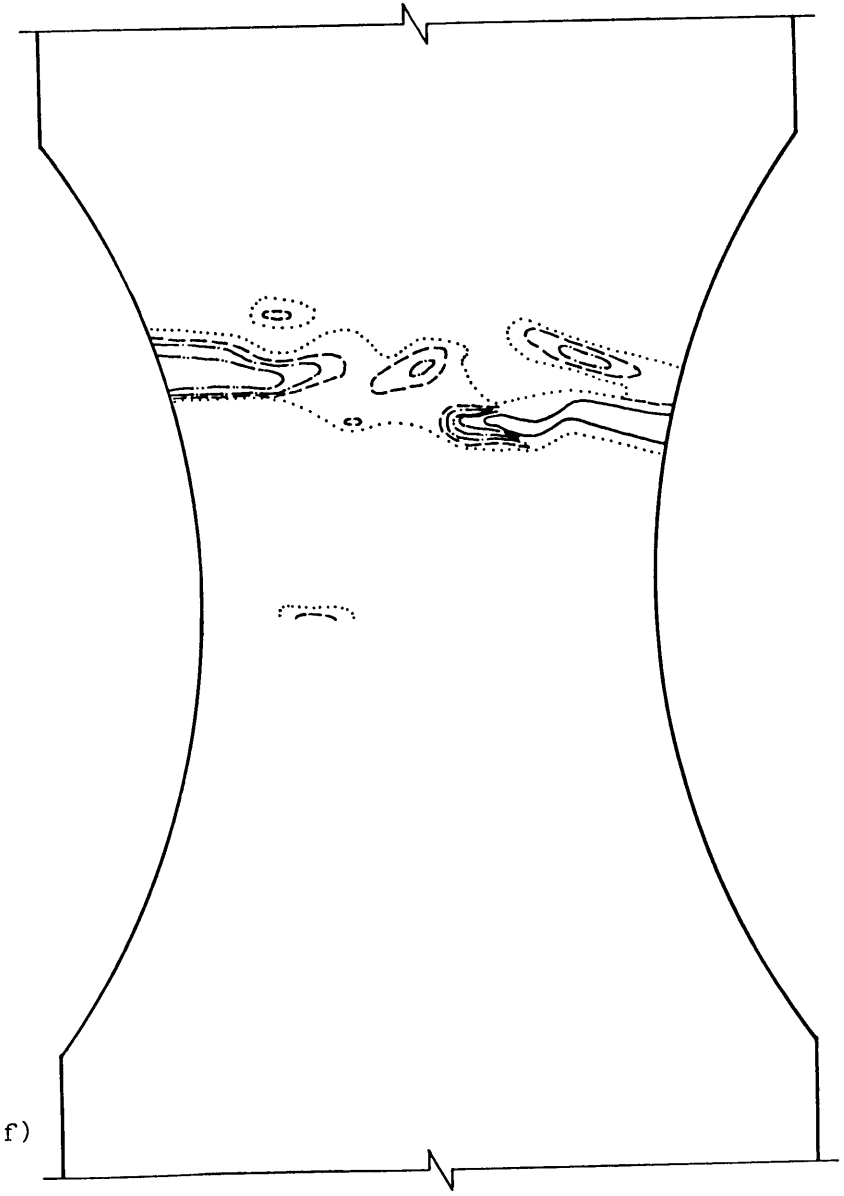

Fig. 8.14 Test L2, strain contour plots (cont)

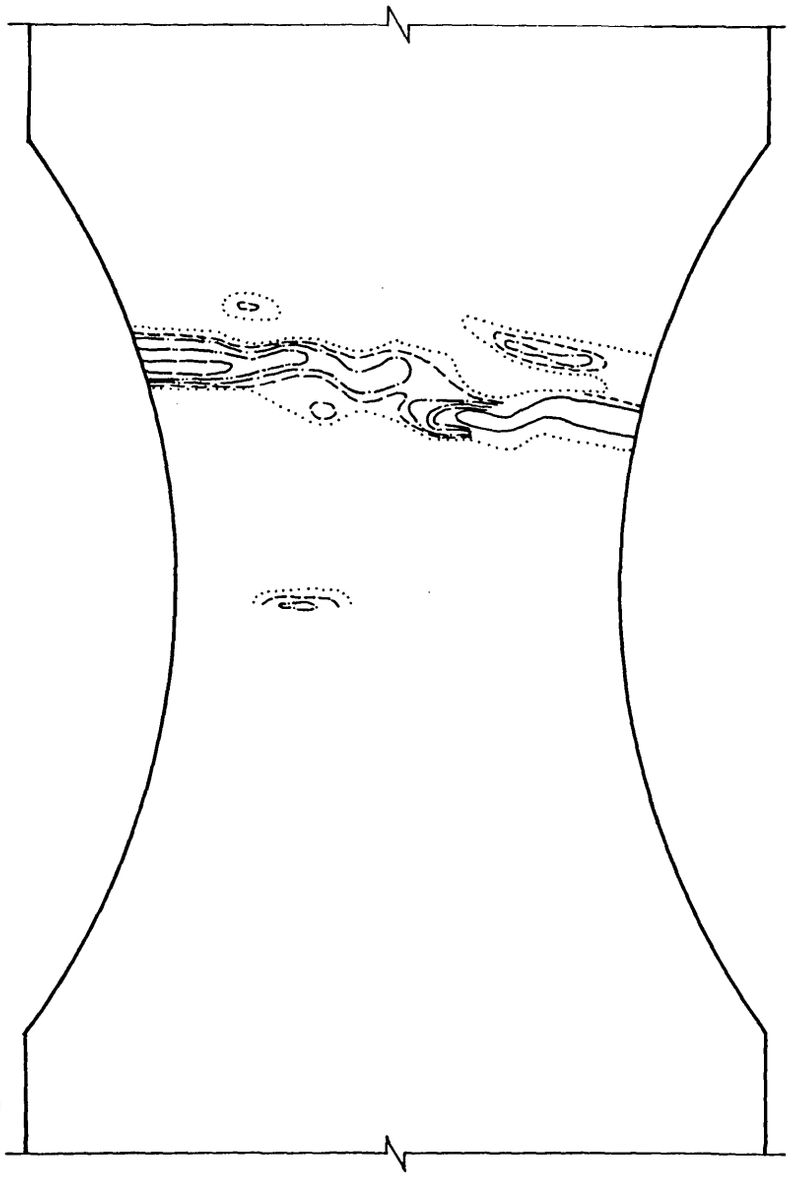

(g)

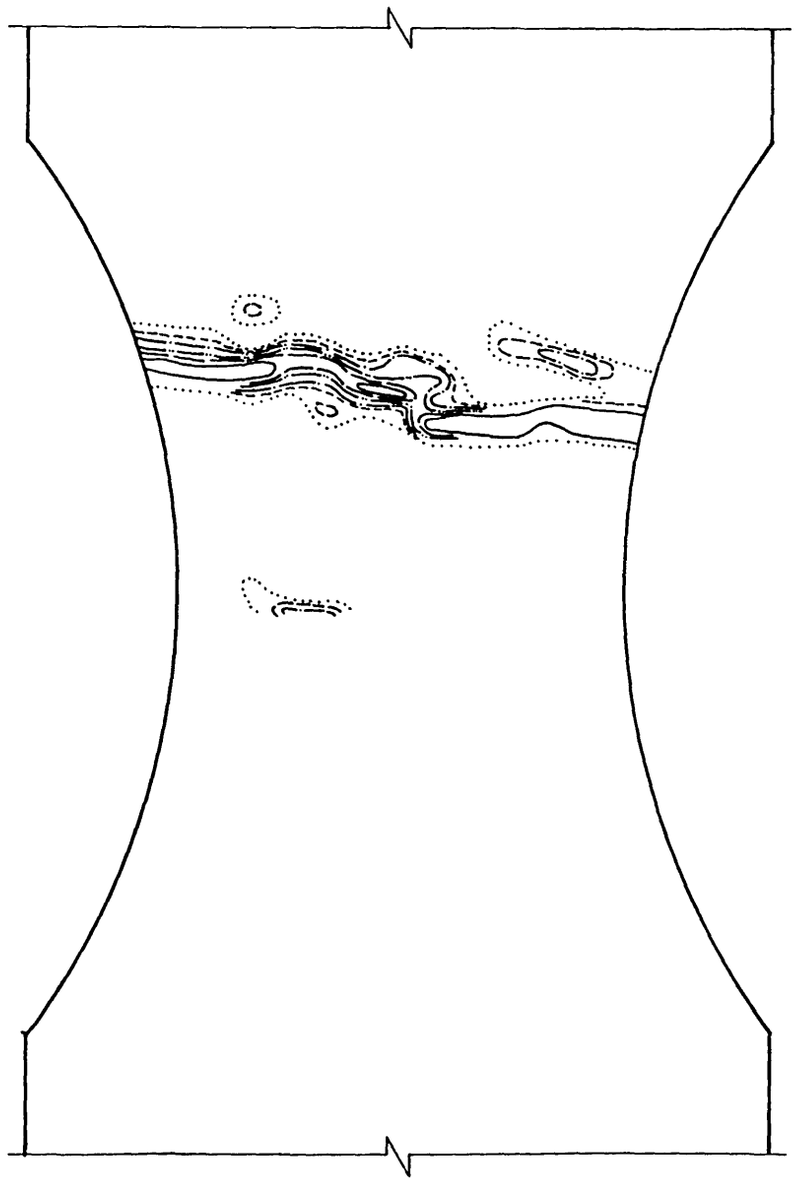

(h)

Fig. 8.14 Test L2, strain contour plots (cont)

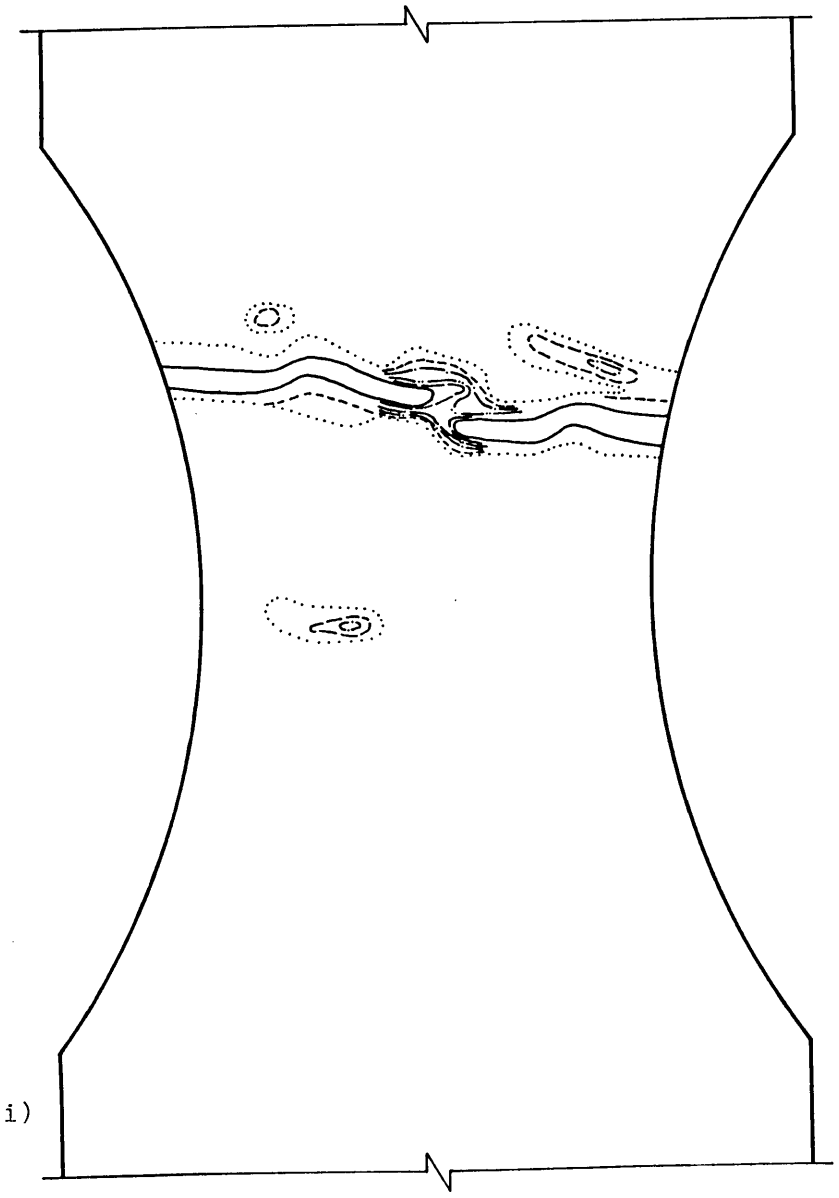

(i)

Fig. 8.14 Test L2, strain contour plots (cont)

The following conclusions may be drawn from the axial strain contour plots.

1. The strain first becomes localised in small zones usually at the edge of the specimen.
2. In 8 out of the 10 tests the localisation was observed to occur before the maximum load was attained.
3. Those tests in which the strain localisation occurred at an early stage also exhibited the greatest non-linearity in the load/extension curve up to the maximum load.
4. In the majority of tests two or more zones were observed with strains greater than 200 microstrain.
5. When pre-peak localisation was observed in a stable test, the zones developed gradually with at least one zone propagating across the specimen. The propagating zone was sometimes met by a second zone propagating from the other edge (Tests J2, L1 & L2; Figs. 8.10, 8.13 & 8.14).
6. In most tests additional specimen extension was required to ensure propagation. In some tests, however, gradual propagation occurred under fixed extension.
7. The first zone to develop was not necessarily the one which led to final failure (Test L2; Fig. 8.14).
8. The zones were of the order of 10mm. wide, had irregular shapes and were orientated in a direction approximately perpendicular to the applied load.
9. In the two tests in which localisation was not observed until after the maximum load had been attained the propagation occurred in a different manner. After a small amount of localisation a zone appeared almost simultaneously across the full width of the specimen but with strains of greater than 500 microstrain only in patches.
10. The strain in a partially developed zone running parallel to the major zone decreased with opening of the major zone (Tests K2 & L2; Figs. 8.12 & 8.14)
11. Zones of compressive strain sometimes occurred adjacent to the major zone (Test J2; Fig. 8.10).
12. Branching of a propagating zone occurred in one test (Test K2; Fig. 8.12).
13. When failure occurred in an unstable manner, the fracture surface

did not necessarily follow the line of any of the zones already formed.

8.3.3 Effects of gauge length and position

The importance of the correct understanding of the relationship between measured strain and gauge length was emphasised in Section 3.1 by comparing the results of stable direct tensile tests described in the literature. In this section the effects of the gauge length and gauge position are demonstrated using the data obtained from the current test series. The full field strain measurement technique allows the choice of gauge length and position to be taken after the test has been completed, however, the accuracy at low strain levels is poor. As a result, the strains measured outside fracture zones should be regarded as approximate.

The average axial strains over various gauge lengths for Test L1 are plotted against average axial stress in Figure 8.15. The positions and lengths of the gauges are given in Figure 8.15a, the effects of gauge length across the fracture zone are demonstrated in Figure 8.15b and the effects of gauge position shown in Figure 8.15c. In this latter figure 20mm. gauge lengths were used across the fracture zone, but, due to the limited area of the fringe photographs, only 10mm. gauge lengths could be used on either side of the zone.

8.3.4 Relationship between field strain and fracture zone opening

In order to investigate the effect on the surrounding material of opening of the fracture zone, the local axial field strain adjacent to the zone has been plotted against the fracture zone opening at various positions across the specimen for each of three tests (Fig. 8.16). This data is used in support of the fracture process zone model presented in Section 9.4. In the analysis of the fringe photographs to obtain the data the field strain has been calculated over a gauge length of approximately 15mm.. The fracture zone opening has been calculated from the opening within a length of approximately 15mm. minus the elastic opening in this length assumed to be equal to the

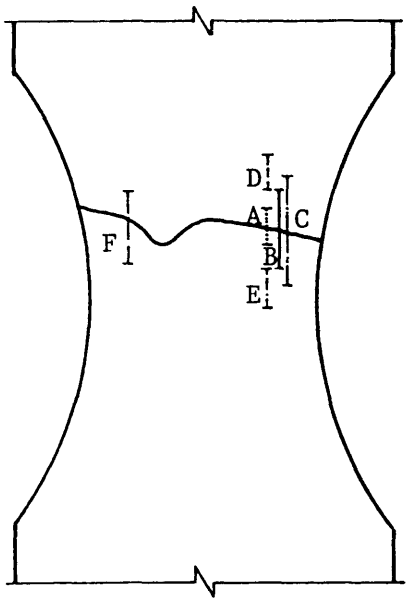

	Gauge lengths (mm)
A	10
B - - - - - - -	20
C -·-·-·-·-	30
D ———	10
E — — — —	10
F —·—·—	20

(a) Gauge lengths and positions

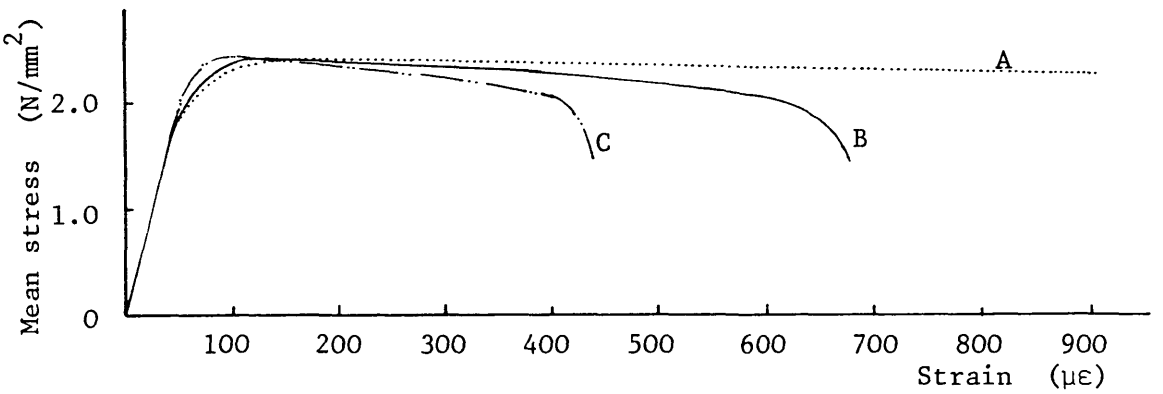

(b) Gauge length effect

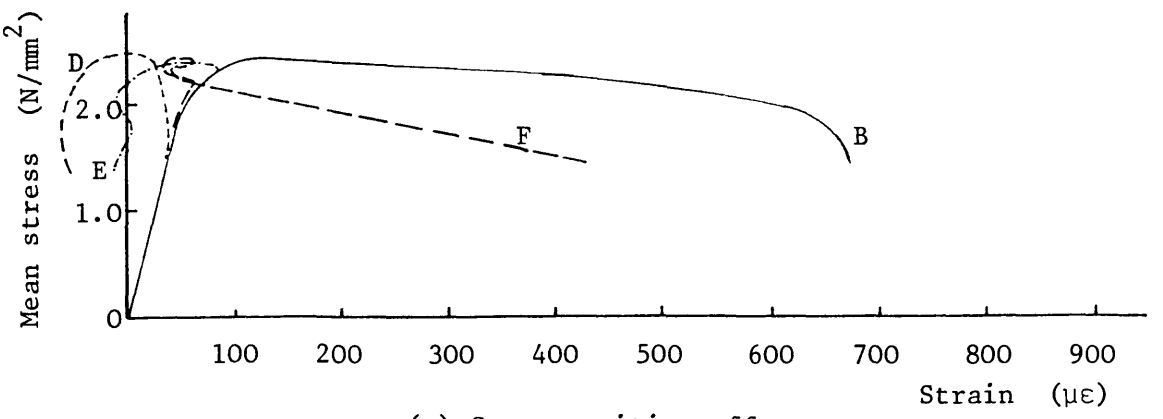

(c) Gauge position effect

Fig. 8.15 Effects of gauge length and position - Test L1

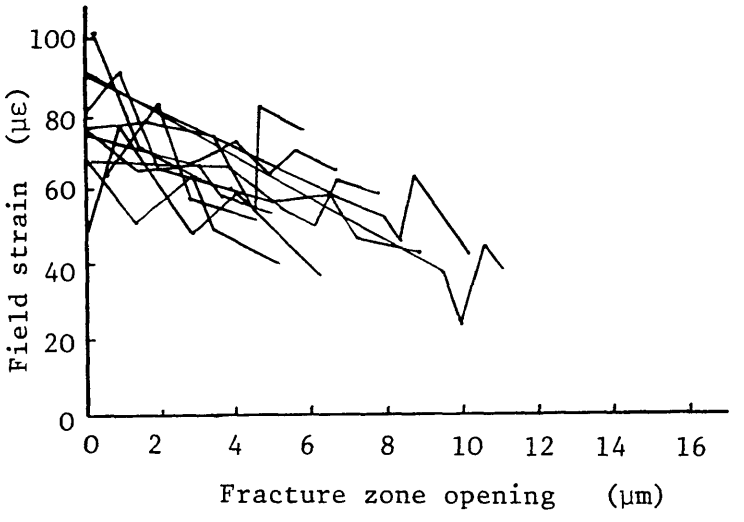

(a) Test C2

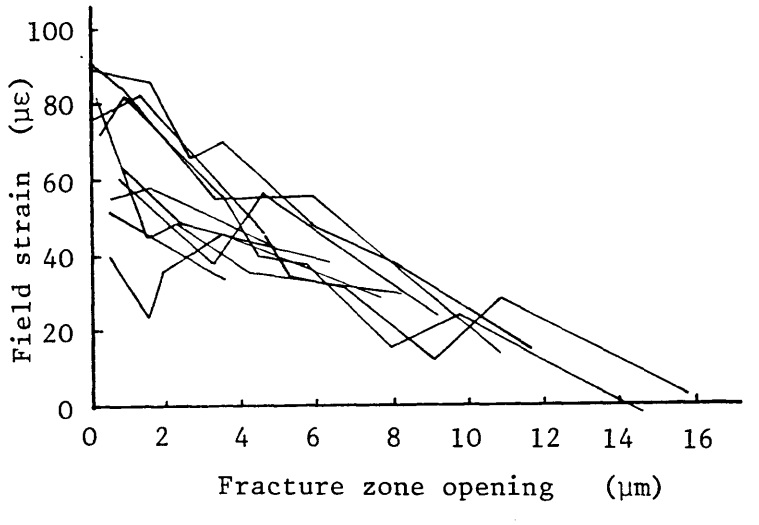

(b) Test G2

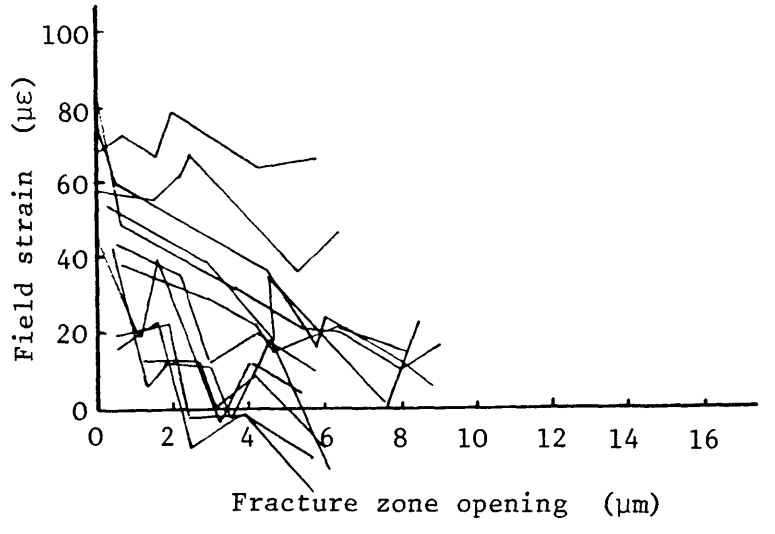

(c) Test L2

Fig. 8.16 Local field strain/fracture zone opening relationships taken at various positions across the specimens

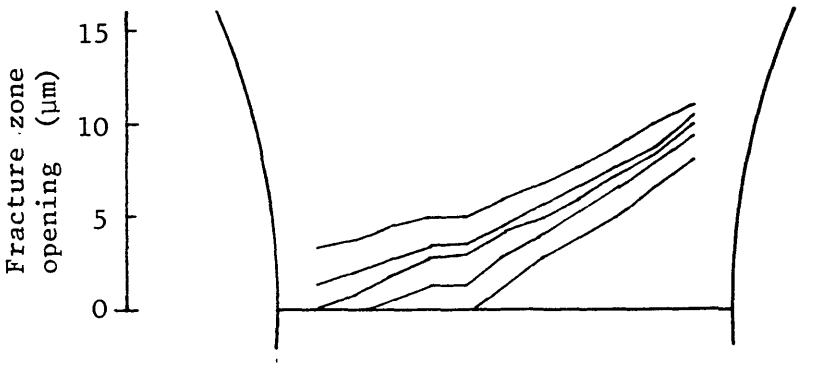

(a) Test C2

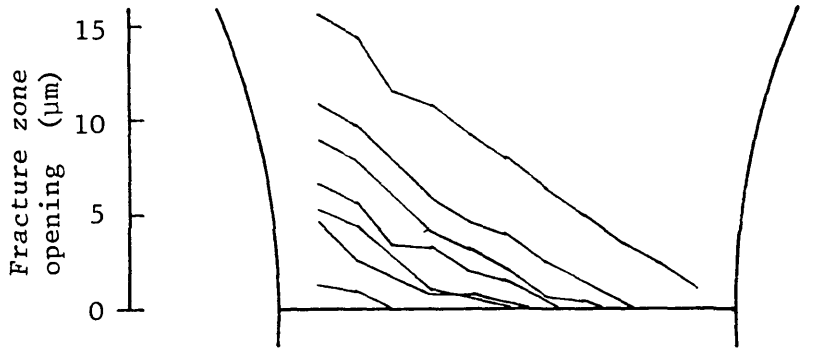

(b) Test G2

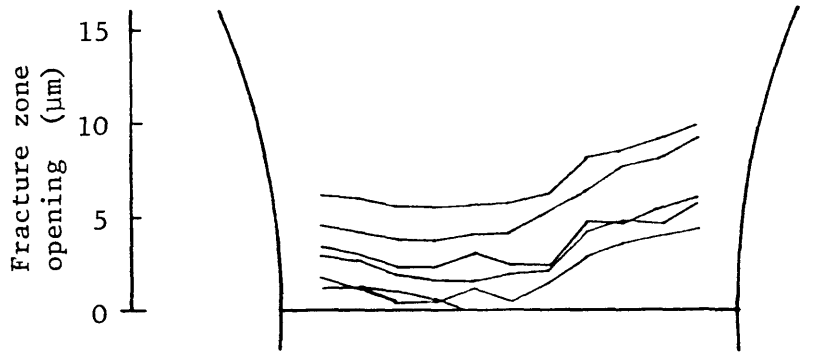

(c) Test L2

Fig. 8.17 Profiles of fracture zone opening across specimen

product of the adjacent field strain and the length. As mentioned in the previous section the field strain measurement can only be taken to be approximate. The fracture zone opening profiles across the specimen for different stages in the three tests are given in Figure 8.17.

8.3.5 Lateral strain and displacement

The full field strain measurement technique allows strains in three directions to be measured and could, in theory, be used to calculated the principal strains and their directions. However, the maximum lateral field strain is of the order of 20 microstrain and as such is below that which can be accurately measured. Figure 8.18 shows two typical lateral strain fringe photographs together with the associated axial strain fringe photographs. In the region of high axial strain, the lateral strain field may be seen to be distorted. However, it must be noted that in this region the interference grating is de-bonded and consequently the measured distortion may not be a true concrete distortion. The only useful information provided by the lateral strain fringe photographs is the measurement of the relative lateral displacement of the concrete above and below the fracture zone. Remembering that the fringes may be thought of as contours of uniform relative displacement it can be seen that in Figure 8.18b no significant relative displacement along the line of the fracture zone has occurred. This was found to be true for all of the tests in which lateral strain fringes were recorded.

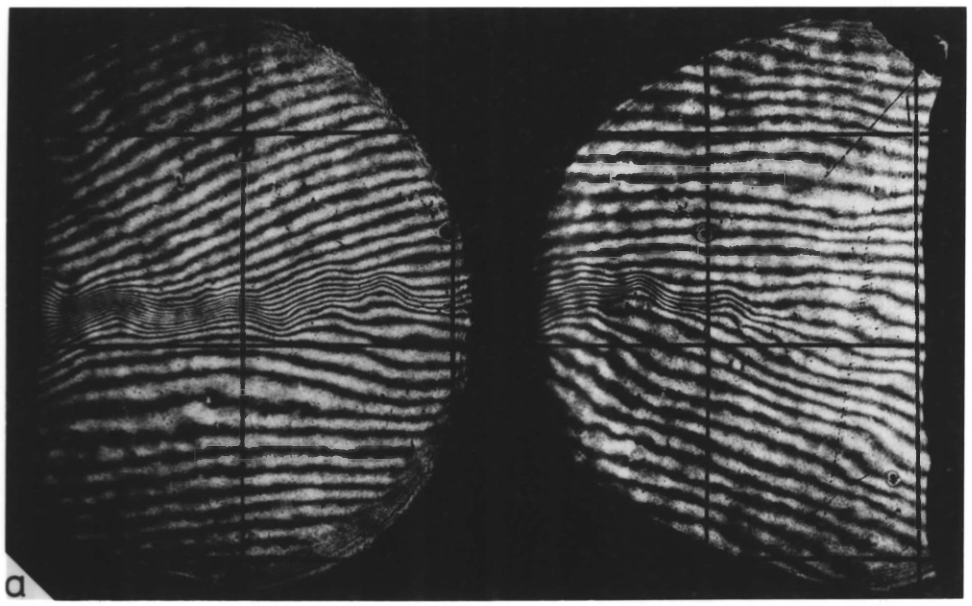

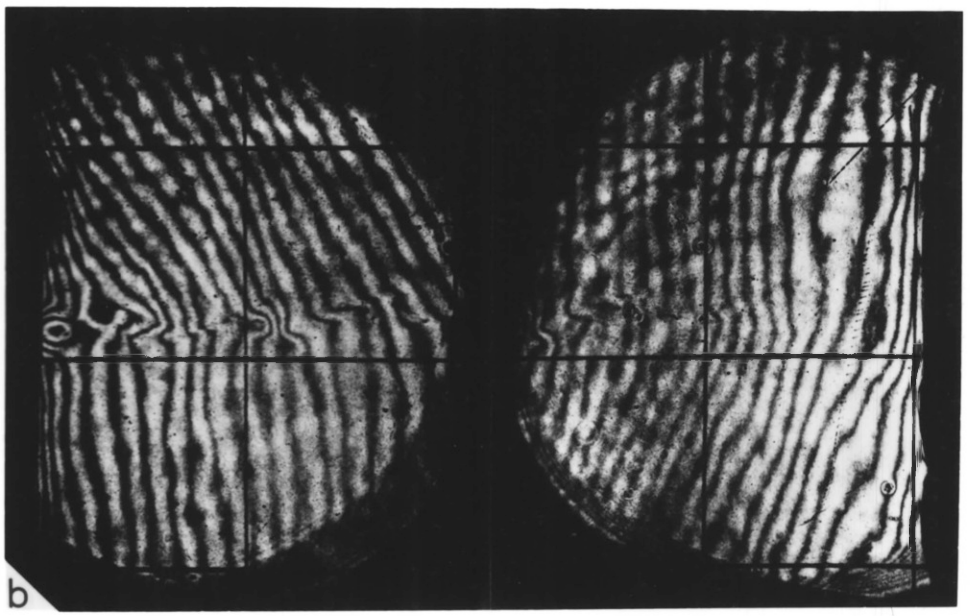

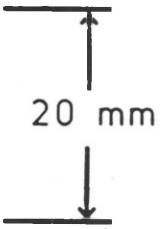

Fig. 8.18 Lateral strain fringe photographs — Test J2
a. Axial strain fringes corresponding to Fig. 8.10 h
b. Associated lateral strain fringes

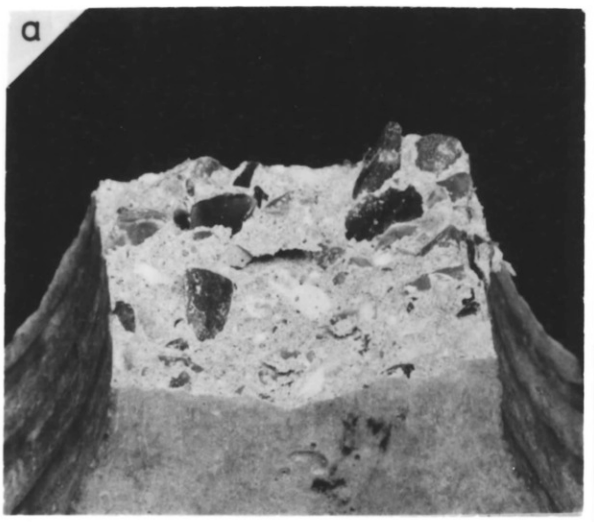

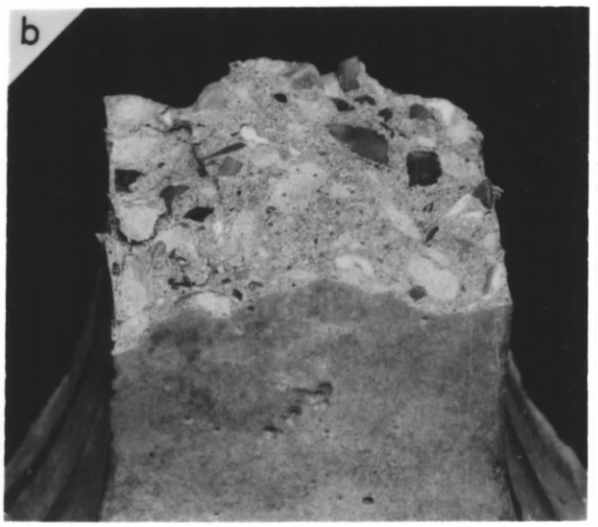

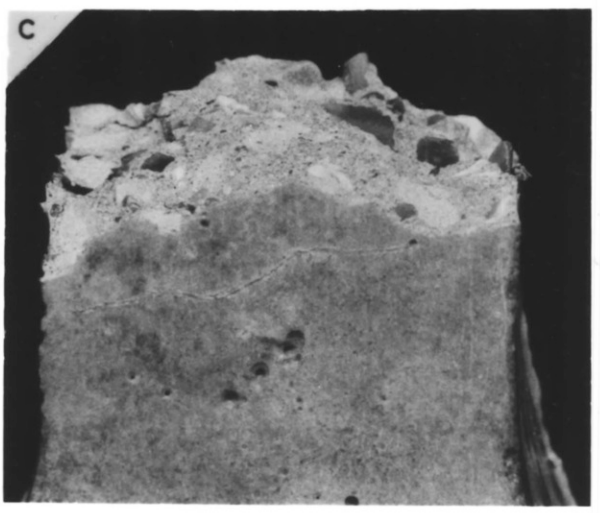

Fig. 8.19 Fracture surfaces — Test F1
a. Upper surface
b. Lower surface
c. Front face of lower portion showing secondary fracture

8.4 Fracture surface

The fracture surface was orientated approximately perpendicularly to the line of the applied load and separated the specimen into two parts (Fig. 8.19a & b). In addition to this major separation, smaller pieces were found to be detached from the surfaces of the two larger parts. The size of these smaller pieces was often of the same order of magnitude as the maximum aggregate size, but occasionally larger pieces were detatched. In Figure 8.19c, a second crack may be seen to run almost the full width of the specimen, approximately parallel to the major fracture at a distance of 10mm..

It was noticeble that the majority of the specimens failed above the specimen centreline and that there was a greater amount of aggregate showing on the upper fracture surface as compared with the lower surface. Generally, the fracture surface passed through the matrix and along the aggregate/matrix interface, however, occasionally aggregate particles were found to have been fractured.

An attempt was made to correlate the profile of the fracture zones shown in the axial strain contour plots with the positions of the larger aggregate particles showing on the fracture surfaces. Occasionally, kinks in the strain contours occurred at positions where an aggregate particle was visible, however, no consistant relationship was observed.

Chapter 9 Discussion of the experimental results

9.1 Suitability of test technique

The suitability of any test must be judged on whether or not it fulfils the initial requirements of the test, whether the results are repeatable and the agreement with similar test results published in the literature. In this section the first two criteria are discussed. The results are discussed in more detail and compared, where possible, with those obtained by other researchers in Sections 9.2, 9.3 and 9.4.

The basic requirements for the test were outlined in Section 3.5. The different requirements have been met with varying degrees of success. Control systems for the testing machine have been developed (Section 4.4.2.2.3) to enable extension controlled loading of the specimen. It has not been possible to ensure stable failure in all specimens. This was not due to machine control problems but to the fact that in some specimens the descending portion of the load/extension curve became vertical. This problem could have been circumvented by the use of shorter specimens (Section 3.2), However, reducing the length of the specimen would have increased the effect of the end conditions on the central portion of the specimen and a balance between these two conflicting requirements was made. In the event, the majority of the tests failed in a stable manner and it is considered that the compromise chosen was appropriate.

The maximum extension obtained in the tests was limited by the load capacity of the actuator and the load carried by the parallel bars. It varied from 92 micron to 182 micron, the upper end of this range being greater than any of the tests reported in the literature. Despite this large extension, complete separation did not occur. It would clearly have been preferable if the extension could have been increased further so that a full measurement of the fracture energy could have been made.

The design of the specimens and their connection to the testing machine was crucial to the success of the test. The minimum specimen dimension was 60mm. which was a factor of six times greater than the maximum aggregate size used. It was suggested in Section 3.3.1 that this factor should be at least 3.5 and so that the maximum aggregate size that could have been used was 17mm. The specimens were cast in such a manner as to ensure no change in material properties across the width of the specimen, and were sealed immediately on removal from the mould to prevent moisture migration.

The use of a necked specimen glued to the testing machine ensured failure within the central portion of the specimen. However, failure was not forced to occur at any predetermined cross-section. In the event failure occurred within the central 80mm. of the specimen for all the tests but with the majority of failure surfaces occurring above the centreline. This can be attributed to a slight reduction in concrete quality in the upper half of the specimen due to less efficient compaction and the rising of entrapped air during compaction leading to a greater air content in the upper half.

The effectiveness of the restraint of end rotation by the parallel bars was not directly measured in the tests, but, in four tests localisation in the strain field could be observed simultaneously at both edges of the face being monitored. This would suggest that the end restraint was effective. If it had not been so, then rotation would have occurred as soon as localisation appeared at one edge with corresponding relief of the strain at the other edge. Also an analysis of the changes in the distribution of loads in the bars during localisation in the strain field, suggested that the maximum relative end rotation that occurred was of the order of 3.5^{-5} rad. thus giving an extension on one face of only 1 micron more than that on the specimen centerline.

The main requirements of the full field strain measurement technique, namely the observation and measurement of the initiation and propagation of fracture process zones, were fulfilled using the moire interferometry technique. One limitation of the technique was that it was only applied to one surface of the specimen and consequently

localisation in the strain field elsewhere in the specimen was not measured. The attempts to use the technique for measurement of the unloading outside fracture zones and for lateral strain measurement were less successful. This was due to inaccuracies in the analysis of fringe patterns for low strains and the results could only be considered as approximate.

The effect of the interference grating on the response of the specimen was described in Section 8.2.7. Tests were conducted on specimens without gratings as a control sample against which those with gratings could be evaluated. The envelopes for the load/extension curves of the two types of specimen (Fig. 8.2) can be seen to be similar, as are the average measured tensile strengths, Young's moduli and fracture energies (Table 8.4). It was possible that the grating might have two effects on the specimen response. The first was to restrain the opening of the fracture zone leading to the formation of secondary fracture zones adjacent to the primary zone. This would have been similar to the effect on crack spacing of reinforcement in reinforced concrete. The second effect of the grating might have been that it would be able to transfer significant load across the fracture zone towards the end of the test. Both of these effects would have led to a change in the shape of the load/extension curve and an increase in the measured fracture energy which did not occur. Secondary fracture zones did appear in several specimens with gratings, however, they were also found to occur in specimens without gratings (Fig. 8.19c). It can be concluded that the grating had no significant effect on the response of the specimen.

The repeatability of the test results may be assessed by considering the coefficient of variation of the parameters measured from the load/extension curve. The coefficients for tensile strength, Young's modulus and fracture energy (up to 100 micron extension) are 12.1%, 13.7% and 13.2% respectively. The coefficients for tensile strength and fracture energy both reduce to 11.0% when the parameter is divided by the cube strength. This indicates a dependence of the variability of these two parameters on the slight changes in concrete quality between different batches, such that the variability due to the testing technique and inherent material heterogeneity is reduced. The numbers of direct tensile tests on any one concrete reported in the

literature are insufficient for a satisfactory determination of the coefficients of variation of the above parameters. However, Hillerborg (1985a), commenting on the use of three-point bend tests for the determination of the fracture energy, suggested that the coefficient of variation was normally between 10% and 15% and in extreme cases was as great as 25%. In the light of these figures, the variability of the current test series seems to be acceptable.

From the above discussion it may be concluded that the test satisfies the initial requirements and that the variability in the results was similar to that found by using other test techniques. The results obtained from the load extension curves are discussed in the next section and the fracture zone is discussed in Section 9.3.

9.2 Load/extension curves

The load/extension curves are shown in Figure 8.1 and described in Section 8.2.2. The curves may be seen to be qualitively similar to those obtained by other researchers (see for example, Figure 3.1). Typically the ascending portion of the curves reported in the literature is initially linear with some non-linearity prior to the attainment of peak load. After the peak load the load drops rapidly followed by a curve of reducing descending slope tending to become asymptotic to the extension axis. The level at which the non-linearity first becomes apparent varies from one researcher to another and indeed from one test to another. The earliest reported non-linearity for damp specimens was at 45% of the maximum load (Terrien, 1980) although this became as low as 28% for dried specimens. In other tests, (Hurlbut, 1985) the curve appeared to be linear almost up to the maximum load. The cause of the pre-peak non-linearity was described by Petersson (1981b) as irreversible strains occuring outside the fracture zone and by Terrien (1980) as microcracking at various positions within the specimen. In Section 9.3.1 it is suggested that the pre-peak non-linearity is due largely to the initiation of one or more fracture zones.

The descending portion of the curve was generally found to be smooth but in some tests a small 'plateau' in the steeper part of the descending portion was observed. Hurlbut attributed this plateau to the fracture zone encountering a piece of aggregate. Plateaux of this nature were encountered in the current project but no evidence is available to confirm or contradict Hurlbut's suggested cause. Hurlbut also attributed the change from the almost vertical descending portion to the curve of reducing descending slope, to the stage at which microcracks coalesce into a larger single discontinuity. However, Gopalaratnam & Shah (1984,5) and Eligehausen & Sawade (1985) observed discrete cracks at earlier stages in the test. The axial strain contour plots presented in Section 8.3.2 suggest that this stage may be related both to the point at which the fracture zone has propagated across the full width of the specimen and also to the relationship between local stress and fracture zone opening. This is discussed more fully in Section 9.3.4.

The ability of specimens to continue to carry load after cracks were observed was attributed by most reseachers to the combination of aggregate interlock and discontinuities in the cracking. This suggestion was supported by Petersson's observation that the post-peak load carring capacity was significantly increased with a change in maximum aggregate size from 2mm. to 8mm.. On the other hand, Eligehausen & Sawade found little difference between 8mm. and 16mm. concretes. This suggests that the aggregate interlock depends more on the presence of coarse aggregate than on it's size.

Due to the different concrete qualities used it is not possible to make a direct comparison between the parameters measured in the current test series and those measured from stable direct tensile tests reported in the literature. However, order of magnitude comparisons may be made and the results of the current test series together with the results from the reported tests on concretes of similar quality are presented in Table 9.1.

Reference	Compressive Strength (N/mm^2)	Tensile Strength (N/mm^2)	Young's Modulus (KN/mm^2)	Fracture Energy (N/m)
Terrien (1980)	-	1.87-2.80	33.7-41.1	-
Petersson (1981b) Mix 2	-	3.3	-	72-114
Gopalaratnam & Shah (1984,5) Series C2 &C3	33.3(cyl)	2.25-3.03	27.4-32.6	37.8-52.0
Cornelissen, Hordijk & Reinhardt (1985a & b)	47.1(cube)	3.20	39.3	100
Eligehausen & Sawade (1985)	35(cube)	3.2	28.0	120
Hurlbut (1985)	22.1(cyl)	2.24-2.82	19.3	60
Current test series	36.0(cube)	2.38	25.4	62.9-128.6

Table 9.1 Results of stable direct tensile tests

The results of the current test series lie within the range of results obtained by other researchers. The parameter in which the largest variation occurs is the fracture energy. This is partly due to the different methods used to evaluate the energy from the load/displacement graphs. In all the results presented in Table 9.1 the fracture energy was calculated from the area under the graph, the

discrepancies arise due to the assumptions made regarding the long tail of the graph and the energy absorbed prior to the attainment of maximum load. Gopalaratnam & Shah calculated the area up to an extension of 61 microns and assumed that the energy consumed beyond this point was negligible, whilst Hurlbut and Petersson used the extension at the end of the test, being approximately 78 microns and 140 microns respectively, as the upper limit. The lower values of maximum extension gave lower values for the fracture energy. On the other hand Cornelissen, Hordijk & Reinhardt and Eligehausen & Sawade fitted exponential curves to their stress/crack opening data and integrated the full area under the curves giving larger values for the fracture energy. Unfortunately, the maximum experimental extensions reported in these two references were 125 microns and 68 microns respectively and no experimental confirmation was obtained regarding the shape of the latter portion of the curves. Reinhardt (1984) in an earlier analysis of the same data as presented by Cornelissen, Hordijk & Reinhardt obtained a value for the fracture energy increased by a factor of 1.35 simply by using a different type of exponential curve.

The differences between the fracture energies reported above highlight the importance of the latter portion of the curves in calculating the fracture energy. The average maximum extension for the stable tests of the current project is 137 micron with six tests exceeding 160 micron. The mean values for the fracture energy calculated up to an extension of 100 micron and, for the six longer tests, up to the end of the test are 77.1N/m and 110.0N/m respectively. In an attempt to estimate the contribution to the fracture energy of that part of the curve beyond 100 microns extension, the energy absorbed between 100 microns extension and the end of the test has been plotted against the extension at the end of the test in Figure 9.1. There is no obvious reduction in the rate of increase of the fracture energy and consequently no limiting extension for the fracture energy calculation can be found. The total fracture energy cannot therefore be calculated but it is known to be greater than 110.0N/m.

In the analysis of the tests presented above, other than those conducted by Petersson, it was assumed that all the energy absorbed by the specimen was required for the fracture processes. As described in Section 2.2.2.3.2, Petersson assumed that in addition to the energy

Fig. 9.1 Fracture energies for latter portion of test

required for fracture, some energy was absorbed by irreversible strains occurring outside the fracture zone prior to the attainment of maximum load. He associated this energy with the pre-peak non-linearity of the load/extension curves and subtracted it from the total energy absorbed to obtain the fracture energy. This analysis is based on the assumption that the fracture zone initiates at peak load and not before. From the results given in Section 8.3.2 this can be seen to be an over-simplification. The primary fracture zone is usually initiated before the maximum load is reached. There are also secondary fracture zones or sites for energy absorption. This would tend to suggest that all energy absorbed is dissipated in fracture process zones, but that the measured area under the load/extension curve may be dependent on the number and size of secondary zones produced. If this was true then the measured fracture energy might be affected by the length of the specimen, the longer specimen having a greater likelihood of producing secondary zones. Hurlbut (1985) tested cylinders with the same cross-section but different heights and was unable to detect any significant difference between the energies measured. However, the aspect ratio of the shorter cylinders was only 1 to 1 so that the effects of the end restraint on the specimen may not be negilgible. Further work would be required to differentiate between the energy absorbed by the primary fracture processes and any energy absorbed in a secondary process not directly associated with the primary fracture. At this stage it would seem reasonable to attribute the full area under the load/extension curve to all the processes required to cause complete separation, ie. the fracture energy.

Beam tests for the determination of the fracture energy were discussed in Section 2.2.2.3.2. It was shown that the measured fracture energy depended on the beam size. Direct tensile testing may prove to be a more appropiate technique for the measurement of fracture energy and the determination of whether or not the fracture energy is a size independent material property.

From the above discussion it may be seen that the results obtained from the load extension curves of the current project are similar to those obtained by other researchers. This, taken together with the discussion in Section 9.1, confirms the suitability of the test

technique developed.

9.3 Fracture process zone

The results which are of primary importance in the current project are those concerning the fracture process zone. These results have been obtained from full field strain measurement and are reported in Section 8.3. In this section the results are discussed and compared with the limited data available in the literature.

9.3.1 Fracture initiation

One of the main limitations of the strain measurement technique adopted is that it is only applied to one face of the specimen. Strain localisation may occur elsewhere in the specimen before it is observed on the measurement face. The stage at which localisation is first observed (Table 8.5) cannot be considered to be the stage at which localisation first occurs since localisation may occur at an earlier stage in the test without being observed. Similarly, the stage at which localisation occurs across the full cross-section may be later than the stage at which it is observed across the full width of the measurement face. This is particularly important when considering the stage at which localisation first occurs. In two specimens, E2 and K1, localisation was not observed until after the maximum load was achieved. Also in these two specimens the observed development of the fracture zone was different to the other tests. Instead of a gradual development of the zone from one side to the other, it appeared almost simultaneously across the full width of the specimen, but with strains greater than 500 microstrain only in patches (Figs. 8.6c and 8.11d). It is suggested that in these two tests the fracture initiated away from the measurement face and was observed only after the fracture zone had propagated across a significant portion of the specimen. Additional support for this suggestion comes by considering the loads in the bars in parallel with the specimen. The changes in the distribution of loads among the four bars, before and after the peak specimen load is obtained, give some indication as to the reduction in load carrying capacity of different parts of the specimen

cross-section due to fracturing. The changes in parallel bar loads are associated with end rotations of the specimen which are extremely small due to the stiffness of the bars, the maximum being of the order of 3.5×10^{-5} rad.. This gives an extension of only 1 micron greater on one side of the specimen than on the centreline. In the case of Tests E2 and K1 this rotation would have resulted from additional extensions on the face remote from the measurement face indicating that this was the face at which the fracture initiated. The direction of the end rotations observed in Tests C2 and L1, and Tests G2, J2 and K2 were such as to result from additional extensions of the right and left hand sides respectively of the measurement face which correspond with the positions of fracture initiation in these tests.

From the above discussion it may be concluded that the fracture process zone is initiated prior to the attainment of maximum load. This promotes one further question; does the initiation of the fracture zone correspond to the onset of non-linearity in the load/extension curve? Again the problem arises that the stage at which initiation occurs cannot be measured, only the stage at which it was observed on the measurement face. All that can be said for certain is that the first appearance of strain localisation and the onset on non-linearity seem to coincide for Tests F2, I2 and J2 and that in the other tests the localisation appears on the measurement face after the onset of non-linearity. It is suggested that the development of fracture zones is the primary cause of non-linearity in the load/extension curve but without further work it cannot be shown to be the only cause. It may well be that microcracking outside recognisable fracture zones also contributes to the observed non-linearity. This, of course, calls into question the definition of fracture process zones. In the current project they are treated as those zones in which the strain is observed to be significantly greater than the strain in the surrounding material. It is possible that this is not the most appropriate deliniation between bulk or distributed phenomena and discrete phenomena but it is the most convenient.

9.3.2 Size of fracture process zones

It can be seen from the axial strain contour plots given in Section 8.3.2, that the width of the observed fracture zone varies but is typically of the order of 10mm.. The maximum aggregate size is 10mm. and, given that the fracture surface passed around the majority of the aggregate particles, it is not surprising that the width of the zone and the maximum aggregate size should be similar. This may not be true in the case of weaker aggregates when the fracture surface might pass through the aggregate particles. Petersson (1981b) demonstrated the effect of the aggregate on the width of the fracture zone by sawing one of his tensile specimens in two to expose the aggregate. During the test the other faces were continually kept wet but the sawn face kept dry. The positions of cracks were observed as damp patches due to the water being transported by capilliary action. When the crack encounted a large aggregate particle it was observed to branch and pass round the aggregate thus leading to a zone of disturbance of a similar width to the size of the aggregate.

Bazant & Oh (1981,3) examined the ratio between fracture zone width and aggregate size by obtaining the best correlation between the results of their crack band analysis (Section 2.4.3) and experimental results in the literature. They found that the best correlation was achieved if the fracture zone width was approximately three times the aggregate size. It is suggested that this correlation depends more on the formulation of the crack band model than on the true physical relationship.

No information is gained from the current tests regarding the length of the fracture zone except that it may be considerable. The fracture zone may be considered to be initiated at the first localisation in the strain field and continue to exist until the stress transferred across it has reduced to zero which may not occur until the opening is greater than 200 microns. Reinhardt (1985) suggested that very large direct tensile specimens would be required for a complete fracture zone, extending from the position of initiation to a stress free crack, to be obtained. Eligehausen & Sawade (1985) suggested that the length of the zone would depend on the type of loading and the

specimen geometry so that it could not be considered to be a material characteristic.

9.3.3 Multiple fracture process zones

In the majority of tests, two or more fracture zones were observed. In some cases two zones joined together to form the major fracture zone. In other cases the development of one zone predominated allowing the other zone to develop only partially before being unloaded. The strain within such secondary zones was observed to reduce during the post-peak portion of the load/extension curve. This reduction in strain indicates either that some of the strain within a fracture zone is reversible or that the zone is subjected to a compressive stress by the rest of the specimen leading to closing up microcracks. In one test the fracture zone was observed to branch around a group of tightly packed aggregate particles. Secondary cracks were also observed in some of the tests in which the strain was not measured.

The branching of cracks was occasionally observed by Eligehausen & Sawade (1985) and Mindess & Diamond (1980) found multiple and branch cracking in mortar at a lower dimensional level using a scanning electron microscope. The majority of other researchers found only one crack, however, this may be attributed in some cases to the effect of notches forcing the fracture to occur at a predetermined cross-section.

Terrien (1980) used acoustic emission to monitor cracking and, by measuring the time difference between acoustic emissions detected at each end of the specimen, was able to conclude that there were several active zones for the emissions but that the final separation occurred by fracture initiating from one of these zones. The acoustic spectra for the initial fracture zones and for the propagation of the zone leading to failure were different. Terrien attributed this phenomenon to different types of cracking, de-bonding of aggregate in the initial fracture zones compared with fracturing of the mortar during propagation. The existance of more than one fracture zone prior to

maximum load was also noted by Cedolin, Dei Poli & Iori (1983) in a necked specimen observed using moire interferometric strain measurement.

9.3.4 Fracture propagation

As noted in Section 9.3.1 fracture process zones are initiated before the maximum load is attained. The initiation and limited propagation of such zones up to maximum load have been suggested as the primary cause of pre-peak non-linearity. In stable tests the zones continue to propagate gradually in a direction perpendicular to the principal tensile stress until the primary zone crosses the whole specimen. From this stage, continued extension of the specimen, or stress relaxation due to creep, led to further gradual opening of the primary zone.

The post-peak portion of the load/extension curve is characterised by an initial rapid drop in load followed by a more gradually descending curve. The transition between these two stages is very marked in some tests whilst in others it is smooth. It is of interest to investigate whether or not any phyical significance can be attibuted to this transition. Hurlbut (1985) suggested that the transition occurred when microcracks coalesced into a single discontinuity across the specimen. This is based on the assumption that the fracturing is uniformly distributed over the whole cross-section. The experimental results of the present project show that the strains are not uniform over the cross-section and that propagation of the fracture process zone occurs during the post-peak portion of the load/extension curve. It may be possible, therefore, that the steeper part of the load/extension curve relates to the propagation of the fracture zone and that the more gradually descending part is a function of the opening of the zone after it has propagated across the full cross-section of the specimen. Considering the axial strain contour plots presented in Section 8.3.2, it can be seen that the transition in the load/extension curve occurs at approximately the same time as the fracture zone is observed to have propagated across the full width of the measurement face for Tests C2, E2, J2 and K2 but seems to occur at a later stage in Tests

G2, K1, L1 and L2. Remembering that the stage at which the zone has propagated across the full cross-section may occur later than the stage at which it is observed to have crossed the measurement face, the results are consistant with the suggestion that the transition in the load/extension curve occurs at the stage when the fracture zone has propagated across the full cross-section. In order to investigate this suggestion further a simple model for the stress transferred across a fracture zone is presented in the next section. Despite the simplifications made in the formulation of the model, the mean load/fracture zone opening curve measured in the tests can be reproduced very accurately (Fig. 9.3), as can the stage at which the fracture is observed to propagate across the whole section. The results from the model suggest that the transition in the load/extension curve may be related to both the stage at which the fracture zone has propagated across the whole specimen and also the shape of the local stress/fracture zone opening relationship.

9.4 Model for stress transferred across a fracture process zone

The models which have previously been suggested for the stress transferred across a fracture process zone (Section 2.4) all assume that each infinitesimal volume of the material behaves in exactly the same way as the overall response of a specimen in the direct tensile test. This presupposes that the zone develops uniformly across the full cross-section of the specimen which, as was shown in Section 8.3.2, does not happen. In this section a simplified model is presented, based on a local stress/fracture zone opening relationship and on the propagation of such a zone. The model is capable of reproducing the mean load/fracture zone opening curve for the tests as well as predicting the stage at which the fracture zone spreads across the whole cross-section.

In Section 8.3.4 the relationship between the local field strain and fracture zone opening was investigated. Although the measurement of field strain was insufficiently accurate for a relationship to be identified with any degree of confidence, it can be seen from Figure 8.16 that the local field strain reduces with increasing fracture zone opening. Assuming that the material outside the fracture zone is approximately elastic, a similar relationship would be appropriate between fracture zone opening and stress transferred. In the model the bi-linear relationship shown in Figure 9.2a has been used. The bi-linear relationship was chosen so that the initial rapid drop in load indicated in Figure 8.16 might be followed by a more gently dropping load. This was required since it is known that stress can still be transferred across a zone with a significant opening. It is suggested that the physical significance of the bi-linear relationship is that there are two basic phases to the fracture. The first consists of microcracks gradually coalescing to produce a single major defect, the second stage then covers the opening of this defect together with aggregate interlock effects. In practice the distinction between these stages may be blurred nevertheless it seems helpful to maintain the distinction for the purpose of analysis.

In order to obtain the load/fracture zone opening curve from the local stress/fracture zone opening relationship it is necessary to make some

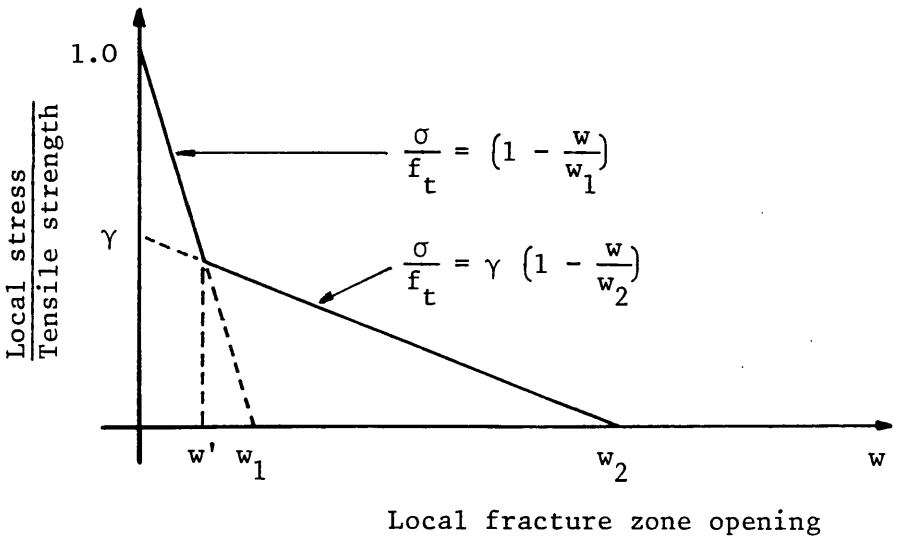

(a) Local stress/fracture zone opening relationship

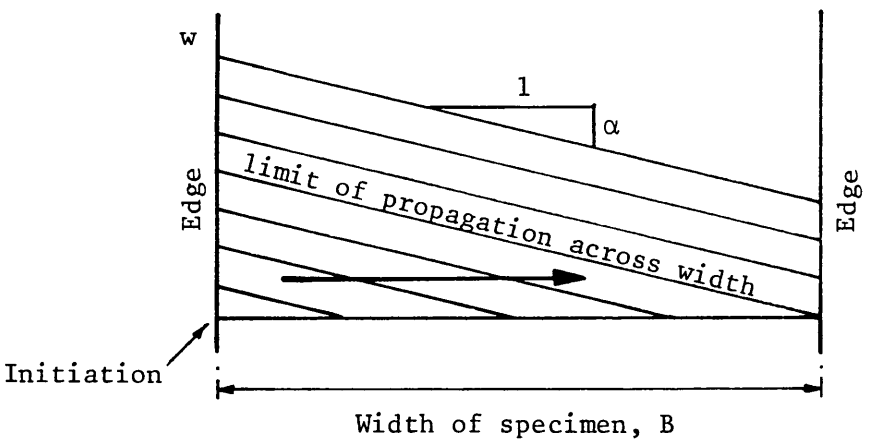

(b) Profile of fracture zone opening during propagation and subsequent opening

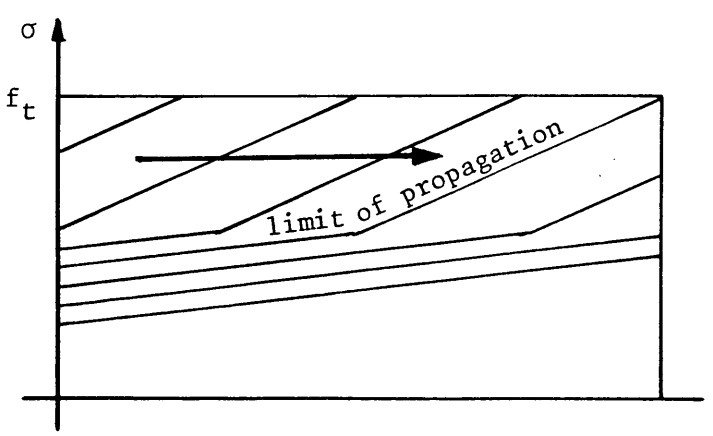

(c) Stress distribution across specimen during propagation and subsequent opening

Fig. 9.2 Model for fracture process propagation and development

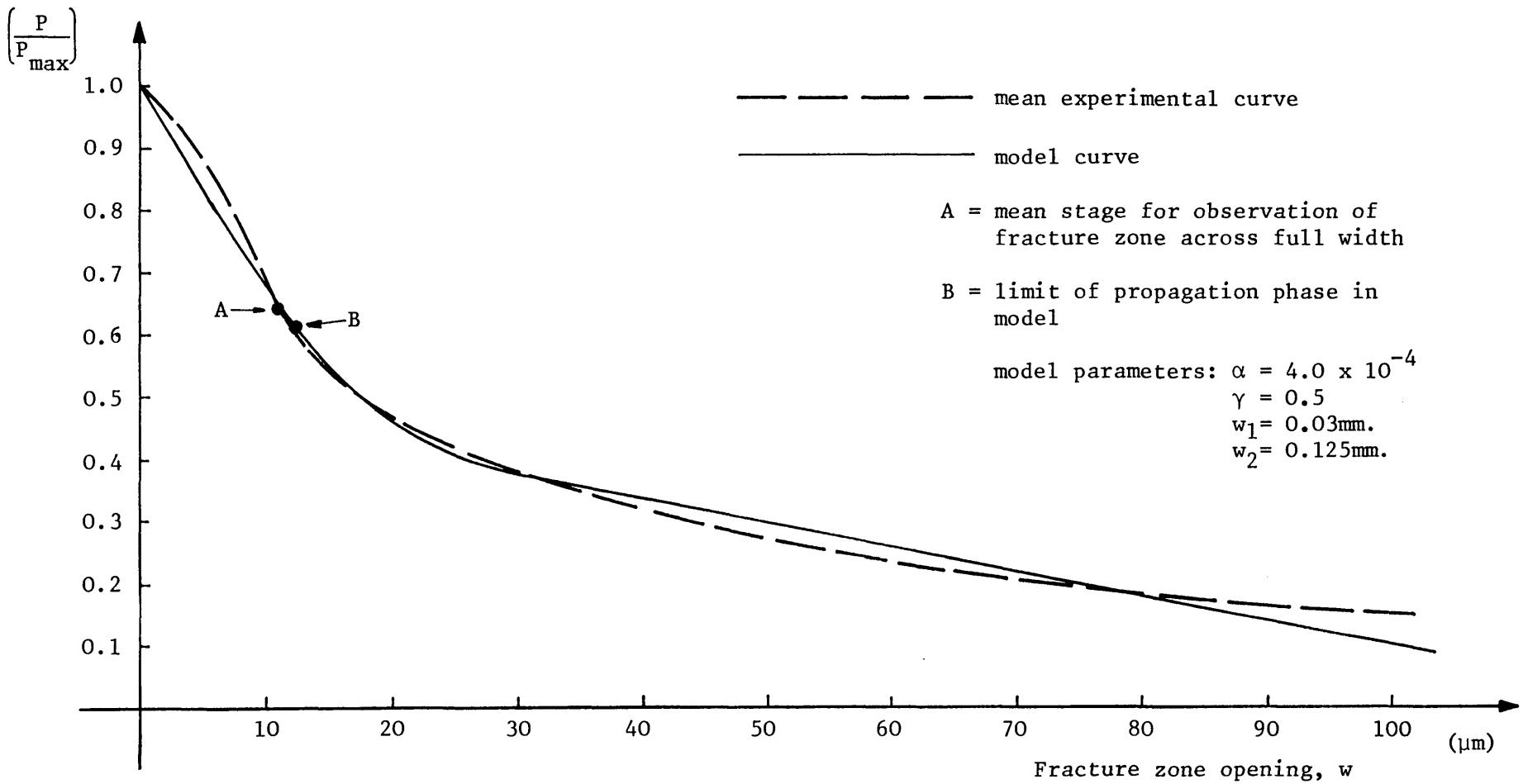

Fig. 9.3 Load/fracture zone opening relationship - best fit for model

assumptions regarding the propagation of the zone and the profile of it's opening. Reinhardt (1984) measured the profiles in wide specimens and the profiles for three tests in the current project are given in Figure 8.17. It seems reasonable to assume the straight line profile shown in Figure 9.2b. For the sake of simplicity it is assumed that fracture initiation occurs at maximum load and that the stress ahead of the fracture zone is equal to the tensile strength. The stress distribution across the cross-section is given in Figure 9.2c for different stages during the propagation and subsequent opening of the zone.

The mean experimental load/fracture zone opening curve is shown in Figure 9.3. This was calculated on the assumption that elastic unloading occurs from the maximum load in all the material outside the fracture zone (Eligehausen & Sawade, 1985). The unloading modulus was taken to be equal to the initial tangent modulus and the load is presented in non-dimensional form. The load/fracture zone opening relationship for the model is simply obtained by averaging the stress and fracture zone opening across the specimen. The best fit of the model to the experimental data is given in Figure 9.3. The average load level at which the fracture zone was observed to have crossed the specimen is shown on the experimental curve and the stage for the limit of the propagation phase in the model is also shown.

The agreement between the model and the experimental data is surprisingly good given the simplicity of the model and the scatter in the experimental data. The important distinction between the model presented in this section and previous models is that this model is based on a local stress/fracture zone opening relationship from which the overall load/fracture zone opening curve of a direct tensile may be obtained. The other models start by approximating the overall load/fracture zone opening curve and then assuming that this approximate relationship can be applied as the local constitutive relationship ignoring the effects of fracture propagation in the tests on which the models were based. It so happens that the optimum approximation to the load/fracture zone opening for concrete suggested by Petersson (1981b), and used by Gustafsson (1985), was a bi-linear relationship similar to the local constitutive relationship used in the current model. The method of application of these two models in

the finite element analysis of concrete structures is identical. The more thorough basis of the current model taken together with the results obtained by Petersson and Gustafsson show the usefulness of the model. For a more complete model of the fracture processes, the effects of pre-peak fracture initiation and variation in the fracture properties across the specimen would have to be included. Further experimental work is required to verify the local stress/fracture zone opening relationship.

Chapter 10 Conclusions

A correct understanding of the fracture processes which occur in concrete under tension is vital for the development of improved material models to be used in the analysis of concrete structures undergoing cracking. A review of current theories for the tensile failure of concrete (Chapter 2) highlighted the disparity of the bases for these theories and the conclusions drawn from them.

In order to obtain a greater understanding of the fracture processes, a stable direct tensile test has been developed (Chapter 4), to be used in conjunction with a technique for full field surface strain measurement (Chapter 6). The suitability of the test technique has been demonstrated in an initial series of tests (Chapters 7, 8 & 9) which has also provided the data upon which several important conclusions can be based. These conclusions may be summarised as follows:

1. Fracture in concrete under tension is not a brittle phenomenon but is characterised by localised strain-softening. The apparent brittleness in some tests is a function of the testing technique rather than the intrinsic material properties.

2. Fracture occurs due to a gradual propagation of fracture process zones in a direction perpendicular to the principal tensile stress.

3. The initiation of fracture process zones in direct tensile tests occurs prior to the attainment of maximum load and may occur as early as at 45% of the maximum load.

4. More than one fracture process zone may be initiated in specimens for which the position of the fracture is not predetermined either by specimen geometry or by loading conditions.

5. Occasionally a propagating fracture process zone may branch, leading to two or more zones running approximately parallel to one another.

6. The coarse aggregate in the concrete tested was Thames Valley Gravel with a maximum aggregate size of 10mm. The fracture process zones in this concrete are approximately 10mm.. It has been suggested (Petersson, 1981b) that the width of the fracture process zone is related to the type and size of the aggregate but the exact nature of this relationship is not yet known.

7. It is suggested that the non-linearity in the ascending portion of the load/extension curves for direct tensile tests is largely due to the pre-peak initiation of fracture process zones.

8. Fracture propagation in stable direct tensile tests begins prior to the attainment of maximum load and continues to occur in the descending portion of the load/extension curve.

9. The load/extension curve obtained in direct tensile tests is not a material relationship but is dependent on the propagation of fracture process zones across the specimen and on the length of the specimen. It is suggested that a more appropriate material relationship is that between the local stress and the fracture zone opening.

10. The descending portion of the load/extension curve for a stable direct tensile test may be approximately subdivided into two stages. In the first stage the load drops rapidly with increasing extension, this is followed by a more gradually descending stage. The transition between these two stages may have two causes. The first is the completion of fracture zone propagation across the full cross-section of the specimen. The second is the shape of the local stress/fracture zone opening relationship which may be approximately described as bi-linear.

11. A simplified model has been proposed, based on a local stress/fracture zone opening relationship, which is able to describe the fracture processes more realistically than previous

models.

12. The length of the fracture process zone is dependent on the testing geometry and the local stress/fracture zone opening relationship. Hence the length of the zone is not an intrinsic material property.

13. The contribution of the tail of the load/extension curve to the measured fracture energy is significant.

The research findings presented in this thesis have provided a greater understanding of the role of fracture process zones in the fracture of concrete. This understanding has enabled a more detailed interpretation of the results of direct tensile tests to be made than had previously been possible. The test results have led to the proposal of a new model for the fracture process zone. The correlation between the test results and the model encourages further development and recommendations for further research are given in Chapter 11. It is hoped that the results of this further research will enable the model to be refined and verified.

Models of the type proposed will have wide application. They will enable the prediction of crack propagation and energy absorption in plain, reinforced and pre-stressed concrete structures. In some situations, such as mass concrete dams or reinforced concrete beams un-reinforced in shear, the models may be used to obtain the ultimate load carrying capacity. It will also be possible to study the effects of structural size on the fracture characteristics obtained. This is essential if the results of laboratory tests on strength and cracking are to be properly applied in the design of concrete structures. It is envisaged that more complex models will be required for the analysis of concrete under multi-axial stress states and predominantly compressive stress states. These more general models, in common with the simple model presented in this thesis, will have to be based on the dual phenomena of localisation and strain-softening in the fracture of concrete.

Chapter 11 Recommendations for further research

11.1 Introduction

The principal part of the work carried out in the present project has been the development of a suitable tensile test technique for the observation of the initiation and propagation of fracture process zones in concrete. A limited series of tests has been conducted from which several useful conclusions can be drawn (Chapter 10). There are, however, drawbacks with the technique and various improvements are suggested in Section 11.2. The full benefits of the work conducted in this project will only be realised when a more comprehensive testing programme is conducted. A suggested outline of this programme is given in Section 11.3. Future research prospects are discussed in Section 11.4.

11.2 Improvements to existing techniques

Many difficulties were encountered in the control of the testing machine (Section 4.4.2.2.2) which were only overcome by cumbersome control systems. Even with these arrangements there was no guarantee that the tests would be successful. The primary root of the problems encountered was the fact that the testing machine was originally intended to be used for high speed dynamic response but was required to work at near-static conditions with very fine control over the movement of the ram. The control problems which resulted could be largely circumvented by changes in some of the equipment used. The key to improving the near-static response of the system is to reduce the mechanical gain so that the electrical gain of the system can be increased without causing dynamic instability. This could be achieved by reducing the flow capacity of the servo-valve to such a level that the maximum flow results in only a gradual movement of the ram. This may have a secondary advantage in deadening the response of the system to unwanted electrical interference.

One other disadvantage of the existing technique is the need for the stiffening bars in parallel with the specimen. This led to a reduction in accuracy in load measurement and also placed a limit on the maximum specimen extension obtainable. The bars are required to increase the axial stiffness of the testing machine and to restrain the relative rotations of the ends of the specimen. One advantage of the bars is that they have allowed the use of Integral Gain as described in Section 4.4.2.2.3. Before the bars could be dispensed with it would be necessary to check that sufficient control could be obtained by using Proportional Gain together with the reduced flow of the servo-valve. If this proved to be possible, then the bars could be removed provided the stiffness requirements were met in some other form. This could be achieved by using a specially designed actuator which would have to be axially stiff (greater than 5000KN/mm) and capable of preventing rotation of the end of the specimen. The maximum stroke of the actuator need not be greater than 5mm. and the maximum displacement rate could be as low as 1.0mm./minute. One further advantage of the new actuator could be the inclusion of hydrostatic bearings to reduce the friction and increase the accuracy of load measurement. It would

be necessary to check that the bearings employed did not allow lateral movement of the ram and rotation of the end of the specimen. A secondary advantage of dispensing with the parallel bars would be that direct measurement of the load on the specimen could be made. This would allow continuous monitoring of the specimen load and facilitate the identification of the maximum load for the purpose of photographing the moire fringe patterns at this critical stage.

The combination of the actuator described above with a suitable low-flow servo-valve would have the following advantages:

1. The complexity of the testing technique would be reduced.
2. The likelihood of damage being done to the specimen through uncontrolled loading and electrical interference would be reduced.
3. The accuracy of the load measurement would be increased together with an improvement in the repeatability of the results.
4. The test could be allowed to continue until complete separation occurred so that the full load/extension curve would be obtained and the fracture energy correctly measured.

The disadvantage with this arrangement is in the cost which would be of the order of £10,000 at current prices.

There is one other possible solution which is to make use of the stiffness of the 100T actuator already available (Section 4.3). This actuator has a friction band of approximately +/- 1KN. which results in two difficulties. The first is that the differential pressure in the actuator could no longer be used to measure the applied load with sufficient accuracy. It would be necessary to introduce a separate very stiff load cell. A conventional strain gauged load cell would either be too flexible to allow stable failure in specimens of the dimensions used or would be insufficiently sensitive to the load. However piezo-electric load cells are available which are very sensitive as well as being very stiff. It may be possible that such a load cell could be used and still allow stable failure to occur. The second difficulty might be in the control of the displacement of the ram. It is not known whether it would be possible to control the ram to the required accuracy (+/- 0.1 micron) when the friction is so large and this would have to be checked before any decision was taken

on the choice of load cell. Should this option work it might achieve similar end results to the specially designed actuator but at a much reduced cost (of the order of £2,000).

11.3 Further tests required

The tests reported in this thesis can only be considered to be the first stage in the research (Section 7.1). Further research is required in order to refine and validate the fracture process zone model proposed in Section 9.4 and to provide data for the application of the model to a variety of concretes. The tests required are described in the following two sections.

11.3.1 Direct tensile tests

The direct tensile tests described in Chapters 8 and 9 were conducted on specimens of the same mix proportions, age and moisture state. A more comprehensive testing progamme is required to investigate the effects of variations in the materials and specimen geometry on the fracture processes measured. The following variations in the mix should be investigated:

1. Effects of aggregate size.
   The current research has indicated that the width of a fracture process zone is dependent on the maximum aggregate size for the type of aggregate used. The fracture energy may also be related to the zone width and hence to the maximum aggregate size and also on the grading of the aggregate.

2. Effects of aggregate surface condition.
   The fracture surface in the tests reported in this thesis often follows the aggregate/mortar interface. Terrien (1980) suggested that microcracks first occur at this interface and it would follow that the strength of the aggregate/mortar bond effects the initiation and propagation of fracture process zones.

3. Effects of aggregate shape.
   It has been suggested that stress transfer across an opening

fracture process zone is largely due to aggregate interlock which would be dependent on the aggregate shape.

4. Effects of aggregate type.
   Aggregate particles were only occasionally fractured in the tests reported in Chapter 8 indicating that the fracture was forced to pass round the aggregate rather than through it. This would not happen with some other types of aggregate. Tests using lightweight aggregate would be of particular interest especially in terms of the factors controlling the width of the fracture process zone and the energy absorbed.

5. Effects of water/cement ratio.
   The quality of the matrix will affect all the parameters measured in the tests. A decrease in water/cement ratio may increase the apparent brittleness of the specimens to such an extent that stable failure cannot be obtained with specimens of the dimensions used.

6. Effects of other mix constituents.
   The effects of changes in other mix constituents are expected to be less significant than those due to changes in aggregate and water/cement ratio, however, this still needs to be confirmed. The variables might include the aggregate/cement ratio, the type of cement and also the use of additives such as plasticisers and air entraining agents.

7. Effects of addition of fibres.
   Fibre reinforcement has little effect on the response of concrete prior to fracture initiation but are expected to significantly alter the fracture energy and fracture propagation.

It will also be necessary to investigate the effects of age and curing conditions on the fracture processes, before the results from the above tests may be properly utilised:

1. Effects of age.
   The tensile strength, Young's modulus and brittleness of concrete all increase with age. The effects on fracture energy, fracture initiation and propagation are less clear.

2. Effects of curing conditions.

   The specimens in the current project were cured in such a manner as to prevent moisture migration either into or out of the specimen. This is typical of concrete within the body of a structure, however, the concrete near the surface which is particularly important when considering durability, may not be cured so effectively.

In addition to the effects of variations in the concrete properties, the effects of variations in specimen geometry and type of loading should also be investigated as follows:

1. Effects of notches in the specimen.

   Most other tests on the fracture properties of concrete have been conducted on specimens which included notches. To enable the correct interpretation of these test results, the effects of the notches have to be evaluated.

2. Effects of specimen size.

   The results of other test techniques have been shown to depend on specimen size. In order that the conclusions drawn from the current project may be fully verified it must be demonstrated that neither the specimen length nor the cross-section affects the local stress/fracture zone opening relationship obtained.

3. Effects of cyclic loading.

   These effects should be studied with particular reference to the growth, if any, of fracture process zones under cyclic loading.

4. Effects of rate of loading.

   The effects of increased rates of loading and also sustained loading both prior to and subsequent to attainment of maximum load should be investigated.

The local field strain/fracture zone opening relationship needs to be more thoroughly investigated. The field strain has not been measured sufficiently accurately for the relationship to be properly evaluated. It is suggested that a combination of electrical resistance strain

gauges, placed to the side of the fracture process zone, together with moire interferometry could be used.

11.3.2 Other tests

In order to confirm that the conclusions drawn from the direct tensile tests regarding the initiation and propagation of fracture process zones, it is necessary to conduct some other type of test in which tensile fracturing can be observed. It is suggested that stable three point bend tests be conducted on specimens of several sizes. The requirements for the stability of such tests are less onerous than for the direct tensile test and there should be no difficulty in modifying the tensile test rig to conduct the beam tests. In these tests the strain distribution is not uniform and the results should provide information on the propagation of fracture in conditions significantly different to those occurring in a direct tensile test.

11.4 Future research prospects

The results of the tests described in Section 11.3 should allow further refinement of the model for stress transferred across a fracture process zone (Section 9.4). This model should then be applied using the finite element method and correlated with the results published in the literature of tests conducted on specimens of other geometries. Provided that reasonable agreement is obtained with a range of different specimen geometries and sizes, the model could then be applied to structural anaysis.

The work described in this thesis has concentrated on Mode I fracture. It has been suggested that this is the primary fracture mode for concrete. So called 'Mixed Mode' fracture can occur when the fracture path is not straight or where non-proportional loading occurs. In this case shear displacement occurs along a previously formed fracture process zone. The effects of this shear displacement and also multi-axial stress fields will have to be investigated before a complete model of the fracture process zone is obtained.

Appendix A

Mathematical model of the adhesive layer between the concrete specimen and the testing machine

The adhesive layer is modelled as an elastic material undergoing plane strain. The unrestrained lateral contractions of the steel platen, adhesive layer and concrete specimen are dependent on the values of the ratio between Poisson's ratio and Young's modulus for each material. This value is very low for steel so that the lateral strain is small, consequently, the boundary conditions along the steel/adhesive interface are that displacements in the x and y directions are assumed to be zero. At the adhesive/concrete interface the boundary conditions are that the normal stress is equal to the applied stress and that the lateral strain is equal to the unrestrained lateral strain of the concrete under uniaxial tension. This last condition overestimates the lateral strain at this interface since it ignores the restraining effect of the shear stresses across the interface, however, without a far more sophisticated model, a more accurate solution cannot be obtained. The current model is considered to be sufficiently accurate to enable an understanding of the problem to be gained. The model and it's boundary conditions are summarised in Figure A.1. The solution has been obtained using an Airy Stress Function expressed as a half range expansion Fourier series.

The Stress function is given by:

$$\phi = \sum_{n=1}^{\infty} \sin \alpha x \, (C_1 \cosh \alpha y + C_2 \sinh \alpha y + C_3 \alpha y \cosh \alpha y + C_4 \alpha y \sinh \alpha y)$$

where $\alpha = \frac{n\pi}{L}$ (A.1)

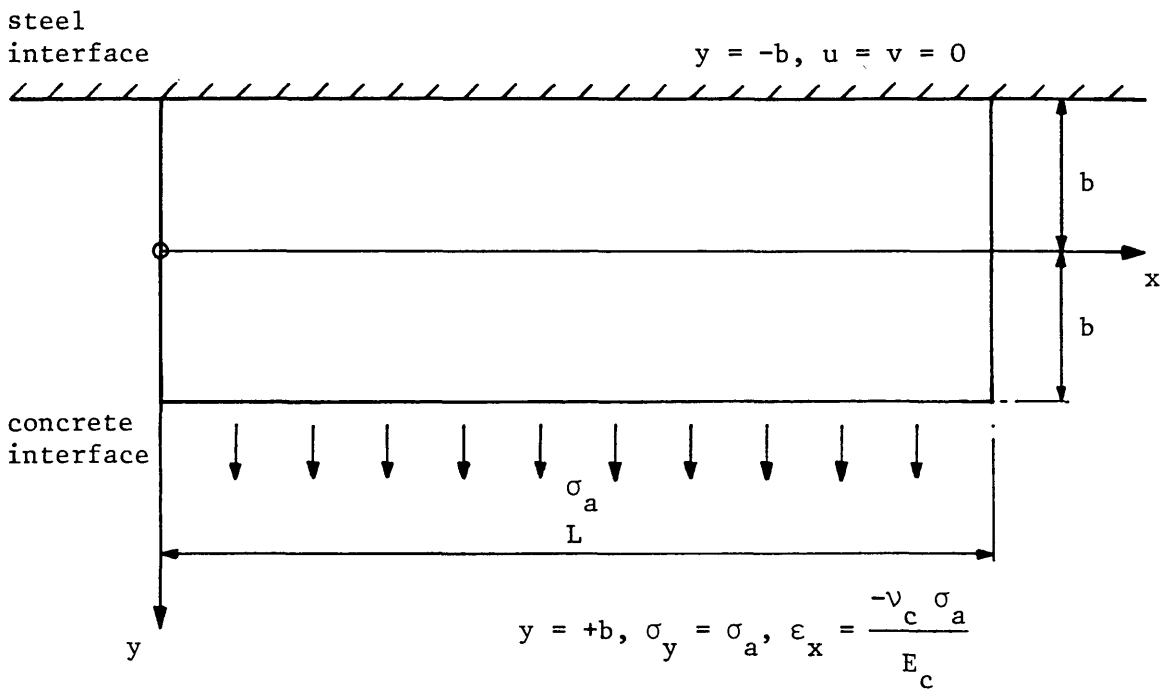

Fig. A.1 Model of adhesive layer

Differentiating to obtain the stresses:

$$\sigma_y = \frac{\partial^2\phi}{\partial x^2} = -\sum \alpha^2 \sin \alpha x \,(C_1 \cosh \alpha y + C_2 \sinh \alpha y + C_3 \alpha y \cosh \alpha y + C_4 \alpha y \sinh \alpha y) \quad \text{(A.2)}$$

$$\sigma_x = \frac{\partial^2\phi}{\partial y^2} = \sum \alpha^2 \sin \alpha x \,\{C_1 \cosh \alpha y + C_2 \sinh \alpha y + C_3(2\sinh \alpha y + \alpha y \cosh \alpha y) + C_4(2\cosh \alpha y + \alpha y \sinh \alpha y)\} \quad \text{(A.3)}$$

$$\tau_{xy} = -\frac{\partial^2\phi}{\partial x \partial y} = -\sum \alpha^2 \cos \alpha x \,\{C_1 \sinh \alpha y + C_2 \cosh \alpha y + C_3(\cosh \alpha y + \alpha y \sinh \alpha y) + C_4(\sinh \alpha y + \alpha y \cosh \alpha y)\} \quad \text{(A.4)}$$

For plane strain:

$$\varepsilon_x = \frac{\partial u}{\partial x} = \frac{1}{E}\left((1-\nu^2)\sigma_x - (\nu+\nu^2)\sigma_y\right) \quad \text{(A.5)}$$

$$\varepsilon_y = \frac{\partial v}{\partial y} = \frac{1}{E}\left((1-\nu^2)\sigma_y - (\nu+\nu^2)\sigma_x\right) \quad \text{(A.6)}$$

By combining Equ. A.2, A.3 and A.5 and integrating the following is obtained:

$$u = -\frac{1}{E}\sum \alpha \cos \alpha x \,\{C_1(1+\nu)\cosh \alpha y + C_2(1+\nu)\sinh \alpha y + C_3\{2(1-\nu^2)\sinh \alpha y + (1+\nu)\alpha y \cosh \alpha y\} + C_4\{2(1-\nu^2)\cosh \alpha y + (1+\nu)\alpha y \sinh \alpha y\}\} + f_1(y) \quad \text{(A.7)}$$

Similarly, by combining Equ. A.2, A.3 and A.6 and integrating:

$$v = -\frac{1}{E}\sum \alpha \sin \alpha x \left(C_1(1+\nu)\sinh \alpha y + C_2(1+\nu)\cosh \alpha y\right.$$

$$+ C_3\{(2\nu^2+\nu-1)\cosh \alpha y + (1+\nu)\alpha y \sinh \alpha y\}$$

$$\left. + C_4\{(2\nu^2+\nu-1)\sinh \alpha y + (1+\nu)\alpha y \cosh \alpha y\}\right) + f_2(y) \qquad (A.8)$$

It is known that:

$$\gamma_{xy} = \frac{\partial u}{\partial y} + \frac{\partial v}{\partial x} = \frac{\tau_{xy}}{G} \qquad (A.9)$$

Differentiating Equ. A.7 and A.8 and substituting with Equ. A.4 into Equ. A.9, it can be shown that:

$$\frac{\partial f_1}{\partial y} + \frac{\partial f_2}{\partial x} = 0$$

Therefore:

$$f_1(y) = D_1 y + D_2$$
$$f_2(y) = -D_1 y + D_3 \qquad (A.10)$$

The applied stress can be expressed as a half range expansion Fourier series:

$$\sigma_a = \sum_{n=1}^{\infty} \sigma_n \sin \alpha x \qquad (A.11)$$

where $\sigma_n = \frac{4\sigma_a}{\alpha L}$ for n odd

$= 0$ for n even

Therefore:

$$\sigma_a = \sum_{n=1,3,5} \frac{4\sigma_a}{\alpha L} \sin \alpha x \qquad (A.12)$$

Since all loading is proportional to the applied stress, which only contains terms with n odd, it follows that the stress function and it's derivatives also only have terms with odd n.

By considering symmetry and applying the boundary conditions the following expressions for the constants are obtained:

$$C_3 = \frac{\frac{P}{V}\left(RT + \alpha b - \alpha b T^2 - V(T + \frac{1}{T})\right) - Q\left(\alpha b T^2 + 2VT - RT - \alpha b\right)}{R - 2V - \alpha b T^3 - 2VT^2 + 2\alpha b T - \frac{\alpha b}{T} + RT^2} \quad (A.13)$$

$$C_4 = Q + \frac{P}{V} - C_3 T \quad (A.14)$$

$$C_1 = P - C_4(2V + \alpha b T) \quad (A.15)$$

$$C_2 = \frac{P}{T} - C_3(2V + \frac{\alpha b}{T}) \quad (A.16)$$

where $P = -\frac{2\nu_c E}{(1+\nu)E_c}\frac{\sigma_a}{\alpha^3 L}\frac{1}{\cosh \alpha b}$

$$Q = \frac{2\sigma_a}{L(1-\nu)\cosh \alpha b}$$

$$R = (2\nu-1)$$

$$T = \tanh \alpha b$$

$$V = (1-\nu)$$

E, E_c = Young's moduli for adhesive and concrete, respectively

ν, ν_c = Poisson's ratios for adhesive and concrete, respectively

These constants may be substituted into Equations A.2, A.3, A.4, A.8, and A.9 to obtain the stresses and displacements of the adhesive under load. A Fortran computer program has been used to evaluate these results taking the first 300 terms of the Fourier series. Of particular interest is the shear stress across the adhesive concrete interface. An outward shear stress applied to the concrete subjects it to triaxial tension and reduces the applied load at which the concrete will fail adjacent to the adhesive. This shear stress is plotted in Figure A.2 for various values of Poisson's ratio and adhesive layer thickness. The Young's moduli of concrete and adhesive have been taken as $30KN/mm^2$ and $7KN/mm^2$ respectively. It should be noted that the model gives erroneous results at the outside edge of the concrete where the shear stress should reduce to zero. The variation in peak outward shear stress with adhesive layer thickness is shown in Figure A.3.

The principal stresses in three dimensional elasticity are given by:

$$s^3 - (\sigma_x + \sigma_y + \sigma_z)s^2 + (\sigma_x\sigma_y + \sigma_y\sigma_z + \sigma_x\sigma_z - \tau_{yz}^2 - \tau_{xz}^2 - \tau_{xy}^2)s$$

$$- (\sigma_x\sigma_y\sigma_z + 2\tau_{yz}\tau_{xz}\tau_{xy} - \sigma_x\tau_{yz}^2 - \sigma_y\tau_{xz}^2 - \sigma_z\tau_{xy}^2) = 0 \qquad (A.17)$$

Then the principal tensile stress is approximately given by:

$$s = (0.5 + \sqrt{(0.25 + 2(\tau_{xy}/\sigma_a)^2})\sigma_a \qquad (A.18)$$

The relationship between peak stress and adhesive layer thickness is shown in Figure A.4.

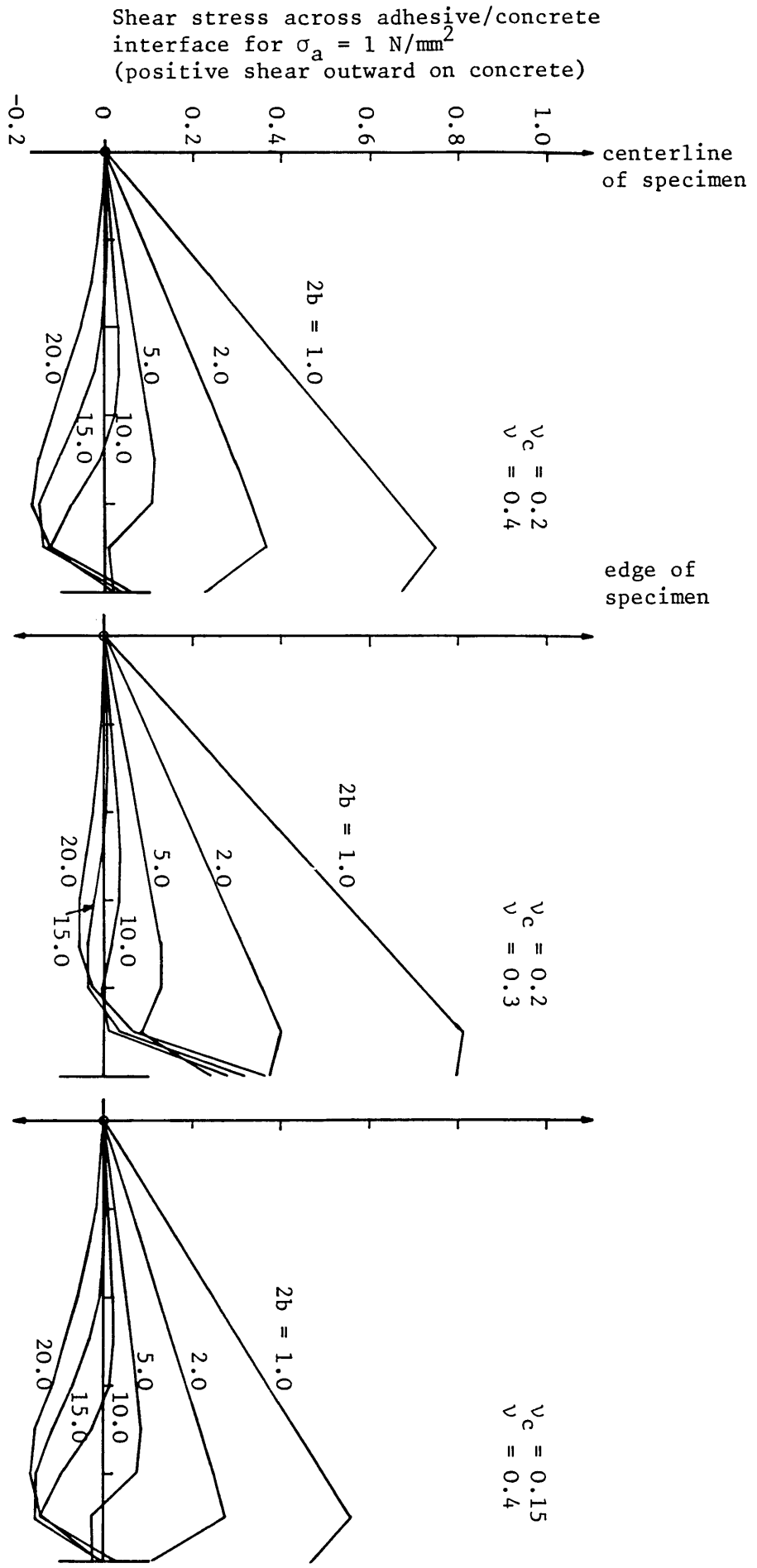

Fig. A.2 Shear stress across the adhesive/concrete interface

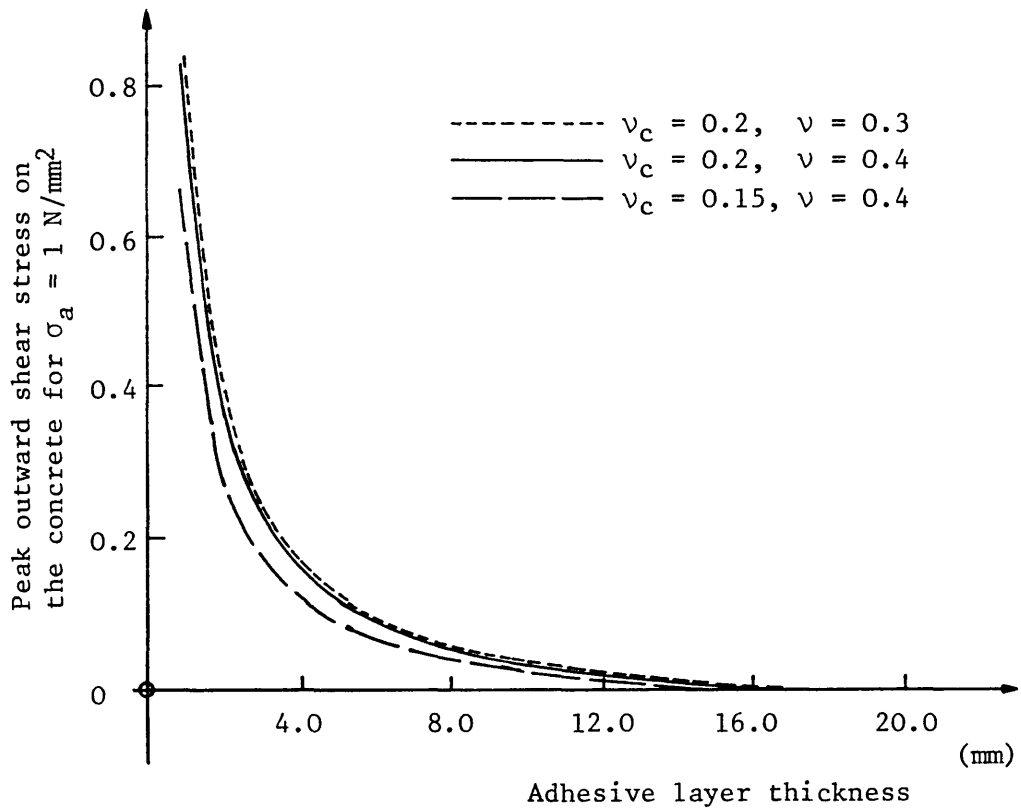

Fig. A.3 Peak outward shear stress

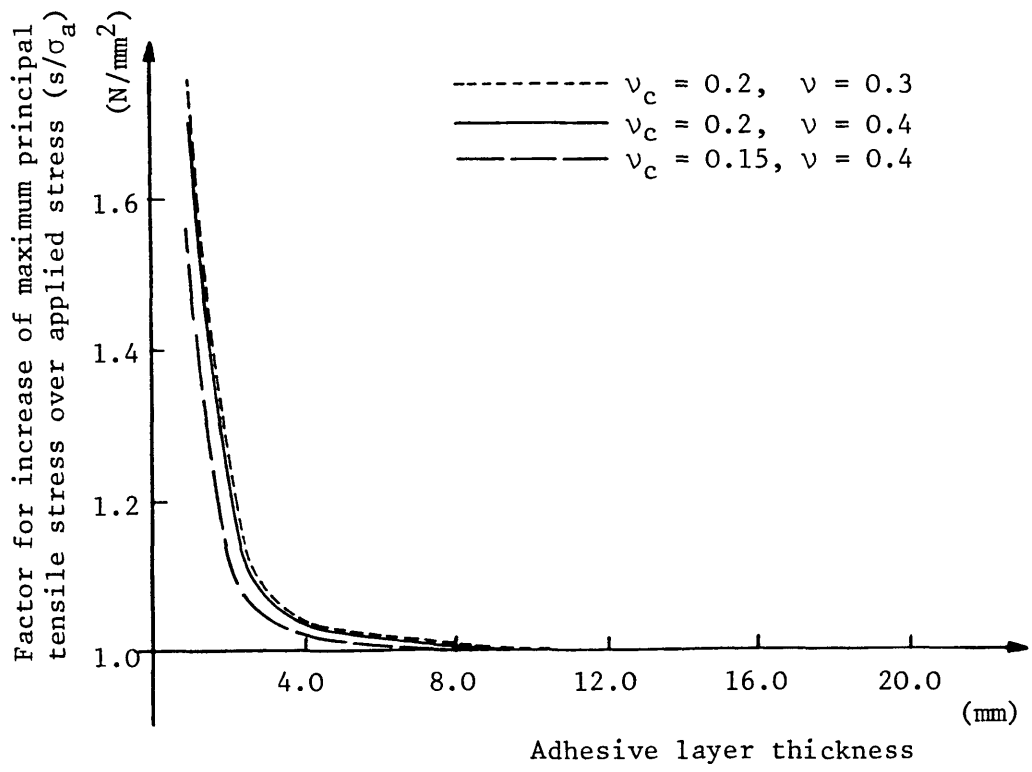

Fig. A.4 Peak increase in principal tensile stress

Appendix B

Specimen casting

The mix proportions used for the concrete specimens are given in Table B.1.

10mm. Aggregate	2.09
Coarse sand	2.09
Fine sand	1.05
Cement	1.00
Free water	0.60

Table B.1 Concrete mix proportions by weight
Aggregate in saturated surface dry condition

The aggregate was partially crushed Thames Valley Gravel and was dried and stored in bins in the laboratory, it was therefore, necessary to determine the moisture content and water absorption of the material in the bins. Moisture content and water absorption tests were conducted in accordance with BS 812 (1975). It proved very difficult to ascertain the saturated surface dry state for the sands with the result that the water absorption tests for the sands were unreliable. Since the sand and coarse aggregate came from the same source it was assumed that the water absorption for all three materials was that obtained for the coarse aggregate. The test results are given in Table B.2.

Material	Moisture content	Water absorption
10mm. Aggregate	0.40%	2.0%
Coarse Sand	0.25%	-
Fine Sand	0.25%	-

Table B.2 Measured aggregate moisture content and water absorption

The aggregate was soaked overnight and drained for half an hour prior to mixing. Sufficient water was added to the mix to obtain the correct combined weight of aggregate and water. The concrete was mixed for 4 minutes in a pan mixer. Three different fresh concrete tests were conducted to BS 1881 (1983), the slump test, the Vebe test and the air content using Method A. The results of these three tests, together with the 28 day cube strength, are given in Table B.3 for the batches in the final test series. The cube strengths were the average of three 4-inch cube results for each batch of concrete, with the exception of batch L for which only two cubes were available. Each batch contained sufficient concrete for the slump test (the concrete from which was re-used for the Vebe test), the air content test, three cubes and two tension specimens.

It is interesting to note that there is a slight change in the concrete properties for the different batches cast during a 10 week period, despite the batch weights remaining identical. Towards the end of the test series the slump was reduced and the cube strength slightly increased. This may be due to the fact that the source for the fine sand was changed approximately half way through the casting programme. It was found that it was more difficult to drain sufficient water from the soaked aggregate in the latter part of the programme. It may be that the new fine sand had a slightly greater water absorption than the original and also a different grading. Since the materials were mixed in the bins it was impossible to verify these conjectures. The coefficient of variation of all the test cube results was only 4.2% and the changes in material properties are not

considered significant. The specimens were cast in 3 layers, in a pair of moulds on a vibrating table.

Batch	Slump (mm)	Vebe time (Sec)	Air content (%)	28 day cube Strength (N/mm^2)
A	75	1.8	1.1	34.4
B	65	1.7	1.0	36.7
C	80	1.9	0.9	34.4
D	60	1.0	1.0	36.3
E	80	1.4	0.9	35.1
F	50	1.8	1.2	35.6
G	65	1.8	1.1	34.5
H	55	2.4	0.9	37.1
I	50	2.4	0.8	37.4
J	70	2.3	0.6	37.5
K	45	2.6	0.8	36.7
L	50	2.2	0.6	36.5

Table B.3 Fresh concrete properties and 28 day cube strengths for the 12 batches used in the final test series

Appendix C

Tests on specimen surface sealers

It was necessary to seal the surfaces of the specimen against moisture migration for up to 8 days. During this period, the specimen end plates were stuck in position, the interference grating was applied and the specimen tested. It was decided that a sealant that could be brushed on was most suitable. There did not appear to be any easily applied material which would seal a damp concrete surface perfectly without strengthening the surface or affecting it in some other way. Tests were conducted on several materials. Damp 4-inch cubes were painted with the curing agent and then suspended in the laboratory atmosphere. The weight loss was measured and, although the tests cannot be considered conclusive since the weight loss must depend on individual cube permeability, they give a good comparison between the different materials. The results for 3 different curing agents with different numbers of applications are given in Figure C.1.

3 coats of Cormix CM90 give the best seal and this material was used in the final test series. It should be noted that although there appears to be a relatively large weight loss in the first few hours of the cube with the chosen material, it was difficult to know exactly when the solvent had evaporated and so the zero reading may not be particularly accurate. Two other advantages of Cormix CM-90 are the short time required between coats (20 minutes) and the fact that it is water rather than spirit based.

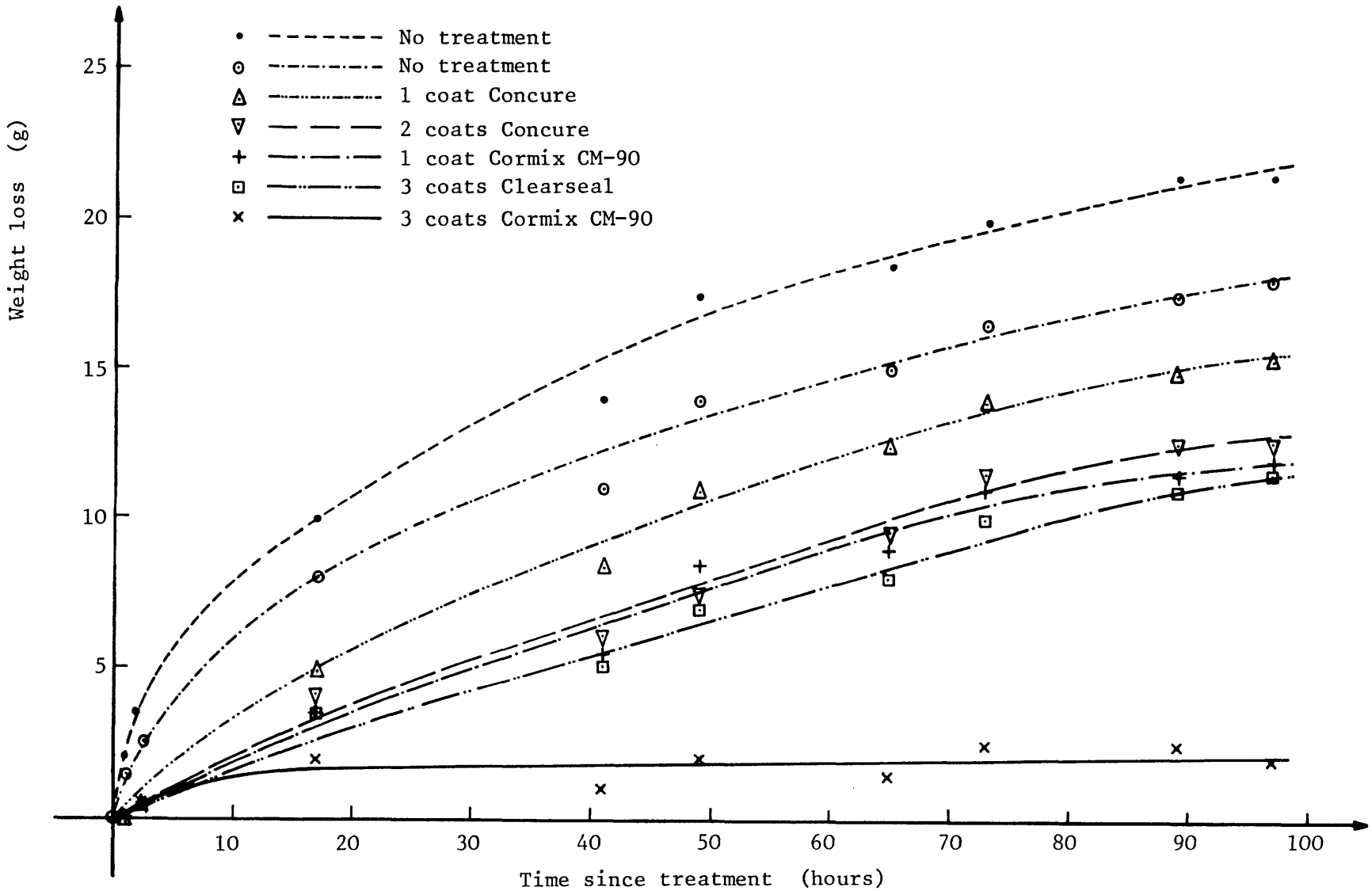

Fig. C.1 Tests on specimen surface sealers

Appendix D

Specimen grating manufacture

Specimen gratings are manufactured by a replication mould process. The first stage is to make a silicone rubber replica on a glass substrate of the master grating. The steps in manufacture of the silicone grating are as follows:-

1. Wash the glass plate (135mm.x110mm.x4mm.) with soap and hot water, rinse and allow to dry.
2. Prime one face of the plate and it's edges with Eccosil Primer S.11 to ensure good adhesion of the silicone rubber to the glass.
3. Mix the silicone rubber (see Table D.1) in a test tube using a wooden dowel in the chuck of an electric drill; de-gas in a vacuum desiccator and centrifuge at 3000rpm. for 5 minutes.
4. Pour the silicone rubber into a 'star shaped' pool at the centre of the master grating with the points of the stars towards the corners of the grating.
5. Gently lay the glass plate, primed side down, onto the silicone rubber without trapping air bubbles, allowing the weight of the plate to squeeze the rubber out into a thin layer.
6. Wipe silicone rubber onto the edges of the plate.
7. Cure for 16 hours, in a draught-free environment, at approximately 22 degrees Centigrade.
8. Remove the silicone rubber replica using bolts in the threaded holes provided in the master grating. The bolts should be tightened very gently to allow slow ingress of air.

The specimen needs special preparation to receive the grating and the following steps need to be taken:

1. The face of the specimen must be as flat as possible and without too many holes. The first step, which may be undertaken when the specimen end plates are being stuck on (Section 7.3.1), is to fill

any surface voids. The face of the specimen is gently rubbed with a carborundum stone, under running water, to expose any voids just below the surface. When the end plates have been stuck on and the lining-up jig tightened, the surface is dabbed dry with a paper towel and Sikadur 31 adhesive worked into the surface voids. This adhesive, which is a two part moisture tolerant, epoxy resin, is supplied by Sika Ltd., Welwyn Garden City, Herts.. Excess adhesive is scraped off before the specimen is sealed (Section 7.3.2).

2. When the adhesive has hardened, the sealer is scraped off over the area of the grating and any excess adhesive removed with a carborundum stone. The specimen is left under water whilst the material for the first layer of the grating is prepared.

The grating is applied in three layers, the first two using a moisture tolerant epoxy resin and the final layer using a special casting resin. The purpose of the moisture tolerant epoxy layers is to seal the damp concrete and provide a dry flat surface for the final layer. It was found that the first layer, on it's own would not seal the concrete sufficiently well. Green dye is added to the second and third layers of the grating to absorb any laser light penetrating the grating and prevent scatter of the light from the concrete surface. The techniques for the application of the three layers are similar and may be summarised as follows:

1. Mix the appropriate resin (Table D.1), de-gas and centrifuge in a similar manner to the silicone rubber.
2. Prepare the surface to receive the grating. For the first layer this means dabbing the surface with paper towels to remove surface moisture. For the second and third layers, scrape away the excess epoxy resin built up at the edges of the previous grating layer and blow with clean compressed air to remove any dust.
3. Support the specimen so that the face is horizontal and pour the resin into a 'star shaped' pool at the centre of the grating.
4. Gently lay a silicone rubber replica grating onto the resin without trapping air bubbles, allowing the weight of the replica to squeeze out the resin. The silicone grating should be new for the final layer but may be one which has already been used for the first two layers.
5. For the first layer, ensure that the resin overlaps the sealer on

the remainder of the specimen.

6. Align the fiducial lines of the silicone grating with the sides of the specimen, ensure that the replica is central with respect to the specimen and fix in position with masking tape.
7. Cure for 16 hours, in a draught-free environment, at approximately 22 degrees Centigrade.
8. Gently prise off the silicone grating by means of a small screw jack, allowing slow ingress of air.

The final grating should be checked in front of the Interferometer before testing. If the grating is not of sufficient quality the final layer should be repeated.

Grating type	Materials	Quantity (g)
Silicone replica	Eccosil 2CN	12.0
	Catalyst 25	0.24
Grating 1st. layer	Sikadur 94 Pt. A	6.00
	Sikadur 94 Pt. B	3.00
Grating 2nd. layer	Sikadur 94 Pt. A	6.00
	Sikadur 94 Pt. B	3.00
	Green dye solution	0.75
Grating 3rd. layer	Stycast 1266 Pt. A	6.75
	Stycast 1266 Pt. B	2.00
	Green dye solution	0.75

Table D.1 Grating materials

Sikadur 94 is supplied by Sika Ltd., Welwyn Garden City, Herts., all other materials are available from Emerson & Cuming Ltd., 1 South Park Rd., Scunthorpe, South Humberside, DN17 2BY.

Appendix E

Test procedure check list

1. CHECK SVDA GAIN SETTINGS: PROPORTIONAL = 050, INTEGRAL = 000, DIFFERENTIAL =000.
2. Upper platen and parallel bars to be fixed firmly in place.
3. All control electronics to be warmed up for at least 2 hours and data logger to be warmed up for at least 1 hour before the test.
4. Hydraulic Power Pack to be warmed up for at least 1 hour before the test, with the pressure turned up to maximum.
5. The Dither signal should be 1.0V amplitude and the external square wave input should be 1mV amplitude.
6. Ramp Generator to be set up: T_1 = 5.00, T_2 = 800.00, T_3 = 100.00, T_4 = 800.00, Compression, Continuous, Single, Ramp multipliers = x100, Output level = 417.
7. If not already done, stick specimen to bottom platen.
8. Fix extension transducer to bottom platen and adjust so that reading is approximately -0.2000mm. when set to level of upper side of top end plate. LOCK firmly in position.
9. Degrease and spread adhesive on top end plate.
10. Set ram to bottom of travel and press 'STOP'.
11. Spray adhesive activator on top platen and wipe area above transducer clean.
12. Bolt bottom platen tightly to ram.
13. Run data logger program 'TEST3'.
14. CHECK GAINS AS IN 1. ABOVE
15. Check holes in bottom platen and parallel bars are in line. Balance displacement knob and press 'START'.
16. Change to 'TEST' mode, run Ramp Generator to check that it works. Reset and return to 'STANDBY' mode.
17. Raise the ram until there is only a 5mm. gap above the specimen.
18. Screw nuts and spherical washers on parallel bars but not so far as to come into contact, take zero readings on data logger and check displayed zeros.

19. Turn up oil pressure to maximum and change to 'TEST' mode.
20. Change Monitor Unit to display extension and check that the 'Static Extension Level' indicator is near the right hand end.
21. Carefully raise ram under displacement control until the extension reading is approximately +0.8000, change to extension control.
22. Check Ramp Generator runs properly and reset.
23. Continue to raise ram under extension control, but keep monitoring the load on the separate digital voltmeter, until some load is registered, then raise the ram using the Ramp Generator running in compression until some small compressive load is maintained. The load should not be more than 1.0KN. (output signal = -0.200V).
24. Take 1st. reading on data logger and check for adhesive drips.
25. Tighten parallel bar nuts evenly to give approximately 3KN. in each bar. Ensure that the specimen remains slightly in compression either by running the Ramp Generator to increase the compression or, once there is a load of at least 1.0KN. applied to each of the parallel bars, increasing the SVDA Integral gain to reduce the compression.
26. Take 2nd. reading.
27. Slowly increase the SVDA Integral gain to 900 compensating all the time by running the Ramp Generator as required, to ensure that the specimen remains slightly in compression.
28. Take 3rd. reading. Run X-Y Plotter and check for vibrations.
29. Leave adhesive to go off for 45 minutes from time of first contact. Take readings every 15 minutes and ensure that the specimen does not go into tension as the adhesive shrinks. Check for slight vibration on plotter and adjust Dither signal if necessary.
30. If Interferometer is to be used, set it up on the carriage whilst adhesive is hardening.
31. Take 6th. reading and check plotter for vibrations.
32. Increase SVDA Integral gain to 950 with compensation from the Ramp Generator as in 27. above.
33. Reset plotter and check vibrations.
34. CHECK VIBRATIONS THROUGHOUT THE TEST, adjusting Dither signal if necessary. Check that plotter does not run off end of scale.
35. Switch to AUTO0.5 reading mode (automatic reading storage at 0.5 micron extension), subsequently changing to FAST reading mode (all readings stored) at a specimen load of 4.0KN and then back down to

AUTO0.5 and AUTO2.0 (automatic reading storage at 2.0 micron extension) as required during the descending portion of the test.

36. If the Interferometer is being used, HOLD the Ramp Generator at zero specimen load for photographs and again at the preselected specimen load levels. Continuously monitor the specimen applied load. If this load begins to fall, or if localisation appears in the strain field, press HOLD and take a set of photographs. Take further photographs as required. Record the reading numbers during which photographs are taken.
37. If the ramp runs out, press 'RESET', set T_1 to 100.00, switch to 'Tension' and press 'RUN'.
38. At end of test, press 'HOLD'.
39. Press key to end data logger program and check graph.
40. RESET SVDA GAIN TO 000, reduce oil pressure to 1000psi. and press 'STOP'.
41. Undo and remove nuts on parallel bars.
42. Balance displacement knob and press 'START'.
43. Lower ram in displacement control to bottom of travel and turn machine off.

Appendix F

Theoretical basis for digitising programs

Three interactive computer programs have been written; LSEC, for the analysis of fringe patterns along a line in the grating principal direction, TSEC, for the analysis of fringe patterns along lines other than in the principal direction, and INTERP, for the interpolation of previously analysed data and the subtraction of zero fields. Data input is by means of a digitising tablet (0.1mm. resolution).

The analysis is based on the discretisation of the normal moire formula:

$$\varepsilon_x = p \frac{\partial N}{\partial x} \qquad (F.1)$$

where ε_x = strain in the principal direction
p = grating pitch
= 1/950 mm.for vertical and horizontal gratings
= $1/(950 \times \sqrt{2})$ mm. for 45 degree gratings
N = fringe order
x = distance in the principal direction.

Equ. F.1 is discretised as follows:

$$\varepsilon_x = p \frac{n}{s} \qquad (F.2)$$

where n = number of fringes between digitised points which must lie on a line in the principal direction
s = distance between digitised points.

The analysis in program LSEC may be visualised by considering the fringe pattern shown in Figure F.1. The positions of the datum point and fringes I and I + 1 are entered into the computer via the digitising tablet. The strain in the principal direction is then calculated from Equ. F.2. and attributed to the point X. By entering the data for several fringe positions the variation of strain in the principal direction may be calculated.

The analysis in program TSEC is similar to that for LSEC except that the distance between fringes is measured along the grating principal direction, now no longer parallel to the line along which the analysis is taken. This is shown in Figure F.2. The positions of the datum point and X, A and B are entered into the computer. The strain is again calculated using Equ. F.2 and attributed to the point X. It should be noted that A and B should be chosen approximately equally spaced on either side of X. By entering several sets of data the variation of strain along the analysis line may be calculated.

As a check on the accuracy of the digitising, two runs of data input are required by each program. The error between the two runs is displayed and the choice is given of storing the average data in an output file or discarding it in favour of re-digitising.

Program INTERP, interpolates each section in the stored strain file, at 0.1mm. intervals, using a cubic spline curve. If required a zero strain field file may then be subtracted. The program outputs the data at 1.0mm. intervals and also the positions of strain contour points.

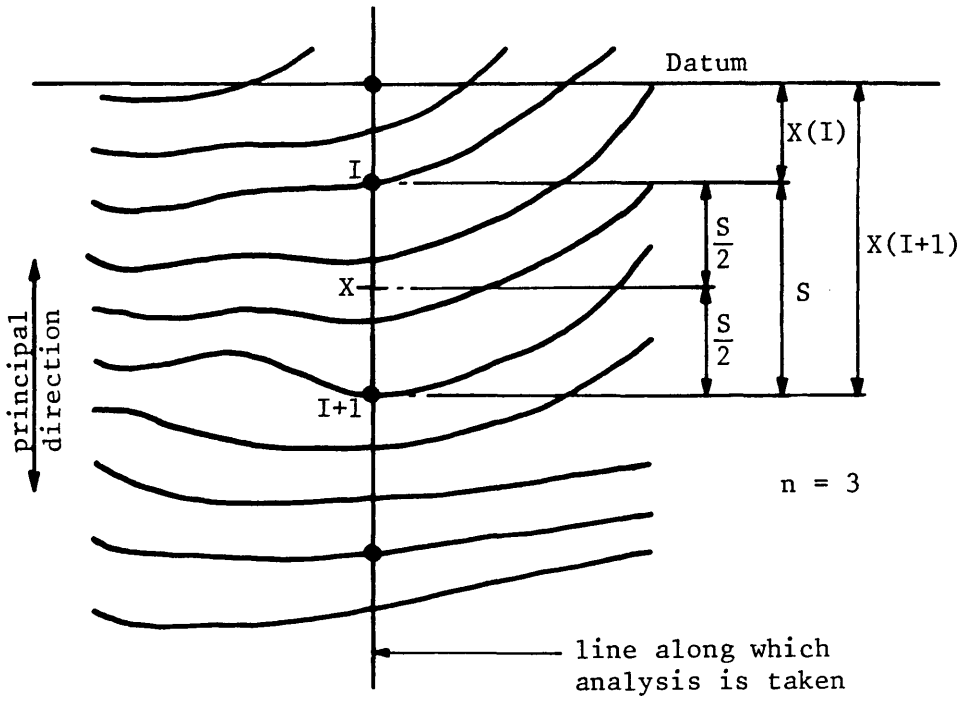

Fig. F.2 Digitising data for longsection

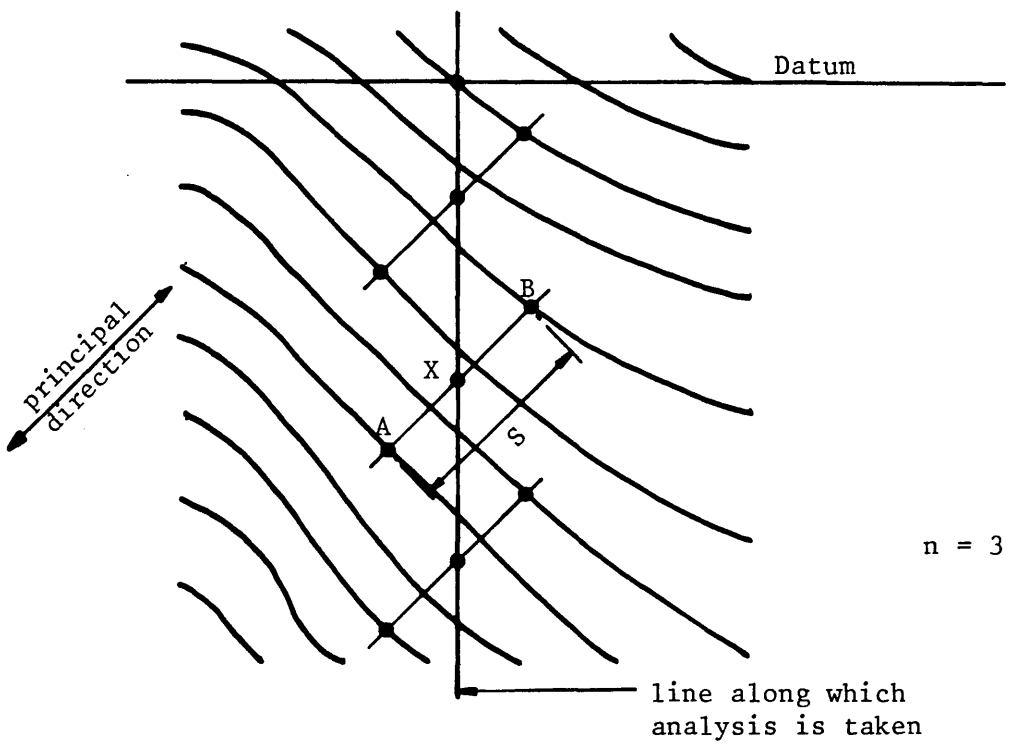

Fig. F.2 Digitising data for transverse section

References

Allison, I.M. and Ennos, A.E. (1981) Evaluating two dimensional strain distributions using speckle pattern photography and photoelasticity. Proc. IUTAM Symp., Optical Methods in Mechanics of Solids, Poitiers, Sept. 1979, Ed. Lagarde, A., Sijthoff and Noordhoff, pp. 323-330.

Archbold, E., Burch, J.M. and Ennos, A.E. (1970) Recording of in-plane surface displacement by double-exposure speckle photography. Optica Acta, Vol. 17, No. 12, pp. 883-898.

Archbold, E. and Ennos, A.E. (1972) Displacement measurement from double-exposure laser photographs. Optica Acta, Vol. 19, No. 4, pp. 253-271.

Archbold, E. and Ennos, A.E. (1975) Laser photography to measure the deformation of weld cracks under load. Nondestr. Test., Vol. 8, Aug., pp. 181-184.

Archbold, E., Ennos, A.E. and Virdee, M.S. (1978) Speckle photography for strain measurement - a critical assessment. 1st. European Cong. on Optics Applied to Metrology, Soc., of Photo-Optical Instrumentation Engineers, Vol. 136, (1977), pp. 258-264.

Barenblatt, G.I. (1962) The mathematical theory of equilibrium cracks in brittle fracture. Advances in Appl. Mech., Vol. 7, pp. 55-129.

Barker, D.B., Hawkins, N.M., Jeang, F.L., Cho, K.Z. and Kobayashi, A.S. (1985) Concrete fracture in CLWL Specimen. J. of Eng. Mech., ASCE, Vol. 111, No. 5, pp. 623-638.

Barr, B.I.G. and Sabir, B.B. (1985) Fracture toughness testing by means of the compact compression test specimen. Mag. of Concr. Res., Vol. 37, No. 131, pp. 88-94.

Basehore, M.L. and Post, D. (1981) Moire method for in-plane and out-of-plane displacement measurements. Exp. Mech., Vol. 21, pp. 321-328.

Basehore, M.L. and Post, D. (1982) Displacement fields (U,W) obtained simultaneously by moire interferometry. Applied Optics, Vol. 21, No. 14, pp. 2558-2562.

Bazant, Z.P. (1984a) Size effect in blunt fracture: Concrete, Rock, Metal. J. of Eng. Mech., ASCE, Vol. 110, No. 4, pp. 518-535.

Bazant, Z.P. (1984b) Imbricate continuum and it's variational derivation. J. of Eng. Mech., ASCE, Vol. 110, No. 12, pp. 1693-1712.

Bazant, Z.P., Belytschko, T.B. and Chang, T-P. (1984) Continuum theory for strain-softening. J. of Eng. Mech., ASCE, Vol. 110, No. 12, pp. 1666-1692.

Bazant, Z.P. and Cedolin, L. (1979) Blunt crack band propagation in finite element analysis. J. Eng. Mech. Div., Proc. ASCE, Vol. 105, EM2, pp. 297-315.

Bazant, Z.P. and Cedolin, L. (1980) Fracture mechanics of reinforced concrete. Fracture in Concrete. Proc. of a session sponsored by ASCE, Hollywood, Ed. Chen, W.F. and Ting, E.C., pp. 28-35.

Bazant, Z.P. and Chang, T-P. (1984a) Is strain-softening mathematically admissible? Engineering Mechanics in Civil Engineering, Proc. of the 5th. Eng. Mech. Div. Speciality Conf., ASCE, Wyoming, Ed. Boresi, A.P. and Chong, K.P., Vol. 2, pp. 1377-1380.

Bazant, Z.P. and Chang, T-P. (1984b) Instability of non local continuum and strain averaging. J. Eng. Mech., ASCE, Vol. 110, No. 10, pp. 1441-1450.

Bazant, Z.P. and Oh, B.H. (1981) Concrete fracture via stress - strain relations, Part 1 - Theory, Part 2 - Verification. Report No. 81-10/665C, Centre for Concrete and Geomaterials, The Technological Institute, Northwestern University, USA.

Bazant, Z.P. and Oh, B.H. (1983) Crack band theory for fracture of concrete. Materiaux et Constructions, Vol. 16, No. 93, pp. 155-177.

Bazant, Z.P. and Oh, B.H. (1985) Microplane model for progressive fracture of concrete and rock. J. Eng. Mech., ASCE, Vol. 111, No. 4, pp. 559-582.

Bedard, C. (1983) Non-linear finite element analysis of concrete structures. Ph.D. thesis, Univ. London.

Boone, P.M. (1970) Holographic determination of in-plane deformation. Optics Technology, Vol. 2, No. 2, pp. 94-98.

Boone, P.M. (1971a) Surface deformation measurements using deformation-following holograms. Nouvelle Revue D'Optique Appliquee, Vol. 1, No. 2, p10.

Boone, P.M. (1971b) A method for directly determining surface strain fields using diffraction gratings. Exp. Mech., Vol. 11, pp. 481-489.

Boone, P.M. (1976) Measurement of displacement, strain and stress by holography. The Engineering Uses of Coherent Optics, Proc. of a Conf., Univ. of Strathclyde, April 1975. Ed. Robertson, E.R., Cambridge University Press, Cambridge, pp. 81-98.

Bowles, D.E., Post, D., Herakovich, C.T. and Tenney, D.R. (1981) Moire interferometry for thermal expansion of composites. Exp. Mech., Vol. 21, pp. 441-447.

Brown, F.W. and Srawley, J.E. (1966) Plane strain crack toughness testing of high strength metallic materials. ASTM Special Technical Publication No. 410, Philadelphia.

Brown, J.H. (1972) Measuring the fracture toughness of cement paste and mortar. Mag. of Concr. Res., Vol. 24, No. 81, pp. 185-196.

Brown, J.H. (1973) The failure of glass-fibre-reinforced notched beams in flexure. Mag. of Concr. Res., Vol. 25, pp. 31-38.

Brown, J.H. and Pomeroy, C.D. (1973) Fracture toughness of cement paste and mortars. Cem. and Conc. Res., Vol. 3, pp. 475-480.

BS 1881 (1983) Testing of concrete. British Standards Institution, London.

BS 812 (1975) Methods for sampling and testing mineral aggregates, sands, and fillers. British Standards Institution, London.

Burch, J.M. and Tokarski, J.M.J. (1968) Production of multiple beam fringes from photographic scatters. Optica Acta, Vol. 15, No. 2, pp. 101-111.

Burdekin, F.M. and Stone, D.E.W. (1966) The crack opening displacement approach to fracture mechanics in yielding materials. J. Strain Anal., Vol. 1, pp145-153.

Burt, N.J. and Dougill, J.W. (1977) Progressive failure in a model heterogeneous medium. J. Eng. Mech. Div., Proc. ASCE, Vol. 103, EM3, pp. 365-376.

Butters, J.N. (1970) Applications of holography to instrument diaphragm deformations and associated topics. The Engineering Uses of Holography. Ed. Robertson, E.R. and Harvey, J.M., Cambridge University Press, Cambridge, pp. 151-169.

Butters, J.N. (1976) Electronic speckle pattern interferometry: a general review background to subsequent papers. The Engineering Uses of Coherent Optics, Proc. of a Conf., Univ. of Strathclyde, April 1975. Ed. Robertson, E.R., Cambridge University Press, Cambridge, pp. 155-169.

Butters, J.N. (1983) Speckle interferometry. Optical Transducers and Techniques in Engineering Measurement, Ch.7, Ed. Luxmoore, A.R., Applied Science Publishers, London, pp. 205-238.

Cady, P.D., Clear, K.C. and Marshall, L.G. (1972) Tensile strength reduction of mortar and concrete due to moisture gradients. J. Am. Concr. Inst., Vol. 69, pp. 700-705.

Carmicheal, G.D.T. and Jerram, K. (1973) The application of fracture mechanics to prestressed concrete pressure vessels. Cem. and Concr. Res., Vol. 3, No. 4, pp. 459-467.

Carpinteri, A. (1985a) Scale effects in fracture of plain and reinforced concrete structures. 'Fracture mechanics of concrete: Structural applications and numerical calculation', Martinus Nijhoff Publishers, Dordrecht, pp. 95-140.

Carpinteri, A. (1985b) Limit analysis for elastic-softening structures: Scale and slenderness influence on the global brittleness. Reprint, EUROMECH 204 Colloquium, Structure and crack propagation in brittle matrix composite materials, Warsaw, Nov. 12-15.

Carreira, D.J. and Chu, K-H. (1986) Stress-strain relationship for reinforced concrete in tension. J. Am. Concr. Inst., Vol. 83, pp. 21-28.

Cedolin, L. and Bazant, Z.P. (1981) Fracture mechanics of crack bands in concrete. Fracture Mechanics Methods for Ceramics, Rock and Concrete, ASTM, STP745, Ed. Freiman, S.W. and Fuller, E.R., pp. 221-236.

Cedolin, L., Dei Poli, S. and Iori, I. (1981) Analisi sperimentale del processo di formazione della frattura nel calcestruzzo. Studi e Ricerche, Corso di Perfezionamento per le Costruzioni in Cemento, Politecnico di Milano, Vol. 3, pp. 47-74.

Cedolin, L., Dei Poli, S. and Iori, I. (1983) Experimental determination of the fracture process zone in concrete. Cem. and Concr. Res., Vol. 13, No. 4, pp. 557-567.

Chen, W-F. and Ting, E.C. (1980) Constitutive models for concrete structures. J. Eng. Mech. Div., Proc. ASCE, Vol. 106, EM1, pp. 1-19.

Chiang, F-P. (1969) Techniques of optical spatial filtering applied to the processing of moire-fringe patterns. Exp. Mech., Vol. 9, pp. 523-526.

Chiang, F-P. (1979) Moire methods of strain analysis. Exp. Mech., Vol. 19, pp. 290-308.

Cho, K.Z., Kobayashi, A.S., Hawkins, N.M., Barker, D.B. and Jeang, F.L. (1984) Fracture process zone of concrete cracks. J. of Eng. Mech., ASCE, Vol. 110, No. 8, pp. 1174-1184.

Cook, D.J. and Crookham, G. (1978) Discussion of Gjorv, Sorensen & Arnesen (1977). Cem. and Concr. Res., Vol. 8, pp. 387-388.

Cooper. G.A. and Figg, J. (1972) Fracture studies of set cement paste. Trans. and J. of the Brit. Ceramic Soc., Vol. 71, pp. 1-4.

Cornelissen, H.A.W., Hordijk, D.A. and Reinhardt, H.W. (1985a) Experiments and theory for the application of fracture mechanics to normal and lightweight concrete. Preprints, RILEM Int. Conf. on Fracture Mechanics of Concrete, Lausanne, Vol. 1, pp. 419-429.

Cornelissen, H.A.W., Hordijk, D.A. and Reinhardt, H.W. (1985b) Post-peak tensile behaviour of lightweight versus normal-weight concrete. Paper presented at Euromech Seminar on Fracture in Brittle Matrix Composites, Warsaw, Nov. 1985.

Daniel, I.M., Rowlands, R.E. and Post, D. (1973) Strain analysis of composites by moire methods. Exp. Mech., Vol. 13, pp. 246-252.

De Backer, L.C. (1975) In-plane displacement measurement by speckle interferometry. Non-destructive testing, Vol. 8, pp. 177-180.

Denby, D. and Leendertz, J.A. (1974) Plane-surface strain examination by speckle-pattern interferometry using electronic processing. J. Strain Analysis, Vol. 9, No. 1, pp. 17-25.

Dougill, J.W. (1967) A mathematical model for the failure of cement paste and mortars. Mag. of Concr. Res., Vol. 19, No. 60, pp. 135-142.

Dougill, J.W. (1971) Further considerations of a mathematical model for progressive fracture of a heterogeneous material. Mag. of Concr. Res., Vol. 23, No. 74, pp. 5-10.

Dougill, J.W. (1983) Path dependence and a general theory for the progressively fracturing solid. Proc. R. Soc. Lond., A390, pp. 341-351.

Dougill,J.W. (1985) Structural and continuum aspects of fracture in brittle matrix composites. Paper for presentation at EUROMECH 204 Colloquium, 'Structure and crack propagation in brittle matrix composite materials', Warsaw, Nov. 12-15.

Dugdale, D.S. (1960) Yielding of steel plates containing slits. J. Mech. Phys. Solids, Vol. 8, pp. 100-104.

Durelli, A.J. and Parks, V.J. (1970) Moire analysis of strain. Prentice-Hall, Inc., Englewood Cliffs, New Jersey.

Durelli, A.J., Jacobson, R.H. and Okubo, S. (1956) Further studies of properties of stresscoat. Proc. SESA, Vol. 13, No. 1, pp. 35-53.

Durelli, A.J., Okubo, S. and Jacobson, R.H. (1955) Studies of some properties of stresscoat. Proc. SESA, Vol. 12, No. 2, pp. 55-76.

Eligehausen, R. and Sawade, G. (1985) Behaviour of concrete in tension. Parts 1 and 2. Betonwerk und Fertigeil-Technik, Heft 5, pp. 315-322 and Heft 6, pp. 389-391.

Ellis, G., Stern, F.B. and Baranowski, S.J. (1966) Brittle coatings. Exp. Mech., Vol. 6, Oct., pp. 19A-24A.

Elvery, R.H. and Haroun, W. (1968) A direct tensile test for concrete under long - or short - term loading. Mag. of Concr. Res., Vol. 20, No. 63, pp. 111-116.

Ennos, A.E. (1968) Measurement of in plane surface strain by hologram interferometry. J. Sci. Instrum., (J. Phys. E), Series 2, Vol. 1, pp. 731-746.

Ennos, A.E. and Archbold, E. (1976) Coherent optical tehniques for studying polmers. Plastics and Rubber: Materials and Applications, Vol. 1, Sept., pp. 116-122.

Evans, R.H. and Marathe, M.S. (1968) Microcracking and stress-strain curves for concrete in tension. Materiaux et Constructions, Vol. 1, pp. 61-64.

Evans, W.T. and Luxmoore, A.R. (1974) Measurement of in-plane displacements around crack tips by a laser speckle method. Eng. Fract. Mech., Vol. 6, pp. 735-743.

Gabor, D. (1948) A new microscopy principle. Nature, Vol. 161, pp. 777-778.

Gabor, D. (1949) Microscopy by reconstucted wave-fronts. Proc. Roy. Soc., A, Vol. 197, pp. 454-487.

Giglio, M., Musazzi, S., Perini, U. and Rossi, P. (1983) Visualizzione de zone microfessurate con tecniche de decorrelazione speckle su campioni intagtiati di calcestruzzo in T.P.B.T. stabili. XI Convegno Nazionale dell'Associazione Italiana per L'Analisi delle Sollecitazioni, Torino, Sept. 1983, pp. 211-220.

Gjorv, O.E., Sorensen, S.I. and Arnesen, A. (1977) Notch sensitivity and fracture toughness of concrete. Cem. and Concr. Res., Vol. 7, pp. 333-344.

Gluckich, J. (1963) Fracture of plain concrete. J. Eng. Mech. Div., Proc. ASCE, Vol. 89, EM6, pp. 127-138.

Glucklich, J. and Cohen, L.J. (1967) Size as a factor in the brittle-ductile transition and the strength of some materials. Int. J. of Fract. Mech., Vol. 3, pp. 278-289.

Go, C.G. and Swartz, S.E. (1984) The COD as a fracture criterion for concrete. Engineering Mechanics in Civil Engineering, Proc. of the 5th. Engineering Mechanics Division Speciality Conf., ASCE, Wyoming, Aug. 1984, Ed. Boresi, A.P. and Chong, K.P., Vol. 1, pp. 563-566.

Go, C.G., Swartz, S.E. and Hu. K-K. (1984) Stress intensity factors for single edge-notch beam. J. Eng. Mech., ASCE, Vol. 110, No. 4, pp629-633.

Gopalaratnam, V.S. and Shah, S.P. (1984) Post-cracking characteristics of concrete in uniaxial tension. Engineering Mechanics in Civil Engineering, Proc. of the 5th. Engineering Mechanics Division Speciality Conf., ASCE, Wyoming, Aug. 1984, Ed. Boresi, A.P. and Chong, K.P., Vol. 2, pp. 1393-1398.

Gopalaratnam, V.S. and Shah, S.P. (1985) Softening response of plain concrete in direct tension. J. Am. Concr. Inst., Vol. 82, pp. 310-323.

Griffith, A.A. (1921) The phenomena of rupture and flow in solids. Phil. Trans. R. Soc., A221, pp. 163-198.

Griffith, A.A. (1924) The theory of rupture. Proc. 1st. Int. Cong. App. Mech. Delft, pp. 55-63.

Gustafsson, P.J. (1985) Fracture mechanics studies of non-yielding materials like concrete: Modelling of tensile fracture and applied strength analyses. Report TVBM-1007, Lund Institute of Technology, Sweden.

Gylltoft, K. (1983) Fracture mechanics models for fatigue in concrete structures. Doctoral thesis 1983:25D, Lulea University of Technology, Sweden.

Gylltoft, K. (1984) A fracture mechanics model for fatigue in concrete. Materiaux et Constructions, Vol. 17, No. 97, pp. 55-58.

Hannant, D.J. (1972) The tensile strength of concrete: a review paper. Struct. Engr. Vol. 50, No. 7, pp. 253-258.

Heilmann, H.G., Hilsdorf, H. and Finsterwalder, K. (1969) Festigkeit und verformung von beton unter zugspannungen. Deutscher Ausschuss fur Stahlbeton, Heft 203, Wilhelm Ernst & Sohn, Berlin.

Higgins, D.D. and Bailey, J.E. (1976) Fracture measurements on cement paste. J. Mat. Sci., Vol. 11, pp. 1995-2003.

Hillemeier, B. and Hilsdorf, H.K. (1977) Fracture mechanics studies on concrete compounds. Cem. and Concr. Res., Vol. 7, pp. 523-536.

Hillerborg, A. (1978) A model for fracture analysis. Report TVBM-3005, Lund Institute of Technology, Sweden.

Hillerborg, A. (1984a) Additional concrete fracture energy tests performed by 6 laboratories according to a draft RILEM recommendation. Report TVBM-3017, Lund Institute of Technology, Sweden.

Hillerborg, A. (1984b) Round robin tests. Draft report, October 1984, Lund Institute of Technology, Sweden.

Hillerborg, A. (1985a) Influence of beam size on concrete fracture energy determined according to a draft RILEM recommendation. Report to RILEM TC50-FMC. Report TVBM-3021, Lund institute of Technology, Sweden.

Hillerborg, A. (1985b) Discussion of Wecharatana & Shah (1983) J. Eng. Mech., ASCE, Vol. 111, No. 1, pp. 113-117.

Hillerborg, A., Modeer, M. and Petersson, P-E. (1976) Analysis of crack formation and crack growth in concrete by means of fracture mechanics and finite elements. Cem. and Concr. Res., Vol. 6, pp. 773-782.

Hughes, B.P. and Chapman, G.P. (1965) Direct tensile test for concrete using modern adhesives. Bulletin RILEM, No. 26, pp. 77-80.

Hughes, B.P. and Chapman, G.P. (1966a) The complete stress - strain curve for concrete in direct tension. Bulletin RILEM, No. 30, pp. 95-97.

Hughes, B.P. and Chapman, G.P. (1966b) The deformation of concrete and microconcrete in compression and tension with particular reference to aggregate size. Mag. of Concr. Res., Vol. 18, No. 54, pp. 19-24.

Hurlbut,B.J. (1985) Experimental and computational investigation of strain-softening in concrete. Structural Research Series 8508, Dept. of Civil, Environmental and Architectural Engineering, Univ. of Colorado, Boulder, USA.

Inglis, C.E. (1913) Stresses in a plate due to the presence of cracks and sharp corners. Trans. Instn. Nav. Archit., Vol. 55, Pt.1, pp. 219-230.

Iori, I., Lu, H., Marozzi, C.A. and Pizzinato, E. (1982a) Metodo per la determinazione dei campi di spostamento nei materiali eterogenei (conglomerati naturali ed artificiali) a bassa resistenza specifica a trazione. L'Industria Italiana del Cemento, No. 4, pp. 275-280.

Iori, I., Lu, H., Marozzi, C.A. and Pizzinato, E. (1982b) Sulla determinazione sperimentale dei campi di spostamento nei calcestruzzi ordinari sottoposti a trazione. X Convegno Nazionale dell'Associazione Italiana per l'Analisi delle Sollecitazioni, Cosenza, pp. 271-279.

Irwin, G.R. (1957) Analysis of stresses and strains near the end of a crack transversing a plate. J. Appl. Mech., Vol. 24, pp. 361-364.

Isenberg, J. (1966) A study of cracks in concrete by X-radiography. RILEM Bulletin, No. 30, pp. 107-115.

Jacquot, P. and Rastogi, P.K. (1983) Speckle metrology and holographic interferometry applied to the study of cracks in concrete. Fracture Mechanics of Concrete. Ed. Wittman, F.H., Elsevier Science Publishers B.V., Amsterdam.

Janson, J. (1978) Damage model for crack growth and instability. Eng. Fract. Mech., Vol. 10, pp. 795-806.

Janson, J. and Hult, J. (1977) Fracture mechanics and damage mechanics, a combined approach. J. de Mecanique Appliquee, Vol. 1, pp. 69-84.

Jeang, F.L. and Hawkins, N.M. (1985) Non-linear analysis of concrete fracture. Report SM85-2, Dept. of Civ. Eng., Univ. of Washington, Seattle, USA.

Jones, R. (1974) Strain distribution and elastic-constant measurement using holographic and speckle-pattern interferometry. J. Strain Analysis, Vol. 9, No. 1, pp. 4-9.

Jones, R. (1976) The design and application of a speckle pattern interferometer for total plane strain field measurement. Optics and Laser Technology, Vol. 8, No. 5, pp. 215-219.

Kachanov, L.M. (1958) On the time to failure under creep conditions. Izu. Akad. Nauk SSSR, Otd. Tekh. Nauk (8), pp. 26-31 (In Russian).

Kachanov, L.M. (1971) Some problems of creep fracture theory. Advances in Creep Design, Ed. Smith, A.I. and Nicolson, A.M., Applied Science Publ., London, pp. 21-29.

Kaplan, M.F. (1961) Crack propagation and the fracture of concrete. J. Am. Concr. Inst., Vol. 58, pp. 591-610.

Kesler, C.E., Naus, D.J. and Lott, J.L. (1972) Fracture mechanics - it's applicability to concrete. Mechanical Behaviour of Materials, Proc. Int. Conf. on Mechanical Behaviour of Materials, Kyoto, Aug. 1971, The Soc. of Materials Science, Japan, Vol. 4, pp. 113-124.

Kim, M.M., Ko, H-Y. and Gerstle, K.M. (1980) Determination of fracture toughness of concrete. Fracture in Concrete. Proc. of a session sponsored by ASCE, Hollywood. Ed. Chen, W.F. and Ting, E.C., pp. 1-14.

Knott, J.F. (1973) Fundamentals of fracture mechanics. Butterworths London.

Kotsovos, M.D. (1978) Mathematical description of the deformational behaviour of concrete under generalised stress states. Interim report, Concrete Materials Research Group, Department of Civil Engineering, Imperial College of Science and Technology, London.

Kotsovos, M.D. and Newman, J.B. (1981) Fracture mechanics and concrete behaviour. Mag. of Concr. Res., Vol. 33, No. 115, pp. 103-112.

Krajcinovic, D. (1979) Distributed damage theory of beams in pure bending. J. Appl. Mech., ASME, Vol. 46, No. 3, pp. 592-596.

Leendertz, J.A. (1970) Interferometric displacement measurement on scattering surfaces utilising speckle effect. J. Sci. Instrum., (J. Phys. E), Series 2, Vol. 3, pp. 214-218.

Legendre, D. and Mazars, J. (1984) Damage and fracture mechanics for concrete (A combined approach). 6th. Int. Conf. on Fracture, New Delhi, India, Dec. 1984.

Lehmann, M. (1972) Fabrication of metallic gratings on photoresist by holographic recording. Proc. of the Engineering Applications of Holography Symposium, Los Angeles, sponsored by Advanced Research Projects Agency of the Dept. of Defence. pp. 327-330.

Loland, K.E. (1980) Continuous damage model for load-response estimation of concrete. Cem. and Concr. Res., Vol. 10, pp. 395-402.

Longhurst, R.S. (1973) Geometrical and Physical Optics. 3rd. edition, Longman, London.

Luxmoore, A.R. (1973) Holographic detection of cracks in concrete. Nondestr. Test., Vol. 6, pp. 258-263.

Luxmoore, A.R. (1974) Holographic detection of cracks. J. Strain Analysis, Vol. 9, No. 1, pp. 50-51.

Luxmoore, A.R., Amin, F.A. and Evans, W.T. (1974) In-plane strain measurement by speckle photography - a practical assessment of the use of Young's fringes. J. Strain Analysis, Vol. 9, No. 1, pp. 26-35.

McCreath, D.R. (1968) The fracture mechanics of concrete. Ph.D. thesis, Univ. London.

McDonach, A., McKelvie, J., MacKenzie, P. and Walker, C.A. (1983) Improved moire interferometry and applications in fracture mechanics, residual stress and damaged composites. Experimental Techniques, June, pp. 20-24.

McDonach, A., McKelvie, J. and Walker, C.A. (1980) Stress anlaysis of fibrous composites using moire interferometry. Optics and Lasers in Engineering, Vol. 1, pp. 85-105.

Marchant, M. and Bishop, S.M. (1974) An interference technique for the measurement of in-plane displacements of opaque surfaces. J. Strain Analysis, Vol. 9, No. 1, pp. 36-43.

Mazars, J. and Lemaitre, J. (1984) Application of continuous damage mechanics to strain and fracture behaviour of concrete. Application of Fracture Mechanics to Cementitious Composites, NATO Advanced Research Workshop, Northwestern Univ., USA, Ed. Shah, S.P., pp. 375-388.

Mindess, S. (1984) The effect of specimen size on the fracture energy of concrete. Cem. and Concr. Res., Vol. 14, pp. 431-436.

Mindess, S. and Diamond, S. (1980) The cracking and fracture of mortar. Fracture in Concrete. Proc. of a session sponsored by ASCE, Hollywood. Ed. Chen, W.F. and Ting, E.C., pp. 15-27.

Mindess, S., Lawrence, F.V. and Kesler, C.E. (1977) The J-Integral as a fracture criterion for fibre reinforced concrete. Cem. and Concr. Res., Vol. 7, pp. 731-742.

Mindess, S. and Nadeau, J.S. (1976) Effect of notch width on K_{1c} for mortar and concrete. Cem. and Concr. Res., Vol. 6, pp. 529-534.

Moavenzadeh, F. and Kuguel, R. (1969) Fracture of concrete. J. of Materials, Vol. 4, No. 3, pp. 497-519.

Moore, D.R. (1983) Photoelastic transducers. Optical Transducers and Techniques in Engineering Measurement, Ch.2, Ed. Luxmoore, A.R., Applied Science Publishers, London, pp. 39-60.

Nallathambi, P., Karihaloo, B.L. and Heaton, B.S. (1985) Various size effects in fracture of concrete. Cem. and Concr. Res., Vol. 15, pp. 117-126.

Naus, D.J. and Lott, J.L. (1969) Fracture toughness of portland cement concretes. J. Am. Concr. Inst., Vol. 66, pp. 481-489.

Newman, J.B. (1973) Deformational behaviour, failure mechanisms and design criteria for concretes under combinations of stress. Ph.D. thesis, Univ. London.

Nicoletto, G. (1983) Uno studio di concentrazione delle deformazioni con la moire interferometry. XI Convegno Nazionale dell'Associazione Italiana per l'Analisi delle Sollecitazioni, Torino, pp. 419-429.

Nicoletto, G., Post, D. and Smith, C.W. (1982) L'applicazione della moire interferometry alla meccanica della frattura. X Convegno Nazionale dell'Associazione Italiana per l'Analisi delle Sollecitazioni, Cosenza, pp. 323-332.

Orowan, E. (1948-9) Fracture and strength of solids. Reports on Progress in Physics, Vol. 12, pp. 185-232.

Palmer, A.C. and Rice, J.R. (1973) The growth of slip surfaces in the progressive failure of over-consolidated clay. Proc. Roy. Soc. Lond. A., Vol. 332, pp. 527-548.

Parks, V.J., Hofer, K.E. and Durelli, A.J. (1962) Extending the stress-analysis range of brittle coatings. Exp. Mech., Vol. 2, pp. 137-141.

Petersson, P-E. (1980a) Fracture energy of concrete : method of determination. Cem. and Concr. Res., Vol. 10, pp. 78-89.

Petersson, P-E. (1980b) Fracture energy of concrete : practical performance and experimental results. Cem. and Concr. Res., Vol. 10, pp. 91-101.

Petersson, P-E. (1981a) Direct tensile tests on prismatic concrete specimens. Cem. and Concr. Res., Vol. 11, pp. 51-56.

Petersson, P-E. (1981b) Crack growth and the development of fracture zones in plain concrete and similar materials. Report TVBM-1066, Lund Institute of Technology, Sweden.

Petersson, P-E. (1982) Comments on the method of determining the fracture energy of concrete by means of three-point bend tests on notched beams. Report TVBM-3011, Lund Institute of Technology, Sweden.

Pflug, L. (1979) Crack detection in bended concrete beam. Proc. of 7th. Nat. Cong. of the Italian Soc. for Stress Analysis, supplement, Cagliari, Sept. 1979, pp. 5-26.

Post, D. (1968) New optical methods of moire fringe multiplication. Exp. Mech., Vol. 8, pp. 63-68.

Post, D. (1979) Photoelasticity. Exp. Mech., Vol. 19, pp. 176-192.

Post, D. (1982) Developments in moire interferometry. Optical Engineering, Vol. 21, No. 3, pp. 458-467.

Post, D. and Baracat, W.A. (1981) High-sensitivity moire interferometry - a simplified approach. Exp. Mech., Vol. 21, pp. 100-104.

Redner, A.S. (1980) Photoelastic coatings. Exp. Mech., Vol. 20, pp. 403-408.

Reinhardt, H.W. (1984) Fracture mechanics of an elastic softening material like concrete. HERON, Vol. 29, No. 2.

Reinhardt, H.W. (1985) Crack softening zone in plain concrete under static loading. Cem. and Concr. Res., Vol. 15, pp. 42-52.

Rice, J.R. (1968) A path independent integral and the approximate analysis of strain concentration by notches and cracks. J. Appl. Mech., Vol. 35, pp. 379-386.

Rice, J.R. and Drucker, D.C. (1967) Energy changes in stressed bodies due to void and crack growth. Int. J. Fracture Mechanics, Vol. 3, pp. 19-27.

Rice, J.R., Paris, P.C. and Merkle, J.G. (1973) Some further results on J-Integral analysis and estimates. Progress in Flaw Growth and Fracture Toughness Testing, ASTM, STP536, pp. 231-245.

RILEM (1963) Inquiry - Direct tensile test of concrete. Bulletin RILEM, No. 20, pp. 83-90.

RILEM (1982) Determination of the fracture energy of mortar and concrete by means of three-point bend tests on notched beams. Proposed RILEM recommendation, 29th. January, 1982, revised version, June 1982. Division of Building Materials, Lund Institute of Technology, Sweden.

RILEM (1984) Determination of the fracture energy of mortar and concrete by means of three-point bend tests on notched beams. Proposed RILEM recommendation, 29th. January, 1982, revised version, October 1984. Division of Building Materials, Lund Institute of Technology, Sweden.

RILEM (1985) Determination of the fracture energy of mortar and concrete by means of three-point bend tests on notched beams. Draft recommendation by 50-FMC Committee, Materiaux et Constructions, Vol. 18, No. 106, pp. 285-290.

Rockey, K.C. (1951) Stress analysis using the brittle laquer process. Trans. Inst. Marine Engrs., Vol. 63, No. 3, pp. 43-54.

Rossi, P., Acker, P. and Francois, D. (1985) Measurements of the fracture toughness K_{1c} of concrete. Paper submitted for the 6th. Int. Conf. on Fracture, New Delhi.

Sack, R.A. (1946) Extension of Griffith's theory of rupture to three dimensions. Proc. Phys. Soc., Vol. 58, pp. 729-736.

Saouma, V.E., Ingraffe, A.R. and Catalano, D.M. (1982) Fracture toughness of concrete: K_{IC} revisited. J. Eng. Mech. Div., Proc. ASCE, Vol. 108, EM6, pp. 1152-1166.

Sciammarella, C.A. (1982) The moire method - A review. Exp. Mech., Vol. 39, pp. 418-433.

Sciammarella, C.A. and Chawla, S.K. (1978) A lens holographic - moire technique to obtain components of displacement and derivatives. Proc. SESA, Vol. 35, No. 2, pp. 373-381.

Sciammarella, C.A. and Gilbert, J.A. (1976) A holographic - moire technique to obtain separate patterns for components of displacement. Proc. SESA, Vol. 33, No. 1, pp. 215-220.

Shah, S.P. and McGarry, F.J. (1971) Griffith fracture criterion and concrete. J. Eng. Mech. Div., Proc. ASCE, Vol. 97, EM6, pp. 1663-1676.

Smith, F.G. and Thomson, J.H. (1971) Optics. J. Wiley and Sons Ltd., London.

Somayaji, S. (1980) Influence of notch dimensions on the effective surface energy and notch sensitivity of cement compounds. Fracture in Concrete. Proc. of a session sponsored by ASCE, Hollywood. Ed. Chen, W.F. and Ting, E.C., pp. 36-49.

Strange, P.C. and Bryant, A.H. (1979) Experimental tests on concrete fracture. J. Eng. Mech. Div., Proc. ASCE, Vol. 105, EM2, pp. 337-342.

Swamy, R.M. (1979) Fracture mechanics applied to concrete. Developments in Concrete Technology, Vol. 1, Ed. Lydon, F.D., Applied Science Publ., London, pp. 221-281.

Swartz, S.E., Hu, K-K. and Jones, G.L. (1978) Compliance monitoring of crack growth in concrete. J. Eng. Mech. Div., Proc. ASCE, Vol. 104, EM4, pp. 789-800.

Terrien, M. (1980) Emission acoustique et "comportement mecanique post-critique" d'un beton sollicite en traction. Bull. Liason, Labo. Ponts et Chaussee, Vol. 105, pp. 65-72.

Van Meir, J.G.M. (1984) Strain softening of concrete under multiaxial loading conditions. Ph.D. thesis, Technische Hogeschule Eindhoven.

Velazco, G., Visalvanich, K. and Shah, S.P. (1980) Fracture behaviour and analysis of fibre reinforced concrete beams. Cem. and Concr. Res., Vol. 10, pp. 41-51.

Vile, G.W.D. (1965) Behaviour of concrete under simple and combined stresses. Ph.D. Thesis, Univ. London.

Vile, G.W.D. (1968) The strength of concrete under short-term static biaxial stress. The structure of concrete and it's behaviour under load, Proc. of an Int. Conf., Cem. and Concr. Assoc., London, pp. 275-288.

Visalvanich, K. and Naamen, A.E. (1980) Evaluation of fracture techniques in cementitious composites. Fracture in Concrete. Proc. of a session sponsored by ASCE, Hollywood, Ed. Chen, W.F. and Ting, E.C., pp. 65-81.

Wadsworth, N.J., Billing, B.F. and Marchant, M.J.N. (1972) The measurement of local in-plane surface displacements using a moire technique. Royal Aircraft Establishment, Farnborough, Technical Report 72046.

Wadsworth, N., Marchant, M. and Billing, B. (1973) Real-time observation of in-plane displacements of opaque surfaces. Optics and Laser Tech., Vol. 5, No. 3, pp. 119-123.

Walker, C.A. and McKelvie, J. (1978) A practical multiplied-moire system. Exp. Mech., Vol. 18, pp. 316-320.

Walsh, P.F. (1972) Fracture of plain concrete. Indian Concr. J., Vol. 46, No. 11, pp. 469,470,476.

Walsh, P.F. (1976) Crack initiation in plain concrete. Mag. of Concr. Res., Vol. 28, No. 94, pp. 37-41.

Ward, M.A. (1964) The testing of concrete materials by precisely controlled uni-axial tension. Ph.D. thesis, Univ. London.

Wecharatana, M. and Shah, S.P. (1980a) Resistance to crack growth in portland cement composites. Fracture in Concrete, Proc. of a session sponsored by ASCE, Hollywood, Ed. Chen, W.F. and Ting, E.C., pp. 82-105.

Wecharatana, M. and Shah, S.P. (1980b) Double torsion tests for studying slow crack growth of portland cement mortar. Cem. and Concr. Res., Vol. 10, pp. 833-844.

Wecharatana, M. and Shah, S.P. (1982?) Experimental methods to determine fracture parameters for concrete. Undated report, probably 1982 or 1983, Technological Institute, Northwestern University, USA.

Wecharatana, M. and Shah, S.P. (1983) Predictions of non-linear fracture process zone in concrete. J. Eng. Mech., ASCE, Vol. 109, No. 5, pp. 1231-1246.

Weissman, E.M. and Post, D. (1982a) Moire interferometry near the theoretical limit. Applied Optics, Vol. 21, No. 9, pp. 1621-1623.

Welch, G.B. and Haisman, B. (1969) The application of fracture mechanics to concrete and the measurement of fracture toughness. Materiaux et Constructions, Vol. 2, No. 9, pp. 171-177.

Westergaard, H.M. (1939) Bearing pressures and cracks. J. Appl. Mech., Vol. 6, No. 2, pp. A49-A53.

Wittmann, F.H. and Metzener-Gheorghita, I. (1985) Fracture toughness of concrete determined on large specimens. Materiaux et Constructions, Vol. 18, No. 104, pp. 93-95.

Wium, D.J.W., Buyukozturk, O. and Li, V.C. (1984a) Hybrid model for discrete cracks in concrete. J. Eng. Mech., ASCE, Vol. 110, No. 8, pp. 1211-1229.

Wium, D.J.W., Buyukozturk, O. and Li, V.C. (1984b) Hybrid model for discrete cracks in concrete. Engineering Mechanics in Civil Engineering, Proc. of the 5th. Engineering Mechanics Division Speciality Conf., ASCE, Wyoming, Aug. 1984, Ed. Boresi, A.P. and Chong, K.P., Vol. 2, pp. 1403-1406.

Ziegeldorf, S., Muller, H.S. and Hilsdorf, H.K. (1980) A model law for the notch sensitivity of brittle materials. Cem. and Concr. Res., Vol. 10, pp. 589-599.